

UNIVERSITY OF SHEFFIELD

DEPARTMENT OF CIVIL AND STRUCTURAL ENGINEERING

THE EFFECTS OF RAISED ACCESS
FLOORING ON THE VIBRATIONAL
PERFORMANCE OF LONG-SPAN
CONCRETE FLOORS

by

Paul Reynolds

A thesis submitted for the Degree of Doctor of Philosophy in Engineering
at the University of Sheffield

February 2000



IMAGING SERVICES NORTH

Boston Spa, Wetherby

West Yorkshire, LS23 7BQ

www.bl.uk

BEST COPY AVAILABLE.

VARIABLE PRINT QUALITY

To Zena

Abstract

There is a current trend towards ever more slender concrete floor structures, which is resulting in more frequent problems with their vibration serviceability. Predictive methods for vibration serviceability must consider not only the structures themselves, but also the non-structural elements which are attached to them, as these may have a significant effect on the dynamic characteristics of the floor structural system. As there has been very little past research in this area, this thesis describes an investigation into the effects of raised access floors on the vibration serviceability of long-span concrete floors.

The development of a new modal testing facility based on electrodynamic shaker excitation, which was capable of producing high quality estimates of the modal properties of full-scale floor structures, is described. This was subsequently utilised to determine the modal properties of three full-scale floor structures, before and after the installation of various configurations of raised access floors. The response of these structures to controlled pedestrian excitation was also measured. Realistic finite element models of all structures were developed and updated using the results from the experimental work. These were subsequently utilised for investigation of the experimentally measured effects of the raised access floors.

It was found that raised access floors had only minor effects on the modal properties of the long-span concrete floors. Reductions in natural frequencies due to the increased mass were, to some extent, offset by the slight increases in stiffness following the installation of the access floors. Modal damping ratios increased for some modes of vibration, but these changes were rather unpredictable and hence they were too unreliable to be used in design.

The response of the structures under controlled pedestrian excitation reduced following the installation of various configurations of raised access floors. The reduction appeared to be greater for relatively deep access floors (500 - 600 mm) than for relatively shallow access floors (150 - 200 mm). Therefore, it is recommended that the effects of access floors may be included in vibration serviceability analyses by applying a reduction factor to predicted responses calculated by assuming a bare floor. The proposed reduction factors are 0.9 for access floors where the finished floor height is less than 500 mm and 0.8 for access floors where the finished floor height is 500 mm or greater.

Acknowledgements

The work described in this thesis was carried out at the Department of Civil and Structural Engineering at the University of Sheffield between October 1995 and September 1998, while the author was working as a full-time postgraduate research student, and between October 1998 and February 2000, while the author was also employed as a Lecturer at the Department. A leave of absence was taken from April to October 1999.

I would like to thank my supervisors, Professor Peter Waldron and Dr Aleksandar Pavic for their support over the last four years. Their encouragement, insight and advice has been invaluable to the success of this research project.

Thanks are also expressed to Messrs Michael Hartley, Mihail Petkovski and Kyriacos Neocleous for their assistance during the field testing phases of this project. These parts of the research would have been impossible without their help.

The financial assistance provided by the 1995 DETR Partners in Technology research grant number CI 39/3/393(cc0952) is also gratefully acknowledged.

In addition, I would like to thank my family, friends and colleagues for their support throughout the course of this project. In particular, I would like to say thanks to Colin and Angela Greensill, and their new baby Jacob, for putting up with me during the ups and downs of the last few years.

Finally, I would like to thank Zena for her love, support and patience throughout the course of this work. Without her, the last four and a half years would have been impossible.

Memorandum

The accompanying thesis entitled "The Effects of Raised Access Flooring on the Vibrational Performance of Long-Span Concrete Floors" is submitted for the degree of Doctor of Philosophy in the Faculty of Engineering at the University of Sheffield. The thesis is based entirely on the independent work carried out by the author in the University of Sheffield between October 1995 and February 2000 (with a leave of absence from April to October 1999) under the supervision of Professor Peter Waldron and Dr Aleksandar Pavic. All the work and ideas recorded are original except where acknowledged in the text or by reference. The work contained in the thesis has not previously been submitted for a degree or diploma at this, or any other, University or Examining Body.

Paul Reynolds
February 2000

Table of Contents

Abstract	iii
Acknowledgements	iv
Memorandum.....	v
Table of Contents.....	vi
List of Tables.....	xiii
List of Figures	xv
Notation	xx
Abbreviations.....	xxiii
1 Introduction.....	1
1.1 The Research Problem.....	1
1.2 Proposed Scope of the Research.....	2
1.3 Thesis Outline	3
2 Background Review	4
2.1 History of the Vibration Serviceability Problem in Floors.....	4
2.1.1 Early Research into Vibration Serviceability of Composite Floors... 4	
2.1.1.1 Human Perceptibility of Vibrations.....	5
2.1.1.2 Analytical Models of Composite Floors.....	5
2.1.1.3 Development of a Design Procedure for Composite Floor	
Vibrations.....	5
2.1.1.4 Limitations of the CSA Guidelines.....	6
2.1.2 Further Research into the Vibrations of Composite Steel-Concrete	
Floors.....	7
2.1.2.1 North American Research Following the CSA Guidelines	
7	
2.1.2.2 SCI Publication 076: Design Guide on the Vibration of	
Floors	8
2.1.2.3 Further North American Research in the 1990s	9
2.1.3 Vibrations of Long-span Reinforced and Post-Tensioned Concrete	
Floors.....	10
2.1.3.1 Dynamic Behaviour of Long-Span Concrete Floors.....	10
2.1.3.2 Concrete Society Technical Report No. 43	11
2.1.4 Experimental Modal Analysis (EMA) of Floors.....	12
2.1.4.1 Operating Deflection Shapes (ODS) Analysis.....	12
2.1.4.2 'True' Experimental Modal Analysis	13
2.2 Prediction and Assessment of Vibration Serviceability	14
2.2.1 The Vibration Source	15
2.2.1.1 External Vibration Sources.....	15

	2.2.1.2	Internal Vibration Sources	16
2.2.2		Modelling the Walking Forcing Function	17
	2.2.2.1	Time Domain Models of the Walking Forcing Function..	17
	2.2.2.2	Frequency Domain Models of the Walking Forcing Function	18
	2.2.2.3	Indirect Modelling of the Walking Forcing Function.....	19
	2.2.2.4	Application of the Walking Forcing Functions to Analytical Models of Structures	20
2.2.3		The Transmission Path	20
	2.2.3.1	Simplified Structural Models for Vibration Analysis.....	21
	2.2.3.2	State-of-the-art Dynamic Analysis of Structures	21
	2.2.3.3	Experimental Determination of Structural Dynamic Properties	22
2.2.4		The Receiver	22
	2.2.4.1	Human Perception of Vibrations	22
	2.2.4.2	Variability of Human Perception to Vibrations.....	24
	2.2.4.3	Human Response to Building Vibrations	25
	2.2.4.4	Current Relevant Codes of Practice and Guidelines.....	26
2.3		The Effects of Non-Structural Elements on the Vibration Characteristics of Floors	27
	2.3.1	The Use of Non-Structural Elements in the Analysis of Vibration Serviceability.....	27
	2.3.2	Quantification of the Effects of Non-Structural Elements.....	28
	2.3.3	The Effects of Access Floors	28
	2.3.4	Survey of World Authorities	30
2.4		Conclusions of the Background Review.....	31
3		Experimental and Analytical Techniques.....	38
3.1		Strategy of the Research Work	38
	3.1.1	Analytical and Experimental Routes to Vibration Analysis	38
	3.1.2	Determination of The Effects of Access Floors on the Vibration Behaviour of Long-Span Concrete Floors.....	40
3.2		Finite Element Analysis.....	40
	3.2.1	The Fundamentals of Structural Finite Element Analysis	41
		3.2.1.1 The Stiffness Matrix	41
		3.2.1.2 The Mass Matrix.....	41
		3.2.1.3 The Damping Matrix.....	42
	3.2.2	Theoretical Modal Analysis	43
	3.2.3	Solution of Equations of Motion.....	44
	3.2.4	Practical Implementation of FE Modelling.....	46
		3.2.4.1 Selection of Analysis Software.....	46
		3.2.4.2 Choice of Element Types.....	46
3.3		Theory of Experimental Modal Analysis.....	47
	3.3.1	Theoretical Background	47
		3.3.1.1 Derivation of the Response Model	47
		3.3.1.2 Use of the Modal Model	48
	3.3.2	Dynamic Signal Analysis	49
		3.3.2.1 Periodic Signals	50
		3.3.2.2 Transient Signals.....	50
		3.3.2.3 Stationary Random Signals.....	51

	3.3.2.4	Calculation of Frequency Response Functions.....	52
	3.3.2.5	Sampled Functions.....	53
	3.3.3	Modal Parameter Estimation.....	53
3.4		Excitation for Experimental Modal Analysis	54
	3.4.1	Instrumented Impact Hammer Excitation.....	54
	3.4.2	Electrodynamic Shaker Excitation	55
	3.4.3	Types of Modal Test Excitation Signals	56
	3.4.4	Band-limited Random Excitation Signals	57
	3.4.4.1	Continuous Random Testing.....	58
	3.4.4.2	Burst Random Testing	58
	3.4.4.3	Use of the Exponential Window	58
	3.4.4.4	Triggered Random Excitation.....	59
	3.4.5	Burst Swept Sine Excitation Signals.....	60
	3.4.6	Pseudo-random (or Periodic Random) Excitation Signals.....	61
	3.4.7	Stepped Sine Excitation	61
3.5		EMA Transducers and Data Acquisition	62
	3.5.1	Response Transducers	62
	3.5.2	Data Acquisition Devices.....	63
	3.5.2.1	Racal StorePlus VL Analogue Instrumentation Tape Recorder.....	63
	3.5.2.2	DI-2200 Spectrum Analyser	63
	3.5.2.3	DAP 2400/e6 Data Acquisition Card.....	64
3.6		EMA Procedures.....	64
	3.6.1	Overview of EMA Procedures	64
	3.6.2	The Preparatory Phase.....	65
	3.6.2.1	Definition of Test Objectives.....	65
	3.6.2.2	Pre-Test Structural Dynamic Analysis.....	65
	3.6.2.3	Checking and Packing of Equipment.....	66
	3.6.2.4	Test Logistics	66
	3.6.2.5	Preparation of Structure	66
	3.6.2.6	Equipment Set-up.....	66
	3.6.3	The Exploratory Phase	67
	3.6.3.1	Excitation/Response Check	67
	3.6.3.2	Immediate Repeatability Check.....	68
	3.6.3.3	Homogeneity Check.....	69
	3.6.3.4	Reciprocity Check.....	69
	3.6.3.5	Coherence Function Check	70
	3.6.3.6	FRF Shape Check.....	71
	3.6.3.7	End of Test Repeatability Check	71
	3.6.4	The Measurement Phase.....	71
	3.6.4.1	Typical 'Swipe' Procedure	72
	3.6.4.2	Data Acquisition and Calculation of FRFs	72
	3.6.5	The Post-test Analysis Phase.....	73
	3.6.5.1	Modal Parameter Estimation.....	73
	3.6.5.2	Modal Complexity Factors	73
	3.6.5.3	Presentation of Results.....	74
3.7		Structural Response Measurement.....	74
	3.7.1	Test Procedures	74
	3.7.2	Processing of the Pedestrian Response Test Data.....	75
	3.7.2.1	Application of Frequency Weighting Curves	75
	3.7.2.2	Calculation of RMS Acceleration.....	75

	3.7.2.3	Calculation of Running RMS Acceleration	76
	3.7.2.4	Calculation of Vibration Dose Value	76
3.8		Finite Element Model Correlation and Updating	77
	3.8.1	Techniques for FE Model Correlation	77
	3.8.2	Finite Element Model Updating	79
4		Experimental Work	92
4.1		Introduction to the Test Structures.....	92
4.2		Test Structure A (Configuration 1).....	93
	4.2.1	Description of the Structure	93
	4.2.2	Pre-Test Analysis	94
	4.2.3	Testing Strategy.....	95
	4.2.4	Test Logistics	96
		4.2.4.1 Test Personnel.....	96
		4.2.4.2 Accommodation and Transport.....	96
	4.2.5	On-Site Preparation	97
		4.2.5.1 Preparation of Structure.....	97
		4.2.5.2 Setting Up Equipment.....	97
	4.2.6	EMA Using BSS Excitation: QA Checks	97
		4.2.6.1 Excitation/Response Check	98
		4.2.6.2 Immediate Repeatability Check	99
		4.2.6.3 Homogeneity Check.....	100
		4.2.6.4 Reciprocity Check.....	100
		4.2.6.5 Coherence Function Check.....	101
		4.2.6.6 FRF Shape Check.....	101
		4.2.6.7 End-Of-Test Repeatability Check.....	101
	4.2.7	EMA Using BSS Excitation: Main Swipe	101
		4.2.7.1 Swipe Details and Procedure	101
		4.2.7.2 Adjustment of Testing Schedule Due to Site Noise	102
		4.2.7.3 Reduction of the Test Grid for Future Modal Test Swipes	103
		4.2.7.4 Playback of Data from Analogue Tape Recorder	103
		4.2.7.5 Modal Parameter Estimation.....	104
	4.2.8	EMA Using BR Excitation: QA Checks	105
		4.2.8.1 Excitation/Response Check	105
		4.2.8.2 Immediate Repeatability Check	105
		4.2.8.3 Homogeneity Check.....	106
	4.2.9	EMA Using BR Excitation: Main Swipe	106
	4.2.10	Comparison of BSS Versus BR Shaker Excitation for EMA	106
	4.2.11	EMA Using Hammer Impact Excitation: QA Checks.....	107
		4.2.11.1 Fast Sampling Excitation/Response Check	107
		4.2.11.2 Slow Sampling Excitation/Response Check.....	108
		4.2.11.3 Immediate Repeatability Check.....	108
		4.2.11.4 Homogeneity and Reciprocity Checks	109
		4.2.11.5 Coherence Function Check.....	109
		4.2.11.6 FRF Shape Check and End-Of-Test Repeatability Check	110
	4.2.12	EMA Using Hammer Impact Excitation: Main Swipe.....	110
		4.2.12.1 Swipe Details and Procedure	110
		4.2.12.2 Modal Parameter Estimation	111

4.2.13	Comparison of Hammer Versus BR Shaker Excitation for EMA..	112
4.2.14	Summary of EMA Results.....	113
4.2.15	Pedestrian Response Measurements.....	114
	4.2.15.1 Design of the Pedestrian Response Tests	114
	4.2.15.2 Processing of the Pedestrian Response Test Data	115
4.2.16	Lessons Learned from Test Structure A (Configuration 1)	117
4.3	Test Structure A (Configuration 2).....	117
4.3.1	Description of the Structure	118
4.3.2	Pre-Test Analysis	118
4.3.3	Testing Strategy.....	118
4.3.4	Test Logistics	118
4.3.5	On-Site Preparation	119
4.3.6	Position of Shaker and Accelerometers for Measurements with Access Floors Installed.....	119
	4.3.6.1 Position of Accelerometers	120
	4.3.6.2 Position of the Shaker	120
4.3.7	EMA Using BR Excitation: QA Checks	121
	4.3.7.1 Homogeneity Check.....	121
	4.3.7.2 Reciprocity Check.....	122
	4.3.7.3 Coherence Function Check.....	122
	4.3.7.4 FRF Shape Check.....	122
4.3.8	EMA Using BR Excitation: Main Swipes.....	122
4.3.9	Summary of EMA Results.....	124
4.3.10	Pedestrian Response Measurements.....	125
4.3.11	Lessons Learned from Test Structure A (Configuration 2)	127
4.4	Test Structure B	128
4.4.1	Description of the Structure	128
4.4.2	Pre-Test Analysis	129
4.4.3	EMA.....	130
	4.4.3.1 QA Checks	130
	4.4.3.2 EMA Strategy	130
	4.4.3.3 EMA Results.....	130
4.4.4	Pedestrian Response Measurements.....	134
	4.4.4.1 Design of the Pedestrian Response Tests	134
	4.4.4.2 Processing of the Pedestrian Response Test Data	135
4.4.5	Lessons Learned from Test Structure B.....	137
4.5	Test Structure C	137
4.5.1	Description of the Structure	138
	4.5.1.1 Specification and Design of Structure C.....	138
	4.5.1.2 Construction of Structure C.....	139
	4.5.1.3 Access Floor Configurations.....	139
4.5.2	Pre-Test Analysis	142
4.5.3	EMA	142
	4.5.3.1 QA Checks	142
	4.5.3.2 EMA Strategy	143
	4.5.3.3 EMA Using Burst Random Excitation in Free-Armature Mode	143
	4.5.3.4 EMA Using Burst Random Excitation in Fixed-Armature Mode	143
	4.5.3.5 EMA Using Stepped Sine Excitation in Fixed-Armature Mode	144

4.5.3.6	EMA Results	144
4.5.3.7	Discussion of the Torsional Modes of Vibration.....	147
4.5.4	Pedestrian Response Measurements.....	147
4.5.5	Lessons Learned from Testing Structure C.....	151
5	Post-Test Analysis of Structures.....	210
5.1	Structure A	210
5.1.1	Correlation Between Pre-Test Model and EMA Results	210
5.1.2	FE Model Updating of Bare Structure A (Configuration 1)	211
5.1.2.1	Details of FE Model Refinements.....	212
5.1.2.2	Details of Parameter Adjustments	212
5.1.2.3	Correlation Between Updated FE Model and Results from EMA.....	213
5.1.2.4	Comparison with Previous FE Model Updating Exercises on Structure A.....	215
5.1.3	Simulation of the Effects of Access Floors.....	216
5.2	Structure B	217
5.2.1	Correlation Between Pre-Test Model and EMA Results	217
5.2.2	FE Model Updating	218
5.2.2.1	Details of FE Model Refinements.....	218
5.2.2.2	Details of Parameter Adjustments	219
5.2.2.3	Correlation Between Updated FE Model and Results from EMA.....	219
5.2.2.4	Comparison with Previous FE Model Updating Exercises on Structure B	221
5.2.3	Simulation of the Effects of Access Floors.....	221
5.3	Structure C	223
5.3.1	Correlation Between Pre-Test Model and EMA Results	223
5.3.2	FE Model Updating	224
5.3.2.1	Updating of Pre-Test Model Using Parameter Adjustments Only.....	224
5.3.2.2	Examination of Boundary Conditions	225
5.3.2.3	Modelling of Structure C Using Solid Elements	226
5.3.2.4	Simulation of the Lack of Contact Above Test Point 9..	228
5.3.2.5	Comparison with Previous FE Model Updating Exercises on Structure C	230
5.3.3	Simulation of the Effects of Access Floors.....	231
5.4	Summary of Conclusions from FE Analysis.....	233
6	Discussion.....	253
6.1	Experimental Work Considerations.....	253
6.1.1	EMA Considerations	253
6.1.1.1	EMA Techniques Available.....	253
6.1.1.2	Practicalities of Performing EMA on Floors with Access Floors	254
6.1.2	Pedestrian Response Testing Considerations.....	255
6.1.2.1	Practicalities of Performing Tests on Floors with Access Floors	255
6.1.2.2	Selection of Vibration Response Assessment Parameter	255

6.2	The Effects of Access Floors on the Vibration Performance of Long Span Concrete Floors	258
6.2.1	Changes in Estimated Modal Parameters	258
6.2.1.1	Changes in Natural Frequencies	258
6.2.1.2	Changes in Modal Damping Ratios	259
6.2.2	Changes in Measured Vibration Response to Pedestrian Excitation	259
6.2.3	Influence of Access Floor Configuration	260
6.2.3.1	Influence of the Finished Floor Height	261
6.2.3.2	Influence of the Mechanical Fixing of Panels to Pedestals	261
6.2.3.3	Influence of the Presence of Stringers	263
6.2.4	Influence of the Sub-Floor Configuration	263
6.3	Inclusion of the Effects of Access Floors in Future Vibration Assessment Analyses	264
6.3.1	Modification of Structural Dynamic Properties	264
6.3.2	Application of a Vibration Response Reduction Factor	264
6.4	Practical Use of Access Floors for Improvement of Vibration Serviceability	266
7	Conclusions and Recommendations for Further Work	267
7.1	Conclusions	267
7.2	Recommendations for Further Work	268
	References.....	270
	Appendix I	A1.1 - A1.21

List of Tables

Table 2.1: Some Sources of Inter- and Intra-Subject Variability	25
Table 2.2: Prominent Experts who were Questioned about the Effects of Non-Structural Elements on the Vibration of Floors.....	30
Table 4.1: Structure A (Configuration 1) - Data Acquisition Parameters Selected for First EMA Swipe Using BSS Excitation.	99
Table 4.2: Structure A (Configuration 1) - Accelerometer Locations and Instrumentation Channels Used for BSS Swipe.....	102
Table 4.3: Structure A (Configuration 1) - Data Acquisition Parameters for Immediate Repeatability Check Using BR Excitation.....	105
Table 4.4: Structure A (Configuration 1) - Data Acquisition Parameters for EMA Swipe Using Hammer Impact Excitation.....	109
Table 4.5: Structure A (Configuration 1) - Accelerometer Locations for Hammer Impact Swipe.....	110
Table 4.6: Structure A (Configuration 1) - Estimated Modal Parameters.....	114
Table 4.7: Structure A (Configuration 1) - Results from Pedestrian Response Tests...	116
Table 4.8: Structure A (Configuration 2) - Specification of Access Floor.	118
Table 4.9: Structure A (Configuration 2) - Accelerometer Locations for 1 st Swipe Using BR Excitation.....	123
Table 4.10: Structure A (Configuration 2) - Accelerometer Locations for 2 nd Swipe Using BR Excitation.	123
Table 4.11: Structure A (Configuration 2) - Estimated Modal Parameters.....	124
Table 4.12: Structure A - Percentage Changes in Modal Parameters Between Configurations 1 and 2.....	125
Table 4.13: Structure A (Configuration 2) - Results from Pedestrian Response Tests.	126
Table 4.14: Structure A - Percentage Changes in Pedestrian Response Test Assessment Parameters Between Configurations 1 and 2.....	127
Table 4.15: Structure B (Configuration 1) - Estimated Modal Parameters.....	131
Table 4.16: Structure B (Configuration 2) - Estimated Modal Parameters.....	131
Table 4.17: Structure B (Configuration 3) - Estimated Modal Parameters.....	132
Table 4.18: Structure B - Percentage Changes in Modal Parameters Between Configuration 1 and Configurations 2 and 3.	133
Table 4.19: Structure B (Configuration 1) - Results from Pedestrian Response Tests.	135
Table 4.20: Structure B (Configuration 2) - Results from Pedestrian Response Tests.	136
Table 4.21: Structure B (Configuration 3) - Results from Pedestrian Response Tests.	136
Table 4.22: Structure B - Percentage Differences in Pedestrian Response Assessment Parameters Between Configuration 1 and Configurations 2 and 3.....	137
Table 4.23: Structure C - Access Floor Configurations Utilised in the Testing.	141
Table 4.24: Structure C - Estimated Modal Parameters from All Floor Configurations	145
Table 4.25: Structure C - Results from Pedestrian Response Measurements Performed by Pedestrian 1.....	149
Table 4.26: Structure C - Results from Pedestrian Response Measurements Performed by Pedestrian 2.....	150
Table 5.1: Structure A (Configuration 1) - Summary of Parameter Adjustments.....	213
Table 5.2: Structure A (Configuration 1) - Natural Frequencies Calculated from the Updated FE Model.....	214

Table 5.3: Structure A (Configuration 2) - Natural Frequencies Calculated from the Updated FE Model with Access Floors Modelled as Added Mass Only.	216
Table 5.4: Structure B (Configuration 1) - Natural Frequencies Calculated from the Updated FE Model.....	220
Table 5.5: Structure B (Configurations 2 and 3) - Natural Frequencies Calculated from the Updated FE Model with Access Floors Modelled as Added Mass Only.	222
Table 5.6: Structure C (Configuration 1) - Natural Frequencies from Updated FE Model and from EMA.	225
Table 5.7: Structure C (Configuration 1) - Comparison of Natural Frequencies from FE Model Using Shell and Solid Elements.	226
Table 5.8: Structure C (Configuration 1) - Comparison of Natural Frequencies from FE Model Using Full Translational Constraints and Simple Supports.	227
Table 5.9: Structure C (Configuration 1) - Parameters for Best Correlation Between Updated FE Model and results from EMA Using Spring Supports.	228
Table 5.10: Structure C (Configuration 1) - Comparison of Natural Frequencies from Updated FE Model Using Spring Supports and from EMA.	228
Table 5.11: Structure C (Configuration 1) - Parameters for Best Correlation Between Updated FE Model Considering Lack of Contact Above Test Point 9 and results from EMA.	229
Table 5.12: Structure C (Configuration 1) - Comparison of Natural Frequencies and Modal Masses from Updated FE Model and from EMA.	230
Table 5.13: Structure C (Configurations 2 to 13) - Natural Frequencies Calculated from the Updated FE Model with Access Floors Modelled as Added Mass Only.	231
Table 5.14: Structure C - Percentage Changes in Natural Frequencies and Modal Masses from EMA Between Configuration 1 and Configurations 4, 5, 8, 9, 12 and 13...	232
Table A1.1: Structure A (Configuration 1) - Summary of Estimated Modal Parameters	A1.2
Table A1.2: Structure A (Configuration 2) - Summary of Estimated Modal Parameters	A1.4
Table A1.3 Structure B (Configuration 1) - Summary of Estimated Modal Parameters	A1.6
Table A1.4: Structure B (Configuration 2) - Summary of Estimated Modal Parameters	A1.9
Table A1.5: Structure B (Configuration 3) - Summary of Estimated Modal Parameters	A1.12
Table A1.6: Structure C (All Configurations) - Summary of Estimated Modal Parameters.....	A1.15

List of Figures

Figure 2.1: Modified Reiher-Meister Criteria (after Lenzen, 1966).	32
Figure 2.2: Idealised Heel-drop Forcing Function (after Lenzen & Murray, 1969).	32
Figure 2.3: Annoyance Criteria for Floor Vibrations (after CSA, 1989).	33
Figure 2.4: Overestimation of Damping When Using the Half-power Bandwidth Method of Estimating Damping for Structures with Close Modes.	34
Figure 2.5: Typical FRF Measurement Presented by Khan (1996).	34
Figure 2.6: Characteristic Double Peak Walking Forcing Function (after Galbraith & Barton, 1970).	35
Figure 2.7: Classical Mass-Spring-Damper SDOF System.	35
Figure 2.8: Continuous Sinusoidal Vibration Ratings (after Reiher & Meister, 1931). .	36
Figure 2.9: Typical Configuration of an Access Floor System (Illustration Courtesy of Tate Access Floors).	37
Figure 3.1: Theoretical and Experimental Routes to Vibration Analysis (after Ewins, 1995).	80
Figure 3.2: Elements and Nodes in Finite Element Analysis.	80
Figure 3.3: Classification of Dynamic Signals (after McConnell, 1995).	81
Figure 3.4: Various Forms of the Fourier Transform (after Randall, 1987).	82
Figure 3.5: Photograph and Illustration of Dytran Model 5803A Instrumented Impact Hammer.	83
Figure 3.6: Hammer Impact Time History and Fourier Transform.	83
Figure 3.7: Force Envelope for the APS Dynamics Model 113 Electrodynamic Shaker (after APS, undated).	84
Figure 3.8: Photograph of Shaker in Free Armature Mode.	84
Figure 3.9: Photograph of Shaker in Fixed Armature Mode.	85
Figure 3.10: Flowchart for the RANGEN Computer Program.	86
Figure 3.11: Exponential and Force Windows for EMA.	87
Figure 3.12: Flowchart for the SG_CTRL Computer Program.	88
Figure 3.13: Logarithmic Burst Swept Sine Signal and Fourier Transform.	89
Figure 3.14: Flowchart for the PSEUDO Computer Program.	90
Figure 3.15: Mounting of the Response Transducers.	91
Figure 3.16: W_k Frequency Weighting Curve from ISO 2631 (after ISO 1997).	91
Figure 4.1: Structure A - Configuration of the Structure.	153
Figure 4.2: Test Structure A (Configuration 1) - Photograph.	153
Figure 4.3: Structure A - Pre-Test FE Model.	154
Figure 4.4: Structure A - First 10 Modes Calculated from Pre-Test FE Model.	155
Figure 4.5: Structure A - Test Grid.	156
Figure 4.6: Structure A - Auto-MAC Calculated for Proposed Test Grid.	156
Figure 4.7: Structure A (Configuration 1) - Photograph of the Data Acquisition Centre Located in the Core Area of the Floor.	157
Figure 4.8: Structure A (Configuration 1) - Excitation/Response Check for BSS Excitation (Time Domain).	157
Figure 4.9: Structure A (Configuration 1) - Excitation/Response Check for BSS Excitation (Frequency Domain).	158
Figure 4.10: Structure A (Configuration 1) - Excitation/Response Check for BR Excitation (Time Domain).	158

Figure 4.11: Structure A (Configuration 1) - Excitation/Response Check for BR Excitation (Frequency Domain).....	159
Figure 4.12: Structure A (Configuration 1) - Comparison Between 4 s and 8 s of BSS Excitation.....	159
Figure 4.13: Structure A (Configuration 1) - Immediate Repeatability Check for BSS Excitation.....	160
Figure 4.14: Structure A (Configuration 1) - SDOF Processing of Immediate Repeatability Check FRF.....	160
Figure 4.15: Structure A (Configuration 1) - Homogeneity Check for BSS Excitation.	161
Figure 4.16: Structure A (Configuration 1) - Reciprocity Check for BSS Excitation. .	161
Figure 4.17: Structure A (Configuration 1) - Point Mobility Coherence Check for BSS Excitation.....	162
Figure 4.18: Structure A (Configuration 1) - Transfer Mobility Coherence Check for BSS Excitation.....	162
Figure 4.19: Structure A (Configuration 1) - FRF Shape Check for BSS Excitation. ..	163
Figure 4.20: Structure A (Configuration 1) - End of Test Repeatability Check for BSS Excitation.....	163
Figure 4.21: Schematic Illustration of the Instrumentation System.	164
Figure 4.22: Structure A (Configuration 1) - Transfer Mobility Immediate Repeatability Check Under Noisy Conditions.	164
Figure 4.23: Structure A (Configuration 1) - Coherence Function for Transfer FRF Between Points 29 and 32.....	165
Figure 4.24: Structure A (Configuration 1) - Comparison of Direct and Replayed FRFs	165
Figure 4.25: Structure A (Configuration 1) - Complex MIF for BSS Swipe Measured at Test Point 32.....	166
Figure 4.26: Structure A (Configuration 1) - MDOF Modal Parameter Estimation (Global-M) for BSS Swipe Measured at Test Point 32.....	166
Figure 4.27: Structure A (Configuration 1) - Estimated Mode Shapes From BSS Swipe	167
Figure 4.28: Structure A (Configuration 1) - Immediate Repeatability Check for BR Excitation.....	168
Figure 4.29: Structure A (Configuration 1) - Homogeneity Check for BR Excitation.	168
Figure 4.30: Structure A (Configuration 1) - Complex MIF for BR Swipe Measured at Test Point 32.....	169
Figure 4.31: Structure A (Configuration 1) - Estimated Mode Shapes from BR Swipe	170
Figure 4.32: Structure A (Configuration 1) - Comparison of Point Mobility FRF for BR and BSS Excitation.....	171
Figure 4.33: Structure A (Configuration 1) - Comparison of Transfer Mobility FRF for BR and BSS Excitation.....	171
Figure 4.34: Structure A (Configuration 1) - Comparison of Mode Shapes and MCFs for BR and BSS Excitation.....	172
Figure 4.35: Structure A (Configuration 1) - Point Mobility Fast Sampling Excitation/Response Check for Hammer Excitation.....	173
Figure 4.36: Structure A (Configuration 1) - Transfer Mobility Fast Sampling Excitation/Response Check for Hammer Excitation (Time Domain).....	173
Figure 4.37: Structure A (Configuration 1) - Point Mobility Slow Sampling Excitation/Response Check for Hammer Excitation (Time Domain).....	174
Figure 4.38: Structure A (Configuration 1) - Point Mobility Slow Sampling Excitation/Response Check for Hammer Excitation (Frequency Domain).....	174

Figure 4.39: Structure A (Configuration 1) - Immediate Repeatability Check for Hammer Excitation.....	175
Figure 4.40: Structure A (Configuration 1) - Problematic Coherence Function Check for Hammer Excitation.....	175
Figure 4.41: Structure A (Configuration 1) - Estimated Mode Shapes From Hammer Impact Swipe.....	176
Figure 4.42: Structure A (Configuration 1) - Comparison of Point Mobility FRF for Hammer and Shaker Excitation.....	177
Figure 4.43: Structure A (Configuration 1) - Comparison of Transfer Mobility FRF for Hammer and Shaker Excitation.....	177
Figure 4.44: Structure A (Configuration 1) - Comparison of Mode Shapes and MCFs for Hammer and Shaker Excitation.....	178
Figure 4.45: Structure A - Walking Paths and Response Measurement Locations for Pedestrian Response Tests.....	179
Figure 4.46: Structure A (Configuration 1) Pedestrian Response Measurement for Walking Path 1 (127 spm) with Response Measured at Test Point 32.....	179
Figure 4.47: Structure A (Configuration 2) - General View.....	180
Figure 4.48: Structure A (Configuration 2) - General Construction of the Access Floor.....	180
Figure 4.49: Structure A (Configuration 2) - Investigation of Accelerometer Position with Access Floors Installed.....	181
Figure 4.50: Structure A (Configuration 2) - Comparison of Accelerometer Positions (Point Mobility Nominally at Test Point 32).....	181
Figure 4.51: Structure A (Configuration 2) - Comparison of Shaker Positions (Point Mobility Nominally at Test Point 32).....	182
Figure 4.52: Structure A (Configuration 2) - Homogeneity Check Using BR Excitation.....	182
Figure 4.53: Structure A (Configuration 2) - Reciprocity Check Using BR Excitation.....	183
Figure 4.54: Structure A (Configuration 2) - Point Mobility Coherence Function Check Using BR Excitation.....	183
Figure 4.55: Structure A (Configuration 2) - Transfer Mobility Coherence Function Check Using BR Excitation.....	184
Figure 4.56: Structure A (Configuration 2) - FRF Shape Check Using BR Excitation.....	184
Figure 4.57: Structure B - Configuration.....	185
Figure 4.58: Structure B (Configuration 1) - General View of Structure B in its Bare Condition.....	185
Figure 4.59: Structure B - General View with Access Floors Installed (Configurations 2 and 3).....	186
Figure 4.60: Structure B - Pre-Test FE Model.....	186
Figure 4.61: Structure B - First 15 Modes Calculated from Pre-Test FE Model.....	187
Figure 4.62: Structure B - Test Grid.....	188
Figure 4.63: Structure B - Auto-MAC Calculated for Proposed Test Grid Using First 15 FE Calculated Modes of Vibration.....	188
Figure 4.64: Structure B (Configuration 1) - Shaker on Bare Floor.....	189
Figure 4.65: Structure B (Configurations 2 and 3) - Shaker on Access Floor Above a Pedestal.....	189
Figure 4.66: Structure B (All Configurations) - Estimated Mode Shapes.....	190
Figure 4.67: Structure B - Walking Paths for Pedestrian Response Measurements.....	191
Figure 4.68: Structure B (Configuration 1) - Pedestrian Response Measurement for Walking Path 1 (138 spm) with Response Measured at Test Point 46.....	191
Figure 4.69: Structure C - General Arrangement Drawing.....	192

Figure 4.70: Structure C - Access Floor Grid Layout.	193
Figure 4.71: Structure C - Photograph of 'Knife-Edge' Support.	193
Figure 4.72: Structure C - Photograph of Showing Pits Constructed for Direct Drive Excitation.	194
Figure 4.73: Structure C - Alternate Dead and Live Prestressing Anchors.	194
Figure 4.74: Structure C - Post-Tensioning in Progress.	195
Figure 4.75: Structure C - Photograph Prior to Concreting Illustrating Formwork, Reinforcement and Prestressing.	196
Figure 4.76: Structure C - Completed Structure with End Platforms Constructed.	197
Figure 4.77: Structure C - Comparison of 200 mm and 600 mm FFH Access Floors. .	197
Figure 4.78: Structure C - Comparison of Epoxy and Polyurethane Based Pedestal Adhesives.	198
Figure 4.79: Structure C - Snap-On Stringer System.	198
Figure 4.80: Structure C - Bolt-On Stringer System.	199
Figure 4.81: Structure C - Pre-Test FE Model.	199
Figure 4.82: Structure C - First 4 Modes Calculated from Pre-Test FE Analysis.	200
Figure 4.83: Structure C - Test Grid for EMA Swipes with Shaker in Free-Armature Mode.	200
Figure 4.84: Structure C (Configuration 1) - Reciprocity Check Between Test Points 4 and 22.	201
Figure 4.85: Structure C - Shaker Attached for Fixed-Armature Measurements.	201
Figure 4.86: Structure C - Test Grid for EMA Swipes with Shaker in Fixed-Armature Mode.	202
Figure 4.87: Structure C (All Configurations) - Estimated Mode Shapes.	203
Figure 4.88: Structure C (Configuration 5) - FRFs Measured Using Stepped-Sine Excitation with Varying Force Levels.	204
Figure 4.89: Structure C - Percentage Changes in Natural Frequencies Between Floor Configuration 1 and Configurations 2 to 13.	204
Figure 4.90: Structure C - Percentage Changes in Modal Damping Ratios Between Floor Configuration 1 and Configurations 2 to 13.	205
Figure 4.91: Structure C - Lack of Contact at Knife-Edge Support Beneath Test Point 9	205
Figure 4.92: Structure C (Configuration 1) - Pedestrian Response Measurement for Pedestrian 1 at a Pacing Rate of 138 spm.	206
Figure 4.93: Structure C - Percentage Changes in RMS Acceleration Response (Entire Record) for 2 nd Harmonic Excitation Between Floor Configuration 1 and Configurations 2 to 13.	206
Figure 4.94: Structure C - Percentage Changes in Peak Running RMS Acceleration Response for 2 nd Harmonic Excitation Between Floor Configuration 1 and Configurations 2 to 13.	207
Figure 4.95: Structure C - Percentage Changes in VDV for 2 nd Harmonic Excitation Between Floor Configuration 1 and Configurations 2 to 13.	207
Figure 4.96: Structure C - Percentage Changes in RMS Acceleration Response (Entire Record) for 3 rd Harmonic Excitation Between Floor Configuration 1 and Configurations 2 to 13.	208
Figure 4.97: Structure C - Percentage Changes in Peak Running RMS Acceleration Response for 3 rd Harmonic Excitation Between Floor Configuration 1 and Configurations 2 to 13.	208
Figure 4.98: Structure C - Percentage Changes in VDV for 3 rd Harmonic Excitation Between Floor Configuration 1 and Configurations 2 to 13.	209

Figure 5.1: Structure A (Configuration 1) - Correlation Between Pre-Test FE Model and EMA Results.....	234
Figure 5.2: Structure A (Configuration 1) - Comparison of the First 6 Modes of the Pre-Test Model and the Results from EMA.....	235
Figure 5.3: Structure A (Configuration 1) - Configuration of Updated FE Model.....	236
Figure 5.4: Structure A (Configuration 1) - Attached Non-structural Elements.....	236
Figure 5.5: Structure A (Configuration 1) - Comparison of the First 10 Modes of the Updated FE Model and the Results from EMA. Continued Overleaf... ..	237
Figure 5.6: Structure A (Configuration 1) - Correlation Between the Updated FE Model and Results from EMA.....	239
Figure 5.7: Structure A (Configuration 1) - Comparison of Experimental and Analytical FRFs.....	239
Figure 5.8: Structure B (Configuration 1) - Correlation Between Pre-Test FE Model and EMA Results.....	240
Figure 5.9: Structure B - Crack Pattern Observed During Tests and Corresponding Division of Slab into Areas for Simulation of the Effects of the Cracking.....	240
Figure 5.10: Structure B - Rotation of Columns Through 45° in FE Model.....	241
Figure 5.11: Structure B - Crack Pattern Observed on Columns.....	241
Figure 5.12: Structure B - Values of Modulus of Elasticity for Various Parts of the Structure Following FE Model Updating.....	242
Figure 5.13: Structure B (Configuration 1) - Comparison of the First 15 Modes of the Updated FE Model and the Results from EMA. Continued Overleaf... ..	243
Figure 5.14: Structure B (Configuration 1) - Correlation Between the Updated FE Model and Results from EMA.....	246
Figure 5.15: Structure B (Configuration 1) - Comparison of Experimental and Analytical FRFs.....	246
Figure 5.16: Structure C (Configuration 1) - Correlation Between Pre-Test FE Model and EMA Results.....	247
Figure 5.17: Structure C (Configuration 1) - Comparison of the First 4 Modes of the Pre-Test Model and the First 5 Modes from EMA.....	248
Figure 5.18: Structure C (Configuration 1) - FE Model Using Solid Elements Instead of Shell Elements.....	249
Figure 5.19: Structure C - Additional Axial Strain Caused by Friction at the Supports.....	249
Figure 5.20: Structure C (Configuration 1) - Configuration of Updated FE Model with Vertical and Horizontal Spring Supports Removed at Point of Lack of Contact.....	250
Figure 5.21: Structure C (Configuration 1) - Comparison of the First 4 Modes of the Updated Model and the First 5 Modes from EMA.....	251
Figure 5.22: Structure C (Configuration 1) - Correlation Between the Updated FE Model and Results from EMA.....	252
Figure 5.23: Structure C (Configuration 1) - Comparison of Experimental and Analytical FRFs.....	252

Notation

- [] Matrix
- { } Vector
- () Element of a matrix or vector
- [\] Diagonal matrix
- []^T Transpose of a matrix
- { }^T Transpose of a vector
- {f} Vector of applied nodal forces
- {q(t)} Vector of time varying generalised coordinates
- {x} Vector of nodal displacements
- {x(t)} Vector of time varying nodal displacements
- {ẋ(t)} Vector of time varying nodal velocities
- {ẍ(t)} Vector of time varying nodal accelerations
- [\ ω_r] Diagonal eigenvalue matrix (natural frequencies)
- [α(ω)] Receptance matrix
- [Ψ] Eigenvector matrix (mode shapes)
- [Φ] Mass-normalised eigenvector matrix (mode shapes)
- [C] Damping matrix
- [D] Structural (hysteretic) damping matrix
- [H(ω)] Inertance matrix
- [I] Identity matrix

- $[K]$ Stiffness matrix
- $[M]$ Mass matrix
- $\alpha_{jk}(\omega)$ Element of the receptance matrix (i.e. a receptance FRF)
- ϕ_{jr} j^{th} element of the r^{th} mode of vibration
- $\gamma^2(f)$ Coherence function
- ζ_r Modal viscous damping ratio of the r^{th} mode of vibration
- η_r Modal loss factor of the r^{th} mode of vibration
- ω Frequency of vibration (rads^{-1})
- ω_r Natural frequency of the r^{th} mode of vibration
- ${}_r A_{jk}$ Modal constant for mode r
- f Frequency of vibration (Hz)
- $f(t)$ Time varying force
- G_{xx} Single-sided auto-spectral density of signal X
- G_{yy} Single-sided auto-spectral density of signal Y
- G_{xy} Single-sided cross-spectral density of signals X and Y
- $H(\omega)$ Element of the inertance matrix (i.e. an inertance FRF)
- $Q(t)$ Time varying generalised force
- i Imaginary unit, $\sqrt{-1}$
- N Total number of degrees of freedom / coordinates
- $q(t)$ Time varying generalised coordinate
- r Current mode number
- R_{xx} Random auto-correlation function of signal X

S_{XX}	Dual-sided auto-spectral density of signal X
S_{YY}	Dual-sided auto-spectral density of signal Y
S_{XY}	Dual-sided cross-spectral density of signals X and Y
t	Time
T	Repeat period / data acquisition period / integration time
$x(t)$	Time varying displacement
$\dot{x}(t)$	Time varying velocity
$\ddot{x}(t)$	Time varying acceleration

Abbreviations

ASCE	American Society of Civil Engineers
AISC	American Institute of Steel Construction
ASD	Auto Spectral Density
BSI	British Standards Institution
CMP	Correlated Mode Pair
COMAC	Coordinate Modal Assurance Criterion
CS	(UK) Concrete Society
CSA	Canadian Standards Association
DETR	(UK) Department of the Environment, Transport and the Regions
DFT	Discrete Fourier Transform
DOF	Degree-Of-Freedom
DTA	(UK) Dynamic Testing Agency
EMA	Experimental Modal Analysis (also known as Modal Testing)
eVDV	Estimated Vibration Dose Value
FE	Finite Element
FEM	Finite Element Method
FFH	Finished Floor Height
FFT	Fast Fourier Transform
FRF	Frequency Response Function
IABSE	International Association for Bridge and Structural Engineering
ICATS	Imperial College Analysis and Testing Software
ISO	International Organisation for Standardisation
MAC	Modal Assurance Criterion
MCF	Modal Complexity Factor
MDOF	Multi-Degree-Of-Freedom
MIF	Mode Indicator Function
NAFEMS	(UK) National Agency for Finite Element Methods and Standards
RFP	Rational Fraction Polynomial
RMS	Root Mean Square
SCI	(UK) Steel Construction Institute
SDOF	Single-Degree-Of-Freedom
UFF	Universal File Format

1 Introduction

There is a current trend for longer spans in floor structures for aesthetic and economic reasons, particularly in modern office building developments. As a result floor slenderness is increasing and it is possible that vibration serviceability may become the governing design criterion for many new floor structure developments.

It has been suggested (Ohlsson, 1988; Eriksson, 1994) that the vibration serviceability performance of such floor structures may be improved through the installation of non-structural elements such as partition walls, raised access floors and suspended ceilings. As vibration serviceability becomes an important design criterion, investigation of such beneficial effects is becoming increasingly relevant. The research work presented in this thesis is concerned with the examination of the effects of one particular type of non-structural element, the raised access floor.

1.1 The Research Problem

Raised access floors (also known as false floors or computer floors) are almost inevitable in new office building developments, as well as in the commercial redevelopment of existing older buildings. Two key benefits of raised access floors, frequently cited in the trade literature, are improved access to services and improved flexibility of building usage (Tate Access Floors, 1996). In addition, it has also been suggested in the literature that the installation of raised access floors may result in the improvement of the vibration serviceability performance of the floors on which they are installed (Osborne & Ellis, 1990; Williams & Waldron, 1994). This has been shown possibly to be quite significant (Williams & Falati, 1999).

However, as will be shown in Chapter 2 of this thesis, little research exists into the quantification of the effects of various types of access floors on the vibration performance of long span floors on which they are installed. Moreover, the scarce results of the past research are often conflicting and inconclusive. It was because of these reasons that the research work presented in this thesis was initiated.

The primary aim of the research presented in this thesis is to identify and quantify the (possibly beneficial) effects of access floors with regards to floor vibration serviceability.

1.2 Proposed Scope of the Research

Raised access floors are probably most commonly utilised in office buildings, where convenient access to communications cabling (such as computer and telephone networks) is required. In addition to this, office buildings are probably most affected by the trend for larger clear spans and increased floor slenderness, because of the drive for increased flexibility of office floor layouts (Pavic, 1999). This means that it is likely that office buildings may be most affected by problems with vibration serviceability.

For these reasons, this study will be primarily concerned with the vibration serviceability of office type floor structures with access floors installed. It has now been widely recognised that the critical dynamic loading condition for these types of structures is a single person walking (Bachmann et al., 1995).

Using a combined experimental and analytical approach, which is common when investigating vibration engineering problems, the research presented in this thesis has the following objectives:

1. The effects of raised access floors on the modal properties (natural frequencies, modal damping ratios, modal masses and mode shapes) of full scale long span concrete floors will be investigated through the use of experimental modal analysis (EMA).
2. The effects of raised access floors on the vibrational response of a number of representative full scale long span concrete floors subjected to pedestrian excitation will be investigated. This will be done because changes in floor modal parameters, following the installation of access floors, may reduce levels of response to pedestrian excitation.
3. Numerical finite element (FE) modelling of the tested structures will be performed, followed by their correlation and updating using the results from the EMA. These will then help a detailed investigation of the results from the experimental work described in 1 and 2.

4. The results from the experimental and analytical work will be interpreted and a recommendation of a practical means by which the effects of raised access floors may be included in future predictions of floor vibration serviceability will be developed.

1.3 Thesis Outline

The research work presented in this thesis is structured into seven chapters. As already seen, this chapter (Chapter 1) provides a brief introduction to the research problem, its relevance, aims and objectives and the proposed scope of the work. Chapter 2 then presents a more detailed background review of past research work in this area and describes the research problem in more detail. The background review includes past research performed into floor vibration serviceability in general as well as research specifically into the effects of access floors on floor vibration. Next, Chapter 3 contains a description of the experimental and analytical techniques used in the course of this investigation. The commissioning of new equipment and development of utility software and procedures utilised in this work are also described. Chapter 4 presents the experimental work performed on each of the full-scale floor structures investigated. This chapter is complemented by limited interpretation of the test results, which is necessary when carrying out this type of experiment. This interpretation was subsequently used in Chapter 5, in which the detailed analytical computer modelling, correlation and updating was performed for each of the structures. Chapter 6 presents an overall discussion of the experimental and analytical data obtained for all of the structures considered. It is in this chapter that recommendations are made for how the effects of access floors may be incorporated into future vibration serviceability predictions. Finally, a summary of the conclusions and recommendations of this research is presented in Chapter 7.

2 Background Review

This chapter presents a literature review of past research which is pertinent to the work that has been carried out by the writer. It is intended to provide the reader with some of the historical developments in the area of floor vibration serviceability and to justify the need for and novelty of the research into the effects of access floors on vibration serviceability, which is presented in this thesis.

2.1 History of the Vibration Serviceability Problem in Floors

There is a long-standing awareness of problems with the vibration serviceability of floors and references to the problem may be found in the literature as far back as the early 19th century. In 1828 Thomas Tredgold, one of the founders of the Institution of Civil Engineers, wrote (Allen & Rainer, 1975):

“Girders should always, for long bearings, be made as deep as they can be got; an inch or two taken from the height of a room is of little consequence compared with a ceiling disfigured with cracks, besides the inconvenience of not being able to move on the floor without shaking everything in the room.”

2.1.1 Early Research into Vibration Serviceability of Composite Floors

One of the first coherent attempts to research the vibration serviceability of floors was performed at the University of Kansas (Lenzen, 1962; Lenzen & Murray, 1969). The work was initiated in 1958 by the Steel Joist Institute in the USA who were becoming concerned by the increase in occurrence of annoying vibrations in composite steel joist - concrete slab floors. This was a direct result of the design of more efficient structural sections possessing adequate static strength, but which were much more lightweight. This research programme lasted more than ten years. It included studies into the human perceptibility of vibrations, the development of analytical models of the floors and the development of a design guide. These will be briefly discussed.

2.1.1.1 Human Perceptibility of Vibrations

Lenzen (1962) stated that only transient vibrations were a problem for vibration serviceability of floors under human-induced excitation, and only if insufficient damping was present to eliminate the vibration within a few cycles of the application of the transient load. In other words, the duration of the vibrations was important.

However, at that time, the only existing research into the human perceptibility of vibrations was that which considered only the effects of steady-state vibrations, such as that performed by Reiher and Meister (Wright & Green, 1959) which had produced perceptibility curves similar to those shown in Figure 2.1. Following a number of tests of human perception of vibrations of composite floors, Lenzen (1966) proposed that the Reiher and Meister curves should be scaled by a factor of 10 to take account of the transient nature of vibrations caused by impact type loads. This has come to be known as the “Modified Reiher-Meister Scale” and is reproduced in Figure 2.1.

2.1.1.2 Analytical Models of Composite Floors

To produce design guidelines that could be used by design practitioners, the researchers at Kansas developed formulae that considered the floor to be a single degree of freedom (SDOF) system considering only the fundamental mode of vibration. The stiffness was calculated using simple beam assumptions. Lenzen (1966) stated that:

“... a more exact method for computing the natural frequency of the floor system was derived in which the stiffness of the slab perpendicular to the joist could be taken into account. Since this refinement made the computations cumbersome, it was not used.”

These types of simplifications have persisted ever since this early work and, as will be shown later in this thesis, have led to many oversimplified guidelines suitable for hand calculation of vibration response of floors.

2.1.1.3 Development of a Design Procedure for Composite Floor Vibrations

The ultimate aim of the research at Kansas University was to develop a checking procedure that could readily be used at the design stage to prevent excessive floor vibrations. In order to do this, a simplified forcing function for which the response of the floor could be calculated was required, in addition to the simplified analytical floor

system. This aim resulted in the heel-drop test, first mentioned in the literature by Lenzen & Murray (1969). The test is performed by "... having a person of average weight with soft-soled shoes rise up on his toes and drop on his heels near the location of the measurement (of the response)" (CSA, 1989).

This was a simple means of applying a more or less standard form of excitation to a real structure, which could be easily simulated analytically using a triangular forcing function (Figure 2.2). The response to this forcing function was then assumed to be related to the response of the structure to normal walking excitation. The measured or calculated frequencies, peak responses and damping values could then be checked against corresponding criteria (Figure 2.3).

Appendix G of the Canadian standard CSA-S16.1-1974 "Steel Structures for Buildings - Limit States Design" (CSA, 1974) was based upon the research performed at the University of Kansas. Although originally intended to serve as an interim measure (Allen & Rainer, 1976), these guidelines have essentially persisted up to the present day and were still included in the latest revision of the code in 1994.

2.1.1.4 Limitations of the CSA Guidelines

Although widely used and reasonably successful for the design and assessment of composite floors, there is a number of limitations of the CSA guidelines.

Firstly, the analytical models recommended are based upon the assumption of a SDOF system. As a result, only the fundamental mode of vibration is assumed to contribute to the response of the floor. In reality, higher modes of vibration may also contribute significantly to the response of the floor, and for many forms of floor construction, these higher modes will have frequencies close to that of the fundamental (closely spaced modes of vibration). This limitation was recognised by some of the developers of the guidelines (Allen & Swallow, 1975), although nothing was proposed to remedy this problem at the time.

The 'damping ratio' used by these guidelines was normally calculated by using the logarithmic decrement of the floor response, which is only theoretically valid for a SDOF system. This has, in the literature, been a source of great confusion with a very wide variety of damping values being suggested. Commonly quoted damping values of up to 14% for a composite floor with partitions and furniture (Allen, 1974) are now understood to be highly in error, and cannot be taken to represent 'modal damping

ratios' which they were meant to be (Wyatt, 1989). Realistic modal damping ratios are important as they can be used in frequency and time domain FE analyses for prediction of the response of MDOF systems.

The CSA guidelines are only applicable to the particular form of construction for which they were developed, i.e. lightweight composite steel-concrete floors (Williams & Waldron, 1994). For other forms of floor construction, such as the typically heavier long-span reinforced or post-tensioned concrete floors considered in this thesis, the guidelines simply are not suitable. This is because the CSA guidelines related the response measured due to a transient event (i.e. a heel-drop) to the likely response of a floor to continuous excitation (i.e. walking). Such a procedure is only likely to be valid for structures of similar mass and stiffness characteristics.

2.1.2 Further Research into the Vibrations of Composite Steel-Concrete Floors

2.1.2.1 North American Research Following the CSA Guidelines

Murray (1981) presented the results of heel-drop tests performed on 91 composite floors which had been rated subjectively as either acceptable or unacceptable. He compared these results with the results of the application of a number of guidelines which were current at that time. He concluded that none of the previous guidelines were reliable and therefore presented yet another empirical formula, which calculated a required amount of damping as a function of natural frequency and peak response. If in the finished structural system this amount of damping was provided, the floor was deemed to be satisfactory.

However, this guideline was once again based on high damping values estimated from heel-drop tests and its scope of application was limited to composite steel joist-concrete slab floors. It was also limited in that the values for fundamental natural frequency and peak amplitude were assumed to be determined from simple-beam formulae, and no account was taken of higher modes of vibration. Nevertheless, Murray was still advocating its use as late as 1988.

In 1981, Rainer and Pernica published a paper in which they examined various methods of determining modal damping ratios. In addition to examining damping values estimated from heel impact tests, they performed various shaker tests and calculated

damping from the linear spectra of the responses. They concluded that the heel impact test tended to overestimate values of modal damping ratios, probably the first time that this had been noted by the civil engineering community. However, the calculation of damping from the shaker tests was performed using the 'half power bandwidth method', which was also likely to be unreliable. This is because it is only theoretically valid for a SDOF system and an overestimation of damping from these tests may occur (Figure 2.4). The final observation from this work is that there was a very large degree of scatter in the measured values of damping, which is an indication of the fact that damping is a very difficult quantity to measure reliably.

An interesting paper by Rainer & Swallow (1986) described a method by which the modal properties (natural frequencies, mode shapes and modal damping ratios) of a structure were obtained from tests using two shakers. This was, in fact, a testing technique known as Operating Deflection Shapes (ODS) analysis, which is described in more detail in Section 2.1.4.1. Unfortunately, the values of damping estimated from these tests were once again likely to be inaccurate since they utilised the SDOF half-power bandwidth method. An indication of this is apparent through inspection of the damping values corresponding to the various modes of vibration, in which it can be seen that higher damping values were obtained for close modes than for well separated modes. This phenomenon was not commented upon by the writers.

2.1.2.2 SCI Publication 076: Design Guide on the Vibration of Floors

In 1989, a Steel Construction Institute (SCI) design guide (Wyatt, 1989) was published. It was primarily aimed at composite floors in offices subjected to pedestrian loading. External forms of excitation, such as traffic, and excitation due to out-of-balance rotating machinery were explicitly excluded from these guidelines. Various methods of calculating natural frequencies were presented and the presence of closely spaced modes of vibration noted. Four methods of computing the fundamental natural frequency of the floor were outlined. These ranged in complexity from estimating the stiffness of the floor using the static deflection at mid-span, through to the use of a dynamic analysis computer program (possibly even FE analysis).

For assessment of the floor response, two methods were proposed depending on whether the floor was classed as a 'low frequency floor' (fundamental natural frequency lower than 7 Hz) or a 'high frequency floor' (fundamental natural frequency greater than 7 Hz). The low frequency response was assumed to be mostly due to resonance, and

the high frequency response was assumed to be due to a series of impulsive heel impacts, each considered as separate transient events.

The suggested damping values of up to 4.5% of critical (for a floor with partitions) were lower than those specified in previous literature, but they are now considered still to be higher than appropriate (ISO, 1992).

2.1.2.3 Further North American Research in the 1990s

In the 1990s, there was a general acceptance that walking is a periodic function and that low frequency floors could be excited in resonance by multiples (harmonics) of the pedestrian pacing rate (walking frequency). The already discussed SCI guidelines had presented a means of considering this phenomenon. However, new guidelines were subsequently developed by Allen and Murray which considered the resonance condition.

Allen (1990) outlined two modelling techniques for floors subjected to rhythmic loading based upon either a SDOF model or a simple beam model (first mode only). He maintained that:

“... there are many modes, but for practical problems where resonance is involved, this assumption [fundamental mode only] is generally close enough”.

However, more recent has shown that this is not necessarily true (Eriksson, 1994; Pavic, 1999).

Murray and Allen proposed a new criterion in 1993 which was based on acceleration limits from ISO 10137 (ISO, 1992), a time domain loading function based on four harmonics of the pacing frequency, and a response function (structural model) based on the fundamental mode of vibration only. In two papers from this year (Allen & Murray, 1993; Murray & Allen, 1993), they acknowledged that resonance of long span floors could occur due to walking excitation. The overestimation of damping ratios from heel impact tests was also acknowledged and the authors suggested, in a rather arbitrary manner, that modal damping ratios for calculation of response should be approximately half of those estimated from heel impact tests.

2.1.3 Vibrations of Long-span Reinforced and Post-Tensioned Concrete Floors

Reinforced concrete floor structures have historically not been a problem as far as vibration serviceability is concerned, due to having a much greater mass and stiffness than their composite counterparts. However, through the use of technologies such as high strength concrete and prestressing, these types of structures are becoming ever more slender as designers strive for increased spans and reduced slab thicknesses (Eriksson, 1994; Pavic, 1999). As a result, problems with the vibration serviceability of such structures may be expected. Therefore, it is becoming necessary for the designers of such structures to consider vibration serviceability at the design stage.

2.1.3.1 Dynamic Behaviour of Long-Span Concrete Floors

Long-span concrete floors typically have greater mass than their composite counterparts, resulting in typically lower natural frequencies (Eriksson, 1994). As such, they are frequently classed as 'low-frequency floors'. When considering pedestrian excitation, vibration problems in these floors are more likely to be caused by excitation of resonance than by impulsive excitation caused by individual footfalls (Eriksson, 1994; Wyatt, 1989).

Unfortunately, the lack of problems in the past with the vibration serviceability of long-span concrete floors has led to a corresponding lack of research interest in the field. Consequently, many of the guidelines which have been reviewed in this Chapter have been aimed at composite floors and therefore have limited applicability to long-span concrete floors.

However, two notable works into the vibration of long-span concrete floors are mentioned here. Firstly, in his doctoral thesis, Khan (1996) investigated the reliability of various analytical methods for prediction of the fundamental natural frequencies of floors by comparing the analytical predictions with values obtained from testing. This work was performed on the assumption that controlling the fundamental natural frequency of a floor is the "best way" to ensure satisfactory vibration serviceability performance. This is questionable. It is now widely recognised (Khan & Williams, 1995; Bachmann et al., 1995; Eriksson, 1996) that vibration serviceability should be assessed through examination of vibration response and that controlling the fundamental natural frequency may result in uneconomic designs for relatively heavy long-span modern

concrete floors. This is particularly so when the floors are prestressed. Another observation regarding this thesis is the very poor quality of the modal test results. The magnitude and phase of a typical frequency response function measurement presented by Khan (1996) is shown in Figure 2.5. It is difficult to understand how the reported fundamental frequency of 4.6 Hz and damping ratio of 3.4% were estimated from this measurement and others like it.

Secondly, Pavic (1999) recently carried out modal testing, FE analysis and FE model correlation and updating of a number of long-span reinforced and prestressed floors. Through this process, he identified a number of parameters which affect significantly the vibration behaviour of such floors which are not currently considered carefully enough in normal civil engineering practice. Probably the most important observation was that in-situ cast columns, which are rigidly connected to the floor which they are supporting, significantly increase the bending stiffness of the floor. This is contrary to normal design practice (Concrete Society, 1994) in which such supports are commonly considered as pin supports.

2.1.3.2 Concrete Society Technical Report No. 43

Pavic's work was initiated by the publication of Concrete Society Technical Report No. 43 (Concrete Society, 1994) entitled 'Post-tensioned Concrete Floors - Design Handbook' in 1994. The aim of this report was to aid the practical day to day design of long-span post-tensioned concrete floors. Appendix G of the report gives a procedure for checking the vibration serviceability of long-span post-tensioned concrete floors at the design stage. It is of particular importance as it is the most recent and comprehensive design guidance document in the UK covering the vibration of post-tensioned concrete floors.

Pavic (1999) presented a deconstruction of the guidelines, illustrating numerous assumptions which were made in order to simplify the vibration serviceability problem for post-tensioned concrete floors. It was found that the guidelines were produced without any experimental verification and they have proven to be unreliable and frequently overconservative for most normal post-tensioned concrete floor structures (Williams and Waldron, 1994; Pavic et al, 1998b; Pavic, 1999). As a direct result of this, the market competitiveness of post-tensioned floors designed using these guidelines has been reduced and there is an immediate requirement for improved design guidelines (Pavic, 1999).

2.1.4 Experimental Modal Analysis (EMA) of Floors

Experimental modal analysis (also called modal testing) is described by Ewins (1995) as:

“... the processes involved in testing components or structures with the objective of obtaining a mathematical description of their dynamic or vibration behaviour”.

This mathematical description normally consists of the natural frequencies, mode shapes and modal damping ratios. Modal testing has traditionally been used by mechanical and aeronautical engineers to design relatively small structures and components through prototyping. More recently, it has been increasingly used as a means of validating FE models of such structures, hence reducing the number of prototypes required. A more detailed explanation of the theory of experimental modal analysis is given in Chapter 3 of this thesis.

The application of experimental modal analysis of civil engineering structures is relatively new. The sheer size of civil engineering structures, combined with technical problems such as the very low responses to be measured in the presence of a great deal of environmental noise, means that sensitive instrumentation and complex signal processing techniques are required (Pavic, 1999). These have not been available until the last few years.

2.1.4.1 Operating Deflection Shapes (ODS) Analysis

The first attempts at experimental modal analysis of civil engineering structures were performed by measuring only the response of the structure due to unmeasured excitation. By examining the ratios of amplitudes of response at various points on the structures, and the phase differences between these points, the natural frequencies and so-called ‘mode shapes’ could be estimated. Since the excitation is not measured in this technique, it is not theoretically possible to completely decouple multiple modes of vibration and the ‘mode shapes’ measured are in fact ‘operating deflection shapes’ which contain contributions from all modes of vibration (Spectral Dynamics, 1994). However, near a resonant frequency, for a system with well separated modes of vibration, an operating deflection shape is a close approximation to a mode shape.

This form of testing was applied to floor structures by Rainer & Swallow (1986) and by Pernica (1987). A reasonable degree of success was achieved and the testing enabled a fairly accurate assessment of the natural frequencies and mode shapes to be determined. However, in both cases, damping ratios were estimated by using the half-power bandwidth method, which, as has already been explained, possibly resulted in overestimation of modal damping ratios.

2.1.4.2 'True' Experimental Modal Analysis

Osborne & Ellis (1990) reported the results of tests on a composite steel-concrete floor in which they presented a "response spectrum" that was created by:

"... converting the measured accelerations to equivalent displacements and then dividing the displacement by the applied force".

In modal testing terms, such a plot is actually called a frequency response function (FRF) and is commonly the basis for single- and multi-degree-of-freedom curve fits which are used to determine the modal properties (natural frequencies, mode shapes and modal damping ratios) of structural systems. They calculated the modal properties of the first two modes of vibration by fitting a "best fit theoretical curve" to the measured FRF, but they did not state the assumed analytical model for that theoretical curve. One point worthy of comment regarding this work is that the modal damping values were about 1%, which is significantly lower than those values reported in much of the literature prior to the 1990s.

In his doctoral thesis, Eriksson (1994) considered the problem of the vibration of low-frequency floors. He used experimental modal analysis as a tool to determine the modal properties of the structures that he was examining (concrete and composite steel-concrete floors with natural frequencies lower than 8 Hz). Excitation was applied using a custom built impactor for the majority of the tests, although a grounded electrodynamic shaker was used on one occasion. The floor response was measured using accelerometers and both the excitation and response signals were processed by a dual channel spectrum analyser. Although some success was achieved, the relative crudity of the test equipment and data processing techniques limited the reliability of the experimental data.

Caetano and Cunha (1993) also describe a modal testing facility which they set up for the testing of various sizes of civil engineering structures. The exciters they described,

in order of applicability to increasing structure sizes, were an instrumented hammer, an electrodynamic shaker and a rotating eccentric mass shaker. In this paper, they also presented a case study of the modal testing applied to a $6.6 \text{ m} \times 6.6 \text{ m}$ reinforced concrete roof plate for which they managed to determine its natural frequencies, mode shapes and modal damping ratios. Interestingly, in addition to SDOF peak-picking and circle fit modal parameter estimation methods, they also applied an MDOF parameter estimation algorithm based on the Rational Fraction Polynomial (RFP) method (Richardson & Formenti, 1985). According to the writers, this technique was simpler to apply and provided better quality estimates of modal parameters than the peak-picking method, an observation which would be expected for this more advanced modal parameter estimation technique.

One of the most comprehensive applications of modal testing technology applied to civil engineering structures, in terms of testing and analysis procedures, was performed by Pavic (1999). He successfully tested a number of structures, applied complex MDOF modal parameter estimation techniques and performed quite complex model correlation and 'manual' model updating to FE models of the same structures. Due to financial constraints however, the only exciter used in this work was an instrumented impact hammer. Probably because of this, the writer described some difficulties in the testing and modal parameter estimation phases of the work, particularly related to complexity of mode shapes. It is likely that by applying these advanced procedures and methods, using an improved method of excitation such as an electrodynamic shaker, it would be possible to obtain more accurate and consistent modal test data.

2.2 Prediction and Assessment of Vibration Serviceability

The problem of the prediction and assessment of the vibration serviceability of structures may be conveniently broken down into three parts. These are described by ISO 10137 *Bases for design of structures - Serviceability of buildings against vibration* (ISO, 1992) as:

1. the "vibration source",
2. the "transmission path", and
3. the "receiver".

Each of these parts is of equal importance to the overall vibration serviceability problem and there has been much research work in these separate areas. Integrated methods, such as proposed in the CSA guidelines, which do not consider these three components separately, are now considered to be obsolete. This is because inaccuracies in, say, the vibration source modelling have tended to be masked by inaccuracies in, say, the modelling of the transmission path. As a result, these methods may only be utilised in the manner in which the writers intended, and separate items from them considering vibration source, path and receiver, should not be used in isolation (Wyatt, 1989). It has also been suggested that there is no point in developing accurate models of vibration source when the acceptable limits are so uncertain. Such a philosophy cannot be justified since improvements in all aspects of the vibration serviceability problem are being made through continuing research (Pavic, 1999).

2.2.1 The Vibration Source

Vibrations in buildings can have a wide variety of causes. These can conveniently be broken down into 'external' and 'internal' vibration sources.

2.2.1.1 External Vibration Sources

Vibrations due to external sources are normally transmitted to the building through an adjoining medium such as the ground, air or water. ISO 10137 (ISO, 1992) gives the following examples:

- Construction, mining or quarry blasting;
- Construction activity (pile driving, compaction, excavation, etc.);
- Road and rail traffic;
- Sonic boom or air blast;
- Fluid flow (wind or water);
- Punching presses or other machinery in nearby buildings;
- Impact of ships on nearby wharves.

Problems with vibrations caused by external sources are generally best treated by isolating the building as a whole (Wyatt & Dier, 1989). However, this is beyond the scope of this thesis and will not be discussed further.

2.2.1.2 Internal Vibration Sources

ISO 10137 also quotes the following examples for internal vibration sources:

- Human excitation;
- Rotating and reciprocating machinery;
- Impact machinery (punches, presses, etc.);
- Moving machinery (trolleys, lift trucks, elevators, conveyors, overhead cranes, etc.);
- Construction or demolition activity in adjoining parts of the building.

Mechanical excitation is generally tackled at source by reduction of out-of-balance or through the use of vibration-isolation mountings for the machine (Wyatt, 1989). Also, excitation due to construction or demolition activities tends to be temporary and case specific. Therefore, such dynamic actions also will not be considered further in this thesis.

Eriksson (1994; 1996) suggested that the owner should specify the intended use of a structure at the design stage so that reasonable dynamic service actions can be considered. He suggested a set of “service action classes” as follows:

- A1. Light domestic type activity;
- A2. Intermittent pedestrian traffic (e.g. office corridor);
- A3. Public pedestrian traffic and light machine installations;
- A4. Crowded open space or mall areas without vehicle traffic;
- A5. Open space areas with vehicle traffic and pedestrians;
- A6. Medium machine installations and vehicle traffic;
- A7. Dance halls and gymnasia;
- A8. Assembly areas for concerts or sports events;
- A9. Heavy machine installations and vehicle traffic.

For the types of buildings considered in this thesis, service action class A2 is obviously applicable. The loading case suggested for this class by Eriksson (1996) was “one person treading in place”. He also suggested a return period for application of this forcing function which is important if vibrations are to be assessed using a “vibration dose” approach (see Section 2.2.4.4).

2.2.2 Modelling the Walking Forcing Function

2.2.2.1 Time Domain Models of the Walking Forcing Function

Many researchers measured time histories of the load applied to the ground by a pedestrian. Harper et al. (1961) measured single step time histories during a study into the abrasion resistance of floor surfaces. Galbraith & Barton (1970) performed similar measurements whilst investigating the feasibility of seismic intruder detection systems. Due to the nature of these works, forcing functions for calculation of structural vibrations were not developed. The time histories presented in these works exhibited the characteristic double peak forcing pattern (Figure 2.6) corresponding to heel strike and toe lift-off. Galbraith & Barton (1970) concluded that the shape of this forcing function was primarily dependent upon the pedestrian weight and the pacing rate. It was found that as the pacing rate increases, the two peaks merge together and the amplitude increases. An important distinction between walking and running is that running occurs when there is a distinct period between footfalls when the pedestrian has no contact with the structure. This is as opposed to walking in which the pedestrian is always in contact with the floor surface. These works also showed that factors such as footwear type and floor surface were of only secondary importance.

The first step towards the production of a continuous time domain forcing function was its modelling as a single sinusoid. In a study of footbridge loading, Blanchard et al. (1977) suggested that a sinusoid with a peak magnitude of 180 N should be used to model the human-induced walking excitation. The magnitude of the force was reduced between 4 and 5 Hz to take account of the reduction of excitation in this range. Finally, it was deemed that bridges with natural frequencies above 5 Hz were "too difficult to excite" and would therefore be acceptable. These guidelines were later incorporated into the UK bridge design code BS 5400 Part 2 (BSI, 1978).

However, many researchers (Matsumoto et al., 1978; Ohlsson, 1982; Tilly et al., 1984; Ellingwood, 1989) presented data which showed that walking excitation is near-periodic containing significant components at multiple harmonics of the pacing rate. This was studied in detail by Rainer et al. (1988) and Rainer & Pernica (1986) who measured time histories of walking forcing functions of pedestrians traversing a 17 m long platform. By performing a Fourier analysis on the forcing function time histories, they determined the magnitude of the components at the first four harmonics of the pacing rate. Using these

“Fourier amplitude coefficients”, an analytical forcing function could be represented by (Rainer et al., 1988):

$$F(t) = P \left(1 + \sum_{n=1}^N \alpha_n \sin(n2\pi f_p t + \phi_n) \right) \quad \text{Equation 2.1}$$

where P is the static weight of person, α_n is the Fourier amplitude of the n^{th} harmonic coefficient, n is a positive integer, f_p is the footstep rate in steps per second, t is time, ϕ_n is the relative phase angle of the n^{th} harmonic and N is the total number of harmonics taken into account.

Various researchers have attempted to determine reasonable values for the coefficients, α_n , with either the first three or the first four harmonics being considered (Rainer et al., 1988; Rainer & Pernica, 1986; Wyatt, 1989). Bachmann et al. (1995) presented quite a comprehensive list of Fourier coefficients for various human activities, including walking, which had been compiled from a number of previous works. Slightly different values for the Fourier coefficients were also presented in ISO 10137.

This form of analytical forcing function is normally applied to a model by adjusting the pacing frequency f_p , so that one of its harmonics coincides with a natural frequency of the structure. The fundamental mode is normally selected although other modes may be selected if they represent a more onerous condition. A problem with this method of application is that a perfect resonance condition is assumed resulting in an upper bound for the predicted response. In practice, it is not possible for a pedestrian to maintain such a perfect pacing rate, even under controlled conditions, and a ‘near resonance’ condition is usually achieved. For a lightly damped structural system this typically results in a large reduction in overall response (Pavic, 1999).

2.2.2.2 Frequency Domain Models of the Walking Forcing Function

Frequency domain forcing functions have the advantage that they are often simpler and less computationally expensive to analyse (Eriksson, 1994). For this reason, several researchers have presented frequency domain forcing functions for human excitation.

Ohlsson (1982) calculated the spectrum of an artificial time domain signal constructed by ‘artificially’ adding four single footfall pulses together with a delay representing the pacing rate. However, the very poor frequency resolution ($\Delta f = 1.57$ Hz) of the calculated Fourier transform resulted in a frequency domain forcing function which was

only valid between 6 Hz and 50 Hz. This was intended to be used for higher frequency timber floors and is of little use for the low frequency floors considered in this thesis.

Eriksson & Ohlsson (1988) and Eriksson (1994; 1996) suggested frequency domain force models which were based upon measurements made on a purpose-built walking platform. These models were developed from an envelope of force auto-spectral densities (ASDs) calculated from a back analysis of response ASDs measured on a structure with known modal properties. However, these force models were intended for application of SDOF models of floor structures using the fundamental mode only. As such, they tend to overestimate the magnitude of the response of floor structures when there are close modes to the fundamental, which is a more realistic scenario. This most significant weakness of the excitation model was illustrated in an extensive study performed by Pavic (1999).

One significant limitation of frequency domain models of walking is the inherent assumption of steady-state vibration. The time taken for the floor response to build up to a full resonance or near resonance condition can be significant (over ten seconds), resulting in a lower overall vibration level than if steady-state conditions are assumed. This phenomenon can only be modelled using time domain analysis methods although it may be possible to consider these effects through the application of dimensionless load factors.

2.2.2.3 Indirect Modelling of the Walking Forcing Function

In order to simplify methods of assessing the vibration serviceability of structures at both the design stage and after construction, Lenzen & Murray (1969) proposed the already mentioned heel-drop test, the results of which were supposed to give an indication of likely vibration levels caused by walking excitation. In reality, it is unlikely that this is true since both the magnitude and duration of this form of dynamic loading is very different from walking and it is likely that the apparent early 'success' of this method was due to it being 'tuned' to the type of floors for which it was developed (i.e. composite steel-concrete).

2.2.2.4 Application of the Walking Forcing Functions to Analytical Models of Structures

An important feature of real walking loads is that they are not stationary in space. Only the most sophisticated analysis techniques (such as time domain FE analyses) are capable of considering this loading characteristic. As a result of this, walking forcing functions are frequently assumed to act at a single point on the structure, normally that which gives the highest response to the dynamic loading. Indeed, the suggested loading case for the aforementioned dynamic service action class A2 (Eriksson, 1996) is a “single person treading in place”. Eriksson suggested that this simplification would not result in a severe loss of accuracy, although Mouring & Ellingwood (1993) reported an overestimation of calculated peak acceleration of 28% for stationary excitation compared with that calculated for an equivalent moving excitation.

This was studied in detail by Pavic (1999) who applied three walking forcing functions to FE models of structures that had also been dynamically tested. The performance of these walking forcing functions was assessed when they were applied both stationary and moving. He found that the most reliable model for walking excitation was that proposed by Eriksson (1994) when applied as a stationary dynamic load, as it had been intended. However, Pavic also concluded that relatively large overestimation errors were apparent and that this should be remedied, in part, through the development of a walking force model which would take account of the movement of the pedestrian.

2.2.3 The Transmission Path

In the context of a vibration serviceability analysis or assessment, the transmission path is defined as the path through which vibration energy is transferred from the vibration source to the receiver. For vibrations in buildings, the transmission path is most frequently assumed to comprise the building structure itself. However, ISO 10137 (ISO, 1992) gives the following more comprehensive range of examples of transmission path:

- Ground, air, or water;
- Structural components (foundations, floors, columns, walls, etc.);
- Non-structural components (pipes, partitions, etc.).

Since external sources of vibration will not be considered in this thesis, consideration of the transmission path will be restricted to those elements that exist within buildings, i.e. structural components and non-structural elements which are attached to the building

structure. Literature describing the modelling of structural components and systems will be reviewed in this section, and literature describing the effects of non-structural elements will be reviewed in Section 2.3.

2.2.3.1 Simplified Structural Models for Vibration Analysis

Much of the past research into the vibration serviceability of floors has attempted to formulate simplified models to represent the behaviour of the structure. The clear motive behind this trend has been to establish design and assessment guidelines that can be readily applied by design practitioners who are unlikely to have a thorough knowledge of structural dynamics. However, these simplified methods have been shown to be inaccurate at best, and completely incorrect at worst (Murray, 1981; Wyatt, 1989; Pavic, 1999). Some of these simplified methods will be outlined here.

The most basic structural dynamic model is an equivalent SDOF system that can be represented by the classical mass-spring-damper arrangement in Figure 2.7. In order to apply this model to real structures, it is necessary to determine an equivalent stiffness and mass, and to assume a meaningful damping ratio. This simplification has been strongly advocated by researchers in North America and there are many papers outlining methods by which the mass and stiffness of the system may be evaluated (Lenzen, 1966; Allen, 1974; Murray, 1985; Allen, 1990; Allen and Murray, 1993).

Wyatt (1989) suggested other simplified methods for practical evaluation of natural frequencies:

- From a global estimate of the self-weight deflection;
- From a combination of component frequencies estimated from self-weight deflection or tabulated frequency formulae;
- By iterative application of static analysis, using common static analysis software at the desk-top PC.

2.2.3.2 State-of-the-art Dynamic Analysis of Structures

Without doubt, the current state-of-the-art in the analytical determination of the modal properties of structures is through the use of FE analysis. Unlike most simplified methods of determining the dynamic properties of structures, the use of FE analysis facilitates easy calculation of modes of vibration higher than the fundamental. It also allows the multi-mode response of a floor structure to be calculated for highly complex

loading scenarios, of which the spatially and temporally varying walking load is a prime example.

2.2.3.3 Experimental Determination of Structural Dynamic Properties

For existing structures, it is possible to determine the transmission path characteristics using experimental modal analysis as described in Section 2.1.4 of this thesis. This has the major advantage that structural idealisation inaccuracies regarding the modelling of mass, stiffness and damping do not exist and the measured structural dynamic properties reflect the real structure. However, this experimental method has the obvious disadvantage that it can only be performed on already built structures and therefore it is difficult to apply it at the design stage.

2.2.4 The Receiver

The receiver is defined in ISO 10137 (ISO, 1992) as the “person, structure or equipment subjected to vibrations”. Vibrations typically cause annoyance to occupants long before reaching levels at which structural damage can occur (Wyatt, 1989) and for this reason, structural damage will not be considered further in this thesis. Damage to or malfunctioning of sensitive equipment (e.g. high precision optical and micro-assembly equipment) is also considered to be a problem (Ungar & White, 1979; Ohlsson, 1988). However, items of equipment typically encountered in office buildings (e.g. personal computers, photocopiers, etc.) are generally robust enough not to be affected by low level vibrations up to the levels which are likely to cause annoyance to occupants (Waller, 1969). Therefore, for the purposes of this research, the limiting vibrational response of offices will be assumed to be dictated by the annoyance threshold of the human occupants.

2.2.4.1 Human Perception of Vibrations

Prior to embarking on a summary of the available literature into the subject of human perception of vibrations, it is necessary to highlight the difference between local vibration and whole-body vibration. Griffin (1996) defined them as follows:

“Whole-body vibration occurs when the body is supported on a surface which is vibrating. *Local vibration* occurs when one or more limbs (or the head) are in contact with a vibrating surface.”

He also quotes three principal possibilities for whole-body vibration to occur: sitting on a vibrating seat, standing on a vibrating floor, or lying on a vibrating bed. Therefore, references relating to whole-body vibration are pertinent to this research.

One of the first studies into the human perception of whole-body vibrations was published by Reiher and Meister in 1931 (Wright & Green, 1959). They subjected ten people of varying ages to sinusoidal excitation at various frequencies and amplitudes. The subjects were then required to rate the vibration as just perceptible, definitely perceptible, annoying, unpleasant and exceedingly unpleasant. This enabled them to compile the graph shown in Figure 2.8, which showed that the perception threshold was dependent on vibration velocity between 5 and 60 Hz (Griffin, 1996).

In 1948, Goldman produced an excellent report that summarised the results of a number of previous research efforts, including the work by Reiher and Meister. He recognised a number of problems concerning the measurement of human vibrations that are still encountered by researchers today. The first of these was that researchers tended to use different experimental conditions (such as position of subject, direction of motion, frequency range and duration of exposure) which were not always clearly outlined in their publications. Such uncertainties bring the repeatability of presented results into question and this was the reason for Griffin (1996) to state that:

“... the full and careful reporting of research studies is vital to the subsequent interpretation and application of the findings”.

Another problem reported by Goldman (1948) was that there was no consistency in terminology used by different researchers. For example, the interpretation of the difference between ‘definitely perceptible’ and ‘annoying’ (used by Reiher & Meister) is almost certain to be different for different subjects. In addition, the works examined by Goldman were intended for different fields of application, hence complicating the interpretation of the results. For example, vibrations that would be acceptable for, say, passengers in aircraft are likely to be completely unacceptable for building structures.

Goldman also recognised a significant limitation of the experimental work performed at that time. This was that the vibration to which subjects were exposed was single

frequency sinusoidal motion. In normal situations, humans are rarely exposed to such vibrations and it is more normal for 'real' vibration to exhibit complex multi-frequency characteristics. Due to the inherent difficulties in studying the effects of complex vibrations, single frequency techniques were the sole method used right up until the 1960's (Griffin, 1996).

In recognition of the complex nature of vibrations to which humans are exposed, a number of methods have been developed which allow the effects of complex vibration to be assessed. These can be broadly divided into two classifications (Griffin, 1996):

- *Rating methods* are methods in which only the worst component of vibration is assessed.
- *Weighting methods* are methods in which the complex vibration is weighted according to differences in human response to vibrations at different frequencies. The frequency weighted complex vibration is then summed in some manner (e.g. RMS) resulting in a single quantity that may be used for assessment.

Weighting methods are now widely considered to be more appropriate than rating methods (Griffin, 1996).

2.2.4.2 Variability of Human Perception to Vibrations

Past studies into the human response to vibration have determined that there is a massive variability in quantities determined for the magnitude of the threshold of perception of vibration, and for the magnitudes of the various comfort criteria. This has been noticed for different individuals (inter-subject variability) and for the same individual at different times (intra-subject variability). Table 2.1, reproduced from Griffin (1996), illustrates the large number of factors that may affect how a person perceives vibrations.

As a result of the very large differences in results which may be expected, it is necessary that any specified criteria for perceptibility or comfort limits are based on the responses of a large number of people followed by a proper statistical analysis (Griffin, 1996). However, it is only in recent years that such statistical analyses have been regularly performed and criteria such as the highly referenced Reiher and Meister criteria from 1931, in which no such statistical analysis was performed, must be viewed with caution.

Table 2.1: Some Sources of Inter- and Intra-Subject Variability

Inter-Subject Variability	Intra-Subject Variability
Body dynamics	Body dynamics
Body dimensions	Body posture
Body masses	Age
Body posture	Health
Age	Experience and training
Gender	Attitude and motivation
Health	Sensitivity and susceptibility
Experience and training	
Attitude and motivation	
Sensitivity and susceptibility	

2.2.4.3 Human Response to Building Vibrations

In many environments humans are willing to tolerate, and indeed expect the presence of vibrations. For example, certain vibrations in ships can be associated with the engines and, paradoxically, the cessation of such vibrations can cause alarm to passengers (Guignard, 1971). However, most occupants of buildings do not expect the structures to be able to move and are therefore willing to tolerate little or no vibration at all. In fact, Steffens (1974) stated that people in buildings will “tend to overestimate the magnitudes of vibratory movements”.

It is therefore clear that much of the concern of occupants of buildings that vibrate, who typically are ignorant of structural engineering, is caused by a fear of collapse, even though there is little chance of this actually happening. Parsons and Griffin (1988) reported that “if the vibration exceeds the perception threshold the disturbance produced by the vibration may become more dependent on vibration frequency”. This implies that there is a certain range of frequencies which cause building occupants to worry about building collapse. Guignard’s (1971) observation that “high frequencies are not as a rule associated with major structural responses indicative of possible danger” points out that it is low frequencies which are most important in terms of building vibration serviceability.

The duration of vibrations is also important for floor vibration serviceability assessment. This is clear from the early work performed by Lenzen (1966), who as already mentioned proposed that the Reiher-Meister criteria from 1931 should be multiplied by a

factor of 10 to take account of the transient nature of floor vibrations. However, a more state-of-the-art approach proposed by Eriksson (1994) is to determine the number of vibration events in accordance with the dynamic service action classes listed in Section 2.2.1.2, and use a vibration dose approach such as that specified in ISO 2631 (ISO, 1997).

2.2.4.4 Current Relevant Codes of Practice and Guidelines

There are numerous codes of practice around the world which are concerned with the assessment of whole-body vibrations. Many of the more important ones were outlined by Griffin (1996) and will not be covered here. However, the following codes of practice have been adopted for the assessment of vibration serviceability performance of floors in this research:

1. ISO 2631:1997 *Mechanical vibration and shock - Evaluation of human exposure to whole-body vibration - Part 1: General requirements* (ISO, 1997), and
2. BS 6472:1992 *Guide to evaluation of human exposure to vibration in buildings (1 Hz to 80 Hz)* (BSI, 1992).

ISO 2631:1997 gives recommendations for the measurement of whole-body vibrations, which are, of course, applicable to the measurement of vibrations on floors. In order to perform a vibration serviceability assessment, it recommends that the following procedure is followed:

1. vibration responses are measured at point of entry to the body,
2. a basic evaluation of weighted root-mean-square acceleration should be performed (using the frequency weighting curves specified in the code), and
3. if it is possible that the basic evaluation will underestimate the effects of vibration (high crest factors, occasional shocks, transient vibration), the running RMS and/or the vibration dose value methods of evaluation should be applied.

Whilst ISO 2631:1997 specifies methods for measurement and evaluation of whole-body vibrations, it does not specify any limits to be applied in accordance with these evaluations. For this purpose, it is necessary to utilise BS 6472:1992 which is the relevant UK code of practice which specifies vibration serviceability limits for building floors.

2.3 The Effects of Non-Structural Elements on the Vibration Characteristics of Floors

All practical office floor structures are likely to contain one or more non-structural elements such as partition walls (part- or full-height), access floors, suspended ceilings, electrical and mechanical services and finishes. However, whilst it has been recognised for a long time that such non-structural elements can significantly affect the vibration performance of a floor structure, quantification of this phenomenon has been quite arbitrary and supported with very little systematic research in the past.

2.3.1 The Use of Non-Structural Elements in the Analysis of Vibration Serviceability

It is interesting to discuss whether the effects of non-structural elements should be utilised in design in vibration serviceability analyses. Indeed, whilst Ohlsson (1988) stated that partitions and other non-structural components can make the difference between acceptable and unacceptable vibration response, he also stressed that:

“... it is the author's opinion that the serviceability limit state design should not rely upon ‘non load-bearing’ components (...) [as they] may be removed any day by the user.”

However, the writer disagrees with this opinion. Whilst partition walls may be removed at any time, it is unlikely that other non-structural elements such as services, suspended ceilings and access floors would be completely and permanently removed during the useable life of a building. Therefore, it is perfectly reasonable to make an appropriate allowance for the effects of these elements when performing a vibration serviceability analysis during design. Furthermore, Allen & Murray (1993) stated that “the damping ratio depends primarily on non-structural components and furnishings”. Therefore, to base vibration serviceability analyses on damping values measured from bare structures is likely to lead to gross overestimation of structural responses. This opinion is shared by Fahy and Westcott (1978) who stated that “vibration tests on incomplete, unoccupied buildings and isolated components are of little practical value”. Nevertheless, it is also the opinion of the writer that it is important to understand the effects of non-structural elements in greater detail before including them in vibration serviceability analyses. This provides the main rationale for conducting the work presented in this thesis.

2.3.2 Quantification of the Effects of Non-Structural Elements

In the early work on the vibration serviceability of composite floor structures performed at the University of Kansas (Lenzen, 1962; 1966; Lenzen & Murray, 1969), measurements of damping of real structures using the heel-impact method led to the conclusion that non-structural elements increased damping significantly. Some later papers published from research in Canada indicated that realistic damping ratios for composite floors were 3% of critical for a bare floor, 6% for a finished floor and 12% for a finished floor with partitions (Allen, 1974; Allen & Rainer, 1975; 1976). Although it is now recognised that these damping values were inappropriately estimated and are much higher than properly estimated modal damping ratios, these measurements clearly indicated the possibility for a significant effect of non-structural elements on the damping of floor structures. Determination of more realistic changes in modal damping ratios caused by the installation of access floors is one of the aims of the work presented here.

It has also been suggested that some non-structural elements, such as access floors, suspended ceilings and services, may increase the stiffness of floor structures, although only to a limited extent (Osborne & Ellis, 1990; Eriksson, 1994). Partitions, however, can significantly increase the stiffness of floors and even act as supports for low-level vibrations (Pernica, 1987).

2.3.3 The Effects of Access Floors

There are only a handful of papers in the literature which described the possibly beneficial effects of access floors with respect to floor vibrations. Williams & Waldron (1994) presented the results of tests carried out on 14 structures, 4 of which contained access floors. They concluded that floors with access floors were quite heavily damped in comparison with floors without access floors. However, on further examination of some of the work on which Williams and Waldron based their paper (Caverson, 1992) it was determined that the damping values were estimated using the half-power bandwidth method, and it is possible that these larger damping values were caused by the likely presence of modes of vibration of the floors close to the fundamental. Osborne & Ellis (1990) presented the results from vibration tests on a composite steel-concrete floor before and after the addition of an access floor. They did not manage to detect significant changes in modal properties of the floor following the addition of the access

floor, but they did report that the perception of floor vibrations due to footfall loading was considerably reduced, although they did not elaborate on this.

Rainer & Pernica (1981) presented data which demonstrated an increase in damping of a composite floor sample following the addition of a suspended ceiling. They speculated that this was caused by friction between the ceiling panels and the supporting T-sections. Bearing in mind the construction of most access floors (Figure 2.9), and the fact that access floors are significantly heavier than suspended ceilings, it is reasonable to expect that access floors may also exhibit this damping mechanism, possibly to a greater extent than for suspended ceilings. However, there is currently no evidence to support this speculation.

A very recent paper by Williams & Falati (1999) describes a series of tests which were performed on a small slab strip constructed at the University of Oxford, some of which concerned the effects of an access floor system on the dynamic properties of the slab. The slab strip was 5.1 m long by 1.0 m wide by 135 mm deep and two configurations of access floors were considered. Firstly, a single row of 7 panels (600 mm × 600 mm square) was installed on the slab with the panels screwed to the pedestals and the pedestals bonded to the slab. Secondly, two rows of 7 panels were installed on the slab with the panels screwed down at all interior corners and left loose around the perimeter of the slab, to simulate a detail which is sometimes used in normal construction. The finished floor height (i.e. distance between the surface of the slab and the top surface of the access floor) was not given.

In these tests, it was determined that the first configuration resulted in a reduction in natural frequency from the slab's bare state of 1.3% and a modest increase in damping of 9.1%. The second configuration resulted in a reduction in natural frequency of 5.0% and a significant increase in damping of 63.6%. The authors concluded, therefore, that access floors may be designed and utilised in such a way as to increase the damping of floor systems and hence improve their vibration serviceability performance.

However, it is important to note the limitations of this work. Firstly, the half-power bandwidth and logarithmic decrement methods were utilised to determine the modal damping ratios. These methods have been shown typically to overestimate damping. However, because the modes of vibration were well separated for this particular structure, it is unlikely that the damping estimates were adversely affected. A more important limitation is that the slab on which the access floors were tested was very small compared to what might be expected in practice, whilst the access floors were the

same size as would be used in practice. This may have led to an overestimation of the effects of the access floors to a degree which is not possible to quantify. So, whilst these tests clearly indicate a possible benefit of using access floors, the magnitude of the benefit remains uncertain.

It is clear that the limited amount of data which has been collected for access floors to date is inadequate and that further research is required to determine the effects of access floors on the vibration serviceability performance of long-span concrete floors.

2.3.4 Survey of World Authorities

Due to the lack of available literature regarding the effects of non-structural elements on the vibration serviceability performance of floors, it was decided at the start of this research to write to a number of prominent experts around the world in the field of floor vibration. Fourteen letters were sent in total and the response rate was quite good with ten of the recipients responding, as indicated in Table 2.2. However, none of the respondents was aware of any significant past or current research into the effects of non-structural elements. This is yet another confirmation that this is an area which requires additional research of greater depth and better quality than in the past.

Table 2.2: Prominent Experts who were Questioned about the Effects of Non-Structural Elements on the Vibration of Floors.

Name	Institution	Replied ?
Dr D E Allen	National Research Council of Canada	Yes
Dr W J Ammann	ETH Zurich, Switzerland	Yes
Prof. H Bachmann	ETH Zurich, Switzerland	Yes
Dr B R Ellis	Building Research Establishment, UK	Yes
Dr P-E Eriksson	Chalmers University of Technology, Sweden	No
Prof. M J Griffin	University of Southampton, UK	Yes
Prof. E Luz	Universität Stuttgart, Germany	Yes
Dr J Maguire	Lloyd's Register, UK	Yes
Prof. T Murray	Virginia Polytechnic Institute	No
Dr G Pernica	National Research Council of Canada	No
Dr A J Pretlove	University of Reading, UK	Yes

Name	Institution	Replied ?
Dr J H Rainer	National Research Council of Canada	No
Dr J Wallascheck	Technische Hochschule Darmstadt, Germany	Yes
Dr T A Wyatt	Wind Engineering Society, UK	Yes

2.4 Conclusions of the Background Review

This chapter has presented an overview of relevant past research work which has been performed in the area of floor vibration serviceability prediction and assessment. It is clear that, in general, simplified techniques for prediction and assessment of floor vibration serviceability have tended to be inadequate. Therefore a more rigorous treatment of the problem through modern experimental and analytical techniques (such as EMA and FE modelling) is warranted.

In addition, this chapter has examined past literature into the effects of non-structural elements, in particular raised access floors. Whilst many writers have commented on the (possibly beneficial) effects of non-structural elements, there has been very little work on the quantification of this phenomenon. The few results which have been presented have tended to be conflicting and inconclusive.

Therefore, there is a need for the effects of access floors to be investigated and quantified in such a way as to facilitate their inclusion in calculations aimed at predicting floor vibration serviceability. It is this research area, which was outlined in Chapter 1, which will be investigated in the remainder of this thesis.

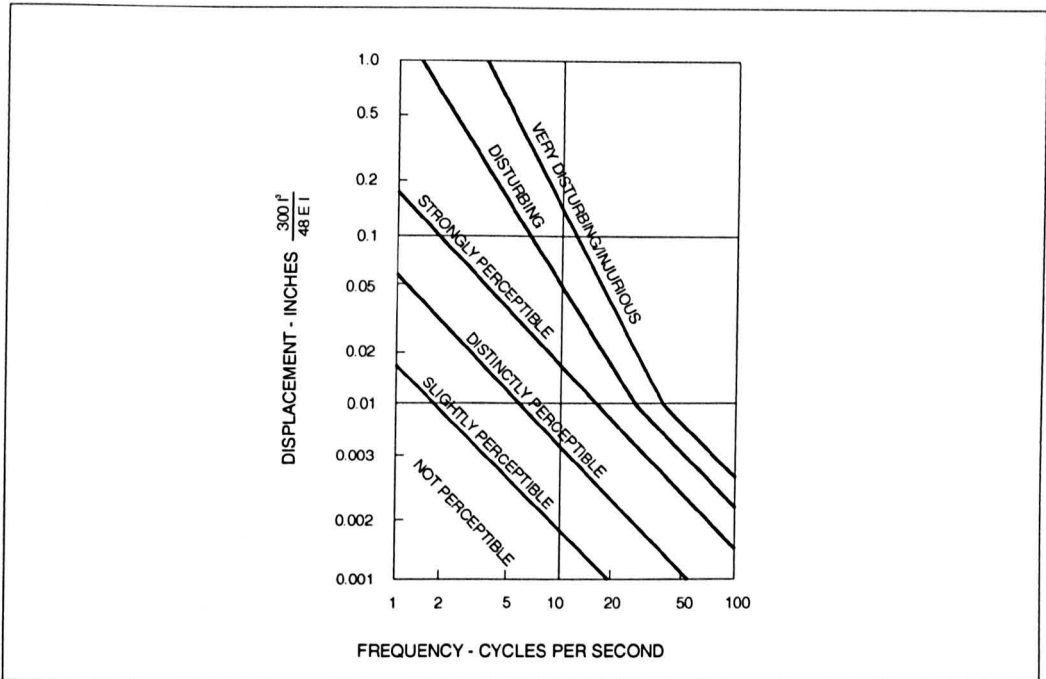


Figure 2.1: Modified Reiher-Meister Criteria (after Lenzen, 1966).

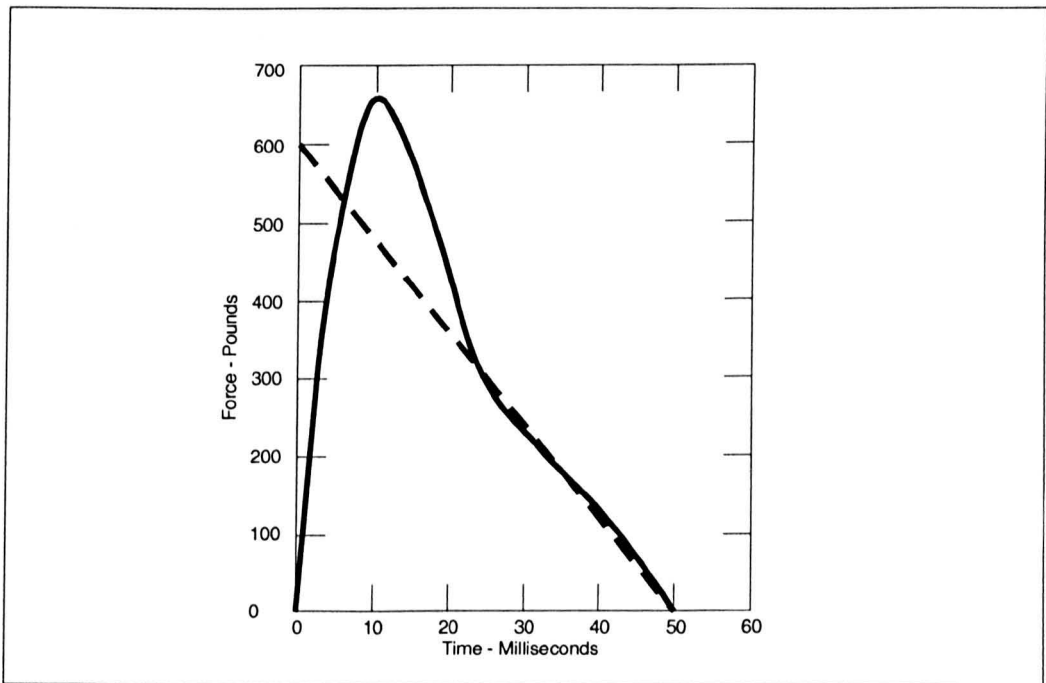


Figure 2.2: Idealised Heel-drop Forcing Function (after Lenzen & Murray, 1969).

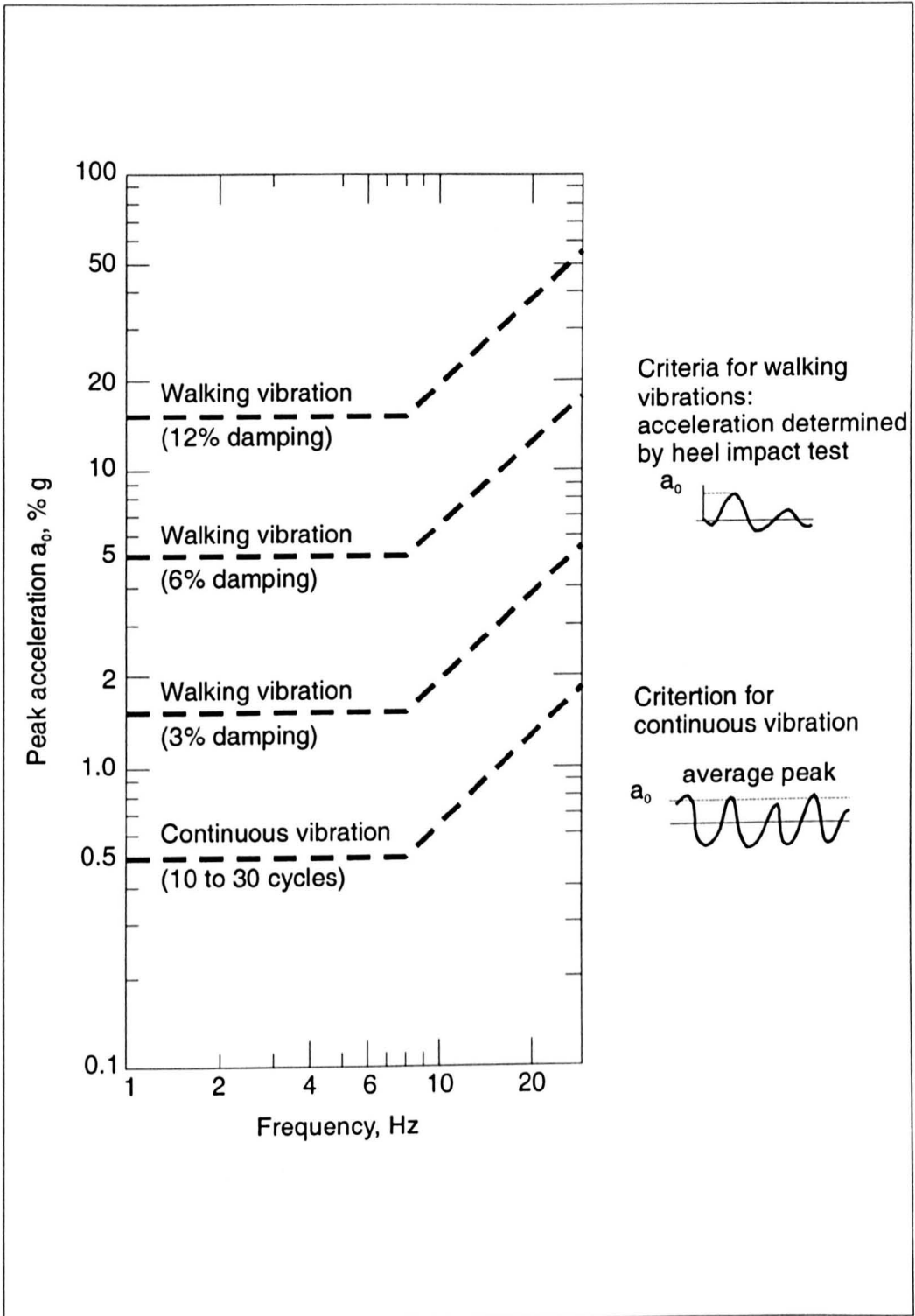


Figure 2.3: Annoyance Criteria for Floor Vibrations (after CSA, 1989).

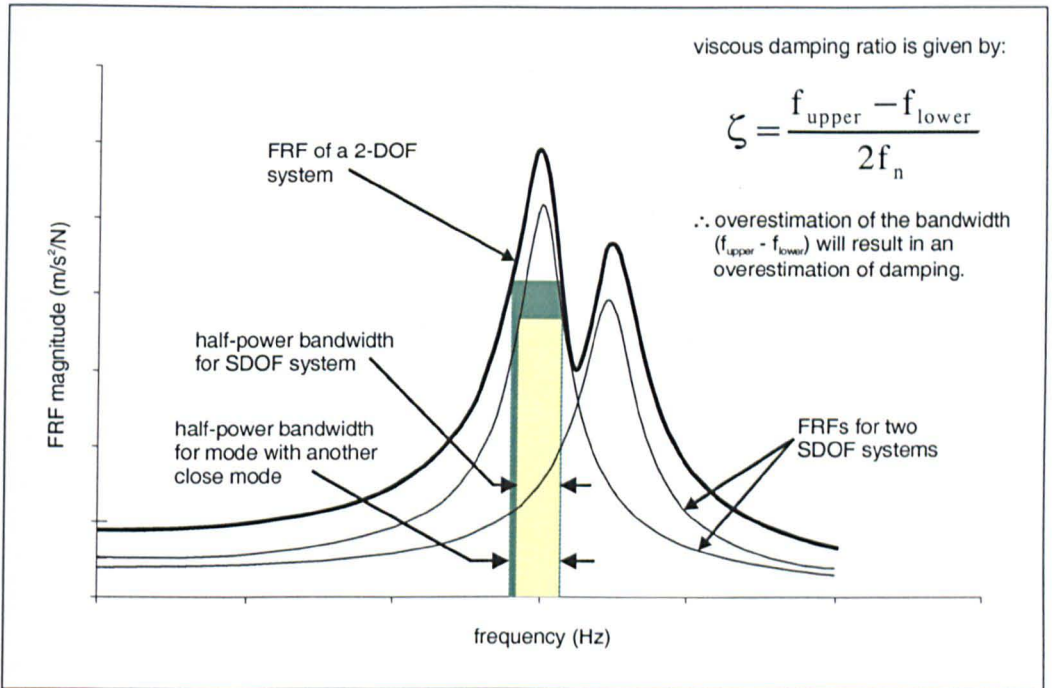


Figure 2.4: Overestimation of Damping When Using the Half-power Bandwidth Method of Estimating Damping for Structures with Close Modes.

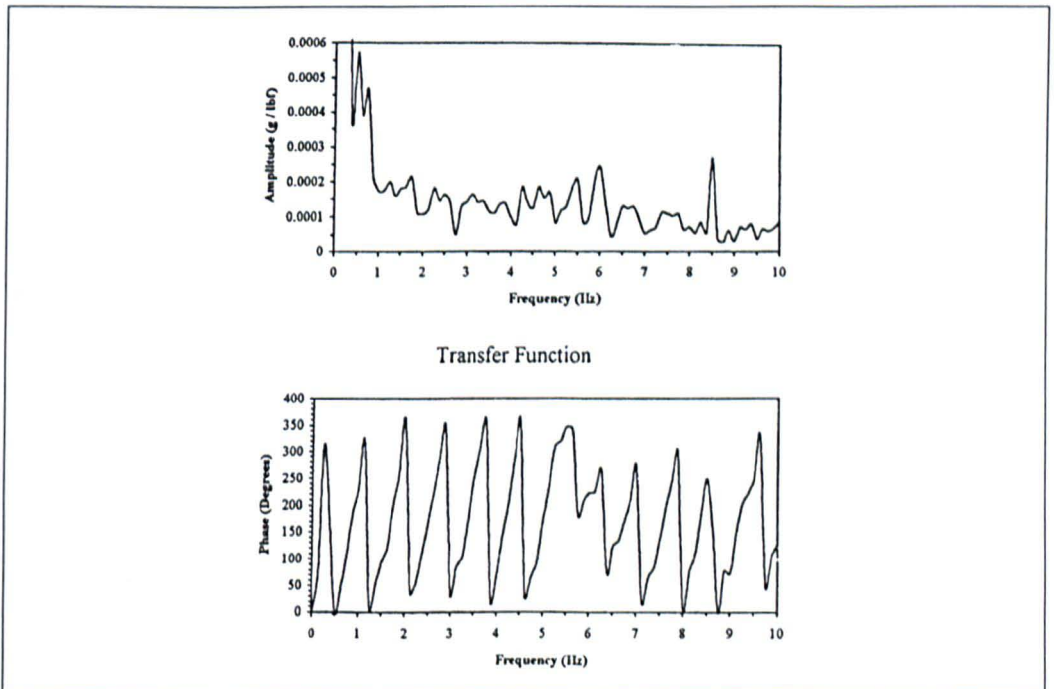


Figure 2.5: Typical FRF Measurement Presented by Khan (1996).

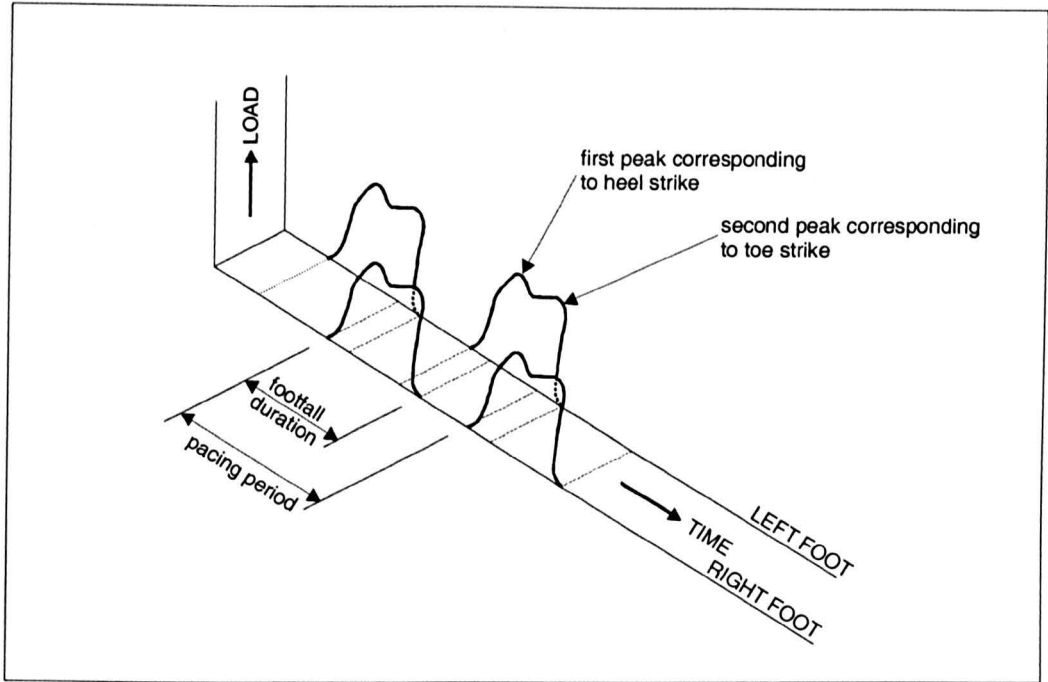


Figure 2.6: Characteristic Double Peak Walking Forcing Function (after Galbraith & Barton, 1970).

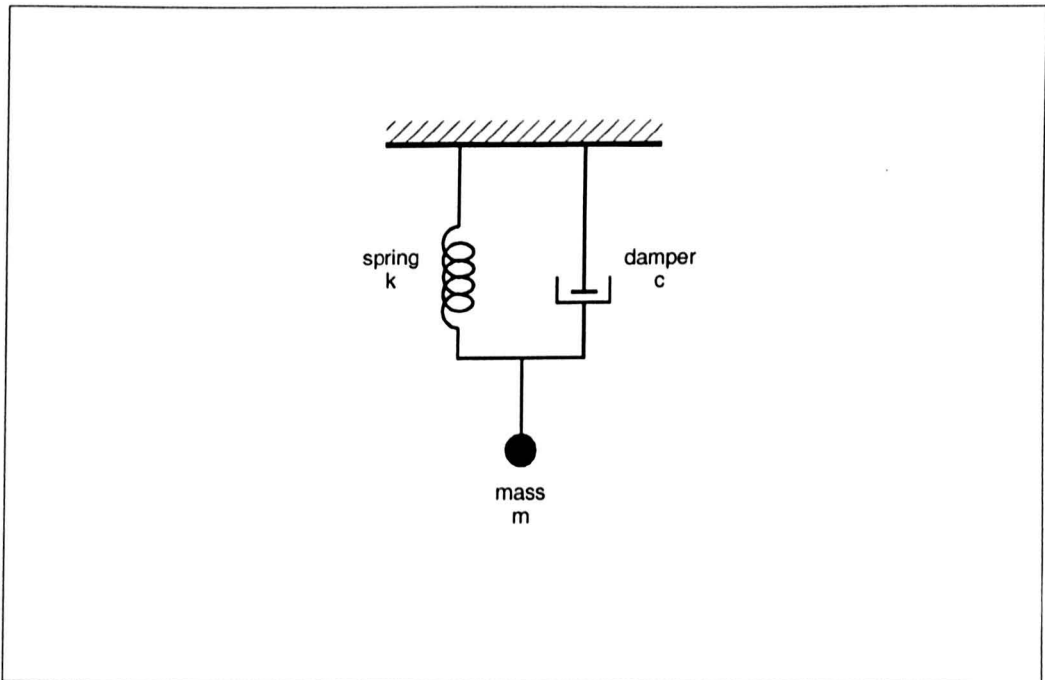


Figure 2.7: Classical Mass-Spring-Damper SDOF System.

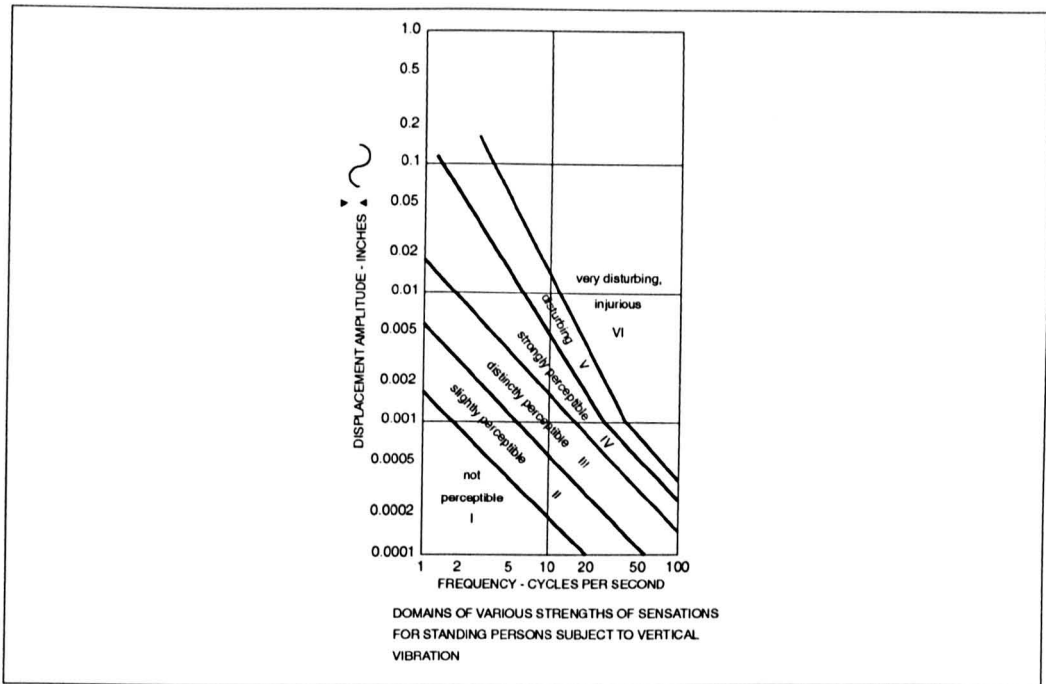


Figure 2.8: Continuous Sinusoidal Vibration Ratings (after Reiher & Meister, 1931).

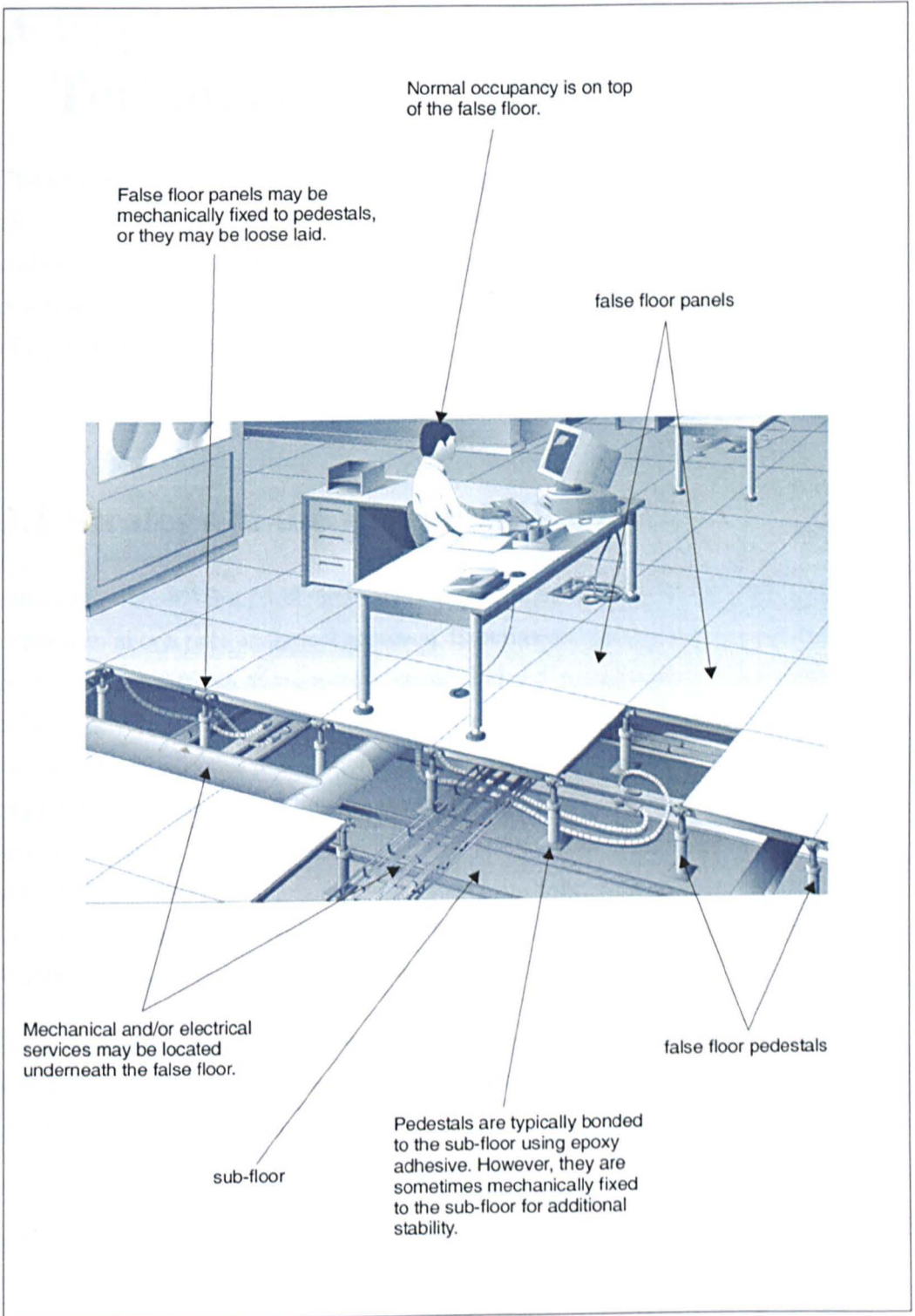


Figure 2.9: Typical Configuration of an Access Floor System (Illustration Courtesy of Tate Access Floors).

3 Experimental and Analytical Techniques

The purpose of this chapter is to outline the important aspects of the experimental and analytical techniques used in the course of the research presented in this thesis. In addition to a brief theoretical background, any important developments made in the practical implementation of these techniques will be discussed, such as commissioning of equipment and development of necessary utility software.

3.1 Strategy of the Research Work

Structural vibration is a problem which is very difficult to study using either a pure experimental or a pure analytical approach. Experiments without analysis can lead to results that are difficult to interpret or understand and, conversely, there seems little point in performing analysis without testing since the accuracy of the analysis cannot be verified. To support this dual analytical and experimental approach to vibration engineering problems, the following recent example is quite enlightening. A pure analytical approach to vibration serviceability of long-span concrete floors supported by unreliable modelling assumptions formed the basis of the method proposed by the Concrete Society (1994). This has been shown repeatedly to be inadequate (Williams & Waldron, 1994; Pavic et al., 1998b; Pavic, 1999).

For these reasons, a dual experimental and analytical approach was adopted for this research whereby experiments were used as a basis for verifying and updating analytical models of the real life structures.

3.1.1 Analytical and Experimental Routes to Vibration Analysis

From an analytical point of view, it is normal to idealise a structure in terms of its stiffness, damping and mass properties, called its spatial model (Ewins, 1995). From this spatial description, it is then possible to calculate its vibration modes in terms of natural frequencies and mode shapes, called the modal model. This is normally performed by modelling the structure using finite elements and performing an eigenvalue extraction

(or theoretical modal analysis) procedure, as described in Section 3.2. Further, it is possible to describe a structure's response to an arbitrary excitation force by calculating its frequency response functions (FRFs), called the response model. This process was described by Ewins (1995) as the "theoretical route to vibration analysis" and is illustrated in Figure 3.1(a).

Conversely, from an experimental point of view, the starting point is usually an existing structure for which a description of its actual vibration behaviour is required. In this case, it is only the response model which is amenable to physical measurement. This is normally performed by measuring the response of a structure due to controlled and measured excitation. Several measurements are required to describe adequately the vibration behaviour of the whole structure. This process is called experimental modal analysis (EMA), but it is also commonly known as modal testing. It is then possible to estimate the vibration modes of the structure through a process called modal parameter estimation (Section 3.3.3) and, further, to estimate its spatial properties using system identification. This was described by Ewins (1995) as the "experimental route to vibration analysis" and is illustrated in Figure 3.1(b).

It is usual in theoretical and experimental modal analysis, when a comparison between analysis and experiments is required, to perform it using the modal model (Figure 3.1). Such a comparison is called model correlation and is described in Section 3.8.1. Additionally, it is possible to utilise the results from experiments to improve upon the original FE model which may contain inaccuracies due to modelling uncertainties such as material properties, geometric tolerances or boundary conditions. This FE model updating process may be based on simple manual trial and error procedures guided by engineering judgement, or it may utilise a more complex computer based numerical method (Friswell & Mottershead, 1995). This topic is covered in more detail in Section 3.8.2.

It is important to note that a fundamental assumption in the application of most of the aforementioned techniques is that the structure under consideration is linear elastic. For the very low-level floor vibrations with which this research is concerned, that assumption has been shown to be reasonable (Eriksson, 1994; Pavic, 1999) and will therefore be made in this work, although linearity checks will be performed during all tests.

3.1.2 Determination of The Effects of Access Floors on the Vibration Behaviour of Long-Span Concrete Floors

As stated in Section 1.1, the primary aim of the research presented in this thesis is to determine the effects that the presence of access floors may have on the vibration serviceability performance of long-span concrete floors. Therefore, for each structure investigated, a research approach containing the following steps will be utilised:

1. The modal properties of the bare structure with no access flooring installed will be determined using EMA.
2. Vibration responses due to controlled occupant-induced excitation will be measured on the bare structure.
3. The modal properties of the structure, with access floors installed, will be determined using identical methods as in step 1. The results of these two sets of measurements will then be compared.
4. Vibration responses due to controlled occupant-induced excitation will be measured on the structure with access floors installed. The results of these measurements will then be compared with those made on the bare floor.
5. Detailed FE models of the structures will be developed. These will be correlated with the EMA results and updated manually to understand in more detail the manner in which the access floors affect the vibration behaviour of the long-span concrete floors.
6. Recommendations will be made regarding how access floors should be modelled in future FE models.

3.2 Finite Element Analysis

The theory of FE analysis is a wide subject area covered by many textbooks. For this reason, the theory presented in this section will be limited to the fundamental equations and assumptions that are pertinent to this work. For a history of and more detailed background to the finite element method, the reader is referred to a textbook published by the UK National Agency for Finite Elements, Methods and Standards (NAFEMS, 1992a) which the writer found particularly relevant to this work.

3.2.1 The Fundamentals of Structural Finite Element Analysis

The finite element method is an approximate analysis technique which basically consists of dividing a structure into a number of parts, called elements. These are connected to each other at their nodes, as shown in Figure 3.2. Each node may have one or more degrees of freedom (DOFs), which are defined as independent displacements (translations and rotations) used to describe the movement of each node. The number and type of elements should be selected so that the deformed shape of the structure can be adequately represented. Deformations within the elements are assumed to follow predefined functions known as shape functions.

3.2.1.1 The Stiffness Matrix

The behaviour of individual elements is described by element stiffness matrices which are square matrices of order equal to the number of nodes in the elements multiplied by the number of degrees of freedom at each node. The elements of the element stiffness matrices are functions of the geometric and material properties of the elements. Once formed, the individual element stiffness matrices are compiled into a stiffness matrix for the whole structure in a process called assembly. The resulting stiffness matrix is a square matrix of order equal to the number of degrees of freedom in the entire structure, and is represented by $[K]$.

The static equilibrium of the structure may now be described by the well known matrix equation:

$$[K]\{x\} = \{f\} \quad \text{Equation 3.1}$$

For dynamic analyses, inertia and damping forces must be included and the governing matrix equation of motion is given by:

$$[M]\{\ddot{x}(t)\} + [C]\{\dot{x}(t)\} + [K]\{x(t)\} = \{f(t)\} \quad \text{Equation 3.2}$$

3.2.1.2 The Mass Matrix

The mass matrix $[M]$ may be formulated to be 'consistent' or 'lumped'. A consistent formulation approximates a continuous distribution of mass throughout the elements by using their shape functions. This results in a mass matrix which contains off-diagonal elements. A lumped formulation assumes the mass to be concentrated at the nodes and

its mass matrix contains only diagonal elements, which is more computationally efficient. It is clear that the consistent formulation represents better the continuous nature of real structures whereas the lumped formulation may save analysis time.

Trial analyses were performed using both the consistent and lumped mass matrix formulations to determine whether the reduction in processing time for the lumped formulation justified its use. For the typical types and sizes of FE model constructed in the course of this work, it was found that the increase in processing time using the consistent mass matrix formulation was not prohibitive and hence the decision was made to use this formulation at all times.

Since the use of a lumped mass matrix tends to overestimate the effective dynamic mass of the system, and since the FEM tends to overestimate structural stiffness, the argument has sometimes been made that the lumped mass approximation should be used to improve natural frequency estimates (NAFEMS, 1992b). However, this procedure tends to degrade the calculated mode shapes, particularly for higher modes. The writer also believes the introduction of inaccuracies into a model on the assumption that they will cancel with other inaccuracies to be an unwise procedure.

3.2.1.3 The Damping Matrix

Various formulations exist for definition of the damping matrix $[C]$. However, selection of the appropriate damping matrix formulation is normally based on convenience of application rather than on a rigorous representation of the actual damping behaviour of the structure being modelled. This is mainly due to the fact that actual damping mechanisms are currently poorly understood (Clough & Penzien, 1993).

Probably the most commonly used assumption for damping is the linear viscous formulation as it facilitates solution of Equation 3.2 for any dynamic loading scenario. In particular, the most common form of viscous damping is Rayleigh damping in which the damping matrix is given by (Petyt, 1990):

$$[C] = a_1 [M] + a_2 [K] \quad \text{Equation 3.3}$$

The main advantage of Rayleigh damping is that the modal damping matrix can be shown to be diagonal (Petyt, 1990). Therefore, this simplifies the solution of the matrix equation of motion (Equation 3.2) by the method of mode superposition. However, when actual damping values for a structure have been determined from EMA, it is possible to

utilise these in place of the Rayleigh formulation for increased accuracy in the solution of Equation 3.2.

3.2.2 Theoretical Modal Analysis

Theoretical modal analysis is used to determine the modal properties of a structure (natural frequencies, mode shapes and modal mass) from its specified, that is assumed, geometrical and material properties. These theoretical modal properties could then be qualitatively and quantitatively compared with the modal properties determined experimentally from EMA. The basic principles of theoretical modal analysis will be outlined here.

Assume that the structure is undamped, and consider the free vibration solution of Equation 3.2, given by:

$$[M]\{\ddot{x}(t)\} + [K]\{x(t)\} = \{0\} \quad \text{Equation 3.4}$$

Matrix Equation 3.4 represents a system of N linear homogeneous simultaneous equations. Assume a trial solution of the form:

$$\{x(t)\} = \{x\} e^{i\omega t} \quad \text{Equation 3.5}$$

and substitute into Equation 3.4 to give:

$$([K] - \omega^2 [M])\{x\} = \{0\} \quad \text{Equation 3.6}$$

Equation 3.6 represents a classical eigenvalue problem for which the only non-trivial solution is given by:

$$\det|[K] - \omega^2 [M]| = 0 \quad \text{Equation 3.7}$$

which can now be used to determine the N values of ω^2 , the eigenvalues, which satisfy this condition. Substitution of the eigenvalues back into Equation 3.6 yields N linearly independent vectors for $\{x\}$ which are called eigenvectors and represent the normal mode shapes of the structure. The complete modal solution may therefore be expressed using the following two $N \times N$ matrices:

$[\omega_r^2]$, a diagonal matrix of eigenvalues, and

$[\Psi]$, a square matrix of eigenvectors.

Many numerical algorithms exist to extract the eigenmatrices from the spatial model, but since these are well established and documented, the theory behind them will not be presented here. Instead, the reader is referred to some of the many readily available texts on the subject (Press et al., 1992; Petyt, 1990). For the purposes of this research, the subspace iteration method of eigensolution, as implemented in a commercial FE software called ANSYS (Section 3.2.4.1), was utilised.

Since the eigenvectors, which are calculated from a modal analysis, describe the mode shapes, they may be scaled using whatever scaling factor is convenient. In practice only two forms of scaling of eigenvectors are commonly used. These are:

1. unity normalisation, and
2. mass normalisation.

Unity normalised eigenvectors have the property that their maximum element is unity. However, it is more usual in modal analysis to use mass normalisation such that:

$$[\Phi]^T [M] [\Phi] = [I] \quad \text{Equation 3.8}$$

which leads to the result that:

$$[\Phi]^T [K] [\Phi] = [\omega_r^2] \quad \text{Equation 3.9}$$

3.2.3 Solution of Equations of Motion

There are two methods of solution of the equations of motion which are commonly utilised in FE analysis. These are 'direct integration' and 'mode superposition'. Due to its computational economy for low frequency vibration analysis problems and the fact that theoretical modal analyses had to be performed for all structures tested in this research, it was decided to utilise the mode superposition method for solution of the equations of motion when this was required. This is outlined briefly here.

For a structure modelled as an N-DOF linear system, it is possible to calculate N eigenvectors as described in Section 3.2.2. As these eigenvectors are orthogonal, they may serve as generalised coordinates to describe any displacement shape assumed by the N-DOF structure (Clough & Penzien, 1993). This transformation may be expressed as:

$$\{x(t)\} = \sum_{r=1}^N \{\psi_r\} q_r(t) \quad \text{Equation 3.10}$$

It is possible to evaluate any arbitrary generalised coordinate (Clough & Penzien, 1993). Firstly, premultiply Equation 3.10 by $\{\psi_r\}^T [M]$ to obtain:

$$\begin{aligned} \{\psi_r\}^T [M] \{x(t)\} &= \{\psi_r\}^T [M] \{\psi_1\} q_1(t) \\ &+ \{\psi_r\}^T [M] \{\psi_2\} q_2(t) \\ &+ \dots \\ &+ \{\psi_r\}^T [M] \{\psi_N\} q_N(t) \end{aligned} \quad \text{Equation 3.11}$$

Because of the orthogonality properties, i.e. $\{\psi_n\}^T [M] \{\psi_m\} = 0$ for $n \neq m$, this reduces to:

$$\{\psi_r\}^T [M] \{x(t)\} = \{\psi_r\}^T [M] \{\psi_r\} q_r(t) \quad \text{Equation 3.12}$$

from which it can be seen that:

$$q_r(t) = \frac{\{\psi_r\}^T [M] \{x(t)\}}{\{\psi_r\}^T [M] \{\psi_r\}} \quad \text{Equation 3.13}$$

The denominator of Equation 3.13 actually equates to the modal mass, m_r , corresponding to the arbitrary scaling of the mode shapes. When Equation 3.13 is substituted back into Equation 3.10, it can be seen that the modal masses cancel demonstrating that the choice of arbitrary mode shape scaling factor is unimportant for mode superposition response analysis. With an assumption of viscous damping, Equation 3.2 may now be converted into a set of N uncoupled equations given by (Clough & Penzien, 1993):

$$\ddot{q}_r(t) + 2\zeta_r \omega_r \dot{q}_r(t) + \omega_r^2 q_r(t) = \frac{Q_r(t)}{m_r} \quad r = 1, 2, \dots, N \quad \text{Equation 3.14}$$

where:

$$m_r = \{\psi_r\}^T [M] \{\psi_r\} \quad \text{and} \quad Q_r(t) = \{\psi_r\}^T \{f(t)\}$$

Therefore, the response of the structure may be calculated by solving each of the uncoupled modal equations and superposing their effects using Equation 3.10. This is the basis of the mode superposition method. In practice, it is common in vibration

engineering to include only a limited number of modes in the mode superposition solution. This is typically of sufficient accuracy for low frequency vibration analyses and it enhances greatly the computational efficiency of the method.

3.2.4 Practical Implementation of FE Modelling

3.2.4.1 Selection of Analysis Software

For this work it was necessary to select a commercial finite element package that would be suitable for the linear elastic modal and dynamic response analyses that were to be performed. This choice was made easy because the ANSYS finite element software was already available at the University of Sheffield, and was therefore readily available to the writer. The software could be run from either a standalone PC or from a central mainframe facility at the University. ANSYS is widely used in the mechanical and aeronautical engineering disciplines and has very powerful linear dynamic analysis capabilities. Furthermore, the ICATS software (ICATS, 1997) used for modal parameter estimation and FE model correlation (Section 3.3.3) had a direct interface with the ANSYS FE code. ANSYS was therefore considered appropriate for use in this work.

3.2.4.2 Choice of Element Types

Since all of the modelling performed in the course of this work was to be linear elastic, a selection of linear elastic elements was made in order to model various aspects of the structures under consideration. These were:

- SHELL63. A 4-noded linear elastic shell element with both bending and membrane capabilities and 6 DOFs at each node. This was chosen for utilisation in the modelling of the reinforced and prestressed concrete slabs considered in this work. The use of orthotropic material properties for the modelling of ribbed slabs was performed in accordance with the recommendations given by Pavic (1999).
- BEAM4. A 2-noded linear elastic beam element with 6 DOFs at each node. This element was chosen typically for the modelling of elements which do not require their centroid to be offset from the location of the FE nodes (e.g. columns).
- BEAM44. A 2-noded linear elastic tapered beam element with 6 DOFs at each node and offset capability. This element was chosen typically for the modelling of beam type elements where the centroid of the section must be offset from the location of the FE nodes (e.g. downstand edge beams).

- COMBIN14. Longitudinal or torsional spring-damper element. This was chosen for the modelling of flexible supports as appropriate.
- SOLID73. An 8-noded linear elastic solid element with 6 DOFs at each node. This element was chosen for the modelling of 3-D elements where the exact structural geometry was important.

3.3 Theory of Experimental Modal Analysis

Ewins (1995) defined EMA as:

“... the processes involved in testing components or structures with the objective of obtaining a mathematical description of their dynamic or vibration behaviour.”

3.3.1 Theoretical Background

Section 3.2.2 described numerical techniques in which the modal model for a structure may be calculated from its spatial properties following the theoretical route to vibration analysis (Figure 3.1) using FE analysis. However, neither the spatial model nor the modal model are amenable to direct physical measurement. For this reason, it is necessary to utilise the response model as follows.

3.3.1.1 Derivation of the Response Model

The matrix equation of motion for the forced vibration of a viscously damped system is given by:

$$[M]\{\ddot{x}(t)\} + [C]\{\dot{x}(t)\} + [K]\{x(t)\} = \{f(t)\} \quad \text{Equation 3.15}$$

It can be shown (Ewins, 1995) that it is possible to calculate the response of the structure to a system of forces using the equation:

$$\{x(t)\} = ([K] - \omega^2 [M] + i\omega [C])^{-1} \{f(t)\} \quad \text{Equation 3.16}$$

which may also be written as:

$$\{x\} = [\alpha(\omega)]\{f\} \quad \text{Equation 3.17}$$

where:

$$[\alpha(\omega)] = ([K] - \omega^2 [M] + i\omega [C])^{-1} \quad \text{Equation 3.18}$$

is defined as the $N \times N$ receptance matrix for the system which constitutes its response model. It should be noted that similar relationships may be derived relating the force input to the velocity and acceleration responses. In these cases, the receptance matrix is replaced by a mobility or inertance matrix respectively. The generic term 'FRF matrix' is frequently used to represent the response model given by Equation 3.17 and it is normally represented as $H(\omega)$.

Since the force input to the structure and the dynamic response of the structure are amenable to physical measurement, it is theoretically possible to obtain a mathematical description of the structure through testing. The challenges involved in obtaining the force and response data, and of converting these data into a meaningful form, are at the heart of EMA.

3.3.1.2 Use of the Modal Model

It is more usual in EMA to define the response model in terms of its modal properties, rather than its spatial properties, in order to simplify the mathematics. Unfortunately, the modal solution of Equation 3.15 using the techniques described in Section 3.2.2 is difficult since a non-proportional viscous damping matrix $[C]$ serves to make the eigenvalues and eigenvectors complex. For this reason, it is more usual in EMA to utilise the 'hysteretic damping' formulation. In this case, the matrix equation of motion is given by (Ewins, 1995):

$$[M]\{\ddot{x}(t)\} + ([K + iD])\{x(t)\} = \{f(t)\} \quad \text{Equation 3.19}$$

where the 'proportional' hysteretic damping matrix $[D]$ is given by:

$$[D] = a_1 [M] + a_2 [K] \quad \text{Equation 3.20}$$

The receptance matrix may therefore be expressed as (Ewins, 1995):

$$[\alpha(\omega)] = [\Phi] \left[(\omega_r^2 - \omega^2) \right]^{-1} [\Phi]^T \quad \text{Equation 3.21}$$

Any individual element in the receptance matrix is a single FRF and may be calculated from:

$$\alpha_{jk}(\omega) = \sum_{r=1}^N \frac{(\phi_{jr})(\phi_{kr})}{\omega_r^2 - \omega^2 + i\eta_r \omega_r^2} \quad \text{Equation 3.22}$$

or:

$$\alpha_{jk}(\omega) = \sum_{r=1}^N \frac{{}_r A_{jk}}{\omega_r^2 - \omega^2 + i\eta_r \omega_r^2} \quad \text{Equation 3.23}$$

where ${}_r A_{jk} = (\phi_{jr})(\phi_{kr})$ is called the modal constant and η_r is known as the 'loss factor' for mode r . It can be shown (Maia et al., 1997) that, at frequencies close to resonance, the loss factor has a value approximately double that of the equivalent modal viscous damping ratio, i.e. $\eta_r \approx 2\zeta_r$.

It is, in fact, FRF relationships based on Equation 3.23 which are most commonly used to obtain the modal parameters of a structure from experimental testing. A number of FRFs are calculated using direct force and structural response measurements, after which curve fitting is performed to estimate the structural modal properties.

3.3.2 Dynamic Signal Analysis

Most EMA is based on the calculation of FRFs from force and response signals, followed by curve fitting techniques which aim to determine modal properties, such as those featuring in Equation 3.23. However, the exact method of calculation of the FRF from the force and response time domain signals depends on the types of signals in question.

The dynamic signals commonly encountered in EMA may conveniently be divided into two classifications: deterministic and random. These may also be sub-divided further; deterministic signals into periodic and transient and random signals into stationary and non-stationary, as illustrated in Figure 3.3. In practice, the signals most frequently encountered in EMA are periodic, transient or stationary random.

3.3.2.1 Periodic Signals

A periodic signal is a deterministic signal which repeats itself in time every T seconds, where T is known as the repeat period. Such a signal may be expressed in terms of a Fourier series (McConnell, 1995):

$$x(t) = \sum_{p=-\infty}^{\infty} X_p e^{ip\omega_0 t} \quad \text{Equation 3.24}$$

where X_p is the complex Fourier coefficient given by:

$$X_p = \frac{1}{T} \int_t^{t+T} x(\tau) e^{-ip\omega_0 \tau} d\tau \quad \text{Equation 3.25}$$

and ω_0 is the lowest frequency component of the signal given by:

$$\omega_0 = 2\pi f_0 = 2\pi \frac{1}{T} \quad \text{Equation 3.26}$$

It can be seen that all frequency components of this signal ($p\omega_0$) are discrete at integer multiples of ω_0 , which describe its 'linear spectrum', as shown in Figure 3.4(b).

For modal testing applications, a dormant linear structure excited by a periodic forcing function will exhibit a periodic response (after any start up transients have died out) with the same period as the forcing function. It is therefore clear that by measuring the forcing function and structural response over a single period, it is possible to determine the linear spectra of both signals and subsequently calculate an FRF (Equation 3.17) using complex division.

3.3.2.2 Transient Signals

Transient signals may be defined as being zero for a long period of time except for a short duration in which there are significant amplitude changes (McConnell, 1995). For the purpose of a theoretical analysis, a transient signal may be considered to be a periodic signal with a repeat period of infinity. Thus, Equations 3.24 and 3.25 become:

$$x(t) = \frac{1}{2\pi} \int_{-\infty}^{\infty} X(\omega) e^{i\omega t} d\omega \quad \text{Equation 3.27}$$

and:

$$X(\omega) = \int_{-\infty}^{\infty} x(t) e^{-i\omega t} dt \quad \text{Equation 3.28}$$

It can be seen that the frequency content of the signal given by $X(\omega)$ is now a continuous function of frequency ω , as opposed to periodic signals, in which the frequency content was given by components at discrete frequencies. Therefore, this continuous function is termed a 'spectral density' (as opposed to 'linear spectrum') and is displayed in Figure 3.4(a).

3.3.2.3 Stationary Random Signals

In order to apply the integral Fourier transform (Equations 3.27 and 3.28), a time domain signal must satisfy the Dirichlet condition (McConnell, 1995):

$$\int_{-\infty}^{\infty} |x(t)| dt < \infty \quad \text{Equation 3.29}$$

Since random signals do not satisfy this condition, it is necessary to utilise the random auto-correlation function defined by:

$$R_{xx}(\tau) = \lim_{T \rightarrow \infty} \frac{1}{T} \int_{-T/2}^{T/2} x(t)x(t+\tau) dt \quad \text{Equation 3.30}$$

For random signals, as τ increases $R_{xx}(\tau)$ tends to zero (McConnell, 1995), which implies no correlation between events a long time apart. Therefore, Equation 3.30 satisfies the Dirichlet condition and it is possible to apply the transient Fourier transform to it. This results in a random auto-spectral density function (ASD) which provides a frequency description of the original signal (Maia et al., 1997). This is given by (McConnell, 1995):

$$S_{xx}(\omega) = \int_{-\infty}^{\infty} R_{xx}(\tau) \cos(\omega\tau) d\tau \quad \text{Equation 3.31}$$

which is a symmetric function of ω . In practical situations, a single-sided function defined for positive ω , $G_{xx}(\omega)$, is normally used and is defined as:

$$\begin{aligned} G_{xx}(\omega) &= 2S_{xx}(\omega) \quad \text{for } 0 < \omega < \infty \\ G_{xx}(0) &= S_{xx}(0) \quad \text{for } \omega = 0 \end{aligned} \quad \text{Equation 3.32}$$

Similarly, the random cross-correlation function is defined as (McConnell, 1995):

$$R_{XY}(\tau) = \lim_{T \rightarrow \infty} \frac{1}{T} \int_{-T/2}^{T/2} x(t)y(t + \tau) dt \quad \text{Equation 3.33}$$

for which its Fourier transform, known as the random cross-spectral density (CSD), is given by:

$$S_{XY}(\omega) = \int_{-\infty}^{\infty} R_{XY}(\tau) e^{-i\omega\tau} d\tau \quad \text{Equation 3.34}$$

In fact, the ASD is actually a special case of the CSD for which the input and output signals are the same.

Through the use of the ASD and CSD, it is therefore possible to side-step the limitations of the transient Fourier transform for random signals, but care is needed to interpret the results as appropriate.

3.3.2.4 Calculation of Frequency Response Functions

So far, three different methods of Fourier analysis of time domain signals have been presented depending on whether the signals are periodic, transient or stationary random. In practice, it is convenient to have a means for calculation of FRFs which is applicable to all types of signal. This can be done through the use of FRF 'estimators' which, provided the force and response signals are processed in the same way, are applicable to all types of signals (McConnell, 1995). One of the most common FRF estimators is the H_1 estimator. This will be outlined in the remainder of this section.

The frequency domain input output FRF relationship for a linear system is given by (McConnell, 1995):

$$Y(\omega) = H(\omega) \cdot X(\omega) \quad \text{Equation 3.35}$$

where $X(\omega)$ is the system input and $Y(\omega)$ is the system output. Multiplying by $X^*(\omega)$ gives:

$$X^*(\omega)Y(\omega) = H(\omega)X^*(\omega)X(\omega) \quad \text{Equation 3.36}$$

which, assuming that both channels are processed in the same way, can be rewritten as:

$$S_{XY}(\omega) = H(\omega)S_{XX}(\omega) \quad \text{Equation 3.37}$$

The H_1 estimator is therefore defined as (McConnell, 1995):

$$H_1(\omega) = \frac{S_{XY}(\omega)}{S_{XX}(\omega)} \quad \text{for } -\infty < \omega < +\infty \quad \text{Equation 3.38}$$

or:

$$H_1(\omega) = \frac{G_{XY}(\omega)}{G_{XX}(\omega)} \quad \text{for } 0 < \omega < +\infty \quad \text{Equation 3.39}$$

The H_1 estimator was implemented in the spectrum analyser utilised in this work (DI, undated). In addition to being applicable to all types of signals, it also has a strong advantage in that the effects of environmental or instrumentation noise, present only on the response channel and uncorrelated with the force channel, will tend to reduce with averaging (DTA, 1993a; McConnell, 1995).

3.3.2.5 Sampled Functions

To facilitate the application of the theory presented in Sections 3.3.2.1 to 3.3.2.4, it is normally necessary to sample time histories at discrete time steps so that they may be stored digitally for further processing. It is therefore impossible to apply integral Fourier transform techniques and, instead, it is necessary to utilise 'discrete' Fourier transform techniques. As can be seen in Figure 3.4(d), this introduces periodicity into both the time and frequency domains.

Whilst the signal analysis concepts are the same as for continuous functions, the periodicity assumed by the discretisation process may lead to errors (e.g. due to aliasing) if the limitations of the discrete functions are not understood. The reader is referred to a reference written by Randall (1987) in which these important effects are explained in detail.

3.3.3 Modal Parameter Estimation

It has already been shown in Section 3.3.1 that the FRF matrix for a structure may be expressed in terms of its modal properties. Modal parameter estimation is a set of techniques by which the modal properties of the structure may be determined from part or all of the FRF matrix.

In this work, the MODENT software, a module of the ICATS suite (ICATS, 1997), was utilised for performing the required modal parameter estimation. In particular, most use

was made of the SDOF circle- and line-fit techniques, and the MDOF 'Global' method (Fillod et al., 1985) of modal parameter estimation. Whilst the writer was aware of the basic theory and advantages and disadvantages of these methods of modal parameter estimation, the MODENT software was treated as a 'black-box'. This means that no attempt was made to master how exactly these methods were implemented. This is, in fact, the level at which the DTA (1993a), Ewins (1995) and Maia et al. (1997) recommend that users of such software familiarise themselves with the theory. For more information regarding a large number of the modal parameter estimation techniques which have been developed, the reader is referred to Maia et al. (1997) or to the DTA Handbook (DTA, 1993a).

3.4 Excitation for Experimental Modal Analysis

As described in Section 3.3.1, it is necessary to provide a measurable source of excitation for EMA. In this work, the excitation was provided using two separate items of equipment:

1. a Dytran model 5803A instrumented impact hammer (Dytran, undated), and
2. an APS Dynamics model 113 electrodynamic shaker (APS Dynamics, undated).

The instrumented impact hammer had been used in the writer's research group at the University of Sheffield prior to the commencement of this work. Consequently, the ancillary equipment and procedures necessary to utilise this form of excitation had already been developed (Pavic, 1999). Therefore, these existing items of equipment and procedures will only be described briefly in this work. However, the APS Dynamics electrodynamic shaker was purchased during the course of this work and the writer was responsible for its commissioning. For this reason, the commissioning and use of the shaker will be described in more detail.

3.4.1 Instrumented Impact Hammer Excitation

The Dytran model 5803A instrumented impact hammer utilised for some of the EMA in this research is shown in Figure 3.5. The mass of the hammer head is 5.4 kg (12 lb) and its nominal force range is 22.2 kN (5000 lbf). The force signal is measured using a piezoelectric force transducer built into the hammer head. The force transducer contains

an integrated amplifier which enables the hammer to be connected to its signal conditioning unit using very long (typically more than 50 m) cables without any significant degradation of the signal. This is obviously an important requirement for the modal testing of large civil engineering structures where it may be necessary to use long cables. The frequency content of the hammer blow is controlled by using hammer tips of different hardnesses. A relatively soft hammer tip will produce an impact of longer duration than a relatively hard one, which results in the energy from the impact being concentrated in a lower frequency band. However, a high degree of control over the frequency content of the excitation using a hammer impact is difficult to achieve.

On floors, the hammer is usually manually operated by a single seated person who is located on top of the test structure. It is typically assumed that for large structures, such as long span concrete floors, the hammer operator does not alter the modal properties of the test structure in any way. A typical hammer impact transient time history together with its Fourier transform are shown in Figure 3.6.

Use of this form of excitation requires a detailed understanding of signal processing issues since it is highly sensitive to data acquisition parameters, filtering and windowing. Pavic, et al. (1998a) give a comprehensive overview of such details pertinent to the equipment used by the writer and they will not be discussed further here.

3.4.2 Electrodynamic Shaker Excitation

The electrodynamic shaker used in this research was a newly acquired APS Dynamics model 113 shaker. The shaker utilises a current carrying conductor located within a dc magnetic field to generate a force, which is proportional to the instantaneous value of the supplied electric current (APS Dynamics, undated). It is therefore possible to generate a time varying force of any form, within the force envelope for the shaker (Figure 3.7), provided a means exists to generate the corresponding electrical control signal.

In this work, the shaker was operated in two different modes. Firstly, operation of the shaker in 'free armature mode' entailed placing the shaker onto the top surface of the structure under test, as shown in Figure 3.8. The force was generated by accelerating reaction masses attached to the shaker armature, hence exerting an equal and opposite force to the shaker body and consequently to the structure itself. The force input to the structure was measured by measuring the acceleration of the shaker armature and by

multiplying it by the mass of the combined armature and reaction mass assembly. It was assumed that the mass of the shaker body was negligible compared to the mass of the test structure, and also that the accelerations of the structure (and hence the shaker body) were negligible compared to the accelerations of the shaker armature.

The shaker was also operated in 'fixed armature mode' as shown in Figure 3.9. This entailed connecting the shaker armature to the structure using a 'stinger' through which the force input was transmitted directly to the underside of the test structure. The shaker body was 'grounded', that is placed onto a firm surface below the structure. The force input to the structure was measured by monitoring the current supplied to the shaker armature and multiplying it by a calibration factor provided by the shaker manufacturer (APS Dynamics, undated). It was assumed that the mass of the shaker armature was negligible compared to the mass of the test structure.

In both free armature and fixed armature modes, an excitation control signal was generated using either a digital signal generator or the output channel of a digital data acquisition card (Section 3.4.3). This control signal was then amplified using an APS Dynamics model 114-EP power amplifier and sent to the shaker.

3.4.3 Types of Modal Test Excitation Signals

Olsen (1984) classified structural dynamic excitation techniques in general into five types: operating, steady-state, periodic, transient and random. Operating excitation is generally not measured and represents the dynamic loading applied to a structure in its operating condition. Since a requirement of EMA is a measurable form of excitation (Ewins, 1995), operating excitation is not suitable. It should be noted, however, that operating excitation is commonly used in civil engineering in 'ambient vibration testing' in which response only measurements are utilised to obtain unscaled mode shapes, natural frequencies and modal damping ratios. This technique is more common on very large structures (such as large buildings, bridges and dams) for which the measurement of the artificial excitation is impractical. However, mode shapes estimated from ambient vibration testing are 'unscaled', meaning that it is not possible to relate the response of the structure to the force input. Therefore, it was not utilised in this work and will not be discussed further.

Steady-state methods usually entail the application of a slowly swept or stepped sine excitation to the structure so that a (near) steady-state sinusoidal response is achieved.

Examination of the magnitude and phase relationship between the excitation and response signals gives a single FRF ordinate at that frequency. By evaluating complex FRF ordinates at all frequencies of interest, a complete FRF may be constructed. Steady-state methods were commonly utilised prior to the advent of the Fast Fourier Transform (FFT) algorithm in the 1960's, but have tended to be superseded in recent years by faster broadband methods based on periodic, transient and random excitation. However, there are some significant benefits of steady-state methods which will be discussed further in Section 3.4.7.

Periodic, transient and random are all broadband forms of excitation containing more than one frequency in which an FRF may be calculated by performing a complex division of the Fourier transform of the response by the Fourier transform of the excitation, as long as both signals are Fourier transformable (Olsen, 1984).

For this work, it was necessary to implement systems for the generation of the excitation signals required to perform EMA on the structures. Systems for the generation of the following types of excitation signals were implemented.

- Band Limited Random
- Burst Swept Sine
- Pseudo-random (or Periodic Random)
- Stepped Sine

3.4.4 Band-limited Random Excitation Signals

The implementation of various forms of random excitation was considered to be important since they tend to produce the best linear approximation (or average) of dynamic systems in which there may be some non-linearity (Brown et al., 1977). This could be true of the structures considered in this work. Since the interest of this research work was only in a relatively narrow range of low frequencies (typically below 50 Hz), it was decided that the frequency content of the signal should somehow be limited to the range of interest, i.e. band-limited.

The possibility of utilising an off-the-shelf band-limited random function generator was explored, but the writer was unable to locate such a device at a reasonable cost. For this reason, it was decided to make use of the function generator and analogue output capabilities of an available DAP 2400/e6 data acquisition card.

A computer program was written which was designed to run on a notebook PC connected to the DAP data acquisition card. The basic principles behind the program are as follows. Commands are sent from the PC to the DAP which instruct it to generate a white noise signal, apply a digital band-pass filter to restrict the frequency content of the white noise to the desired frequency range, and convert the signal into an analogue voltage of appropriate magnitude using one of the on-board digital-to-analogue converters. The resulting band-limited random output signal may be of a pre-specified duration or it may be continuous. A flowchart for the program, called RANGEN (Reynolds, 1996a), is presented in Figure 3.10. The procedures for modal testing using both a continuous random signal and short duration random bursts are outlined here.

3.4.4.1 Continuous Random Testing

In this form of testing, a continuous random forcing function is applied to the structure. Both the force input and response of the structure are measured over a number of finite duration data acquisition periods. Since these signals are not periodic in the analyser window, they suffer from leakage errors. These may be reduced through the use of time domain windows such as the Hanning window, but they will always result in some distortions in the measured FRFs.

3.4.4.2 Burst Random Testing

To eliminate the aforementioned leakage errors in continuous random testing, it is possible to apply the random excitation in finite duration bursts which are fully contained within the data acquisition period. The excitation signal can now be analysed as a transient without any leakage errors. The response signal must also be transient, that is that the structural vibrations die out completely within the acquisition period. This form of excitation will hereafter be referred to as Burst Random (BR) excitation.

3.4.4.3 Use of the Exponential Window

However, for structures with low damping, typical in civil engineering, it is possible that the structural response does not attenuate completely within the data acquisition period. In this case leakage errors will occur. Also, when a short duration excitation is utilised, the remainder of the excitation time history represents nothing more than measurement noise which may contaminate the FRF. To reduce these effects, it is common to apply an 'exponential window' to the time domain signals defined by (Fladung & Rost, 1997):

$$w(t) = e^{-at}$$

Equation 3.40

where a is the time constant of the exponential function. This is illustrated in Figure 3.11. It can be shown that, provided identical windows are applied to both the excitation and response channels, the only consequence regarding estimated modal parameters is an increase in apparent system damping which may be subsequently corrected using the formula (Taber et al., 1985):

$$\zeta_r = \zeta_r^d - \frac{a}{2\pi f_r} \quad \text{Equation 3.41}$$

where ζ_r is the 'actual' modal damping ratio of the r^{th} mode, whilst ζ_r^d is the modal damping ratio and f_r is the natural frequency of the r^{th} mode estimated from EMA.

A secondary but very important effect of the exponential window is that, due to the increased apparent system damping, the peaks of the FRFs are wider than when the exponential window is not utilised. Typically for civil engineering structures with very low damping, problems are encountered describing the very sharp peaks in the FRFs using the available frequency resolution. The wider peaks produced by application of the exponential window can be described better using the available frequency resolution and therefore result in better and more consistent estimates of modal parameters (Reynolds & Pavic, 2000).

An additional window function is also commonly applied in addition to the exponential window when performing EMA using transient forms of excitation. This is called a force window and is applied only to the excitation signal. This window takes a unity value for a pre-specified proportion of the data acquisition duration, which should include the entire excitation signal. Theoretically, the window then takes a value of zero for the remainder of the signal. In practice, for the DI2200 spectrum analyser utilised in this work, the window then takes a value of the mean of the remainder of the signal, which is normally very close to zero. This enables the effects of a dc offset to be discounted. The force window is illustrated in Figure 3.11. It is designed to reduce the effects of noise on the excitation signal after the excitation itself has stopped.

3.4.4.4 Triggered Random Excitation

The term 'triggered random excitation' was coined by Taber et al. (1985) to describe the BR testing method where the excitation is applied for the full duration of the acquisition

period. In this case, the exponential window is assumed to attenuate the excitation and response signals sufficiently to reduce leakage to an acceptable level.

3.4.5 Burst Swept Sine Excitation Signals

Burst swept sine (BSS) excitation uses a sinusoidal excitation signal which is swept smoothly between pre-specified frequency limits in a relatively short duration. Such a signal will contain energy at all frequencies between the lower and upper limits. Similarly to the BR excitation, provided both the excitation and response signals are fully contained within the data acquisition period, they may be treated as transient and the FRF may be calculated without leakage errors. Two possible types of sweep are commonly utilised, linear and logarithmic, with logarithmic being preferred since a linear sweep tends to concentrate the excitation energy at the higher frequencies (Olsen, 1984).

For this research, a computer program called SG_CTRL (Reynolds, 1996b) was developed to generate a digitised burst swept sine signal which could be downloaded to a Hewlett-Packard HP33120A digital function generator. This signal could subsequently be output to the shaker amplifier. Both the linear and logarithmic sweeps were implemented using the following equations (University of Manchester, 1991):

$$f(t) = \sin\left(\omega_0 t + \frac{1}{2} \lambda t^2\right) \quad (\text{linear}) \quad \text{Equation 3.42}$$

$$f(t) = \sin\left[\frac{\omega_0}{\beta} (e^{\beta t} - 1)\right] \quad (\text{logarithmic}) \quad \text{Equation 3.43}$$

where ω_0 is the initial frequency in radians, λ is the linear sweep rate in radians/s² and β is the logarithmic sweep time constant given by

$$\beta = \frac{1}{T} \ln\left(\frac{\omega_{\text{final}}}{\omega_0}\right) \quad \text{Equation 3.44}$$

In addition, a linear ramp was applied to the start and end of the excitation signal to reduce the effects of the transient response of the shaker. A flowchart for the program is presented in Figure 3.12. A typical logarithmic BSS excitation signal produced by the shaker, together with its Fourier transform is shown in Figure 3.13.

3.4.6 Pseudo-random (or Periodic Random) Excitation Signals

A pseudo-random signal is generated by defining its frequency content and using the inverse Fourier transform to obtain a time history. The magnitude of each line of the linear spectrum is specified to be unity in the frequency range of interest, whereas the phase is randomly generated. Due to the periodicity properties of the DFT, the resulting time history is periodic with a repeat period given by the reciprocal of the frequency resolution of the artificially generated spectrum. However, on first inspection the time history appears random hence its name. Periodic random testing is a variation of pseudo-random where different time histories are generated and utilised for each average. Provided that the data acquisition window used in modal testing has the same duration as the repeat period of the pseudo-random signal, both the excitation and response time histories may be Fourier transformed without leakage.

A computer program called PSEUDO was written which enables the user to generate a pseudo-random signal by specifying a lower frequency limit, an upper frequency limit and a required time history duration. The program would then download this signal to the Hewlett-Packard HP33120A digital function generator so that it could be replayed on demand at the touch of a button. A flowchart for the program is presented in Figure 3.14.

3.4.7 Stepped Sine Excitation

Despite the already mentioned unpopularity of steady-state testing, it was considered prudent to develop the capability to perform stepped sine testing for two main reasons. Firstly, a stepped sine excitation signal gives the best possible signal-to-noise ratio for a shaker/amplifier system with finite power output (Brown et al., 1977). This is particularly important if there is a requirement to test a structure which cannot be excited sufficiently using broadband excitation signals. Secondly, sinusoidal excitation is the best form of excitation for quantifying any non-linear behaviour in a test structure (DTA, 1993b). Whilst there was no intention of studying non-linearities in detail in this work, the ability to examine the degree of non-linearity in the test structures under low-level vibration was considered worthwhile.

A computer program was written which implemented an automated stepped sine testing procedure. It was designed to make use of existing equipment since there were no additional funds available. To this end, it made use of the available Hewlett-Packard

HP33120A signal generator for generation of the excitation signal and the DAP data acquisition card for measurement of the actual force input to the structure and the response. The resolver method (University of Manchester, 1991) was utilised for calculation of the FRF from the measured sinusoidal force and response signals.

To begin with, the program was developed with the frequency steps being specified by means of a start frequency, an end frequency and a number of frequency steps, i.e. equidistant frequency lines. However, the program was later adapted so that non-uniform frequency spacing could be specified.

3.5 EMA Transducers and Data Acquisition

The previous section described the production and measurement of EMA excitation in some detail. Prior to the description of the procedures used in the practical implementation of EMA in this work, it is convenient to describe briefly the other principal items of equipment used.

3.5.1 Response Transducers

When measuring the dynamic response of structures, it is possible to examine the displacement, velocity or acceleration and convert between these quantities using simple time differentiation or integration. However, current technology dictates that it is acceleration which is the structural response which is most convenient to measure.

The responses of the structures tested in this work were measured using low-noise, low-frequency piezoelectric accelerometers. Two different models were used: Endevco model 7754-1000 and Dytran model 3100B24. Two of each type of accelerometer were available for this work. Both the Endevco and Dytran accelerometers incorporate integrated amplifier circuitry which converts the charge produced by the piezoelectric crystals into a voltage. This enables the accelerometers to be connected to their signal conditioning units using very long cables (sometimes greater than 50 m) with minimal distortion of the signals. This was verified during the research work by performing calibration checks using very short and very long cables and comparing the results. Any differences observed were negligible.

In order to measure floor responses, the accelerometers were mounted on levelled steel base plates and then placed onto the top surface of the floor structure under test. This arrangement is illustrated in Figure 3.15. Since the accelerations of the floors were expected to be less than 1 g, no attempt was made to fix firmly the accelerometers to the floors.

3.5.2 Data Acquisition Devices

In this work, three different data acquisition devices were utilised depending on the requirements of the testing. A typical instrumentation configuration, applicable to one of the modal tests described later, is illustrated in Figure 4.21.

3.5.2.1 Racal StorePlus VL Analogue Instrumentation Tape Recorder

The 16-channel Racal StorePlus VL tape recorder (Racal, 1994) was acquired to record simultaneously up to 14 analogue signals from the force and response transducers. The remaining two channels are required for storing time, event and flutter compensation data. The recording of analogue signals rather than digital is recommended by the DTA (1993a) so that they may be replayed following a return from site with different digital data acquisition parameters. This ensures that optimum digital sampling and processing of the data is performed.

3.5.2.2 DI-2200 Spectrum Analyser

A Diagnostic Instruments model DI-2200 dual channel spectrum analyser (DI, 1995) was utilised in EMA to sample digitally the force and response signals and to perform immediate calculation of FRFs. The FRF data were stored directly onto a PCMCIA memory card which was used to transfer data quickly to a notebook PC for subsequent processing.

An additional firmware application called Long Time Record (LTR) was purchased in the course of this work, which facilitated the use of the spectrum analyser for recording relatively long time histories. This was utilised mainly for response measurements as described in Section 3.7 of this thesis.

3.5.2.3 DAP 2400/e6 Data Acquisition Card

The DAP 2400/e6 data acquisition card is a 16-channel, 12-bit device enabling the fast digital sampling of analogue instrumentation signals. It also possesses two analogue output channels facilitating its use as a control signal source for the electrodynamic shaker. The data acquisition card was mounted in a Keithley Dac-Pac expansion box, which was connected to a notebook PC.

3.6 EMA Procedures

The practical implementation of EMA has, for mechanical and aeronautical engineering applications, become a mature technology which is commonly used in design. However, the application of this technology to civil engineering applications, where structures are typically orders of magnitude more massive, is fraught with unique difficulties and complications. The procedures used to perform EMA on the civil engineering structures tested in this work will be described here.

3.6.1 Overview of EMA Procedures

The EMA performed during this work was structured to follow pre-defined procedures to ensure that high quality data was acquired on site. This was of utmost importance since in most cases a return to site to repeat any substandard measurements would not have been possible. The guidelines provided by the UK Dynamic Testing Agency (DTA, 1993a) were followed as much as practicably possible. However, since these guidelines were written primarily for the mechanical and aeronautical engineering disciplines, some had to be ignored or modified due to the specifics involved in testing full scale civil engineering structures.

EMA procedures may be broken down into four phases, as follows (DTA, 1993a):

Phase 1: The 'preparatory phase' entails definition of the test objectives, performing some preliminary pre-test analysis, arranging the test logistics, preparing the structure and setting up the equipment following arrival on site.

Phase 2: The 'exploratory phase' entails performing preliminary measurements to determine the suitability of the structure for modal testing and to aid in the selection of data acquisition parameters.

Phase 3: The 'measurement phase' is the main data acquisition phase where all required FRF data are obtained.

Phase 4: The 'post-test analysis and modal parameter estimation phase' is normally performed following return from site and entails the determination of modal properties of the structure from the measured data, together with any other required analysis.

3.6.2 The Preparatory Phase

3.6.2.1 Definition of Test Objectives

The DTA (1993a) specify a number of levels of test depending on the intended use of the data. These range from Level 0 (only estimation of natural frequencies and damping) to Level 4 (high quality measurements for use in further analyses such as response prediction and modification assessment). For the purposes of this work, the main objective of the tests was to obtain the best quality modal test data possible so that the effects of access floors may clearly be identified, possibly through the use of FE model updating. Test Level 3 was therefore deemed to be applicable.

3.6.2.2 Pre-Test Structural Dynamic Analysis

Prior to performing EMA on site, it is very important to have some idea as to the likely dynamic properties of the structure. This information gives the test leader some understanding of the dynamic behaviour of the structure and aids in the selection of transducer, exciter and data acquisition centre locations (Flanigan & Hunt, 1993).

Therefore, for all of the structures investigated in this research, analytical FE models were developed prior to testing. The test grid was selected on the basis of these models, as were the reference accelerometer locations. The adequacy of the test grid not to suffer from spatial aliasing was determined by performing an auto-MAC analysis (Maia et al., 1997). The FE models also gave valuable information regarding the likely frequency ranges of interest, hence aiding in the initial selection of data acquisition parameters on site.

3.6.2.3 Checking and Packing of Equipment

The proper functioning of all equipment was checked prior to departure to the test site. Packing was performed with the aid of checklists to ensure that nothing was forgotten. Wherever possible, spare parts were taken for critical items of equipment should failure occur on site.

3.6.2.4 Test Logistics

Whilst the arranging of accommodation and transport for a site test may appear a trivial matter, it should nevertheless be given proper consideration. The writer was involved in a test in central London prior to this research in which five hours each day were spent travelling between the accommodation and the site. Clearly, this was not an ideal situation and the writer therefore was very careful regarding the selection of the accommodation for the testing performed in this research. However, this was particularly difficult when the testing was performed in London and there typically was no provision for car parking in hotels close to the site.

3.6.2.5 Preparation of Structure

Whenever site testing was being organised, the owners/managers of the test structure were instructed to remove any items of construction and other equipment, or building materials from the floor under test. Moreover, any artificial boundary conditions (e.g. temporary props) were instructed to be removed if possible. In addition to ensuring that the modal properties of the structures were not affected by such materials, the removal of loose attachments reduced the likelihood of the 'rattling' phenomenon occurring (DTA, 1993a).

3.6.2.6 Equipment Set-up

Following arrival on site, all equipment was set up as appropriate. Pre-prepared forms were utilised to identify precisely which items of equipment were used and which cables were used to connect them. This was to ensure that any faults which were identified following a return from site, through examination of the test data, could be rectified. The test grid was marked and a photographic and video survey of the structure was made so that there was a visual record of the condition of the structure at the time of the test.

3.6.3 The Exploratory Phase

The exploratory phase consisted of making a number of measurements to determine the suitability of the structure for modal testing and to determine the data acquisition parameters which would be utilised in the EMA. This exercise was also performed with the aid of a set of pre-prepared forms to ensure that the whole process was systematic and thorough. It consisted of a number of checks which are described in the remainder of this section.

3.6.3.1 Excitation/Response Check

The excitation/response check consisted of applying an excitation to a structure, and simultaneously measuring the excitation signal and the corresponding response of the structure with a sampling rate which would describe properly both signals. For hammer excitation, a sampling rate of 102400 samples/s was used whereas for shaker excitation, where the frequency content of the excitation was more closely controlled, a sampling rate of 512 samples/s was used. Measurements were made for both point mobility and transfer mobility between remote test points. Both the time domain signals and the corresponding spectra were examined visually for the following purposes:

- The signals should have looked reasonable to the experienced test personnel. For example, a hammer blow should last approximately up to 10 ms and have a characteristic 'half-sine wave' shape when applied using the softest hammer tip on a concrete floor surface. For the point mobility measurement, the response should start almost immediately whereas there is usually a small delay for remote transfer mobility due to the speed of wave propagation through the structure. For shaker excitation, the shape of the measured excitation signal should correlate well with that provided to the shaker amplifier. The frequency content and magnitude of the signals should also have looked reasonable. Any deviation from these observations, or the existence of other unexplained peculiarities, such as low frequency drifts, DC offset or sharp peaks in the excitation spectrum, which should have been fairly flat, would warrant further investigation.
- The high sampling rate gave an indication of the actual analogue voltages which may be expected in the transducer and signal conditioning electronics. This could not be checked adequately using lower sampling rates since the anti-aliasing filters, which remove high frequency components of a signal prior to analogue to digital conversion, tend to reduce the apparent magnitude of the signal. This indication of voltage range was then utilised in the setting of gain factors and sensitivities of the

signal conditioning electronics, the spectrum analyser and the analogue tape recorder.

- When using hammer excitation, there is a strong possibility for the accelerometer to 'jump' following the hammer impact. Such jumping would spoil measured FRFs and would be apparent from a visual examination of the time history. If observed, this would necessitate the reduction of the strength of the hammer blow to a level which would not cause the accelerometer to jump.
- Indications of loose transducer cables may be recognised from these time domain plots, particularly when aggravated by the motion of the hammer itself or the response of the structure.

3.6.3.2 Immediate Repeatability Check

The 'immediate' repeatability check consisted of measuring two nominally identical point mobility FRFs, one immediately after the other, using exactly the same equipment set-up. These two FRFs were then superimposed on the display of the spectrum analyser and, in theory, they should have been identical. In practice, small differences between the two FRFs, caused by experimental errors, would have been tolerable. However, large discrepancies may have indicated problems with the level of unmeasured extraneous excitation. In this case, the only two options available would be to increase the number of frequency domain averages to attempt to average out the effects of the extraneous excitation on the measurements, or to attempt to reduce the level of environmental noise. It is not usually practical to reduce the environmental noise and so the former option is usually taken.

However, since this check was usually the first time that FRFs were measured for any particular structure under test, it was normal for this check to be also used for experimentation with different data acquisition parameters to ensure the acquisition of good quality FRF data. The parameters which were typically investigated included:

1. the exponential window time constant,
2. the type, duration, frequency content and other parameters related to the excitation signal, and
3. trigger level and amount of pre-trigger used on the spectrum analyser.

To assist with the selection of the optimum data acquisition parameters, it was considered normal procedure to attempt to perform some SDOF curve fitting of some of the measured FRFs at this time. This was required to determine the 'processability' of the

data. If it was found that the data was difficult to process using these techniques, it was usually possible to improve the situation by changing one or more of the data acquisition parameters.

3.6.3.3 Homogeneity Check

The homogeneity check was the first of two checks aimed at checking the linearity of the structural behaviour. It consisted of measuring two consecutive point mobility FRFs, one with a high level of excitation and another with a relatively low level of excitation. ISO 7626 Part 5 (ISO, 1994) recommends that a factor of 10 is used between the magnitudes of the two excitation signals. However, for civil engineering structures it was noted that such a high factor generally was not possible since the low magnitude excitation resulted in a response which was completely obscured by vibrations caused by environmental noise. For this reason, a factor of approximately 2 was used instead.

Any significant discrepancies between the two measurements, other than those caused by the poorer signal-to-noise ratio of the low level excitation, would have indicated that the structure was not behaving as a linear system, a fundamental assumption when performing modal testing. If a floor structure was determined to behave non-linearly, corrective measures would have been limited to removing any furniture, partitions, access floors or other non-structural elements which may have introduced non-linearities into the structure. However, it is the experience of the writer that such modifications would also modify the dynamic behaviour of the structure and any subsequent measurements would not represent the behaviour of the structure in service. Since most structures are in any case weakly non-linear, this check was generally used only to indicate the degree of non-linearity which was subsequently treated as an experimental error.

3.6.3.4 Reciprocity Check

The reciprocity check was the second of the two linearity checks performed on the test structures, which was based on Maxwell's Reciprocity Theorem (Clough & Penzien, 1993). This theorem states that, for a linear structure, a transfer mobility FRF measured with the exciter at a point A and the response transducer at a point B will be identical to one measured with the response transducer at point A and the exciter at point B.

In practice, this check was performed by measuring two transfer mobility FRFs, swapping the locations of the exciter and the accelerometer between the two measurements. The FRFs were then compared on the screen of the spectrum analyser. Possible remedial measures in the case of large discrepancies being observed between the two measurements are the same as those presented for the homogeneity check presented in Section 3.6.3.3.

3.6.3.5 Coherence Function Check

The coherence function is defined as (DTA, 1993a):

$$\gamma^2(f) = \frac{G_{YX}G_{YX}^*}{G_{XX}G_{YY}} \quad \text{Equation 3.45}$$

and it defines the proportion of the response which is completely accounted for by a linear response to the measured excitation (DTA, 1993a). Values of coherence lie between 0 and 1, with a poor coherence indicating (Maia et al., 1997):

1. leakage errors in the estimation of the spectra,
2. non-linearities of the structure,
3. instrumentation noise on the force, response or on both channels, and/or
4. unmeasured extraneous excitation.

The coherence function check consisted of calculating the coherence function for two FRF measurements, one point mobility and one transfer mobility, using the spectrum analyser. The value of the coherence function in the regions of the modes of vibration of the structure was examined to ensure that it was close to unity.

For the measurements made in this work, a low value of the coherence function was typically caused by a high level of environmental noise. The first three of the possible causes of low coherence listed could normally be discounted because:

1. the acquisition time used in the measurements was selected to prevent leakage errors,
2. the possibility of non-linear behaviour of the structure was eliminated typically by satisfactory homogeneity and reciprocity checks, and
3. instrumentation noise on the excitation and response channels was typically many orders of magnitude lower than the excitation and response signals themselves.

Due to the 'noisy' nature of measurements made on civil engineering structures, values of coherence above about 0.8 were considered to be sufficient, although the DTA (1993a) prefers values higher than 0.9 for high quality measurements.

3.6.3.6 FRF Shape Check

Ewins (1995) and BS 6897 Part 2 (BSI, 1990) describe a number of preliminary visual checks which may be performed on measured FRF data to assess qualitatively its adequacy. Consequently, a point mobility FRF was measured, plotted using logarithmic scales on the spectrum analyser and examined to ensure that the following conditions were satisfied:

1. An anti-resonance should always exist between adjacent resonances.
2. There should be a negative phase shift through resonances and a positive phase shift through anti-resonances. For point mobility inertance FRFs, the value of phase should always be between 0 and -180 degrees.
3. For a grounded structure, which is invariably the case when testing prototype civil engineering structures, the region of the FRF at lower frequencies than the first mode of vibration should approximately represent the static stiffness behaviour of the structure.

3.6.3.7 End of Test Repeatability Check

The use of the 'end of test' FRF repeatability check was presented by Pimentel (1997). The purpose of this check was to measure an FRF following the end of a series of FRF measurements for comparison with an FRF measurement made prior to commencement of the series of measurements. Any significant differences between the two FRFs would have indicated possible problems with slowly varying phenomena, such as temperature variations affecting the modal properties of the structure or a slow variation in the amount of environmental noise.

3.6.4 The Measurement Phase

The measurement phase is the main data production phase of EMA. By this time, all necessary data acquisition parameters should have been chosen and any abnormalities in the equipment or structure should have been identified.

3.6.4.1 Typical 'Swipe' Procedure

Once the preliminary checks were completed, the reference accelerometers were placed into position on the structure and the exciter was moved to the first point. The test then proceeded by exciting the structure and recording the excitation and response data onto the analogue tape recorder for all channels, and onto the dual channel spectrum analyser. Assuming that no problems were observed, the exciter was then moved to the next test point and the procedure repeated. This procedure continued until all test points had been recorded. To simplify the terminology, this set of data will hereafter be termed a modal test 'swipe'.

A set of FRF measurements, corresponding to excitation at all test points in turn and response measurement at a single reference test point, forms a single row of the FRF matrix (Section 3.3.1). Theoretically, this provides enough data for estimation of all natural frequencies, modal damping ratios and mode shapes (Ewins, 1995). However, in practice, it is quite possible that the chosen response measurement location is close to or on a node of some modes of vibration of the test structure. This is likely to result in poor estimates of those modes of vibration or even a complete failure to identify them at all. For this reason, it is recommended (DTA, 1993a; Ewins, 1995) that as many rows of the FRF matrix are measured as is practicable and used in the subsequent parameter estimation.

3.6.4.2 Data Acquisition and Calculation of FRFs

For each excitation point in a typical swipe, the force signal and all response signals were stored on tape, in analogue form, using the Racal StorePlus VL instrumentation tape recorder. By recording the analogue signals, the measurement data could be resampled digitally using a variety of data acquisition parameters to improve the quality of the data analysis performed.

However, whilst on site, the force signal and one of the response signals were also sampled digitally using the DI-2200 spectrum analyser. This enabled immediate calculation of FRFs which could be monitored continuously to ensure that reasonable data were being acquired.

Following return from site, the remainder of the response channels were replayed from the tape recorder into the spectrum analyser, one at a time, to provide a full set of FRF data. All files were subsequently transferred to a PC for further parameter estimation.

3.6.5 The Post-test Analysis Phase

The post-test analysis phase consisted of processing the measured FRF data to extract the modal properties of the structure and presenting them in a meaningful manner.

3.6.5.1 Modal Parameter Estimation

The first step in modal parameter estimation was to calculate various Mode Indicator Functions (MIFs), which are functions which indicate frequencies at which modes of vibration may lie (Rades, 1994).

The next step in the modal parameter estimation was to perform SDOF or MDOF curve fitting on the measured FRF data. Whilst a number of algorithms had been implemented in MODENT (ICATS, 1997) and were therefore available to the writer, it was found that the most successful were the Circle-Fit and Line-Fit SDOF, and the Global MDOF algorithms. The first two were used to give some preliminary indications of likely modal parameters, whilst the last method served for performing the bulk of the estimations.

3.6.5.2 Modal Complexity Factors

Once the estimations had been made, the estimated mode shapes were examined using Modal Complexity Factors (MCFs) which were also implemented in the MODENT software (ICATS, 1997). Indications of high complexity may have indicated non-proportional damping in the structure or problems with the measurement or data analysis techniques (Imregun & Ewins, 1995). Three MCFs were utilised as follows:

- MCF1: Phase differences between consecutive coordinates are averaged and expressed as a percentage of the 'maximum' complexity defined by $360/N$, where N is the number of coordinates. Higher values of MCF1 indicate increasing complexity. As a consequence of how it was defined (Imregun & Ewins, 1995), it is possible for the value of MCF1 to be higher than 100%.
- MCF2: Mode shape coordinates are plotted as lines extending from an origin where their length is proportional to the mode shape coordinate magnitude and their angle is equal to the mode shape coordinate phase. MCF2 is defined as the area enclosed by the ends of these lines divided by the area of a circle with a radius equal to the maximum mode shape coordinate magnitude. This is normally expressed as a percentage where higher values of MCF2 indicate increasing complexity. By definition, all values are less than 100%.

- **MCF3:** This is similar to MCF1 except that the phase differences are weighted by the magnitude of the two neighbouring coordinates. Higher values of MCF3 indicate increasing complexity.

3.6.5.3 Presentation of Results

The modal properties estimated from the testing were natural frequencies, modal damping ratios, modal masses and mode shapes. The first three of these parameters were simply tabulated whereas still and animated graphical representations of the mode shapes were produced. Due to the large quantity of data generated, only a representative sample of the graphical data is included in this thesis.

3.7 Structural Response Measurement

Structural response measurement was described by Maia et al. (1997) as 'Operational Testing' and may be defined as being the measurement of the dynamic response of a structure to unquantifiable operational excitation. In the case of the office floors considered here, the relevant form of excitation is from their human occupants. To assess the possible benefits of access floors on vibration performance of office floors, the response of the floors was measured before and after the addition of access floors to quantify any possible reductions. The pedestrian excitation was strictly controlled so that one of the previously measured natural frequencies was excited.

3.7.1 Test Procedures

More specifically, the basic method of performing the pedestrian response testing was (Pavic & Reynolds, 1999):

- EMA was always performed prior to the pedestrian response tests to select the most onerous walking paths, pacing frequencies and transducer locations.
- The floors were instrumented with transducers positioned at the point(s) where maximum modal response was expected, as predicted from the measured mode shapes. The pedestrian was instructed as to which walking path to follow, and at which frequency controlled by means of a metronome.

- The pedestrian was instructed to start walking and continue for a pre-specified duration. The response of the floor was recorded using the DI-2200 spectrum analyser (with the LTR firmware installed) and the Racal StorePlus VL tape recorder.
- Response channels from the tape recorder not processed on site and were replayed and sampled following return from site. All data were then transferred to a PC for further processing.

3.7.2 Processing of the Pedestrian Response Test Data

Once digitally sampled, it was necessary to process the test data to obtain a parameter which would quantify the severity of the vibration response. For this purpose, it was decided to utilise the recommendations of ISO 2631 (ISO, 1997) as described in the following sub-sections.

3.7.2.1 Application of Frequency Weighting Curves

Prior to assessment of the severity of the vibration response, it is necessary to apply a frequency weighting to take account of the differing human perception of vibration at different frequencies. In the case of the application of ISO 2631:1997 to the office floors, the W_k frequency weighting curve was considered to be appropriate (Figure 3.16). In practice, this frequency weighting was performed using the commercial DATS signal processing software, and its modules which had been written at the request of the writer's research group (Mercer, 1997).

3.7.2.2 Calculation of RMS Acceleration

As stated in Section 2.2.4.4, a basic evaluation of the vibration response may be performed by calculating the weighted RMS acceleration, which may be done using equation 3.46:

$$a_w = \left[\frac{1}{T} \int_0^T a_w^2(t) dt \right]^{\frac{1}{2}} \quad \text{Equation 3.46}$$

This calculation is normally performed over the entire duration of a measurement of length T seconds.

3.7.2.3 Calculation of Running RMS Acceleration

A problem with the basic RMS method of assessment of vibration measurements is that it averages together periods of high and low response of the structure. For example, in buildings, periods with no pedestrian activity will tend to reduce the effects of periods of significant pedestrian activity. However, it may actually happen that the periods of high pedestrian activity are sufficient to cause annoyance to human occupants of the floors.

The 'running RMS' method utilises the concept of selecting an integration time for calculation of RMS accelerations which is chosen to be consistent with the application under consideration. Whilst the recommendation for this integration time given in ISO 2631:1997 is 1 second (for which the running RMS is defined as the Maximum Transient Vibration Value or MTVV), it is likely that that is more applicable to vibrations in vehicles. Eriksson (1994) suggested that a more reliable integration time for floors may be 10 s, a value that was also used by Pavic (1999) in the interests of standardisation of reporting. For this reason, the running RMS vibration responses reported in this thesis will also make use of the 10 s integration time.

3.7.2.4 Calculation of Vibration Dose Value

For comparison with the results of the RMS and running RMS values calculated from the pedestrian response tests, the vibration dose value (VDV) will also be evaluated for all measurements, as defined by equation 3.47.

$$\text{VDV} = \left\{ \int_0^T [a_w(t)]^4 dt \right\}^{\frac{1}{4}} \quad \text{Equation 3.47}$$

Since it is based on the fourth power of acceleration, it is more sensitive to peaks than the RMS acceleration methods (ISO, 1997) and it has been suggested that it is therefore more applicable to environments where there is intermittent vibration (Griffin, 1996).

3.8 Finite Element Model Correlation and Updating

FE model correlation (Maia et al., 1997) entails the application of visual and numerical techniques to determine the level of agreements and sources of discrepancies between the actual vibration behaviour of a structure and that predicted by an FE model of it. Some techniques simply give a value indicating the degree of correlation whereas others attempt to pinpoint the geometric position of the problem areas of the structure which cause discrepancies. Those that have been used in the course of this work are described in this section.

Taking the process one step further, FE model updating (Friswell & Mottershead, 1995) entails performing modifications to the original FE model, in a logical and systematic manner, in order that the degree of correlation between it and the test data is improved.

3.8.1 Techniques for FE Model Correlation

A simple starting point for correlating FE models with corresponding modal test data is by comparing the measured and calculated natural frequencies. If plotted on a chart with the measured natural frequency on the abscissa and the calculated natural frequency on the ordinate, perfect correlation would be indicated if all points trace a line at an angle of 45° . If a straight line is traced at an angle greater/lower than this, it would indicate that the FE model has too high/low global stiffness (or too low/high global mass). If the points do not trace out a straight line at all, then it is more likely that a local phenomenon (e.g. inappropriate idealisation of a local boundary condition or discontinuity) is to blame for the discrepancies (Ewins, 1995).

The next stage in performing a correlation may be to produce a static or animated display of the mode shapes from testing and analysis, preferably from the same viewpoint and to the same scale. This enables the analyst to recognise visually any discrepancies between the measured and calculated mode shapes. It is the writers experience that this tends to be quite insensitive and normally only blatant modelling inaccuracies are visible. A 2-D graph variation of this technique is to plot the modal amplitudes of the measured and calculated mode shapes against each other (Ewins, 1995). A perfectly correlated mode shape will trace out a straight line at 45° whereas deviations from a straight line indicate lack of correlation.

The Modal Assurance Criterion (MAC) quantifies the deviation from a straight line of a plot of the modal amplitudes. It is normally calculated for all experimental and analytical modes and presented in matrix form which may be calculated from equation 3.48.

$$\text{MAC}(\{\phi_x\}_i, \{\phi_A\}_j) = \frac{|\{\phi_x\}_i^T \{\phi_A^*\}_j|^2}{(\{\phi_x\}_i^T \{\phi_x^*\}_i)(\{\phi_A\}_j^T \{\phi_A^*\}_j)} \quad \text{Equation 3.48}$$

where i and j are the experimental and analytical mode numbers. Each element of the MAC matrix may take a scalar value between 0 and 1, with 0 indicating that mode shapes are completely linearly independent and 1 indicating that they are linearly dependent. In practice these extreme values are seldom obtained but it is recommended (DTA, 1993a) that values above about 0.9 may be taken to indicate a good correlation. However, for tests performed under difficult conditions, which is frequently the case with civil engineering structures, it may be necessary to accept lower values of MAC as indicating a good correlation between analytical and measured modes (NAFEMS, 1992b). Typically, it is the writer's experience that values above 0.8 indicate a reasonable correlation when testing civil engineering structures. These high values should, obviously, lie on the diagonal of the MAC matrix provided that all modes have been calculated and measured and that there is a good correlation between them. High values of MAC away from the diagonal tend to indicate possible problems with spatial aliasing (DTA, 1993a).

The final FE model correlation technique utilised in this work was the Coordinate Modal Assurance Criterion (COMAC), which is described as an error location technique (Lieven & Ewins, 1988). It measures the degree of correlation of each DOF averaged over a set of correlated mode pairs (CMPs) and is defined as:

$$\text{COMAC}(i) = \frac{\left(\sum_{j=1}^{n_{\text{CMP}}} |\phi_A(i, j) \phi_x^*(i, j)| \right)^2}{\sum_{j=1}^{n_{\text{CMP}}} |\phi_A(i, j)|^2 \sum_{j=1}^{n_{\text{CMP}}} |\phi_x(i, j)|^2} \quad \text{Equation 3.49}$$

where i is the test point under consideration and j is the number of the CMP. If a particular DOF underperforms in all CMPs, this will be picked up as a lower COMAC value and would warrant further investigation, either from the modelling or the testing side.

3.8.2 Finite Element Model Updating

Finite element model updating is a means by which analytical FE models of structures may be improved to correlate more closely with corresponding experimental data. This is normally done through the systematic and reasonable modification of uncertain modelling parameters.

It is possible to classify FE model updating techniques broadly into two groups, depending on the implementation of the technology. These are 'manual' and 'automatic'. Automatic FE model updating is a developing technology which makes use of software which implements quite complex algorithms for adjusting FE models so that they correlate better with the modal test data. However, automatic FE model updating techniques were not utilised in the course of this work.

Instead, the writer concentrated on the use of manual FE model updating techniques which basically consisted of using the correlation results to make carefully reasoned and logical adjustments to the FE model in order to improve its correlation with the test data. In many cases, this involved refinement of the FE model to simulate better details which were identified as being inappropriately or too crudely modelled initially. In other cases, it involved adjustment of the material properties of the structure within reasonable limits.

When performing such updating it is of paramount importance to ensure that there is a physical reason for updating any parameter or detail. Failure to do so may result in a well correlated FE model which has very little physical meaning.

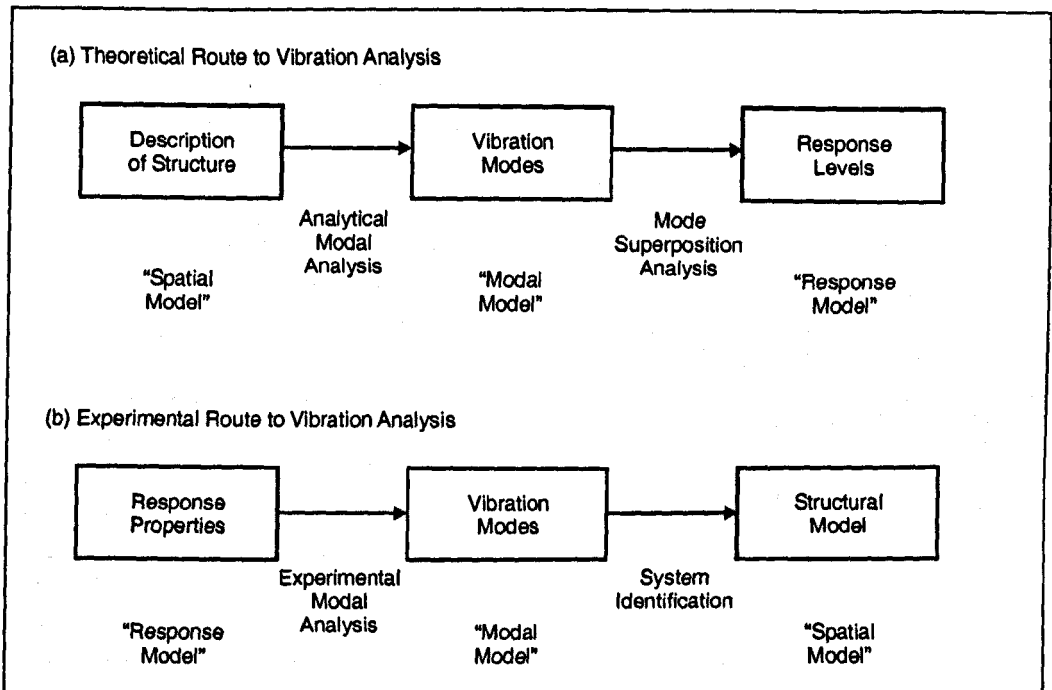


Figure 3.1: Theoretical and Experimental Routes to Vibration Analysis (after Ewins, 1995).

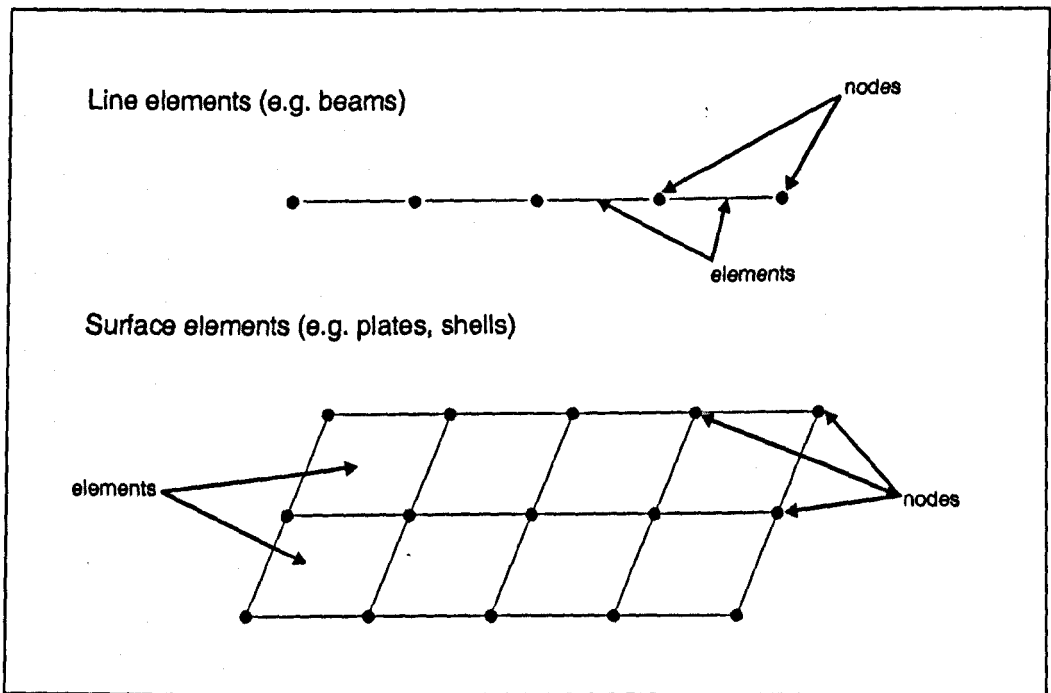


Figure 3.2: Elements and Nodes in Finite Element Analysis.

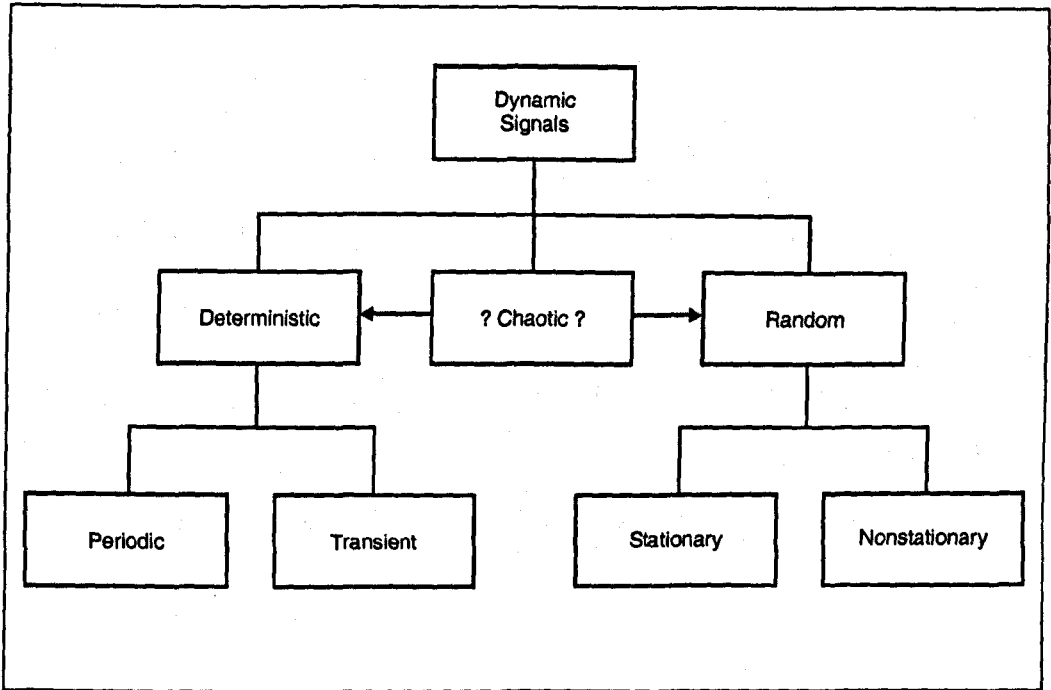


Figure 3.3: Classification of Dynamic Signals (after McConnell, 1995).

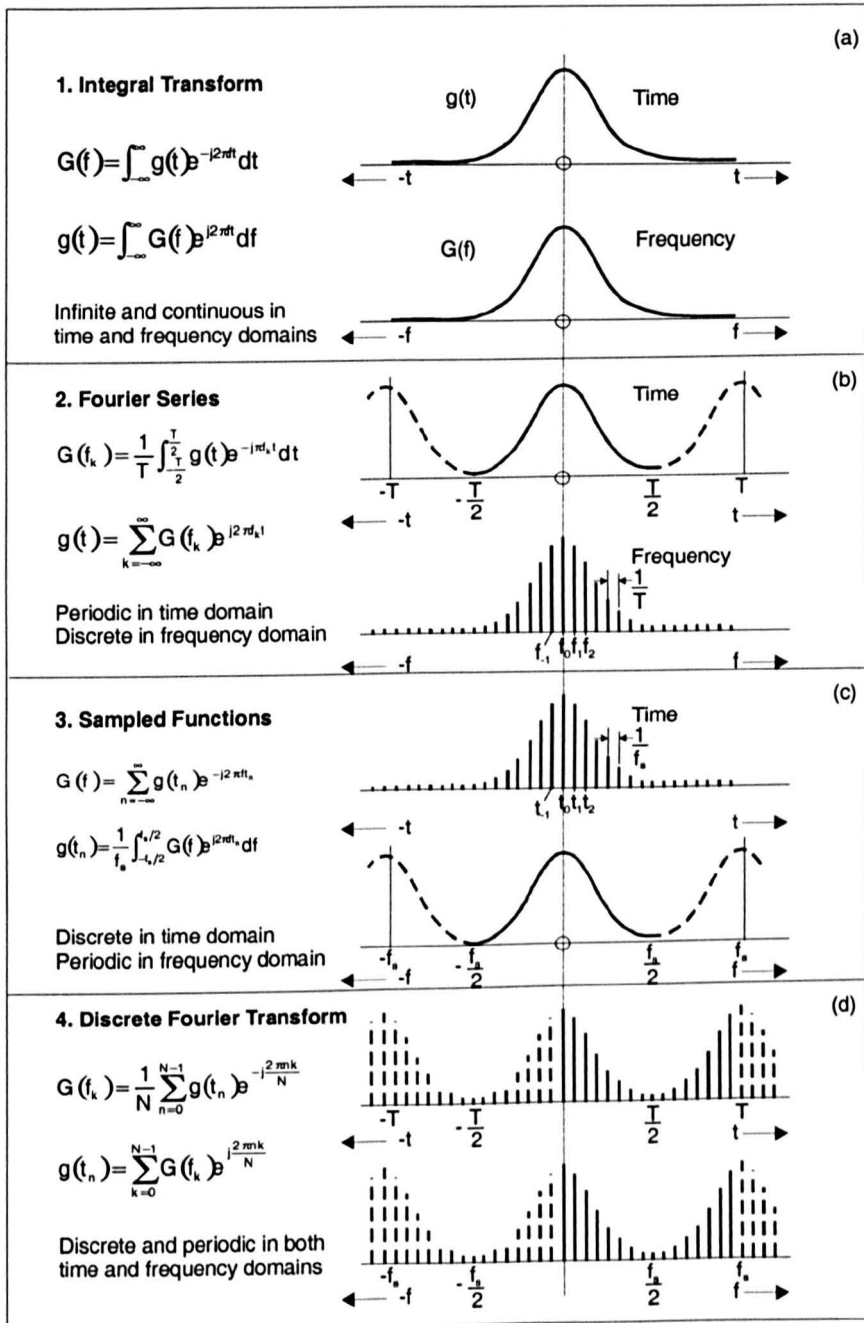


Figure 3.4: Various Forms of the Fourier Transform (after Randall, 1987).

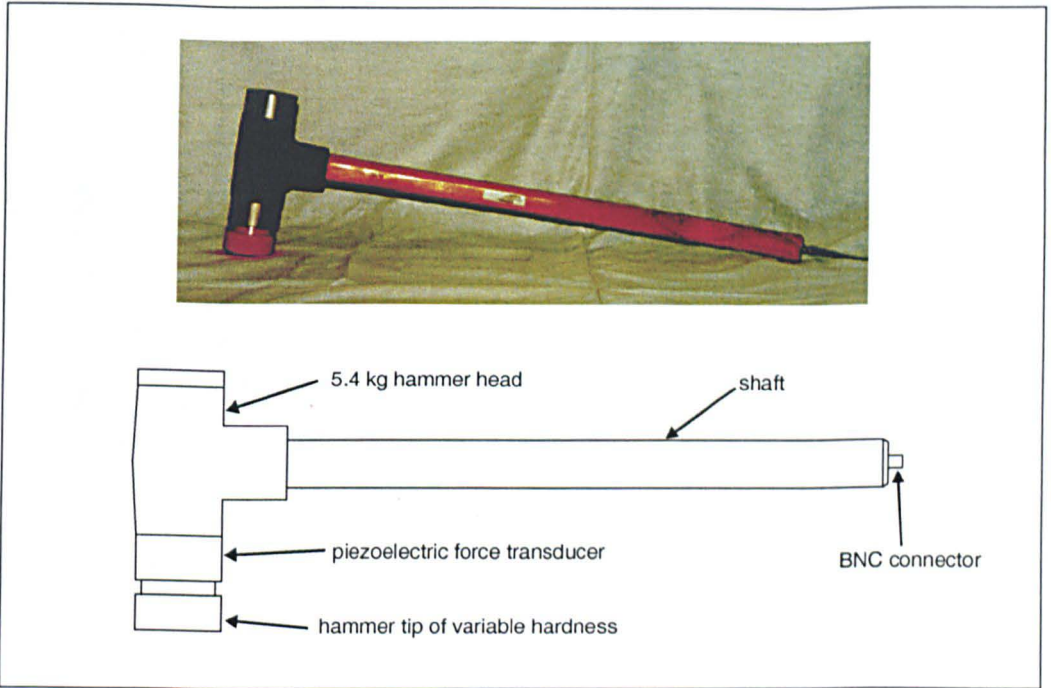


Figure 3.5: Photograph and Illustration of Dytran Model 5803A Instrumented Impact Hammer.

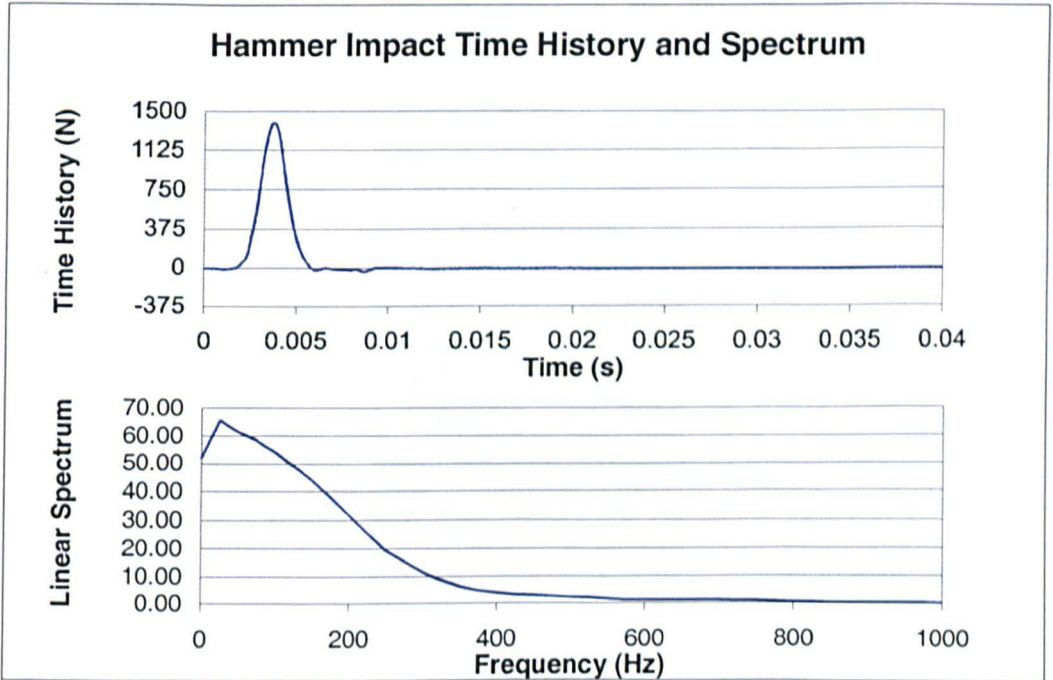


Figure 3.6: Hammer Impact Time History and Fourier Transform.

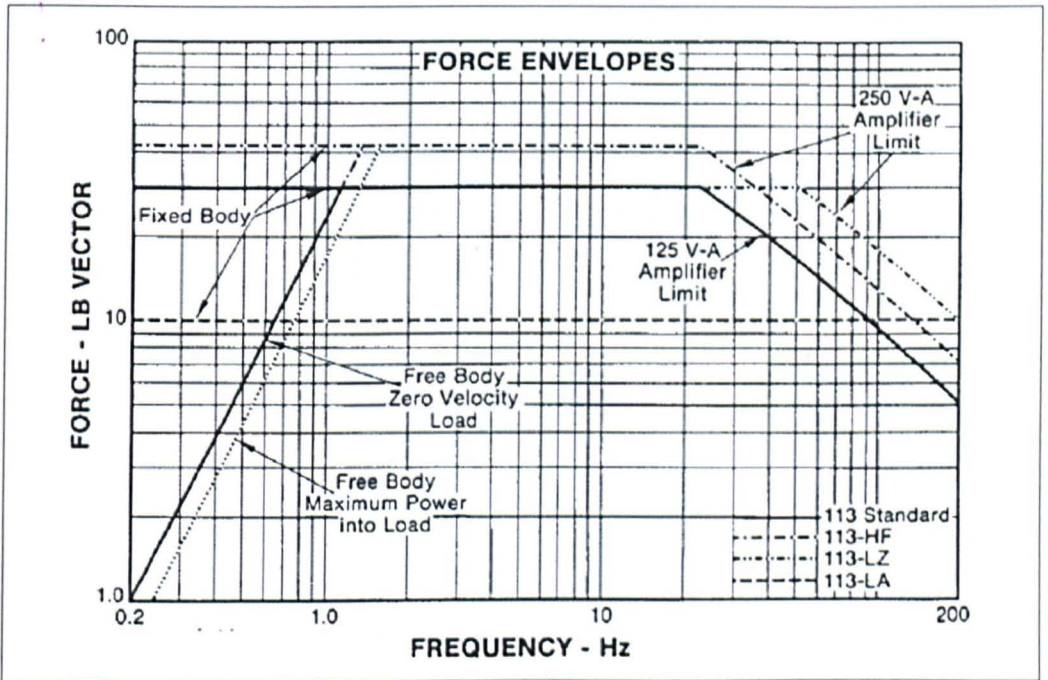


Figure 3.7: Force Envelope for the APS Dynamics Model 113 Electrodynamic Shaker (after APS, undated).

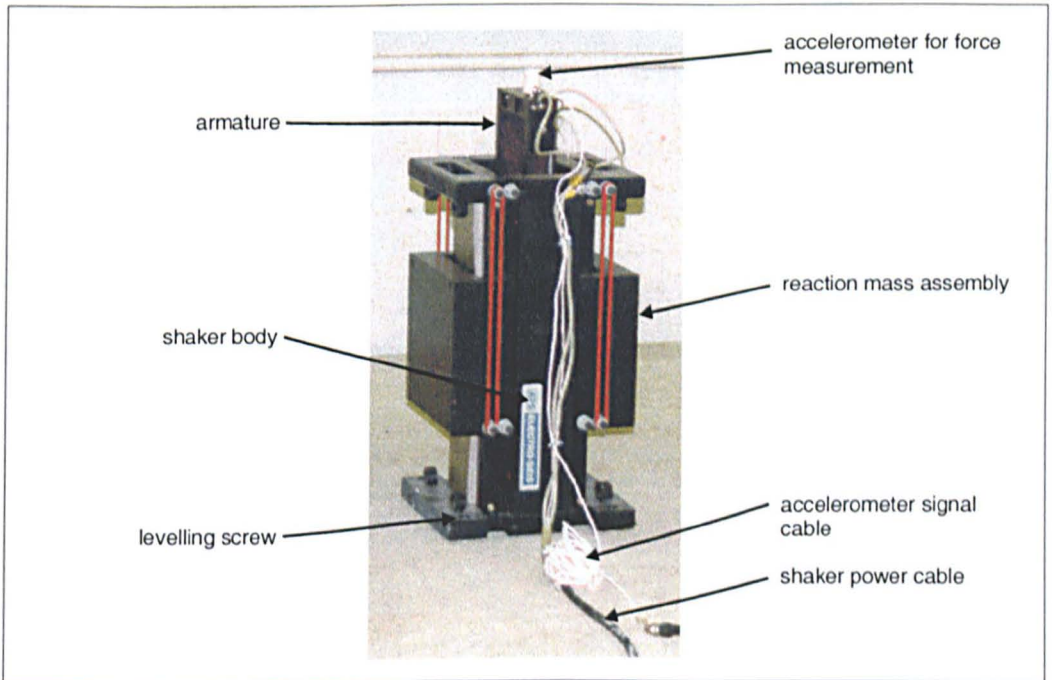


Figure 3.8: Photograph of Shaker in Free Armature Mode.

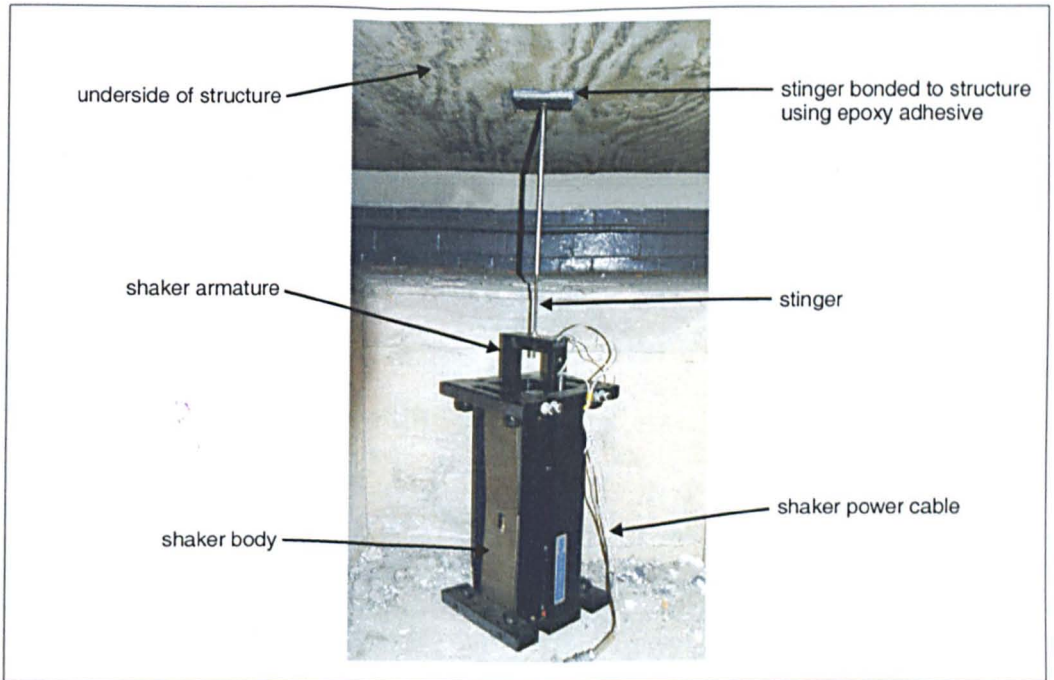


Figure 3.9: Photograph of Shaker in Fixed Armature Mode.

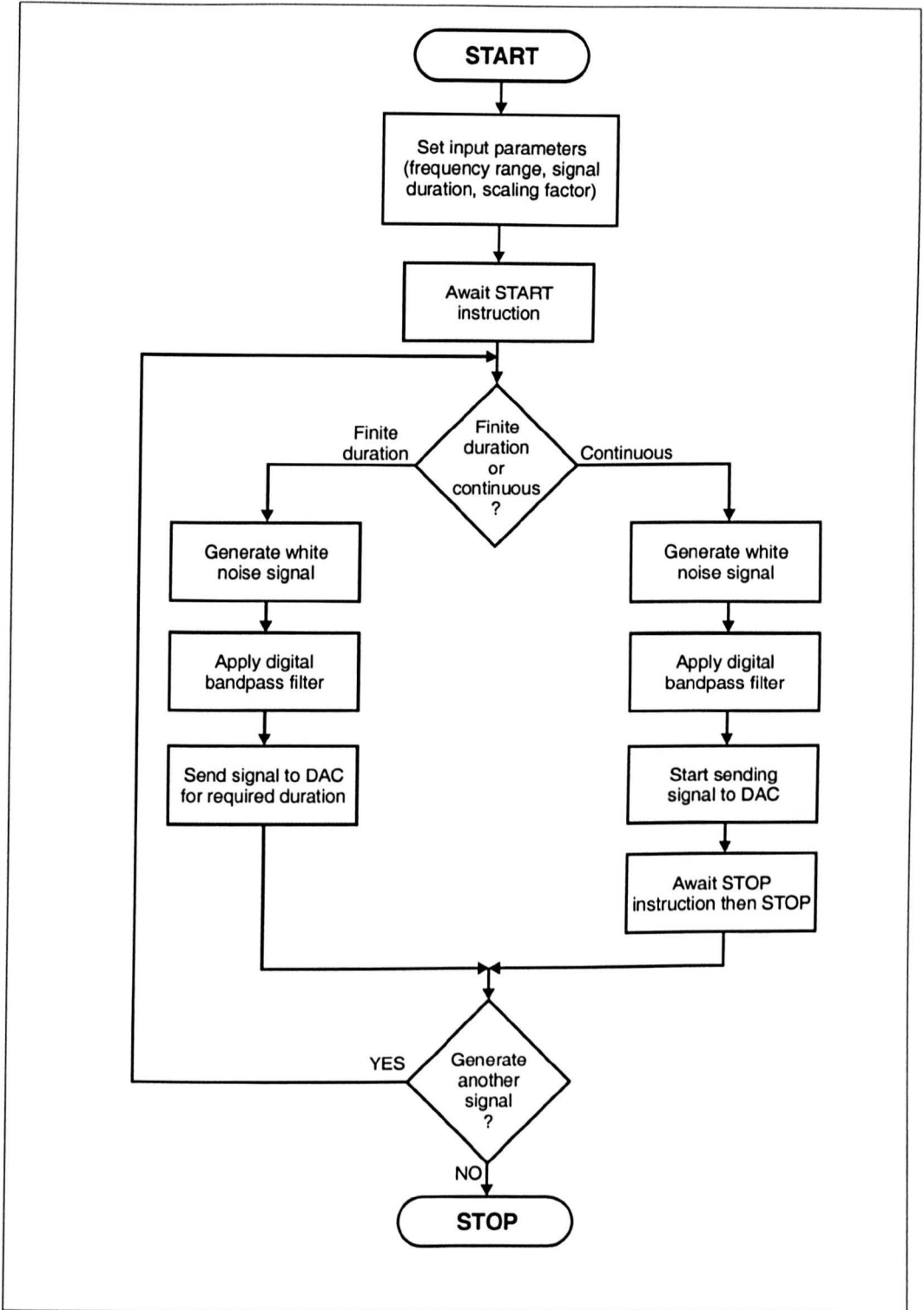


Figure 3.10: Flowchart for the RANGEN Computer Program.

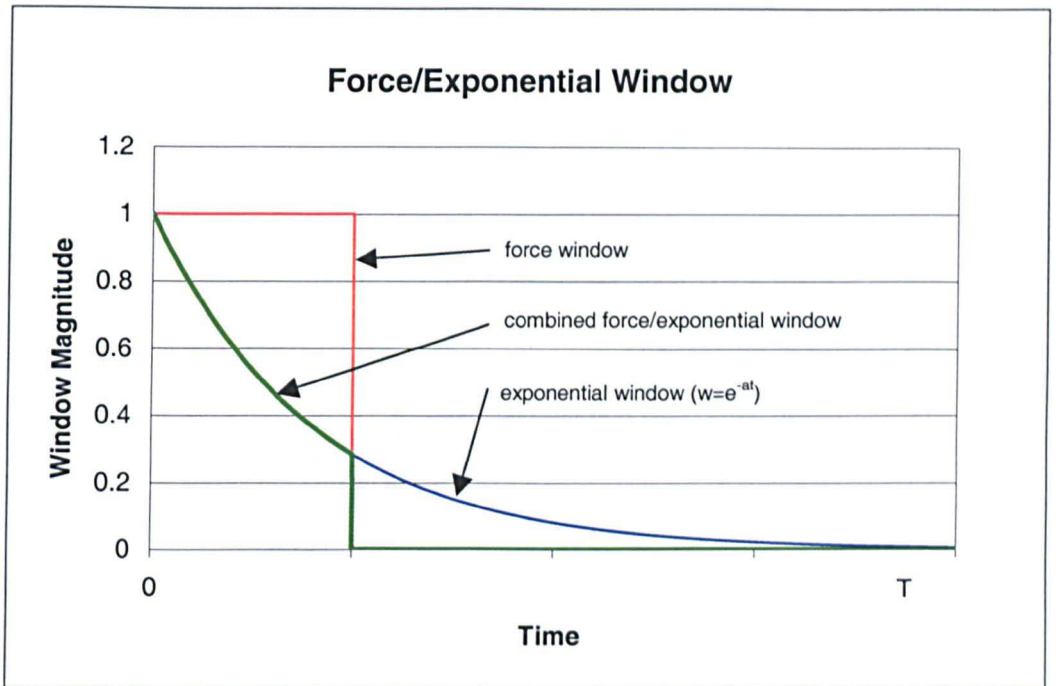


Figure 3.11: Exponential and Force Windows for EMA.

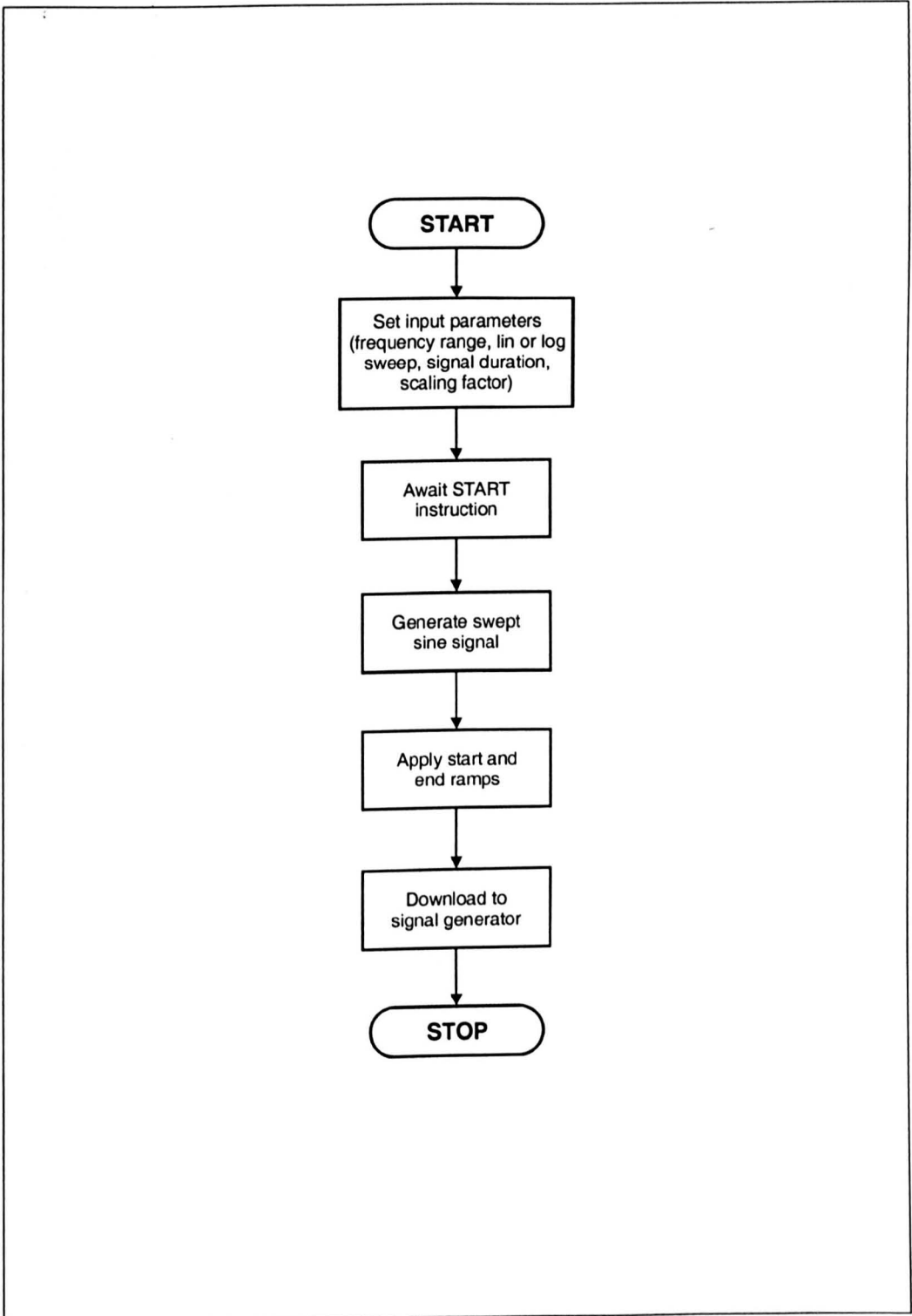


Figure 3.12: Flowchart for the SG_CTRL Computer Program.

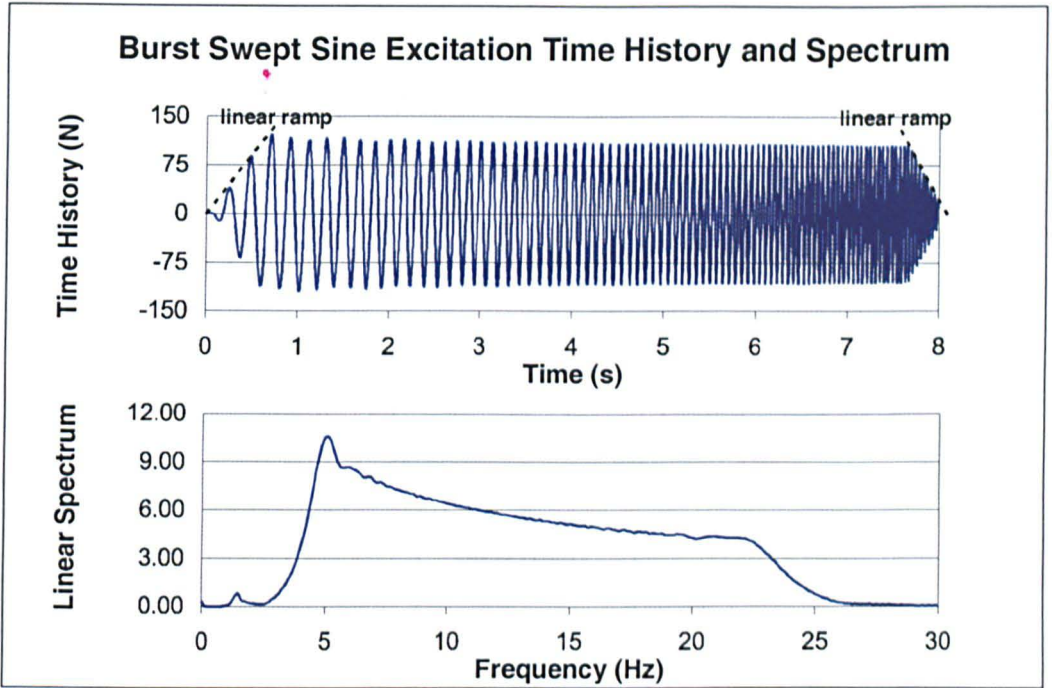


Figure 3.13: Logarithmic Burst Swept Sine Signal and Fourier Transform.

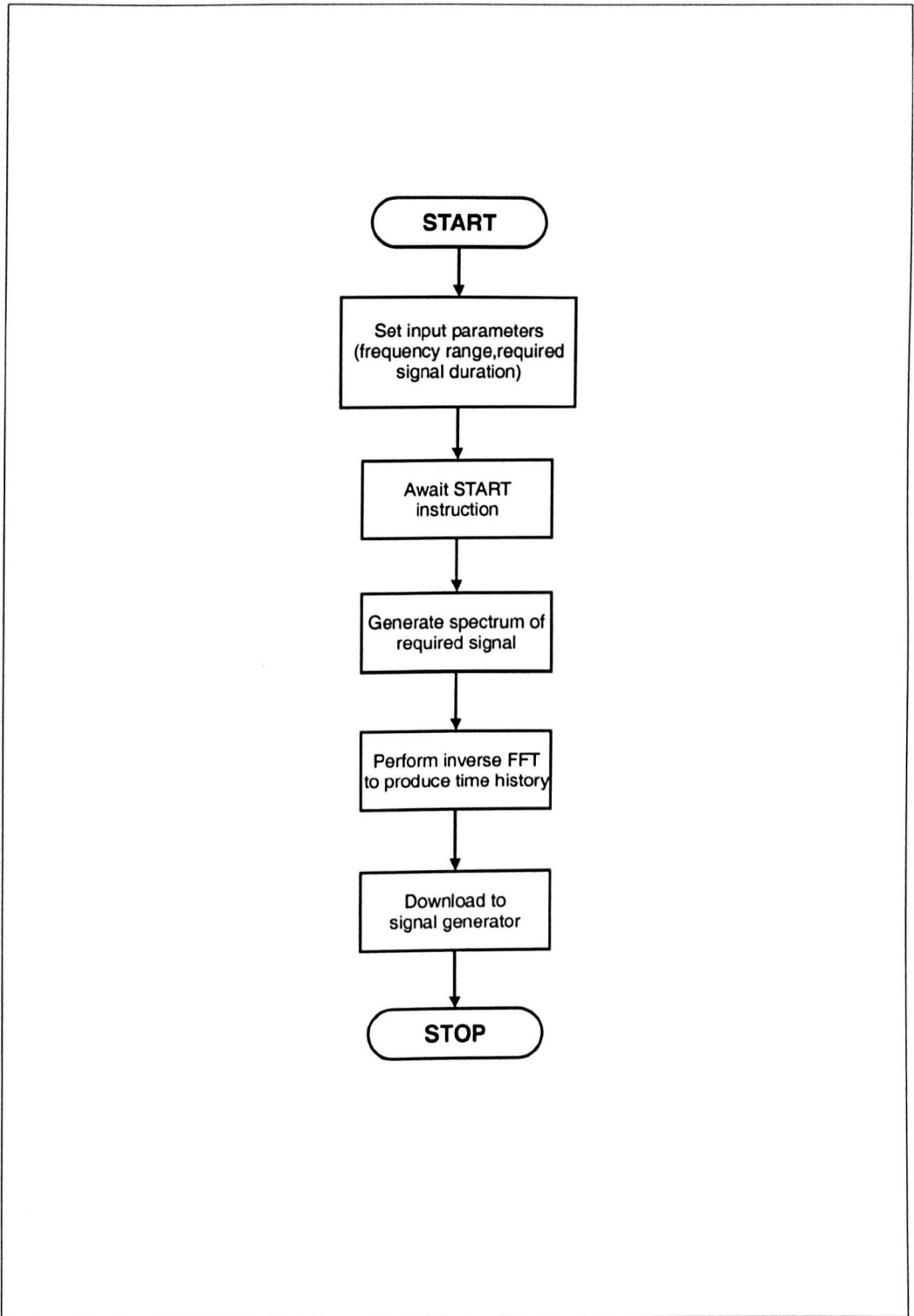


Figure 3.14: Flowchart for the PSEUDO Computer Program.

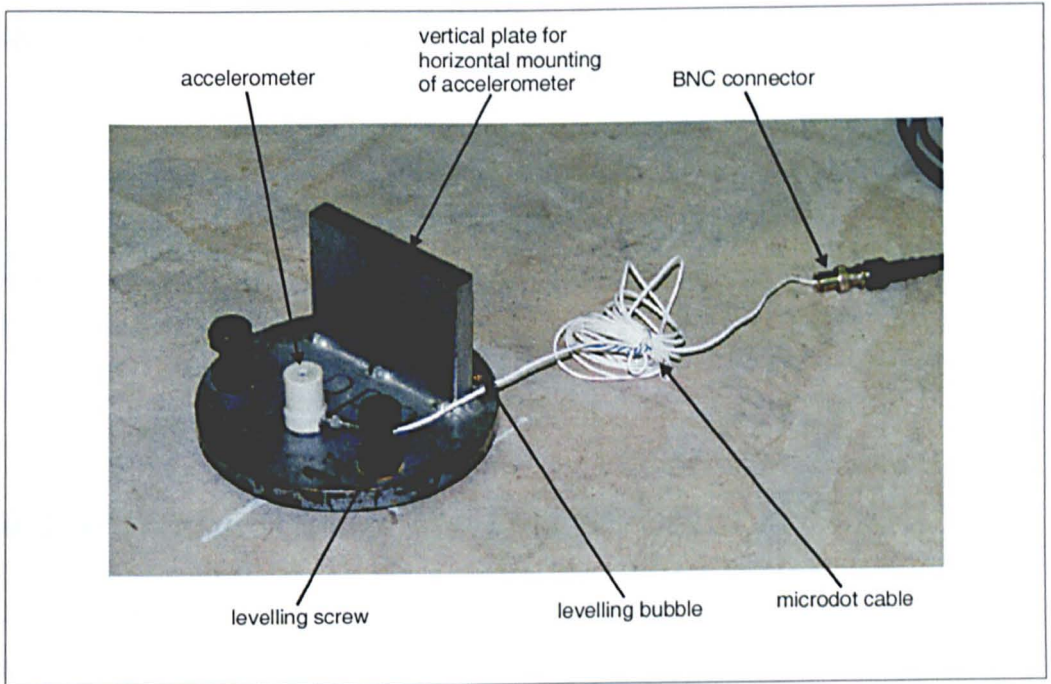


Figure 3.15: Mounting of the Response Transducers.

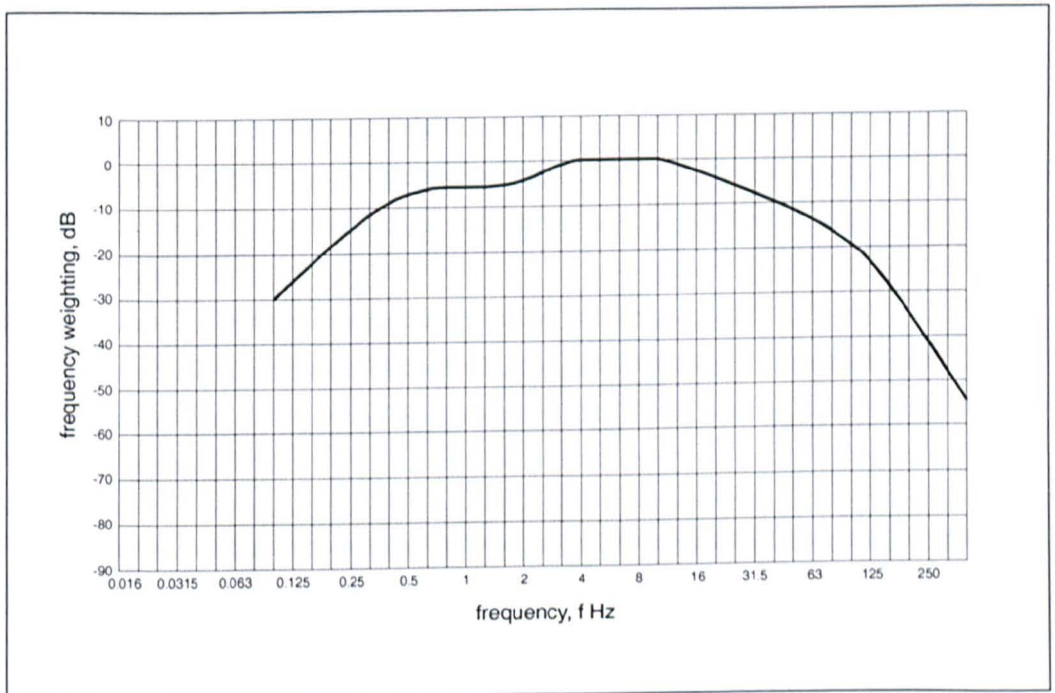


Figure 3.16: W_k Frequency Weighting Curve from ISO 2631 (after ISO 1997).

4 Experimental Work

This chapter contains analysis and test data from each of the structures tested in the course of this research. The structures were selected for the DETR Partners in Technology research contract (Pavic et al., 1998b) which provided resources for this work. Due to time and financial constraints, no attempt was made to test additional structures.

4.1 Introduction to the Test Structures

To examine the effects of access floors on them, three long-span concrete structures were dynamically tested and analysed. These structures, listed in the chronological order in which they were tested, were as follows:

1. Structure A: a ribbed post-tensioned concrete slab (31 m × 14.5 m main area) in a multi-storey office building in London. This was tested in two configurations; its bare condition and with an access floor installed.
2. Structure B: an experimental high strength concrete slab (15 m × 15 m) constructed and tested in laboratory conditions in London. This was tested in three configurations; its bare condition and with two different configurations of access floors installed.
3. Structure C: a purpose-built post-tensioned concrete slab strip (11.2 m × 2 m) constructed in a laboratory at the University of Sheffield. This was tested in 13 configurations; its bare condition and with 12 different configurations of access floors installed.

At first glance, it may seem peculiar to have tested these structures in order of reducing size, starting with a full-size real-life structure and ending with small-scale laboratory tests. It would, perhaps, have been more logical to perform the tests on Structure C first and to use these as an aid in the construction of the test plans for the two larger structures. For Structure B, it would have been possible to make an appropriate selection of access floor configuration (possibly the most beneficial) determined from the tests on Structure C. For both Structures A and B, it would have been possible to customise the selection of the modal and response tests to be performed, based on the results measured

on Structure C. However, the chronology of the tests on these structures was dictated strictly by their availability, which was not under the control of the writer.

In this chapter, a detailed account of the testing of the first structure (i.e. Structure A Configuration 1) will be presented. This account will illustrate procedures adopted, the results of preliminary checks and other test specifics. All subsequent rounds of tests were conducted in a similar manner. Therefore, they will be presented in less detail, focusing only on their most important test specifics and the results obtained.

4.2 Test Structure A (Configuration 1)

Test Structure A was the third floor of a multi-storey office building in central London, Configuration 1 being the bare floor prior to the installation of the access floors. The duration of this testing was five days, from 24 to 28 June 1996.

4.2.1 Description of the Structure

Figure 4.1 shows the configuration of Structure A, a post-tensioned and reinforced concrete floor slab. The main area of the floor comprised an approximately 31 m by 14.5 m ribbed post-tensioned concrete slab of overall depth 350 mm. This gives it a slenderness ratio of approximately 41, which can be considered to be quite slender (Khan & Williams, 1995). Within the main area, the 'ribbed' zone was constructed of a 110 mm thick slab acting integrally with 650 mm wide and 240 mm deep ribs at 1 m centres. The 'ring' zone consisted of a 350 mm deep solid slab cast around the 'ribbed' zone. The 'core' area consisted of a 300 mm deep reinforced concrete solid slab with various openings to permit the passage of stairs, lifts and services. The floor was supported around its perimeter by a system of monolithically cast in-situ beams, columns and shear walls, and it was connected to the lift shaft by means of a dowel connector, as shown in Figure 4.1.

At the time of these tests, the building was mostly clad, and electrical and mechanical services, suspended ceilings and core area partitions were installed. A photograph showing the bare floor configuration at the time of testing is presented in Figure 4.2.

4.2.2 Pre-Test Analysis

The purpose of a pre-test analysis is to give an indication of likely natural frequencies and mode shapes of the structure prior to testing. These are then used in selecting a test grid and accelerometer and exciter locations. In this case, a pre-test analysis was not strictly necessary since the previous EMA results obtained by Pavic (1999), for which the writer assisted in the testing, were available. Nevertheless, the writer deemed it to be prudent to develop an FE model of his own to aid numerical modelling skills and understanding of the likely behaviour of the structure.

The FE model developed initially according to normal civil engineering modelling practice was constructed first. This was presented in detail in Reynolds et al. (1998). In this model, pin supports were assumed at all floor supports, including the columns. This model gave quite a poor correlation with the EMA results presented by Pavic (1999) and so a more detailed pre-test FE model was constructed.

The final pre-test FE model constructed is illustrated in Figure 4.3. The ribbed area of the slab was modelled using orthotropic shell elements of equivalent depth 326 mm and the ring and core areas of the slab were modelled using isotropic shell elements of depth 350 mm and 300 mm respectively. All columns and edge beams were explicitly modelled using beam elements with offset capability. The modulus of elasticity taken for all elements was 38 kN/mm^2 , in accordance with the recommendation of Wyatt (1989). The modulus of elasticity of the ribbed slab in the direction perpendicular to that of the ribs was reduced to 9.8 % of the value in the direction of the ribs. This value was calculated to include the stiffness of the 110 mm deep slab together with a contribution due to the transverse stiffness of the wide ribs. The supporting columns were assumed to be 3.62 m long (the actual height between the floors above and below) and all six DOFs were constrained at their ends. The slab was also assumed to be pin supported at the locations of shear walls and at the connection to the lift shaft.

The first 10 modes of vibration calculated from this analysis are presented in Figure 4.4, in which it can be seen that the majority of the modes exhibit more bending in the less stiff direction of the slab, as expected. Because of the high degree of orthotropy, the natural frequencies at which these modes occurred were quite close (Pavic, 1999), with the first two natural frequencies (at 6.22 Hz and 6.31 Hz) only being separated by 0.09 Hz. The existence of such closely spaced modes serves to highlight the importance of using MDOF parameter estimation in EMA to ensure that such modes are properly estimated.

Based on this analysis, and experience of the previous testing on this structure (Pavic, 1999), the 76 point test grid illustrated in Figure 4.5 was chosen. This was the same grid as used by Pavic (1999), the reason for this being that the writer wanted to be able to compare directly the results if necessary. The auto-MAC calculated for this test grid is presented in Figure 4.6. The absence of off-diagonal shaded squares in this figure confirmed that there was unlikely to be a problem with spatial aliasing when using this test grid.

Finally, it was necessary to select the reference accelerometer locations to be used for the EMA with roving excitation. Experience gained whilst assisting with the tests performed by Pavic (1999) had shown that it had been difficult to estimate accurately modal parameters on this large structure unless the accelerometers were positioned quite close to the antinodes of the modes that were being measured. Since a maximum of 3 response accelerometers were available to the writer at the time of testing, it was decided to ensure that the first three modes of vibration were measured accurately. These were considered to be most important as they could be excited by pedestrian excitation. Therefore, the selection of test points 32, 35 and 38 as the response locations was made (Figure 4.5).

4.2.3 Testing Strategy

Prior to constructing a detailed test plan for this structure, a general list of test objectives was drawn up. These were.

- Since this was the first opportunity to utilise the newly-acquired electrodynamic shaker, a comparison between the modal test results produced for this form of excitation and the results produced by the previously used hammer impact excitation was required.
- The use of an electrodynamic shaker for modal test excitation opens up many possibilities regarding the excitation signal (Reynolds & Pavic, 1996). A comparison between the two methods of excitation that had been implemented at the time, namely burst swept sine and burst random, was required.
- High quality modal test results (DTA Level 3) were required as they were needed in the subsequent updating of an FE model of the structure, and for comparison with similar measurements to be made on the structure with access floors installed.
- High quality pedestrian response measurements were required for comparison with similar measurements to be made on the structure with access floors installed.

A detailed plan for this round of tests was constructed prior to departure, based on the likely durations of the various activities. Three EMA swipes were planned, two using shaker excitation (one with BR and one with BSS excitation) and one using the hammer.

4.2.4 Test Logistics

4.2.4.1 Test Personnel

Since it would not have been possible for a single person to perform this testing work alone, the writer enlisted the assistance of two fellow students from the University of Sheffield. Their responsibilities included assisting with transporting, setting up, operating and packing the test equipment, in addition to being the test subjects for the pedestrian response measurements.

4.2.4.2 Accommodation and Transport

For these tests, the decision was made to utilise accommodation situated within central London, close to the test structure. However, it was not possible to find accommodation with parking facilities. Therefore, it was decided that a combination of one-way hire vans (Sheffield to London and London to Sheffield) and taxis (in London) should be utilised according to the following procedure.

- A one-way hire van was collected from Sheffield and all necessary equipment was packed into it.
- The van was driven to the location of the accommodation and the majority of the equipment was unloaded. The van was then returned to the hire company.
- Following each day of testing, the test personnel travelled back to the accommodation using taxis, taking the most critical and expensive items of test equipment (the computers, the tape recorder and the spectrum analyser) back to the hotel with them. The remainder of the equipment had to be left on the site, which was deemed to be secure.
- At the start of each day of testing, the test personnel travelled back to the test structure by taxi, taking the equipment with them.
- Following the last day of testing, another one-way hire van was collected from the hire company in London. The equipment was loaded into the van which was then driven back to Sheffield.

These rather complicated travelling arrangements were highly successful in that less than one hour was spent travelling to and from the site each day, compared with the already mentioned five hours of travelling for the previous test.

4.2.5 On-Site Preparation

4.2.5.1 Preparation of Structure

During the negotiations for the testing, the main contractor in charge of the site was instructed to remove all items of equipment and materials from the test floor, prior to arrival of the test personnel on site. Following arrival, the test personnel made a photographic and video survey of the structure to ensure that any deviations from the construction drawings were recorded. Also, notes were taken regarding the configurations of the various non-structural elements which had already been installed. Following this, the test grid was marked on the floor using chalk.

4.2.5.2 Setting Up Equipment

It was necessary to select a location for the data acquisition centre which would be convenient, yet not interfere with the measurements. Since it was not practical to set it up on a separate part of the structure due to other site activities, it was decided to place it on the 'core' area of the floor structure, as shown in Figure 4.7. From the experience of previous tests on this structure (Pavic, 1999), the dynamic response of this area of the floor was known to be significantly lower than the main area. Therefore, the presence of the data acquisition equipment and the test personnel here would have only a minor effect of the dynamic behaviour of the whole floor.

4.2.6 EMA Using BSS Excitation: QA Checks

Once the structure and equipment had been prepared for the first EMA swipe, a full set of data quality assurance (QA) checks were performed in accordance with the procedures outlined in Section 3.6.3.

4.2.6.1 Excitation/Response Check

At this point in the testing, it was not known which shaker excitation signal would produce the best modal test data. For this reason, the excitation/response check was performed for both the BSS and the BR excitation.

Figure 4.8 shows a plot of the results from the excitation/response check performed at test point 32 of Structure A using BSS excitation. From this plot, the following observations can be made:

- The excitation signal measured by the transducer on the shaker (and therefore applied to the floor) was a faithful reproduction of the signal supplied to the shaker amplifier, and therefore did not indicate any problems. The magnitude of the excitation was also as expected.
- The shape and magnitude of the response was as expected and did not indicate any problems.
- The approximate level of vibrations caused by environmental noise relative to those caused by the excitation could be gauged. Whilst it is obviously of a significant magnitude, it was possible to average it out fairly quickly using the H_1 estimator.

Figure 4.9 contains a plot of the ASD of the excitation and response signals presented in Figure 4.8. The following observations may be made.

- The frequency content of the measured excitation signal was consistent with that generated and output to the shaker amplifier. It exhibited the classical shape of a logarithmic swept sine signal, with decreasing spectral amplitudes at higher frequencies.
- The shape of the response ASD looked reasonable, with a number of peaks indicating the frequencies of possible modes of vibration of the structure.

Figure 4.10 shows a plot of the excitation and response signals measured from the excitation/response check performed using BR excitation. Also, the ASDs of these signals are presented in Figure 4.11. These were deemed to be reasonable for the BR excitation under consideration. However, it is clear that, due to the random nature of the signal, a number of frequency domain averages would be required to produce a smoother excitation ASD.

Based upon the measurements presented in this section, it was thought that it was likely that the BSS excitation would produce better quality FRF measurements than the BR

excitation, due to the smooth nature of the excitation ASD. Therefore, the decision was made to use the BSS excitation for the first shaker swipe.

4.2.6.2 Immediate Repeatability Check

As explained in Section 3.6.3.2, the 'immediate repeatability' FRF check was used as an opportunity to investigate various data acquisition parameters and various excitation characteristics. The finally adopted data acquisition and excitation parameters, used in this EMA swipe, are presented in Table 4.1.

Table 4.1: Structure A (Configuration 1) - Data Acquisition Parameters Selected for First EMA Swipe Using BSS Excitation.

Parameter	Setting/Value
Acquisition Bandwidth	Zoom 3 - 23 Hz
Acquisition Duration	20 s
Frequency Resolution	0.05 Hz
No. of Frequency Domain Averages	5
Force Window Duration (% of Acquisition)	25%
Exponential Window Time Constant	0.25
Excitation Type	Logarithmic Burst Swept Sine
Excitation Duration	4 s
Excitation Frequency Limits	4 - 25 Hz

One very important observation made whilst performing this check was that there was a problem with using 8 s duration swept sine bursts. It was found that the FRF became very 'noisy' at the upper range of frequencies excited. This is illustrated clearly in Figure 4.12 which shows a comparison between FRFs measured using 4 s and 8 s durations of BSS excitation. It can be seen from this figure that the 'noise' effect was less pronounced for the 4 s excitation than for the 8 s excitation. It was therefore concluded that higher frequencies were being attenuated by the exponential window to such an extent that digitisation errors were becoming significant. Therefore, the shorter swept sine bursts of 4 s duration were utilised for all subsequent measurements.

Figure 4.13 shows the 'immediate repeatability' check performed by measuring a point mobility FRF at test point 32 using BSS excitation. It is clear that the two FRFs overlaid

well, although the second measurement was slightly more noisy than the first. It is likely that this was caused by the presence of an additional short term source of environmental noise whilst the second measurement was being made. However, it was not considered to be significant and, therefore, the immediate repeatability check did not highlight any significant problems with the test set-up, the data acquisition parameters or with the level of background noise.

However, in addition to overlaying the two measured FRFs and performing a visual inspection, a limited amount of SDOF curve fitting was performed using the ICATS (1997) suite of modal parameter estimation software. The purpose of this was to check the processability of the measured data. A typical circle fit performed on the first peak of this measurement is presented in Figure 4.14. As can be seen from this figure, it was possible to process the measured data quite easily, indicating that there was unlikely to be significant problems when processing the data for the entire swipe.

4.2.6.3 Homogeneity Check

For the homogeneity check, a factor of 2 was utilised between the magnitude of the high- and the low-level excitation. The results from this check, performed when measuring the point mobility FRF at test point 32, are shown in Figure 4.15. It is clear that the measurement made using the low-level excitation is significantly more 'noisy' than the measurement made using high-level excitation. This would be expected and is common for civil engineering structures. Figure 4.15 also indicates that the frequency and approximate magnitude of the peaks corresponding to the modes of vibration of the structure are the same for both measurements, indicating that any non-linear behaviour of the structure was likely to be insignificant.

4.2.6.4 Reciprocity Check

The reciprocity check was performed for this structure by measuring transfer mobility FRFs between points 32 and 38, and is presented in Figure 4.16. It can be seen that there are some small discrepancies between the two FRFs measured in this check. These are attributed to the effects of environmental noise which can be significant, especially on large civil engineering structures. In this case, the two FRFs were considered to be sufficiently similar so as to not be a cause for concern with regard to the linearity of the structure.

4.2.6.5 Coherence Function Check

Figures 4.17 and 4.18 indicate the point mobility (at point 32) and transfer mobility (between points 32 and 38) checks of coherence function, respectively. It can clearly be seen that the values of both coherence functions were above 0.9 at all FRF peaks corresponding to resonances of the structure. This was deemed to be satisfactory (Section 3.6.3.5).

4.2.6.6 FRF Shape Check

A point mobility FRF measurement was made and plotted on the spectrum analyser using log-log scales (Figure 4.19). It can clearly be seen that all three of the requirements stated in Section 3.6.3.6 are satisfied.

4.2.6.7 End-Of-Test Repeatability Check

Following the end of the swipe for which these QA checks were being performed, the end of test repeatability FRF measurement was performed and compared with the same FRF measurement made at the beginning of the test (Figure 4.20). There is a very good correlation between the two measurements, with both the magnitude and phase plots overlaying very well. However, there was a slight discrepancy between the two measurements in the vicinity of the second mode of vibration, which had a higher peak for the end of test measurement than for the initial measurement. It is possible that this was the result of the shaker and/or response accelerometer not being positioned in exactly the same location for the post-swipe measurement as for the pre-swipe measurement. However, since the difference was small, it was not expected to pose any significant problems for the subsequent data analysis and modal parameter estimation.

4.2.7 EMA Using BSS Excitation: Main Swipe

Following the satisfactory preliminary data quality assurance checks, the main data collection exercise, i.e. a full swipe, was performed.

4.2.7.1 Swipe Details and Procedure

By the time this point in the testing schedule had been reached, the writer had already decided on details such as the test grid, the accelerometer locations and the excitation

and data acquisition parameters. For this particular swipe, the test grid is illustrated in Figure 4.5, the excitation and data acquisition parameters are indicated in Table 4.1 and the accelerometer locations are indicated in Table 4.2 below.

Table 4.2: Structure A (Configuration 1) - Accelerometer Locations and Instrumentation Channels Used for BSS Swipe.

Transducer ID	Location	DI-2200 Channel	Racal Channel
A1	Roving Shaker	1	3
A2	Test Point 32	2	4
A3	Test Point 35	---	6
A4	Test Point 38	---	7

As can be seen from Table 4.2, only the excitation transducer and one of the response accelerometers could be attached to the DI-2200 spectrum analyser since it was only a dual-channel device. However, in accordance with the general instrumentation strategy outlined in Section 3.5, all accelerometers were connected to the Racal StorePlus VL tape recorder for playback and further analysis following return from site. This included accelerometer channels already monitored by the spectrum analyser. A schematic illustration of the instrumentation system utilised is presented in Figure 4.21.

Once the accelerometers had been positioned on the structure and levelled, the shaker was positioned at the first test point. The FRF was measured for this point and stored on the spectrum analyser. The development of the FRF was examined carefully to ensure that it was not being spoiled by environmental noise. The analogue transducer signals were also stored on the tape recorder. The shaker was then moved to each test point in turn and this procedure was repeated.

To ensure that the data being acquired was of usable quality, some limited MDOF parameter estimation was performed on site using a notebook PC and the ICATS software.

4.2.7.2 Adjustment of Testing Schedule Due to Site Noise

The timing of the first modal test swipe for this structure was such that the first 22 FRFs were measured during the evening of the first day of testing, after all normal site activity had ceased. When the test personnel arrived back on site the following morning, there

was a great deal of noisy site activity in progress, as expected. This resulted in clearly much poorer modal test results, as illustrated in the immediate repeatability check for a transfer mobility measurement between points 23 and 32 presented in Figure 4.22.

Whilst it may have been possible to continue the swipe under these conditions and accept that the acquired data would have been of a poorer quality, it was clearly desirable to perform the remainder of the tests under the quiet conditions experienced the previous evening. For this reason, the writer obtained permission for the remainder of the tests to be performed during the evenings, rather than during the day as had originally been planned.

4.2.7.3 Reduction of the Test Grid for Future Modal Test Swipes

Whilst performing the modal test swipe, it was noticed that FRFs measured at test points around the perimeter of the main area and in the core area were quite unstable (i.e. they changed significantly between subsequent averages). It was hypothesised that this was the result of insufficient excitation at these points, which corresponded to stiff locations on the structure. As a result, the vibrations caused by the controlled excitation were being overwhelmed by the vibrations caused by environmental noise.

To prove or disprove this hypothesis, it was decided to make a number of measurements of coherence at some of these points. A typical coherence measurement for a transfer mobility FRF between stiff point 29 and point 32 is presented in Figure 4.23. It can be seen that the values of coherence are low, even where there appear to be peaks corresponding to modes of vibration of the structure (compare this with good quality coherence functions shown in Figures 4.17 and 4.18). This indicates that the vibrations measured by the accelerometers were uncorrelated with the excitation and were most likely caused by environmental noise and not by the shaker excitation.

For this reason, it was decided that in all future modal test swipes on this structure, test points around the perimeter of the 'main area' of the floor and in the 'core area' would be omitted. This more than halved the number of test points from 76 to 33, and they are represented as red crosses in Figure 4.5.

4.2.7.4 Playback of Data from Analogue Tape Recorder

The transducer signals produced by all of the transducers, including those sampled on site using the spectrum analyser, were recorded using the Racal StorePlus VL analogue

tape recorder. After replaying and processing these signals, it was found that, provided all scaling factors had properly been accounted for, the FRFs generated from the replayed analogue data were almost identical to the FRFs measured directly on site. This is illustrated in Figure 4.24 where two FRFs, one measured directly on site and one replayed from tape are overlaid. Such checks on the quality of the replayed data gave the writer good confidence in the ability of the tape recorder to faithfully replicate the transducer signals following a return from site.

4.2.7.5 Modal Parameter Estimation

Following data acquisition, the modal test data was transferred to a PC in the form of Universal File Format (UFF) Frequency Response Function (FRF) files (Spectral Dynamics, 1994). These files were imported into the ICATS suite of modal parameter estimation software for analysis.

The first stage of the modal parameter estimation was the computation of a Mode Indicator Function (MIF) for use as an indication of the frequencies of possible measured modes of vibration (Rades, 1994). The Complex MIF for the BSS swipe, calculated as a summation of the squares of all measured FRFs (Equation 4.1), is presented in Figure 4.25.

$$\text{MIF}_{\text{complex}} = \sum [H_{i,j}(\omega)]^2 \quad \text{Equation 4.1}$$

Having obtained an indication of the frequencies of possible modes of vibration, the Global method of modal parameter estimation (Fillod et al., 1985), as implemented in the ICATS software (ICATS, 1997), was utilised for estimation of the modal parameters of the structure. A screenshot from this analysis process, presented in Figure 4.26, shows a typical curve-fit for the first two modes of vibration. The results (natural frequencies, modal damping ratios and mode shapes) from the modal parameter estimation for this FRF swipe are presented in Figure 4.27. Note that, due to the placement of the reference accelerometer, not all modes of vibration were estimated from this swipe alone.

This modal parameter estimation procedure was repeated for all of the datasets replayed from tape following return from site.

4.2.8 EMA Using BR Excitation: QA Checks

EMA was also performed on this structure using BR excitation, as described in Section 3.4.4.2. Once again, a full set of data quality assurance checks was performed to ensure the acquisition of good quality data. However, only a limited number of these checks are illustrated here in the interests of brevity.

4.2.8.1 Excitation/Response Check

The excitation/response check had already been performed as part of the previous shaker swipe and is described in Section 4.2.6.1. The time and frequency domain plots from this check are displayed in Figures 4.10 and 4.11 respectively.

4.2.8.2 Immediate Repeatability Check

The immediate repeatability check is presented in Figure 4.28. As can be seen, the two FRFs measured were very similar and it was assumed from this check that the effects of background noise were small. The excitation and data acquisition parameters selected in the course of performing this check are presented in Table 4.3.

Table 4.3: Structure A (Configuration 1) - Data Acquisition Parameters for Immediate Repeatability Check Using BR Excitation.

Parameter	Setting/Value
Acquisition Bandwidth	Zoom 3 - 23 Hz
Acquisition Duration	20 s
Frequency Resolution	0.05 Hz
No. of Frequency Domain Averages	7
Force Window Duration (% of Acquisition)	45%
Exponential Window Time Constant	0.35
Excitation Type	Band Limited Burst Random
Excitation Duration	8 s
Excitation Frequency Limits	4 - 25 Hz

Since BR excitation was not adversely affected by the exponential window in the same way as the BSS excitation, it was possible to utilise longer excitation signals. This

would be expected to improve the quality of the measured FRFs due to the improved signal-to-noise ratio.

4.2.8.3 Homogeneity Check

The homogeneity check is presented in Figure 4.29. Similar to the homogeneity check performed using BSS shaker excitation (Section 4.2.6.3), the FRF measured using low-level excitation was noisier than that measured using high-level excitation, although the correlation between the two measurements was good.

4.2.9 EMA Using BR Excitation: Main Swipe

A swipe of 33 points was performed using the data acquisition parameters selection in Table 4.3. The swipe procedure and accelerometer locations were identical to those described for BSS excitation, with the obvious exception of the excitation signal itself.

The complex MIF (Rades, 1994) calculated for the FRF dataset sampled on site (i.e. accelerometer at Test Point 32), presented in Figure 4.30, is similar to that calculated from the FRFs measured using BSS excitation (Figure 4.25). This would be expected if both forms of excitation were producing the same results, as they should, and served as an indication that the data that had been collected were of good quality. The remainder of the modal parameter estimation was performed in the same manner as described in Section 4.2.7.5 for BSS excitation, and the results are presented in Figure 4.31.

4.2.10 Comparison of BSS Versus BR Shaker Excitation for EMA

In order to assess the difference in quality of the modal test data measured using BSS shaker excitation and BR shaker excitation, a comparison of the two sets of data was required. To perform such a comparison, the following measures were utilised:

1. a visual comparison of point and transfer mobility FRFs (modulus and phase plots),
2. a comparison of the estimated modal parameters, particularly mode shapes, and
3. a visual and numerical comparison of the MCFs.

Firstly, by examining the point and transfer mobility FRFs presented in Figures 4.32 and 4.33 respectively it can be seen that at frequencies below approximately 11 Hz, the FRFs

measured using both forms of excitation are of similar quality. The peaks corresponding to modes of vibration on the BSS FRF are slightly larger in magnitude than those on the BR FRF due to the difference in the time constant of the exponential window utilised in the FRF measurements (Tables 4.1 and 4.3). However, above approximately 11 Hz, the FRF measured using BSS excitation is more 'noisy' than that measured using BR excitation, for the reasons already discussed in Section 4.2.6.2.

Secondly, an examination of the mode shapes and MCFs for the first three modes of vibration estimated from the measured FRF data (Figure 4.34) shows little difference between the two sets of data.

Based on these comparisons, it was decided to use BR excitation in future modal tests on this structure since it would not be necessary to consider the detrimental effects of the exponential window on the upper range of excitation frequencies. In addition, because of the manner in which the different excitation signals were generated, as described in Chapter 3, the BR excitation was found to be more convenient than the BSS excitation on site.

4.2.11 EMA Using Hammer Impact Excitation: QA Checks

A full set of data quality assurance checks was performed using hammer impact excitation using the procedures outlined in Section 3.6.3.

4.2.11.1 Fast Sampling Excitation/Response Check

Figures 4.35 and 4.36 present the excitation/response check performed for point and transfer mobility respectively, using a fast sampling rate of 102400 samples/s. The point mobility measurement was performed at test point 32 and the transfer mobility measurement was performed with excitation at test point 38 and the response at test point 32.

The results of this check were used to ensure that the hammer blow and structural response looked reasonable and to examine the magnitude of the voltages produced by the transducers. If the voltage produced by the hammer was in excess of the maximum specified in the manufacturer's documentation, then the strength of the hammer blow would have required adjustment. Also, if the structural response exceeded 1 g

(9.81 m/s^2) then the accelerometer would have required physical fastening to the structure, rather than simply being placed onto the surface of the floor.

4.2.11.2 Slow Sampling Excitation/Response Check

Figures 4.37 and 4.38 present the time histories and transient ASDs, respectively, of the hammer excitation and structural response measured using a sampling rate of 512 samples/s. This sampling rate was used to assess the shapes of the input and output signals in the time and frequency domains when a low sampling rate was used. This was required to determine the length of the hammer blow after anti-aliasing (AA) filtering so that the duration of the force window could be set appropriately to include 'ringing' effects caused by AA filtering.

It is interesting to observe from Figure 4.38 that the ASDs are quite 'spiky', particularly for the excitation signal. This was due to a combination of a poor signal to noise ratio for both signals and leakage, which was exaggerated because of the very low energy content of the excitation.

4.2.11.3 Immediate Repeatability Check

The immediate repeatability check is presented Figure 4.39. As a result of experimentation with data acquisition parameters in the course of performing this check, the data acquisition parameters presented in Table 4.4 were selected for the main hammer impact swipe.

Table 4.4: Structure A (Configuration 1) - Data Acquisition Parameters for EMA Swipe Using Hammer Impact Excitation.

Parameter	Setting/Value
Acquisition Bandwidth	Zoom 3 - 23 Hz
Acquisition Duration	20 s
Frequency Resolution	0.05 Hz
No. of Frequency Domain Averages	10
Force Window Duration (% of Acquisition)	3 %
Exponential Window Time Constant	0.5
Excitation Type	Hammer Impact Excitation
Excitation Duration	≈ 0.005 s
Excitation Frequency Limits	N/A

It can be seen from Figure 4.39 that the immediate repeatability check was quite poor and there were significant differences between the two FRFs. This was probably caused by the poor signal to noise ratio due to the very short duration of the excitation and corresponding structural response. However, the main peaks corresponding to probable modes of vibration were reasonably similar. It was anticipated that the results from the hammer impact EMA were likely to be difficult to process and any estimated modal parameters were likely to be of poor quality. Nevertheless, it was decided to proceed with the main swipe so that the results of this form of excitation could be compared with the results obtained from using shaker excitation.

4.2.11.4 Homogeneity and Reciprocity Checks

The homogeneity and reciprocity checks were deemed to be pointless, considering the poor quality of the results from the immediate repeatability check. Therefore, precious time was not wasted performing these checks.

4.2.11.5 Coherence Function Check

The coherence function check was performed on site and is presented in Figure 4.40. It exhibits a peculiar behaviour in that the coherence is unity at every frequency, contrary to prior expectations. This behaviour was thought to be caused by a lack of sufficient dynamic range in the DI-2200 Spectrum Analyser, although this was not proven by the

writer. For this reason, the coherence function measurement for hammer impact excitation was assumed to be unreliable and was not utilised further.

4.2.11.6 FRF Shape Check and End-Of-Test Repeatability Check

The FRF shape check and end-of-test repeatability check were performed and did not exhibit any anomalous behaviour. They are not presented here.

4.2.12 EMA Using Hammer Impact Excitation: Main Swipe

4.2.12.1 Swipe Details and Procedure

The procedure for the hammer impact swipe was similar to those described earlier for shaker excitation. Once again, by this point in the testing, the excitation and data acquisition parameters had already been chosen from the quality assurance checks (Table 4.4). The reduced test grid was utilised (Figure 4.5) to enable the comparison of the same data gathered in two tests which should produce nominally identical modal testing results. The hammer and accelerometer locations are indicated in Table 4.5.

Table 4.5: Structure A (Configuration 1) - Accelerometer Locations for Hammer Impact Swipe.

Transducer ID	Location	DI-2200 Channel	Racal Channel
Hammer	Roving	1	2
A1	Test Point 51	---	3
A2	Test Point 32	2	4
A3	Test Point 35	---	6
A4	Test Point 38	---	7

Similar to the previous swipes, only the excitation and one response transducer were connected to the DI-2200 spectrum analyser. The excitation and all response transducers were connected to the Racal StorePlus VL tape recorder to further processing following return from site.

Once the accelerometers had been positioned on the structure and levelled to measure vertical accelerations, the hammer operator was instructed to sit at the first test point.

After leaving a few seconds for any structural response caused by the motion of the hammer operator to die out, the FRF measurement commenced with the test leader instructing the hammer operator to make the first impact. Following this impact, the hammer operator had to remain as motionless as possible to minimise the application of unmeasured excitation to the structure. When the acquisition duration was complete, the hammer operator was again instructed to impact the structure and remain still. This procedure was repeated until all frequency domain averages had been acquired.

At this point, it is useful to illustrate some practicalities regarding the hammer testing as performed on site.

- The hammer operator was instructed to make impacts of similar strength. It was found that the instrumentation was easily over- or under-ranged when varying strength hammer blows were used.
- The hammer operator had to be seated. This aided in the production of consistent strength hammer blows and was also less tiring for the hammer operator.
- It was necessary for the hammer operator and test leader to be in continuous contact using hands-free radios, particularly when the test point at which the hammer operator was located was some distance from the data acquisition centre.

Throughout the course of the FRF measurements using hammer impact excitation, it was found that the FRFs were prone to significant changes between averages. This was a consequence of the poor signal to noise ratio of the force and response signals caused by performing EMA using very short duration hammer blows combined with quite long duration data acquisition periods, which were necessary to obtain adequate frequency resolution for further processing. For this reason, the test leader was required to be very vigilant in the examination of FRF measurements to ensure that they were becoming more stable with increasing number of averages, indicating that the effects of environmental noise were being averaged out. Any measurements that appeared to be spoiled had to be repeated. For this particular swipe, FRF measurements at four out of 33 test points were spoiled in the manner and had to be repeated.

4.2.12.2 Modal Parameter Estimation

Following data acquisition, the FRF data were processed further in the same way as for the previous swipes. The results of the parameter estimation (natural frequencies, modal damping ratios and mode shapes) from the dataset sampled directly on site are presented in Figure 4.41.

4.2.13 Comparison of Hammer Versus BR Shaker Excitation for EMA

It was considered necessary to assess the difference in quality of the modal test data measured using hammer impact excitation and BR excitation, to determine whether the additional financial expense of using shaker excitation was warranted. To do this, the same comparative measures were used as in Section 4.2.10 for the comparison of the two forms of shaker excitation.

On examination of point and transfer mobility FRFs measured using hammer and BR shaker excitation, presented in Figures 4.42 and 4.43 respectively, it can be seen that the FRFs measured using hammer impact excitation are visibly more distressed than those measured using BR shaker excitation. This is so, even though an exponential window with a slightly higher time constant, which normally has a smoothing effect, was applied when acquiring the data using hammer impact excitation.

Following MDOF modal parameter estimation using the ICATS Global-M algorithm, the estimated modal parameters and MCFs for the first three modes of vibration for hammer impact and BR shaker excitation are illustrated in Figure 4.44. It is clear from a visual comparison of the mode shapes that those measured using shaker excitation are of better quality than those measured using hammer impact excitation. In addition to this, the values of the MCFs also indicate that the mode shapes estimated using hammer impact excitation are more complex than those measured using shaker excitation. Since the structure itself could not alter the complexity of the mode shapes between these swipes, the additional complexity observed for hammer impact excitation was thought to be caused by the much poorer signal-to-noise ratio or by rattling. It is also possible that the presence of the hammer operator, possibly acting as a non-proportional damper, was inducing some mode shape complexity. In summary, the evidence indicates that the modal measurements made using shaker excitation were far superior to those measured using hammer impact excitation.

It is also interesting to note that EMA using shaker excitation was quicker than using hammer impact excitation. This is contrary to the common belief in the mechanical and aeronautical engineering disciplines that the use of hammer impact excitation is a quick method of performing EMA (Brown et al., 1977). The reasons for this are related to the specifics of the application of EMA to full-scale floors. Firstly, due to a worse signal to noise ratio, the number of frequency domain averages required when measuring the FRFs using hammer impact excitation (10 averages - see Table 4.4) was larger than

required for shaker excitation (7 averages - see Table 4.3), resulting in an additional 1.5 minutes of data acquisition required per test point. In addition to this, the number of spoiled FRF measurements requiring repetition was larger for hammer impact excitation (4 of 33 FRFs spoiled) than for the shaker excitation using BR excitation (2 of 33 FRFs spoiled) in approximately the same environmental conditions.

The already presented results for EMA using hammer impact excitation showed that it is possible to utilise hammer impact excitation to measure reasonably meaningful modal parameters on this structure. However, due to the availability of the superior electrodynamic shaker excitation, it was decided that the hammer would not be utilised for further EMA during the course of this research. It was, however, taken to site for the remainder of the field tests to serve as a backup excitation device in case the shaker should malfunction.

4.2.14 Summary of EMA Results

After processing all directly sampled and replayed FRF datasets, a number of sets of modal parameters were obtained, which, although quite consistent, were not exactly in agreement. These are included in Appendix I of this thesis. However, to perform correlation of these modal test results with FE models of this structure, it was necessary to select representative values of natural frequencies, modal damping ratios and modal masses from this large quantity of data. It was decided not to use a simple arithmetic average of all the values produced from all measurements since it was quite obvious that modal parameter estimations for specific modes were best when using response accelerometer points close to an antinode of the mode estimated. For this reason, the results of poor modal parameter estimations were first discarded and then an arithmetic average of the remainder of the results was taken. These values are presented in Table 4.6.

Table 4.6: Structure A (Configuration 1) - Estimated Modal Parameters.

Mode Number	Natural Frequency (Hz)	Modal Damping Ratio (%)	Modal Mass (kg)
1	6.41	0.95	70000
2	6.79	1.30	63000
3	8.16	1.00	58000
4	9.92	0.85	---
5	11.78	2.30	68000
6	15.02	2.15	48000
7	17.40	1.55	103000
8	18.18	1.75	60000

4.2.15 Pedestrian Response Measurements

Following the EMA, pedestrian response measurements were designed so that the most onerous walking paths, accelerometer locations and pacing rates were utilised (Pavic & Reynolds, 1999).

4.2.15.1 Design of the Pedestrian Response Tests

The walking paths to be utilised in the pedestrian response measurements were based on the mode shapes estimated from the EMA and some consideration of the possible future usage of the floor. Three walking paths were selected as illustrated in Figure 4.45. Walking Path 1, along the length of the entire main area of the floor, was expected to produce maximum responses. Walking Paths 2 and 3 were thought to be more realistic considering the future usage of the floor as an office building. Two accelerometer response locations were utilised at test points 32 and 38 (Figures 4.5 and 4.45). It could be seen from the mode shape plots (Figure 4.31) that these points were most likely to produce the maximum vibration responses, as they were experimental antinodes for modes 2 and 1 respectively.

Two pacing frequencies were utilised in the pedestrian response tests. Firstly, to excite the first mode of vibration, a pacing rate of 127 steps-per-minute (spm) was utilised for all three walking paths, its third harmonic tuned to the 6.41 Hz frequency of the first mode. Secondly, a pacing rate of 136 spm was chosen to excite the second mode of

6.79 Hz, also with its third harmonic. However, this was only utilised for Walking Paths (WP) 1 and 3 since WP 2 was located approximately along a nodal line of the second mode of vibration.

For all tests, a male test subject weighing approximately 75 kg was instructed to walk back and forth along the prescribed walking paths. His pacing rate was controlled by a metronome, for a pre-specified duration. The acceleration vibration responses were recorded using the analogue Racal instrumentation tape recorder, as well as simultaneously being digitised using the DI-2200 spectrum analyser with the LTR firmware installed. Immediate digitising of the data enabled the writer to examine the measured time histories on site and to repeat any tests which might have been spoiled by environmental noise or faulty instrumentation, for example. However, this was found not to be necessary in these tests.

4.2.15.2 Processing of the Pedestrian Response Test Data

Following return from site, the test data were transferred to a PC. All subsequent processing was performed using the DATS signal processing software in accordance with the procedures specified in Section 3.7 of this thesis.

For each of the tests, the three assessment parameters have been calculated. These are:

1. RMS accelerations for the entire measured time history,
2. peak running RMS calculated using a 10 s integration time, and
3. vibration dose value based on an assumed 8 hour exposure time.

The values of the three parameters pertinent to this series of response measurements (Structure A, Configuration 1) are shown in Table 4.7.

Table 4.7: Structure A (Configuration 1) - Results from Pedestrian Response Tests.

Walking Path	Mode (frequency)	Pacing Rate (spm)	Response Point	RMS Entire Record (%g)	Peak Running RMS 10 s Int. (%g)	VDV 8 h Exp. (m/s ^{1.75})
1	1 (6.41 Hz)	127	32	0.050	0.061	0.087
1	1 (6.41 Hz)	127	38	0.051	0.070	0.094
1	2 (6.79 Hz)	136	32	0.066	0.100	0.118
1	2 (6.79 Hz)	136	38	0.061	0.088	0.107
2	1 (6.41 Hz)	127	32	0.036	0.050	0.065
2	1 (6.41 Hz)	127	38	0.038	0.053	0.068
3	1 (6.41 Hz)	127	32	0.034	0.046	0.063
3	1 (6.41 Hz)	127	38	0.045	0.057	0.084
3	2 (6.79 Hz)	136	32	0.045	0.056	0.080
3	2 (6.79 Hz)	136	38	0.048	0.057	0.089

An illustration of the processing procedure is included in Figure 4.46 which shows the time history recorded from the first of the tests listed in Table 4.7. The salient points to note from this figure are as follows:

- The start of the time history, prior to the start of the walking excitation and, therefore, having lower acceleration amplitudes corresponding to ambient excitation only, was removed from the analysis. This was done to prevent the artificial reduction of the RMS acceleration, averaged over the entire record, and of the vibration dose value.
- The level of the RMS acceleration of the portion of the time history that was analysed is illustrated in Figure 4.46. It is important to note that it is impossible for this parameter to make due consideration of the non-stationary nature of the acceleration response due to pedestrian excitation.
- The running RMS level using 10 s integration time is illustrated. It can be seen that it provides a mechanism by which variations in the magnitude of vibration may be gauged. Taking the peak of this running RMS, as tabulated in Table 4.7, provides a conservative measure for assessment purposes (Eriksson, 1994).

4.2.16 Lessons Learned from Test Structure A (Configuration 1)

From the experience gained in this round of EMA and pedestrian response measurements, the following important points were noted.

- BR excitation was considered to be more reliable than BSS excitation over the entire frequency range of interest. This was due to the fact that the application of the exponential window to measurements made using BSS excitation resulted in higher frequencies being attenuated more than lower frequencies, resulting in discretisation errors. BR excitation, because of its broadband nature, did not exhibit this behaviour.
- EMA performed using the shaker as an excitation source produced better quality FRF data than when using the instrumented hammer in less time. For this reason, the decision was made not to use the hammer in any further tests. However, it is important to realise that the application of EMA on such structures is feasible using hammer impact excitation, which has the advantage of being cheaper than using the electrodynamic shaker.
- Data acquired during quiet overnight conditions was of a superior quality compared with data acquired during more noisy daytime conditions. To enhance the quality and scientific value of data measured on large civil engineering structures, it is recommended that future testing is performed in quiet conditions whenever possible. This typically means overnight testing of structures situated in cities or on active building sites.
- It was difficult to acquire reliable modal test data at very stiff locations on the structure, such as over columns or very stiff beams. These test points were not utilised for future modal test swipes in order to reduce the testing time required.

4.3 Test Structure A (Configuration 2)

Configuration 2 of Structure A was tested two weeks after Configuration 1. The duration of the testing was four days, from 15 to 19 July 1996.

4.3.1 Description of the Structure

The structure was in an identical state to that described for Configuration 1 (Section 4.2.1), with the exception that an access floor system had been installed on it. The specifications of this particular access floor system are presented in Table 4.8.

Table 4.8: Structure A (Configuration 2) - Specification of Access Floor.

Manufacturer	Tate Access Floors
System Type	Series 900 GCS Concore [®] Medium Grade
Finished Floor Height	150 mm
Pedestal Fixity	Pedestals bonded to floor using epoxy adhesive
Panel Fixity	Panels screwed to the pedestals

Figure 4.47 shows a general view of Structure A with the access floor (Figure 4.48) installed.

4.3.2 Pre-Test Analysis

No attempt was made to develop an FE model of this structure with the access floors installed prior to the testing, because any such modelling would have been merely speculative. It was unknown how the access floors would actually affect the mass, stiffness and damping properties of the post-tensioned concrete floor slab.

4.3.3 Testing Strategy

After having acquired high quality modal and pedestrian response test data from Structure A (Configuration 1), the prime objective of this round of testing was to acquire similar high quality data for comparative purposes.

4.3.4 Test Logistics

The logistics of this round of tests were almost identical to those for Structure A (Configuration 1). However, for this round of tests, overnight testing was planned prior to arrival on site.

4.3.5 On-Site Preparation

Similarly to the previous round of tests, the data acquisition centre for testing was location in the 'core area' of the floor (Figure 4.1) and the whole of the floor was cleared of site equipment and building materials. It is important to note that no special preparation was applied to the access floor, which had been installed by the contractor. It was the intention of the writer to obtain data which would demonstrate the effects of the access floor after being installed under typical conditions.

4.3.6 Position of Shaker and Accelerometers for Measurements with Access Floors Installed

When performing modal and structural response measurements, a decision had to be made about where to place the shaker and the accelerometers. Referring to response measurements only, the guidelines in ISO 10137 (ISO, 1992) state that:

"... measurement points should be located in a place where people are likely to sense the vibrations".

In addition, BS 6472 (BSI, 1992) states that:

"... measurements of vibration should normally be taken on a building structural surface supporting a human body".

The rationale behind these guidelines is that it would not be required to take account of any transfer function between the measurement point and the point of entry to the receiver.

Obviously, in the case of access floors, any building occupants would be located on top of them. Therefore, on first thought, that would appear to be the logical place where to measure the vibration response and to apply the modal test excitation using the shaker. However, the EMA was concerned with measuring the global modes of vibration of the dynamic system comprising the bare floor and access floors. Therefore, it was considered worthwhile to perform some trial measurements to investigate if differences in EMA results, due to different locations of the shaker and accelerometers, would occur.

4.3.6.1 Position of Accelerometers

Three possible accelerometer positions were considered:

1. on the surface of the sub-floor (i.e. the structural floor supporting the access floor),
2. on the surface of the access floor directly above a pedestal, and
3. on the surface of the access floor in the centre of a panel supported by four pedestals.

These positions are illustrated in Figure 4.49 which shows a test set-up with three accelerometers nominally at the same test point, but in the three aforementioned positions.

Three point mobility FRFs measured using these accelerometer locations, with the shaker located on the surface of the access floor over another pedestal, are presented in Figure 4.50. It is clear from this plot that point mobility FRFs measured using accelerometers located on the top surface of the access floor were visibly altered from an equivalent FRF measured using an accelerometer located on the surface of the concrete sub-floor. This effect was much more significant for the case where the accelerometer was located in the centre of an access floor panel than when the accelerometer was located over a pedestal.

It is possible that this behaviour was caused by local vibrations occurring within the access floor system. This may be justified to some extent by a simple examination of the peaks corresponding to modes of vibration of the floor presented in Figure 4.50. It can be seen that, for the lowest modes of vibration, the peaks have similar size and shape for all three measurements. It is only away from these peaks and at higher frequencies that the shapes of the FRFs are changed.

It was decided to investigate the sensitivity of the whole EMA and parameter estimation procedure to these 'nominally identical' FRFs by performing an entire swipe of EMA using these three accelerometer positions. Based on this study, as will be seen later (Section 4.3.8), it was decided for other FRF swipes to place the accelerometers directly onto the sub-floor.

4.3.6.2 Position of the Shaker

With respect to the placement of the shaker, a similar comparison was performed with shaker excitation applied on the top surface of the sub-floor (after removing and

appropriate access floor panel as shown in Figure 4.48) and on top of the access floor above a pedestal. This comparison is presented in Figure 4.51. It can be seen that the difference between these two configurations was quite small.

The practicalities of removing a panel at every test point to position the shaker on the concrete sub-floor would have increased significantly the total test time, which was quite limited. Therefore, for the first swipe the shaker was placed above the nearest pedestal to each test point so that a full swipe of measurements would be assured. It was assumed that errors introduced by the inaccuracy in the geometric position of the shaker would be negligible. After performing the first FRF swipe, however, it was decided that there was enough time to remove a panel at each test point for the second FRF swipe, so that the shaker could be positioned on the sub-floor. No significant differences were observed between the modal parameters estimated from these swipes and it was therefore concluded that either shaker location could be utilised in future tests.

4.3.7 EMA Using BR Excitation: QA Checks

A full set of data QA checks were performed for this structure prior to the commencement of the first EMA swipe. They were deemed particularly important for this structure as it was unknown whether or not the installation of the access floors would introduce significant non-linearities into the structure, or cause other problems.

The excitation/response checks and the repeatability checks were performed and produced results similar to those presented for Configuration 1 (Section 4.2.6). However, the results of the homogeneity, reciprocity, coherence and FRF shape checks may have indicated peculiar (possibly non-linear) behaviour of the structure and are therefore presented in this section.

4.3.7.1 Homogeneity Check

The results from the homogeneity check, performed at test point 32 with a factor of 2 between the magnitude of the high- and low-level excitation, are presented in Figure 4.52. It can be seen that, similarly to the homogeneity check for Structure A (Configuration 1), the quality of the FRF measured using low-level excitation was quite poor as a result of the decreased signal-to-noise ratio. However, there was no visible indication from this QA check of any problems with non-linearity.

4.3.7.2 Reciprocity Check

The results of the reciprocity check, performed between test points 32 and 38, are presented in Figure 4.53. Once again, the plots of the two FRFs overlay very well and it was concluded that there was no indication of the occurrence of non-linear behaviour that would spoil the modal test data.

4.3.7.3 Coherence Function Check

The results of the point and transfer mobility coherence function checks, performed at test point 32 and between test points 32 and 38, respectively, are presented in Figures 4.54 and 4.55. For all of the peaks in the FRF magnitude plots, the corresponding coherence was above 80%, which was considered to be acceptable. The coherence was slightly lower than that measured for Configuration 1 but this was attributed to the effects of background noise caused by some workmen who had stayed late on site.

4.3.7.4 FRF Shape Check

The FRF shape check for point mobility at test point 32 is presented in Figure 4.56. Whilst it is unfortunately quite noisy, a result of the presence of workmen on site during the acquisition of the test data, it is clear that the shape of the FRF was reasonable (Section 3.6.3.6), and it therefore gave no cause for concern.

4.3.8 EMA Using BR Excitation: Main Swipes

Two swipes of EMA were performed, both with 33 test points in total following the experience gained from the testing on Structure A (Configuration 1) (see Figure 4.5).

The first swipe was performed to examine the effects of performing EMA with accelerometers located at different positions on top of and below the access floor, as already described in Section 4.3.6.1. Therefore, for this swipe all three response accelerometers were positioned at nominally the same test point (point 32), as illustrated in Table 4.9 and in Figure 4.49. During this FRF swipe, the shaker was always positioned over the pedestals nearest to the actual locations of the test points, as there insufficient time available to remove access floor panels at each test point to position the shaker on the sub-floor. It was found, as expected, that all accelerometer positions gave similar modal parameter estimations. However, the accelerometer positioned on the sub-

floor was least affected by noise within the access floor system (Section 4.3.6.1) and was therefore most reliable. In future swipes, the accelerometers were positioned on the sub-floor only.

Table 4.9: Structure A (Configuration 2) - Accelerometer Locations for 1st Swipe Using BR Excitation.

Transducer ID	Location	DI-2200 Channel	Racal Channel
A1	Roving Shaker	1	3
A2	Test Point 32 (on sub-floor)	2	4
A3	Test Point 32 (on access floor over pedestal)	---	6
A4	Test Point 32 (on access floor in centre of a panel)	---	7

For the second swipe, all of the response accelerometers were positioned on the sub-floor, in the locations indicated in Table 4.10. To measure better the fourth mode of vibration, which had been only poorly estimated from the measurements on Structure A (Configuration 1), one of the response accelerometers was positioned at point 37 instead of point 38 (Figure 4.5).

Table 4.10: Structure A (Configuration 2) - Accelerometer Locations for 2nd Swipe Using BR Excitation.

Transducer ID	Location	DI-2200 Channel	Racal Channel
A1	Roving Shaker	1	3
A2	Test Point 37	2	4
A3	Test Point 35	---	6
A4	Test Point 51	---	7

To ensure that the data from these tests would be completely comparable with the data measured on Structure A (Configuration 1), identical data acquisition parameters were used as for BR excitation on that structure (Table 4.3).

4.3.9 Summary of EMA Results

A summary of the estimated modal parameters for Structure A (Configuration 2) is presented in Table 4.11. These values were calculated by collating and averaging the results of all measured datasets, which are presented in Appendix I of this thesis.

Table 4.11: Structure A (Configuration 2) - Estimated Modal Parameters.

Mode Number	Natural Frequency (Hz)	Modal Damping Ratio (%)	Modal Mass (kg)
1	6.28	1.05	60000
2	6.69	1.65	55000
3	8.04	0.90	61000
4	9.82	1.50	100000
5	11.60	2.10	68000
6	14.65	2.00	62000
7	17.15	1.74	81000
8	17.78	1.50	71000
9	20.11	2.10	58000
10	21.42	1.55	79000

Comparison of these results with those presented in Table 4.6 for the same structure prior to the addition of access floors revealed the percentage changes presented in Table 4.12.

Table 4.12: Structure A - Percentage Changes in Modal Parameters Between Configurations 1 and 2.

Mode Number	Percentage Change in Natural Frequency (%)	Percentage Change in Modal Damping Ratio (%)	Percentage Change in Modal Mass (%)
1	-2.0	+11	-14
2	-1.5	+27	-13
3	-1.5	-10	+5
4	-1.0	+76	---
5	-1.5	-9	0
6	-2.5	-7	+29
7	-1.4	+12	-21
8	-2.2	-14	+18
9	---	---	---
10	---	---	---

It can clearly be seen that for all modes of vibration compared, the natural frequency reduced more or less by a small percentage. This would seem to indicate that the increase in mass of the system due to the addition of the access floor was more significant than any increase in stiffness. Quantification of any increase in stiffness could not be determined from this simple comparison and this was scheduled for investigation in the post-test FE modelling presented in Chapter 5 of this thesis.

Damping estimations are traditionally more unreliable than natural frequencies, which may account for the less conclusive distribution of results. However, it can be seen that on the whole, there appeared to be an increase in damping of the structure following the addition of the access floors. The modal mass estimations, probably the most imprecise parameter of all, actually reduced for the first two modes of vibration contrary to expectation. It is probable that this was not a structural trait, but a result of experimental errors in the EMA data.

4.3.10 Pedestrian Response Measurements

To produce pedestrian response measurements which were comparable with those for Configuration 1, identical walking paths and response points were selected as presented

in Section 4.2.14. The pedestrian always walked on the top surface of the access floor and the responses were measured on the surface of the sub-floor. Due to the small changes in natural frequencies of the first two modes of vibration, the pacing rates designed to excite these modes were adjusted slightly from 127 to 126 spm for the first mode and from 136 to 134 spm for the second mode. When comparing the results, it was assumed that these small changes in pacing rate would not alter the force input from the pedestrian.

Table 4.13: Structure A (Configuration 2) - Results from Pedestrian Response Tests.

Walking Path	Mode (frequency)	Pacing Rate (spm)	Response Point	RMS Entire Record (%g)	Peak Running RMS 10 s Int. (%g)	VDV 8 h Exp. (m/s ^{1.75})
1	1 (6.28 Hz)	126	32	0.040	0.051	0.070
1	1 (6.28 Hz)	126	38	0.046	0.067	0.078
1	2 (6.69 Hz)	134	32	0.053	0.076	0.096
1	2 (6.69 Hz)	134	38	0.052	0.071	0.091
2	1 (6.28 Hz)	126	32	0.030	0.038	0.054
2	1 (6.28 Hz)	126	38	0.037	0.049	0.067
3	1 (6.28 Hz)	126	32	0.026	0.033	0.046
3	1 (6.28 Hz)	126	38	0.039	0.057	0.068
3	2 (6.69 Hz)	134	32	0.035	0.049	0.064
3	2 (6.69 Hz)	134	38	0.040	0.047	0.075

Comparison of the results presented in Table 4.13 with those presented in Table 4.7 for the same structure prior to the addition of access floors revealed the percentage changes presented in Table 4.14.

Table 4.14: Structure A - Percentage Changes in Pedestrian Response Test Assessment Parameters Between Configurations 1 and 2.

Walking Path	Mode	Pacing Rate (spm)	Response Point	Percentage Change in RMS Entire Record (%)	Percentage Change in Peak Running RMS 10 s int. (%)	Percentage Change in VDV 8 h Exp. (%)
1	1	127/126	32	-20	-16	-20
1	1	127/126	38	-10	-4	-17
1	2	136/134	32	-20	-24	-19
1	2	136/134	38	-15	-19	-15
2	1	127/126	32	-17	-24	-17
2	1	127/126	38	-3	-8	-1
3	1	127/126	32	-24	-28	-27
3	1	127/126	38	-13	0	-19
3	2	136/134	32	-22	-13	-20
3	2	136/134	38	-17	-18	-16
Average over all tests				-16	-15	-17

It can be seen that every test performed on this structure exhibited a reduction in response following the installation of an access floor, no matter which assessment parameter was utilised. This varied in magnitude between 0% and 28%, but on average over all tests, a reduction of about 16% was observed.

4.3.11 Lessons Learned from Test Structure A (Configuration 2)

- When access floors were installed, the shaker excitation could be reliably applied to either the sub-floor, or to the access floor above a pedestal location, provided that the response measurements were made on the surface of the sub-floor. Results measured when the shaker was in the centre of an access floor panel were spoiled possibly by the effects of local panel vibration.
- Accelerometers were best located on the sub-floor when performing pedestrian response measurements. Measurements attempted with accelerometers on top of the access floors showed that high-frequency accelerations, outside the range of frequencies perceptible to humans, could be produced by relative movements of

closely-fitting adjacent access floor panels. These accelerations were sometimes accompanied by clicking sounds and tended to spoil the quality of the measured response data by over-ranging the accelerometers and signal conditioning electronics.

4.4 Test Structure B

Test structure B was a high strength concrete flat slab constructed at the laboratories of Taywood Engineering Ltd. in London. Due to its large size, only two configurations of access floors were supplied by Hewetson Raised Access Floors and were dynamically tested, in addition to the bare structure. All tests on this structure were performed in April and May 1997.

4.4.1 Description of the Structure

Structure B was a 15 m square, 250 mm deep normally reinforced high strength concrete slab, supported by four 300 mm square columns at 9 m centres (Figure 4.57). The slenderness ratio of 36 is high for a classically reinforced structure. The characteristic strength of the concrete was approximately 120 N/mm^2 at the time of testing (Price, 1996). The slab was constructed as part of a separate investigation into the use of high strength concrete. Four weeks after construction, the slab was loaded to 13.125 kN/m^2 which caused heavy cracking.

The cracked floor structure was tested in three configurations.

Configuration 1: In its bare condition (i.e. no access floors) (Figure 4.58).

Configuration 2: With a Hewetson RMG 600 medium grade access floor system installed with an FFH of 500 mm (Figure 4.59). For this configuration, the panels were loose laid onto the pedestals.

Configuration 3: Same as Configuration 2 but with the panels mechanically fixed to the pedestals.

Access to the slab was provided by two wooden staircases that had been constructed leading up to the slab. Since the tops of these were supported on the slab and may have affected the vibration behaviour of it, the site personnel were instructed to detach these

staircases. Also, handrails were present around the full perimeter of the slab. These could not easily be detached from the slab and they had to remain in place for safety reasons. However, as they were very light compared with the slab, they were assumed to have no effect on its vibration behaviour.

4.4.2 Pre-Test Analysis

The FE model constructed for structure B prior to testing is illustrated in Figure 4.60. The slab was modelled using isotropic shell elements of depth 250 mm. The columns were modelled using beam elements of length 1.725 m (the distance from the footings to the mid-plane of the slab), and all 6 DOFs were constrained at the location of the footings. Due to the very high strength of the concrete used in this structure, an initial estimate for the modulus of elasticity was made of 50 kN/mm^2 (Pavic, 1999). Also, an estimate of the density of the concrete was made of 2600 kg/m^3 . At this stage, no attempt was made to model the cracking which existed on the slab.

The first 15 modes calculated from the pre-test analysis are shown in Figure 4.61. Interestingly, the importance of the pre-test analysis was highlighted with this particular structure. With it being plate-like supported by four columns, one might intuitively have considered the centre of the slab to be a good location to place an accelerometer to measure the first mode of vibration. However, as the results of the pre-test analysis showed, the centre point was actually at a node of the first mode of vibration and the use of the centre point as a reference would have resulted in this mode being missed from the measurements completely (Pavic, 1999).

Another important point to note from this analysis was the presence of a number of repeated modes, caused by the symmetry present in the plate-like structural configuration. In practice, it was unlikely for these modes to be repeated exactly due to construction tolerances, but it was likely that these modes would be quite closely spaced. This once again highlights the importance of using an MDOF method of parameter estimation.

Based on the results of this analysis, the test grid illustrated in Figure 4.62 was selected. This was similar to the grid used in the previous hammer impact tests reported by Pavic (1999), except that four additional points (50 to 53) were used to attempt to improve the parameter estimations of the local corner modes (Modes 5, 6, 7 and 8 in Figure 4.61).

The auto-MAC calculated for points 1 to 49 is illustrated in Figure 4.63 and does not highlight any problems.

4.4.3 EMA

4.4.3.1 QA Checks

As for all structures, the EMA commenced with a full series of quality assurance checks as already described in detail for Structure A. These were performed once for all configurations of the structure and, in general, indicated no significant problems.

4.4.3.2 EMA Strategy

Bearing in mind the experience gained in the EMA performed on Structure A, it was decided to use BR shaker excitation for all swipes. In each configuration of the structure, the shaker was used in reaction mode either on the sub-floor (Figure 4.64) or on the access floor above a pedestal (Figure 4.65) depending on whether or not an access floor was installed.

Two EMA swipes were performed for Configuration 1 of the structure with accelerometer response locations at test points 5, 18, 22, 25, 35 and 43. For configurations 2 and 3, an additional swipe was performed with all accelerometers nominally at test point 39, but with one on the sub-floor, one on the access floor above a pedestal and one on the access floor in the centre of a panel.

4.4.3.3 EMA Results

A summary of the estimated modal parameters for the three configurations of Structure B are presented in Tables 4.15 to 4.17 (natural frequencies, modal damping ratios and modal masses). The results for all measured datasets are included in Appendix I of this thesis. The mode shapes did not change significantly between the various configurations of the structure and are therefore presented for all configurations in Figure 4.66.

Table 4.15: Structure B (Configuration 1) - Estimated Modal Parameters.

Mode Number	Natural Frequency (Hz)	Modal Damping Ratio (%)	Modal Mass (kg)
1	4.31	0.73	25000
2	4.65	0.54	20000
3	6.63	0.81	16000
4	6.76	0.92	15000
5	8.29	1.68	5000
6	8.70	1.57	6000
7	---	---	---
8	9.04	1.36	5000
9	12.42	0.46	15000
10	15.02	0.48	16000
11	15.09	1.23	27000
12	15.32	1.40	25000
13	20.03	0.54	16000
14	20.75	0.39	17000
15	21.09	0.39	14000

Table 4.16: Structure B (Configuration 2) - Estimated Modal Parameters.

Mode Number	Natural Frequency (Hz)	Modal Damping Ratio (%)	Modal Mass (kg)
1	4.23	0.63	29000
2	4.64	0.58	23000
3	6.47	0.90	18000
4	6.75	1.13	15000
5	8.15	1.69	6000
6	8.53	1.60	6000
7	---	---	---
8	8.82	1.31	6000
9	12.20	0.56	15000

10	14.72	0.89	21000
11	---	---	---
12	15.04	1.59	30000
13	19.63	0.49	22000
14	20.34	0.40	18000
15	20.65	0.39	16000

Table 4.17: Structure B (Configuration 3) - Estimated Modal Parameters.

Mode Number	Natural Frequency (Hz)	Modal Damping Ratio (%)	Modal Mass (kg)
1	4.25	0.66	26000
2	4.74	1.02	20000
3	6.57	1.06	19000
4	6.81	1.19	17000
5	8.23	1.56	8000
6	8.56	1.77	7000
7	---	---	---
8	8.87	1.47	9000
9	12.26	0.54	15000
10	14.76	0.55	23000
11	14.89	1.21	20000
12	15.07	1.59	26000
13	19.72	0.49	20000
14	20.47	0.41	17000
15	20.72	0.39	15000

The differences between the modal parameters estimated for the different configurations of Structure B are illustrated more clearly in Table 4.18, in which the percentage differences between the modal parameters estimated for the bare structure and the configurations with access floors installed are tabulated.

Table 4.18: Structure B - Percentage Changes in Modal Parameters Between Configuration 1 and Configurations 2 and 3.

Mode Number	Percentage Change in Natural Frequency from Config. 1 (%)		Percentage Change in Modal Damping Ratio from Config. 1 (%)		Percentage Change in Modal Mass from Config. 1 (%)	
	Config. 2	Config. 3	Config. 2	Config. 3	Config. 2	Config. 3
	1	-1.9	-1.4	-14	-10	+16
2	-0.2	+1.9	+7	+89	+15	0
3	-2.4	-0.9	+11	+31	+13	+19
4	-0.2	+0.7	+23	+29	0	+13
5	-1.7	-0.7	+1	-7	+20	+60
6	-2.0	-1.6	+2	+13	0	+17
7	---	---	---	---	---	---
8	-2.4	-1.9	-4	+8	+20	+80
9	-1.8	-1.3	+22	+17	0	0
10	-2.0	-1.7	+85	+15	+31	+44
11	---	-1.3	---	-2	---	-26
12	-1.8	-1.6	+14	+14	+20	+4
13	-2.0	-1.6	-9	-9	+38	+25
14	-2.0	-1.4	+3	+5	+6	0
15	-2.0	-1.8	0	0	+14	+7

Similarly as for Structure A, the data in Table 4.18 show that, in general, the natural frequencies of the slab reduced following the installation of the access floor. However, for modes 2 and 4 measured on Configuration 3 of the structure, the natural frequency actually increased relative to the bare floor. In these two cases, the access floor clearly increased the stiffness of the slab system so as to offset any reduction caused by the increased mass due to the access floor. It is also possible that there was still an increase in stiffness for modes where the natural frequencies reduced, although not enough to offset the increase in mass. Such stiffness changes could not be quantified on the basis of these tests alone, and this was therefore scheduled for investigation in the post-test FE analysis presented in Chapter 5 of this thesis.

The modal damping ratios increased significantly following the installation of the access floor, particularly for configuration 3 where the access floor panels were mechanically

fixed to the pedestals. It is possible that the increased friction caused by this mechanical fixing acted as a damping mechanism for the composite concrete slab/access floor system.

In general, the modal masses increased for configurations 2 and 3 as expected. However, there was a large degree of scatter in these data which was probably caused by the increased susceptibility of the modal mass estimates to experimental errors.

4.4.4 Pedestrian Response Measurements

4.4.4.1 Design of the Pedestrian Response Tests

For the bare structure (Configuration 1), the pedestrian response measurements were made following the first EMA swipe. At this time, the exact nature of the problem caused by the faulty spectrum analyser firmware had not been identified and it had not yet been possible to perform parameter estimation. Therefore, the walking paths were selected on the basis of previous testing experience on this structure (Pavic, 1999) and the pre-test FE model (Section 4.4.2). Four walking paths were selected and are presented in Figure 4.67. For each walking path, the response measurement location was selected as being as close as possible to an antinode of the mode being excited. As no natural frequencies had yet been estimated, the pacing rate was selected to correspond to frequencies of peaks on the measured FRFs, which the writer thought corresponded to the modes of vibration.

Unfortunately, the extensive cracking of the structure had caused the first two modes of vibration to swap since the previous round of testing (Pavic, 1999). The mode which had previously been the second was now the first and vice-versa. As no mode shapes had yet been estimated in these tests, the writer was unaware of this and failed to identify correctly the natural frequency of the first mode of vibration from a simple examination of the FRFs. For this reason, the pedestrian response measurements corresponding to this mode of vibration (walking paths 3 and 4) were not meaningful for Configuration 1 of the structure and therefore had to be discounted. However, the second natural frequency was correctly estimated from the FRFs and the pedestrian response measurements were considered to be valid.

For Configurations 2 and 3, the pedestrian response measurements were performed following EMA and modal parameter estimation in accordance with the recommended procedure (Pavic & Reynolds, 1999).

Similar to the pedestrian response measurements on Structure A, a male test subject weighing approximately 75 kg was instructed to walk back and forth along the prescribed walking paths, using a metronome to control the pacing rate. The same experienced test subject used in the pedestrian response measurements on Structure A, was also used for all three configurations of Structure B.

4.4.4.2 Processing of the Pedestrian Response Test Data

Following return from site, the pedestrian response test data were processed in the standard way (Section 3.7). The three previously selected response assessment parameters were calculated for all tests and are presented in Tables 4.19, 4.20 and 4.21 for Configurations 1, 2 and 3 of the structure respectively. A typical pedestrian response measurement is presented in Figure 4.68. This figure also shows the level of the RMS of the entire record and the running RMS with a 10 s integration time.

Table 4.19: Structure B (Configuration 1) - Results from Pedestrian Response Tests.

Walking Path	Mode (frequency)	Pacing Rate (spm)	Response Point	RMS Entire Record (%g)	Peak Running RMS 10 s Int. (%g)	VDV 8 h Exp. (m/s ^{1.75})
1	2 (4.6 Hz)	138	46	0.585	0.714	0.915
2	2 (4.6 Hz)	138	22	0.578	0.699	0.917

Table 4.20: Structure B (Configuration 2) - Results from Pedestrian Response Tests.

Walking Path	Mode (frequency)	Pacing Rate (spm)	Response Point	RMS Entire Record (%g)	Peak Running RMS 10 s Int. (%g)	VDV 8 h Exp. (m/s ^{1.75})
1	2 (4.64 Hz)	138	46	0.506	0.650	0.791
2	2 (4.64 Hz)	138	22	0.416	0.577	0.674
3	1 (4.22 Hz)	127	25	0.225	0.295	0.358
4	1 (4.22 Hz)	127	25	0.201	0.253	0.317

Table 4.21: Structure B (Configuration 3) - Results from Pedestrian Response Tests.

Walking Path	Mode (frequency)	Pacing Rate (spm)	Response Point	RMS Entire Record (%g)	Peak Running RMS 10 s Int. (%g)	VDV 8 h Exp. (m/s ^{1.75})
1	1 (4.74 Hz)	142	46	0.267	0.373	0.451
2	1 (4.74 Hz)	142	22	0.316	0.395	0.516
3	2 (4.26 Hz)	128	25	0.220	0.291	0.350
4	2 (4.26 Hz)	128	25	0.226	0.316	0.364

The differences between the pedestrian response assessment parameters for the different configurations of Structure B are illustrated more clearly in Table 4.22, in which the percentage differences between the bare structure and the configurations with access floors installed are tabulated.

Table 4.22: Structure B - Percentage Differences in Pedestrian Response Assessment Parameters Between Configuration 1 and Configurations 2 and 3.

Walking Path	Percentage Change in RMS Entire Record from Config. 1 (%)		Percentage Change in Peak Running RMS 10 s Int. from Config. 1 (%)		Percentage Change in VDV 8 h Exp. from Config. 1 (%)	
	Config. 2	Config. 3	Config. 2	Config. 3	Config. 2	Config. 3
1	-14	-54	-9	-48	-14	-51
2	-28	-45	-17	-43	-27	-44
Average	-21	-50	-13	-46	-20	-47

It can be seen from Table 4.22 that reductions in response were measured between Configurations 1 and 2 and Configurations 1 and 3, regardless of which response parameter was utilised. The reductions appeared to be more significant in the case of Configuration 3 (approximately 45%) than for Configuration 2 (approximately 15%).

4.4.5 Lessons Learned from Test Structure B

- The incident with the faulty spectrum analyser firmware illustrated how vulnerable site test opportunities are to unforeseen problems with test equipment. Whilst good EMA data was eventually obtained, the incorrect pacing rate used in the pedestrian response measurements resulted in some of them having to be discarded. Any future upgrades in hardware or software were treated with utmost suspicion and were checked thoroughly prior to further site testing.
- Performing pedestrian response measurements without properly estimated natural frequencies and mode shapes resulted in failure to excite properly the first mode of vibration for Configuration 1 of the structure. This highlights the importance of performing EMA prior to performing pedestrian response measurements, to ensure that the maximum possible structural acceleration responses are achieved.

4.5 Test Structure C

Test Structure C was a purpose-built in-situ cast post-tensioned slab strip constructed and tested in one of the laboratories at the University of Sheffield, Department of Civil

and Structural Engineering. Since this was a smaller scale structure, it was possible to test a much wider range of access floor configurations than were tested on the previous two structures. These tests were performed mainly between May and December 1998.

4.5.1 Description of the Structure

4.5.1.1 Specification and Design of Structure C

As Structure C was purpose built for this project, it was necessary to consider the requirements for the structure so that the most benefit may be obtained from it. It was also, of course, necessary to consider restrictions on its configuration, such as financial and spatial constraints. In light of these, the following list of specifications was drawn up:

1. The floor should be large enough to be representative of a real concrete floor. This would be important to ensure that the benefits of installing access floors in terms of vibration serviceability would not be over-emphasised in the measurements. A reasonable size structure was also required so that its vibration response to human excitation would be comparable with real floors.
2. The natural frequency of the floor should be in the range excitable by the second and/or third harmonic of walking excitation.
3. The floor should have as simple as possible configuration to facilitate its future ease of modelling using finite elements.
4. The floor dimensions should be selected with consideration of the 600 mm modular unit of access floor panels.

Bearing in mind these specifications, the configuration of the structure was selected to be a simply supported in-situ cast post-tensioned slab strip of span 10.8 m (total length 11.2 m including 200 mm overhangs over the supports), width 2.0 m and depth 275 mm. A general arrangement drawing is included in Figure 4.69. This configuration had a high but realistic span-to-depth ratio of about 40 and was predicted to have a first natural frequency of about 4.2 Hz, as calculated from FE models and checked using an equation for calculating the natural frequency of a simple beam (Blevins, 1979). This could be excited by both the second and third harmonics of walking excitation. The dimensions of the structure enabled an 18 by 3 grid of access floors to be installed on its surface (Figure 4.70), with adequate allowance for the full width of the access floor pedestal bases to be properly adhered to the surface of the structure. The supports were designed

to simulate as closely as possible true 'knife-edge' simple supports (Figure 4.71) and provision was made to excite the structure in direct drive mode through the construction of two pits beneath the slab strip (Figure 4.72).

The slab strip was post-tensioned using a system of 12 parabolic profiled unbonded tendons, each with one live and one dead anchor, alternately stressed from both ends (Figures 4.73 and 4.74). The reinforcement and prestressing design and detailing was performed by Freyssinet Ltd., whilst the remainder of the design was performed by the writer.

4.5.1.2 Construction of Structure C

Construction of Structure C took place in February and March 1998. Freyssinet Ltd. provided, placed and stressed the unbonded tendons and an external contractor performed the remainder of the construction of the slab strip.

A photograph of the slab strip formwork, reinforcement and prestressing prior to concreting is shown in Figure 4.75. The 12 tendons can clearly be seen with 6 of the live anchors at the end of the slab strip in the foreground of the photograph. The photograph in Figure 4.71 shows one of the supports, which clearly was designed to perform as a 'knife-edge'. Note that the upper bearing plate was not bonded in any way to the angle section on which it was supported.

Finally, following the completion of the slab strip, two adjustable platforms were constructed at each end of it. These may be seen in the photograph of the completed slab strip in Figure 4.76. The purpose of these platforms was to enable pedestrians to turn around whilst performing walking response tests without applying any dynamic loading to the structure.

4.5.1.3 Access Floor Configurations

It had been agreed that Tate Access Floors, the suppliers of the access floors for Structure A, would supply and install the raised access floors for examination on this structure. To decide which access floor configurations should be tested, the most common variables regarding the construction of access floors were identified as:

1. the finished floor height (FFH),
2. the grade of the access flooring panels,

3. the fixity between panels and the pedestals (whether or not they were mechanically fixed at the corners),
4. the fixity between the pedestals and the sub-floor (whether they were bonded using adhesive or whether they were bonded and mechanically fixed),
5. the type of adhesive used to bond the pedestals to the sub-floor, and
6. whether or not stringers were utilised (and if so, what type).

Bearing in mind the above variables possible when specifying access floor systems, a reference access floor system, of a configuration commonly utilised in practice, was taken to be as follows:

- 200 mm FFH
- Medium grade panels
- Pedestals bonded to the concrete using epoxy adhesive
- Panels mechanically fixed to the pedestals
- No stringer system installed

The following variations on this reference system were investigated:

1. increased FFH (Figure 4.77),
2. heavy grade panels,
3. pedestals bonded to the concrete using a soft, polyurethane based adhesive (Figure 4.78),
4. panels loosely placed onto the pedestals (i.e. no mechanical fixing), and
5. two types of stringer system (snap on and bolt on) installed (Figures 4.79 and 4.80).

A complete list of the access floor configurations used in the testing of Structure C is presented in Table 4.23.

Table 4.23: Structure C - Access Floor Configurations Utilised in the Testing.

Floor Config. ID	FFH (mm)	Access Floor System	Pedestal Fixity	Pedestal Adhesive Type	Panel Fixity	Stringer Type
1			Bare concrete slab strip – no access floors installed.			
2	600	Series 900 GCS	Glued	Epoxy Based	Mechanically Fixed	None
3	600	Series 900 GCS	Glued	Epoxy Based	Loose Laid	None
4	200	Series 900 GCS	Glued	Polyurethane Based	Mechanically Fixed	None
5	200	Series 900 GCS	Glued	Polyurethane Based	Loose Laid	None
6	200	Series 900 CRS	Glued	Epoxy Based	Mechanically Fixed	None
7	200	Series 900 CRS	Glued	Epoxy Based	Loose Laid	None
8	200	Series 900 GCS	Glued	Epoxy Based	Mechanically Fixed	None
9	200	Series 900 GCS	Glued	Epoxy Based	Loose Laid	None
10	200	Series 900 GCS	Glued	Epoxy Based	Mechanically Fixed	Snap On
11	200	Series 900 GCS	Glued	Epoxy Based	Mechanically Fixed	Bolted
12	200	Series 900 GCS	Glued & Mech. Fixed	Epoxy Based	Mechanically Fixed	None
13	200	Series 900 GCS	Glued & Mech. Fixed	Epoxy Based	Loose Laid	None

- Notes: 1) Shaded rows indicate installation steps performed by qualified access flooring installers.
 2) Floor grades as follows: Series 900 GCS – medium grade, Series 900 CRS – heavy grade.

4.5.2 Pre-Test Analysis

The pre-test FE model constructed for Structure C is illustrated in Figure 4.81. The slab strip was modelled using isotropic shell elements which were pin supported at the locations of the knife-edge supports. The density of the concrete was assumed to be 2400 kg/m^3 and the modulus of elasticity was 38 kN/mm^2 (Wyatt, 1989). The first four modes of vibration calculated from this model are illustrated in Figure 4.82.

In addition to performing an FE analysis, the first few bending natural frequencies were calculated by hand using the relevant theoretical formulae for simple beams (Blevins, 1979). The use of these equations were only possible for this structure due to the simplicity of its construction. For real buildings, such theoretical expressions are rarely directly applicable and the use of FE techniques is probably the only method of obtaining good predictions of vibration behaviour.

Based on the pre-test FE model results, a test grid covering the whole of the slab strip was selected as shown in Figure 4.83. The auto-MAC calculated for this test grid using the first four modes of vibration indicated the likelihood that there would not be any problems with spatial aliasing.

4.5.3 EMA

4.5.3.1 QA Checks

Testing of Structure C commenced with performing preliminary QA checks on the bare structure (Configuration 1). Due to its construction and testing under laboratory conditions, these checks indicated that very high quality EMA data could be expected from the tests. However, a small peculiarity regarding the structure was noted in that the torsional mode of vibration predicted by the pre-test FE analysis was actually split into two experimental modes. Additionally, the first of these appeared to behave in a non-linear manner as indicated by the reciprocity check between test points 4 and 22 presented in Figure 4.84. The reason for this became more clear following a full modal test swipe and it will be discussed further in Section 4.5.3.7.

4.5.3.2 EMA Strategy

Because Structure C was being tested under convenient laboratory conditions, it was possible to utilise several different EMA techniques to increase confidence in the estimated modal parameters. These would have not been possible when testing Structures A and B due to time limitations. The following EMA techniques were utilised on each of the configurations of Structure C:

1. EMA measurements made using the shaker in free-armature mode with burst random excitation, in the same way as for Structures A and B,
2. EMA measurements made using the shaker in fixed-armature mode with burst random excitation, and
3. EMA measurements made using the shaker in fixed-armature mode with stepped sine excitation.

The implementation of these different EMA techniques will be described in more detail in Sections 4.5.3.3 to 4.5.3.5.

4.5.3.3 EMA Using Burst Random Excitation in Free-Armature Mode

For the EMA swipes performed with burst random excitation in free-armature mode, twenty-seven test points were used in the grid illustrated in Figure 4.83. This grid was designed so that it would be possible to position the shaker at each point on the surface of the sub-floor by lifting only a single access floor panel. Also, by measuring points along the edges of the slab strip, torsional and bending modes of vibration could be examined using these swipes. One swipe was performed for each configuration of the structure, with the response points 14, 16 and 22.

4.5.3.4 EMA Using Burst Random Excitation in Fixed-Armature Mode

Next, for the EMA swipes performed using burst random excitation in fixed-armature mode, the shaker was positioned in the pits which had been constructed beneath Structure C for this purpose. It was attached to the soffit of the slab strip by means of a stinger which had been bonded to the slab strip using epoxy adhesive. This arrangement is shown in Figure 4.85. Two swipes were performed for each configuration of the structure, with the shaker positioned at point 14 for one of the swipes and then at point 16 for the other. For both swipes, a test grid consisting of 19 points along the centreline of the slab strip only was used as illustrated in Figure 4.86. Obviously, these swipes

were not expected to show torsional modes of vibration. The main purpose of these tests was to verify the modal parameters of the bending modes measured using the reaction mode testing, by an alternative method of force measurement, which was only possible because the testing of the structure was conducted under controlled laboratory conditions.

4.5.3.5 EMA Using Stepped Sine Excitation in Fixed-Armature Mode

The final swipe of EMA measurements made for each configuration was made using stepped sine excitation at four levels of peak sinusoidal excitation force (33 N, 66 N, 99 N and 133 N corresponding to 25%, 50%, 75% and 100% respectively of the peak sinusoidal force output of the shaker). The shaker was attached in fixed-armature mode at test point 14 and only the first mode of vibration was examined. The purpose of this test was as an indicator of possible non-linear behaviour of the structure/access floor system. Due to the very long testing times anticipated for these tests, only 9 test points (points 10 to 18 in Figure 4.83) were utilised.

Due to time constraints during the test schedule, only Configurations 1 to 11 (Table 4.23) were tested during May to August 1998. Configurations 12 and 13 were then tested in December 1998.

4.5.3.6 EMA Results

A summary of the EMA results is presented in Table 4.24 for all configurations of the structure. A detailed list of the estimated modal parameters from the various swipes is included in Appendix I of this thesis. The estimated mode shapes, which did not change significantly between the various configurations of the structure, are illustrated in Figure 4.87.

Table 4.24: Structure C - Estimated Modal Parameters from All Floor Configurations.

Floor Configuration ID	Mode 1			Mode 2			Mode 3			Mode 4			Mode 5		
	Freq. (Hz)	Damp. (%)	M. Mass (kg)	Freq. (Hz)	Damp. (%)	M. Mass (kg)	Freq. (Hz)	Damp. (%)	M. Mass (kg)	Freq. (Hz)	Damp. (%)	M. Mass (kg)	Freq. (Hz)	Damp. (%)	M. Mass (kg)
1	4.55	0.53	6990	17.02	0.46	6990	26.02	2.55	3550	28.92	1.35	6990	37.71	1.12	7700
2	4.50	0.57	7230	16.56	0.74	8660	27.00	1.64	4980	28.69	2.60	7350	36.90	1.18	8180
3	4.46	0.60	7240	16.66	0.50	7240	26.49	1.62	5350	28.75	2.42	9900	36.79	1.72	---
4	4.48	0.51	7390	16.75	0.46	7240	24.78	1.95	9620	28.67	1.37	6410	36.78	1.32	8300
5	4.46	0.51	7370	16.66	0.47	7480	23.30	2.08	19490	28.07	1.17	4650	37.00	1.78	6310
6	4.48	0.55	7410	16.74	0.46	7380	25.17	1.95	7460	28.66	1.54	7630	36.97	1.15	7940
7	4.45	0.52	7410	16.63	0.47	7370	24.64	2.06	10260	28.51	1.43	7190	36.48	1.52	8170
8	4.52	0.54	7330	16.84	0.46	7330	25.31	1.86	7190	28.77	1.48	8260	37.12	1.18	8550
9	4.47	0.53	7310	16.75	0.45	7220	24.96	1.90	7350	28.61	1.44	7580	37.17	1.21	12790
10	4.54	0.53	7200	16.84	0.46	7130	25.29	1.81	7630	28.76	1.60	7520	37.16	1.17	8370
11	4.58	0.54	7230	16.91	0.45	7160	25.20	1.78	6490	28.85	1.39	8700	37.27	1.15	8000
12	4.50	0.44	7450	16.82	0.41	7190	24.50	1.78	5490	28.47	1.72	8400	36.85	1.28	7650
13	4.44	0.47	7190	16.72	0.42	7110	23.98	1.50	7040	28.15	1.69	9010	---	---	---

The data from all of the EMA swipes for each configuration of Structure C, using the various methods for excitation described earlier, gave more or less identical estimated modal parameters. The following general points were noted.

- Natural frequencies estimated from the tests utilising the shaker in free-armature mode were consistently 0.01 Hz lower than those estimated from the tests with the shaker in fixed-armature mode. This obviously insignificant difference was probably a result of the additional mass of the shaker body acting as part of the structural system.
- The results from stepped sine EMA on all configurations of the structure showed evidence of very weak non-linearity. This is illustrated in Figure 4.88 which shows the FRF peak corresponding to the first mode of vibration of the structure (Configuration 5) for all four forcing levels. It can be seen that with increasing force level, the magnitude of the peak reduced and the natural frequency reduced very slightly. This is typical of a stiffness softening non-linearity (DTA, 1993b). However, as the effect of this non-linearity was very small, the structure was assumed to be linear.

To help visualise the data in Table 4.24, Figure 4.89 shows percentage changes in natural frequencies between Configuration 1 (the bare slab) and Configurations 2 to 13 (with access floors installed). Only modes 1, 2, 4 and 5 are displayed since the parameter estimations made for the 3rd mode were more erratic for reasons that will be discussed later (Section 4.5.3.7). In addition, Figure 4.90 shows percentage changes in modal damping ratios. By examining the obtained values, the following conclusions were drawn:

- Similarly as for Structures B and C, a general trend was noted for the natural frequencies of the system to reduce following the installation of access floors. The obvious conclusion from this is that the increase in mass due to the access floor systems was more significant than any increase in stiffness provided by them. The only exception to this was for Configuration 11, when bolted stringers were installed. It therefore appears that the bolted stringers served to increase the stiffness of the structural system.
- Configurations 2 and 3 appeared to have more significantly increased modal damping ratios than the rest of the configurations. Since these were the only measurements made with an increased FFH of 600 mm (the rest had an FFH of 200 mm), it is possible that the increased height was advantageous. This could be a result of the increased lever arm between the pedestal bases and the access floor

panels resulting in increased relative displacements occurring between the pedestals and the panels. A consequent increase in damping caused by friction at the connections between the pedestals and the panels may have resulted.

The values in Table 4.24 also indicate that, in general, the modal mass estimated from Configurations 2 to 13 was greater than that estimated from Configuration 1. This is obviously expected and serves as a reassurance that the estimated modal parameters are correct.

4.5.3.7 Discussion of the Torsional Modes of Vibration

As indicated in Figure 4.87 and Table 4.24, there were in fact two torsional modes of vibration measured from the EMA with quite close natural frequencies. However, it was clear from examination of the mode shapes that only the higher of the two modes of vibration was a classical torsional mode. The lower of these two modes appeared to represent a 'rocking' motion of the structure with very little bending taking place. This was the mode which also appeared to behave in a non-linear manner as mentioned in Section 4.5.3.1.

Upon examination of the knife-edge supports of the structure, it was discovered that there was a lack of contact at one of its corners below test point 9. This can be seen from the photograph and close-up presented in Figure 4.91. It was concluded that this 'rocking' mode of vibration was likely to be caused by a (non-linear) contact problem between the slab strip and its supports.

It was also noted that modal parameter estimations made for this mode of vibration were quite erratic. This would be expected to be caused by the non-linear nature of this mode because modal parameter estimation algorithms have an inherent assumption of linearity.

4.5.4 Pedestrian Response Measurements

For the pedestrian response measurements, four test subjects were planned; the writer and three volunteers who were recruited on the basis of their availability. All tests were performed with the pedestrians walking along the length of the slab strip for a pre-specified pacing rate and duration, turning only on the platforms at each end. For each

measurement, the acceleration responses were measured on the surface of the sub-floor at test point 14, the centre of the slab strip.

For each floor configuration, two pacing rates were selected so that their second and third harmonics would coincide with the first natural frequency of the test structure (Tables 4.25 and 4.26). For this reason, similarly as for Structures A and B, the pedestrian response tests had to take place following the analysis of the EMA data to determine the exact first natural frequency of the structure. In each case, the slower pacing rate could be described to be a 'slow walk' and the faster rate could be described as a 'brisk walk' (Bachmann & Ammann, 1987).

Unfortunately, after the tests had commenced, it became apparent that two of the test subjects were unable to maintain the pacing rates provided by the metronome. This was particularly visible when reviewing video footage of the tests, which had been recorded at all times. For this reason, these two sets of test data had to be discarded and the results presented here were measured from tests performed by the two pedestrians who were able to maintain the pacing rate. Tables 4.25 and 4.26 contain the results from the pedestrian response tests for all configurations of the structure for Pedestrians 1 and 2 respectively. The processing of a typical pedestrian response measurement on this structure is illustrated in Figure 4.92.

**Table 4.25: Structure C - Results from Pedestrian Response Measurements
Performed by Pedestrian 1.**

Floor Config. ID	Frequency Excited	Harmonic Excited	Pacing Rate (spm)	RMS Entire Record (%g)	Peak Running RMS 10 s Int. (%g)	VDV 8 h Exp. (m/s ^{1.75})
1	4.55	2	136	2.40	2.96	3.56
1	4.55	3	90	0.83	1.06	1.28
2	4.50	2	135	1.59	2.24	2.48
2	4.50	3	90	0.66	0.96	1.04
3	4.46	2	134	1.58	2.19	2.45
3	4.46	3	89	0.66	0.84	1.03
4	4.48	2	134	2.11	2.71	3.17
4	4.48	3	89	0.71	1.00	1.12
5	4.46	2	134	1.58	1.99	2.42
5	4.46	3	89	0.74	1.11	1.16
6	4.48	2	134	1.99	2.82	3.00
6	4.48	3	89	0.77	1.01	1.21
7	4.45	2	133	1.77	2.24	2.66
7	4.45	3	89	0.64	0.97	1.05
8	4.52	2	135	2.02	2.48	3.02
8	4.52	3	90	0.59	0.78	0.93
9	4.47	2	134	1.74	2.24	2.62
9	4.47	3	89	0.66	1.04	1.06
10	4.54	2	136	2.02	2.45	3.00
10	4.54	3	90	0.68	1.07	1.11
11	4.58	2	137	1.66	2.12	2.49
11	4.58	3	91	0.79	1.04	1.22
12	4.50	2	135	1.84	2.34	2.73
12	4.50	3	90	1.09	1.45	1.66
13	4.44	2	134	1.16	1.66	1.81
13	4.44	3	89	0.99	1.30	1.53

**Table 4.26: Structure C - Results from Pedestrian Response Measurements
Performed by Pedestrian 2.**

Floor Config. ID	Frequency Excited	Harmonic Excited	Pacing Rate (spm)	RMS Entire Record (%g)	Peak Running RMS 10 s Int. (%g)	VDV 8 h Exp. (m/s ^{1.75})
1	4.55	2	136	1.70	2.28	2.58
1	4.55	3	90	0.77	1.07	1.21
2	4.50	2	135	1.14	1.59	1.77
2	4.50	3	90	0.64	0.79	0.96
3	4.46	2	134	0.92	1.51	1.50
3	4.46	3	89	0.69	0.92	1.07
4	4.48	2	134	1.35	1.62	2.00
4	4.48	3	89	0.84	1.09	1.30
5	4.46	2	134	1.10	1.39	1.67
5	4.46	3	89	0.99	1.23	1.50
6	4.48	2	134	1.78	2.49	2.73
6	4.48	3	89	0.69	0.93	1.07
7	4.45	2	133	1.72	2.13	2.55
7	4.45	3	89	0.60	0.77	0.90
8	4.52	2	135	1.82	2.31	2.74
8	4.52	3	90	0.63	0.77	0.96
9	4.47	2	134	1.70	2.29	2.56
9	4.47	3	89	0.65	0.92	1.02
10	4.54	2	136	1.86	2.14	2.77
10	4.54	3	90	0.61	0.78	0.95
11	4.58	2	137	1.90	2.43	2.85
11	4.58	3	91	0.50	0.71	0.80
12	4.50	2	135	1.91	2.50	2.85
12	4.50	3	90	0.74	1.02	1.13
13	4.44	2	134	1.28	1.61	1.97
13	4.44	3	89	0.76	1.12	1.17

To visualise the data in Tables 4.25 and 4.26 better, several plots have been constructed to illustrate the changes between the response parameters measured between configuration 1 and configurations 2 to 13 for both test subjects. These are as follows.

- Figure 4.93: Percentage changes in RMS acceleration response (entire record) for 2nd harmonic excitation.
- Figure 4.94: Percentage changes in peak running RMS for 2nd harmonic excitation.
- Figure 4.95: Percentage changes in VDV for 2nd harmonic excitation.
- Figure 4.96: Percentage changes in RMS acceleration response (entire record) for 3rd harmonic excitation.
- Figure 4.97: Percentage changes in peak running RMS for 3rd harmonic excitation.
- Figure 4.98: Percentage changes in VDV for 3rd harmonic excitation.

Detailed inspection of these charts revealed the following salient points.

1. In general, there was a reduction in the measured response of the floor for both pedestrians, both excitation harmonics and when using all response parameters from that measured on the bare floor. When averaged over all access floor configurations, the response was reduced by between 1.18% and 26.88%.
2. The reductions in response measured for 2nd harmonic excitation were higher than those measured for 3rd harmonic excitation. Examination of Tables 4.25 and 4.26 shows that the magnitude of the response was higher for 2nd harmonic excitation than for 3rd harmonic excitation, which would be expected due to the faster pacing rate and the fact that the Fourier amplitude coefficient corresponding to the 2nd harmonic is higher than that corresponding to the 3rd harmonic (Bachmann et al., 1995). It is therefore possible that the reduction in response is amplitude dependent.
3. In general, configurations of access floors in which the panels were mechanically fixed to the pedestals exhibited lower reductions in response than those configurations in which the panels were loose laid onto the pedestals. It is possible that the connection between the pedestals and the panels acted as a friction damper, which could not be engaged when the panels were mechanically fixed.

4.5.5 Lessons Learned from Testing Structure C

- The inability of two of the pedestrians to maintain pacing rates consistent with the beat provided by the metronome was a significant drawback, resulting in 50% of the pedestrian response test data having to be discarded. In future, if tests are performed with the intention to provide best possible human excitation tuned to specific

frequencies, potential pedestrians should be evaluated to ensure that they are able to maintain a constant pacing rate.

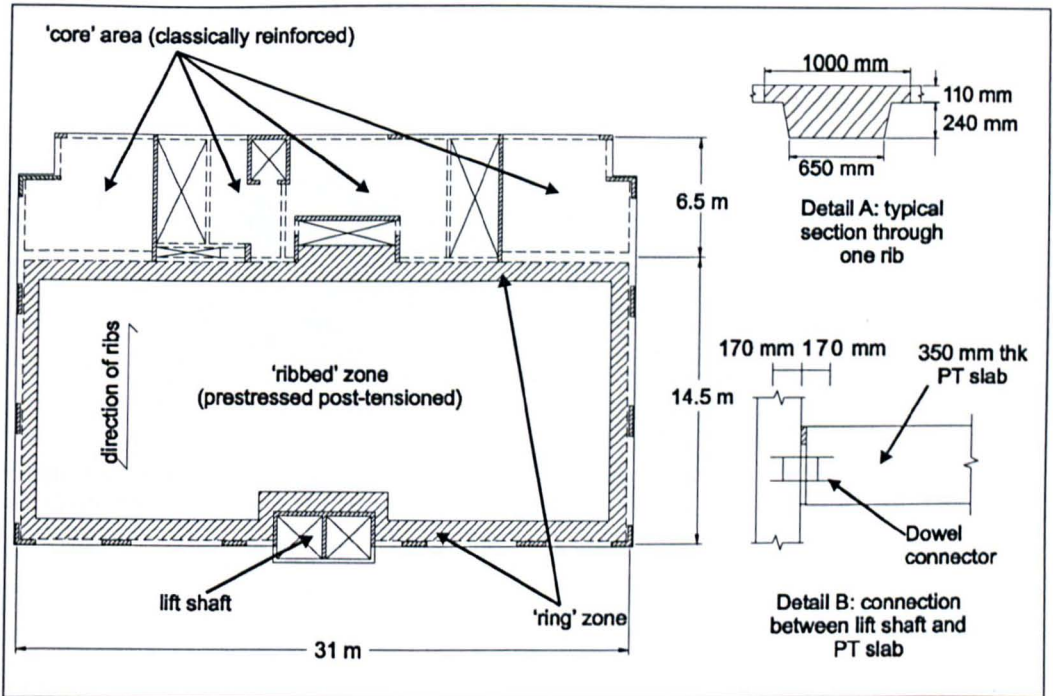


Figure 4.1: Structure A - Configuration of the Structure.



Figure 4.2: Test Structure A (Configuration 1) - Photograph.

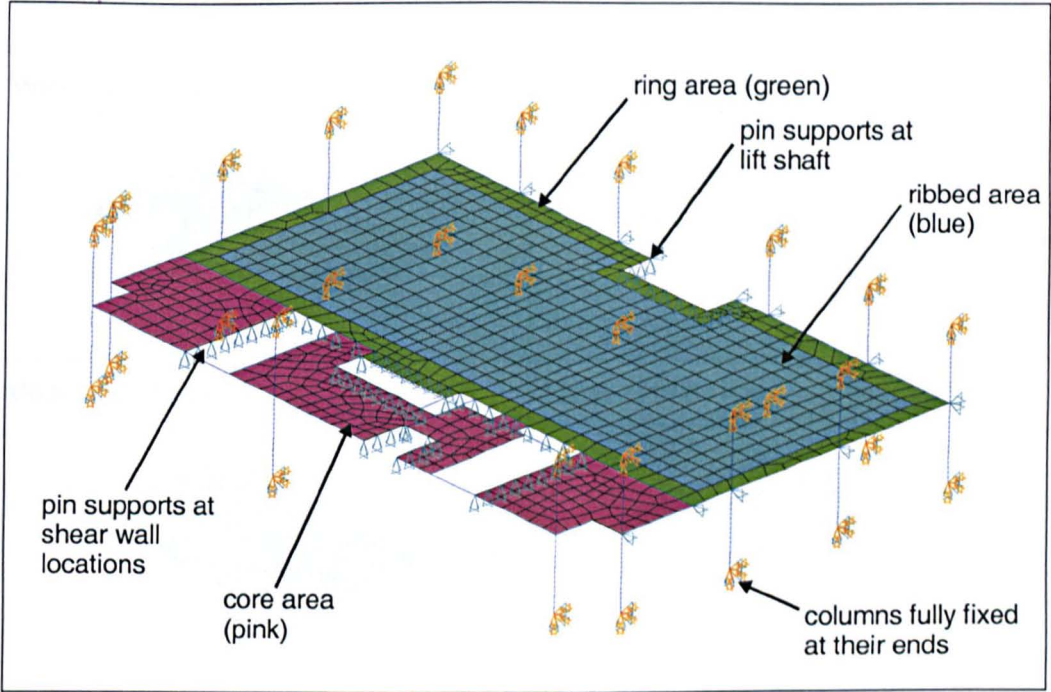


Figure 4.3: Structure A - Pre-Test FE Model.

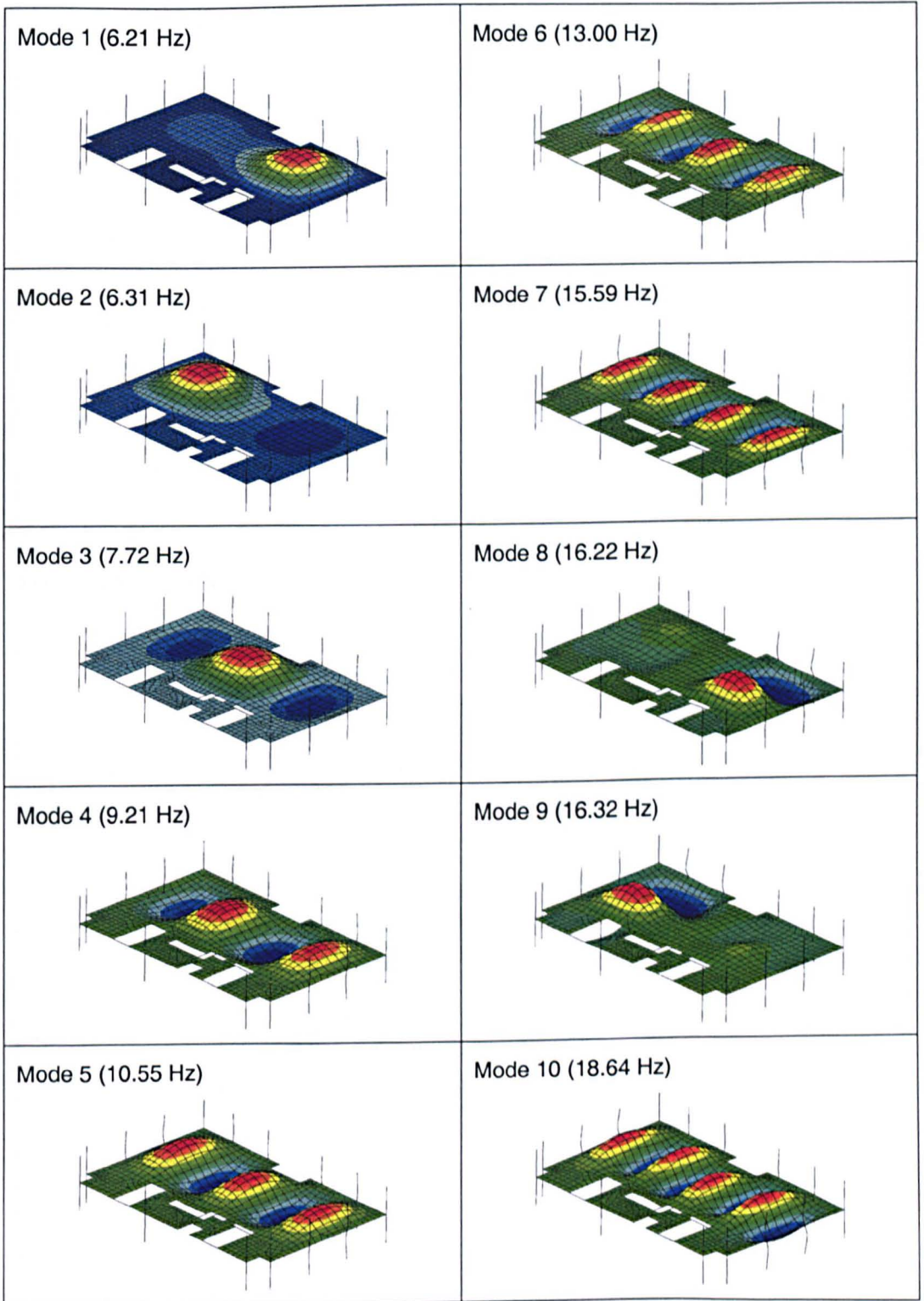


Figure 4.4: Structure A - First 10 Modes Calculated from Pre-Test FE Model.

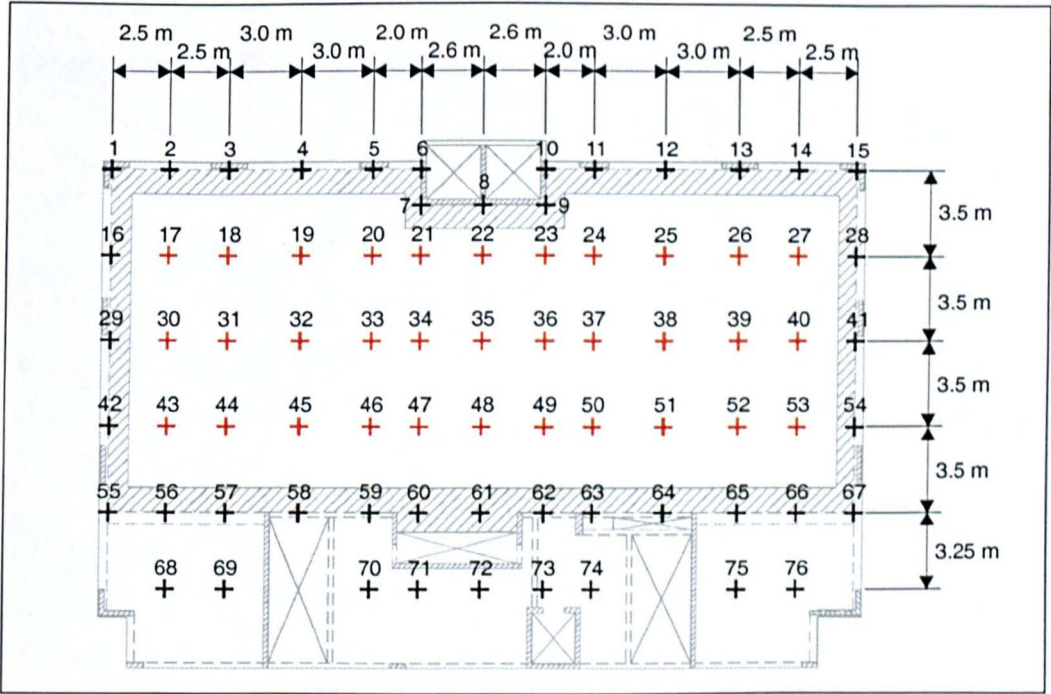


Figure 4.5: Structure A - Test Grid.

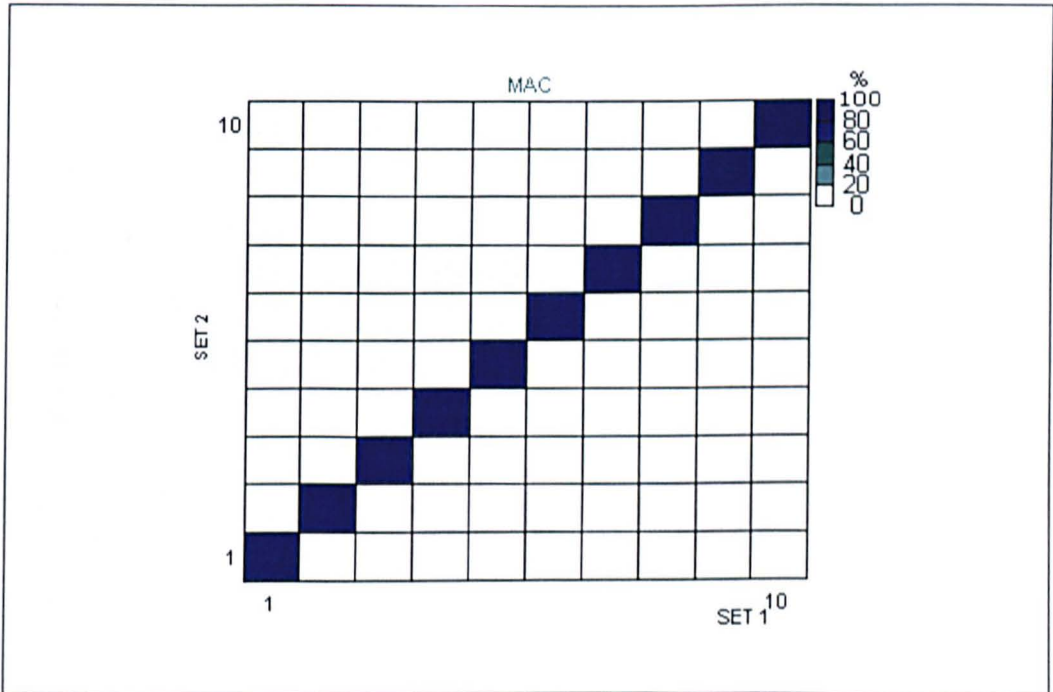


Figure 4.6: Structure A - Auto-MAC Calculated for Proposed Test Grid.



Figure 4.7: Structure A (Configuration 1) - Photograph of the Data Acquisition Centre Located in the Core Area of the Floor.

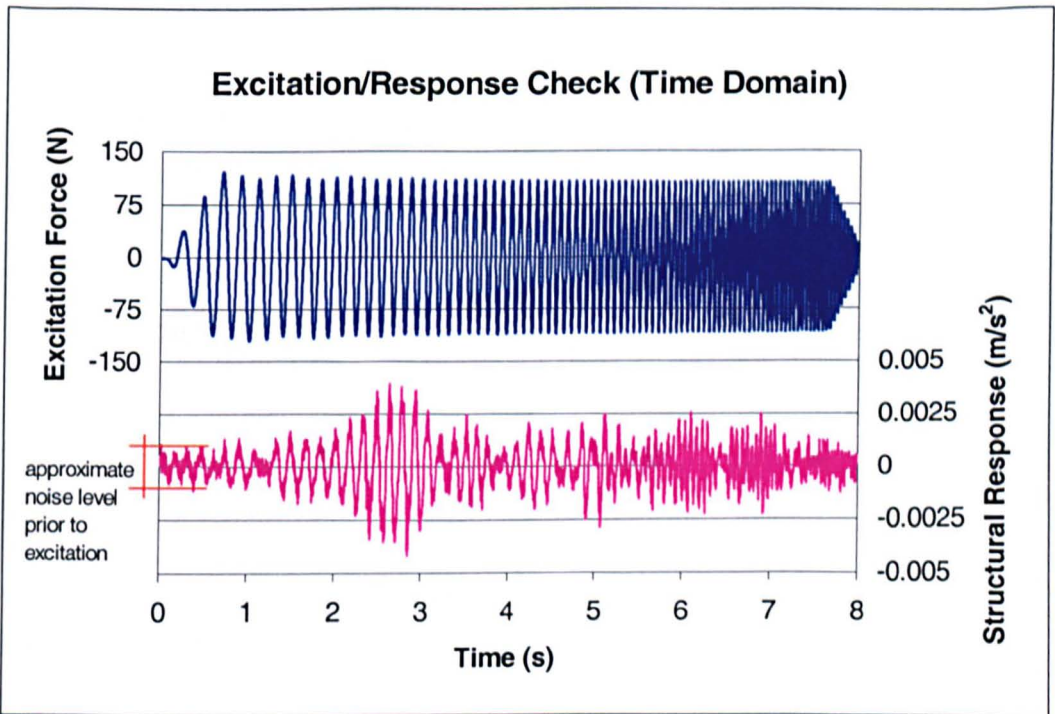


Figure 4.8: Structure A (Configuration 1) - Excitation/Response Check for BSS Excitation (Time Domain).

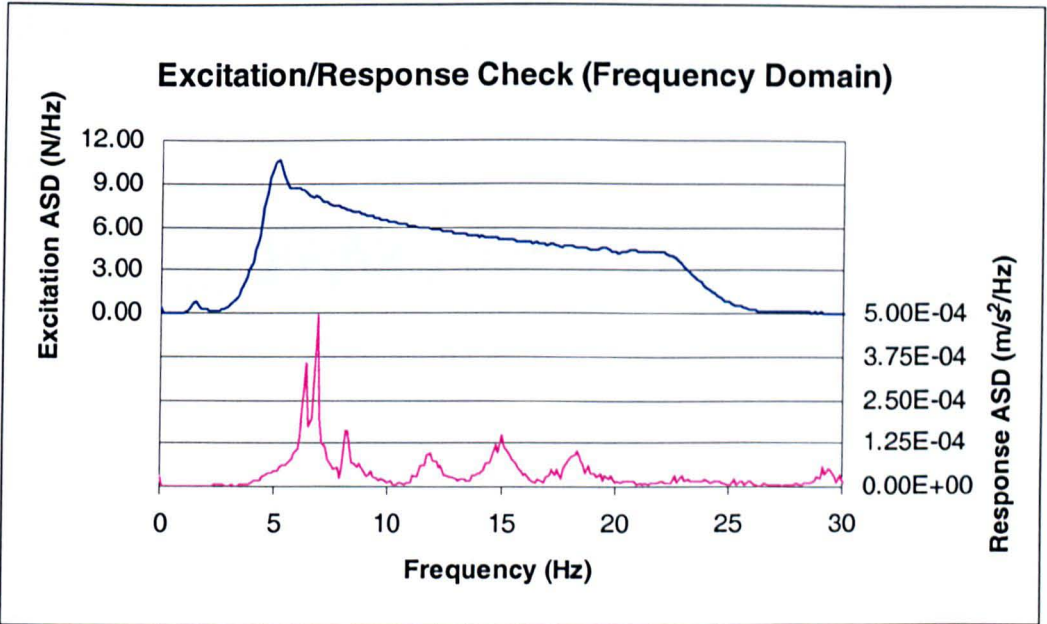


Figure 4.9: Structure A (Configuration 1) - Excitation/Response Check for BSS Excitation (Frequency Domain).

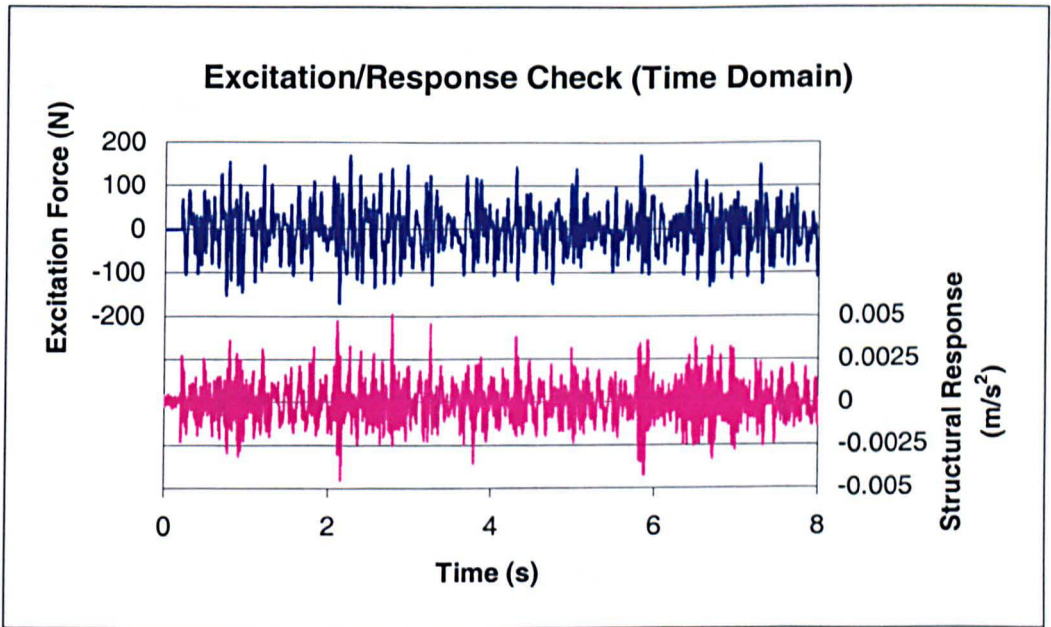


Figure 4.10: Structure A (Configuration 1) - Excitation/Response Check for BR Excitation (Time Domain).

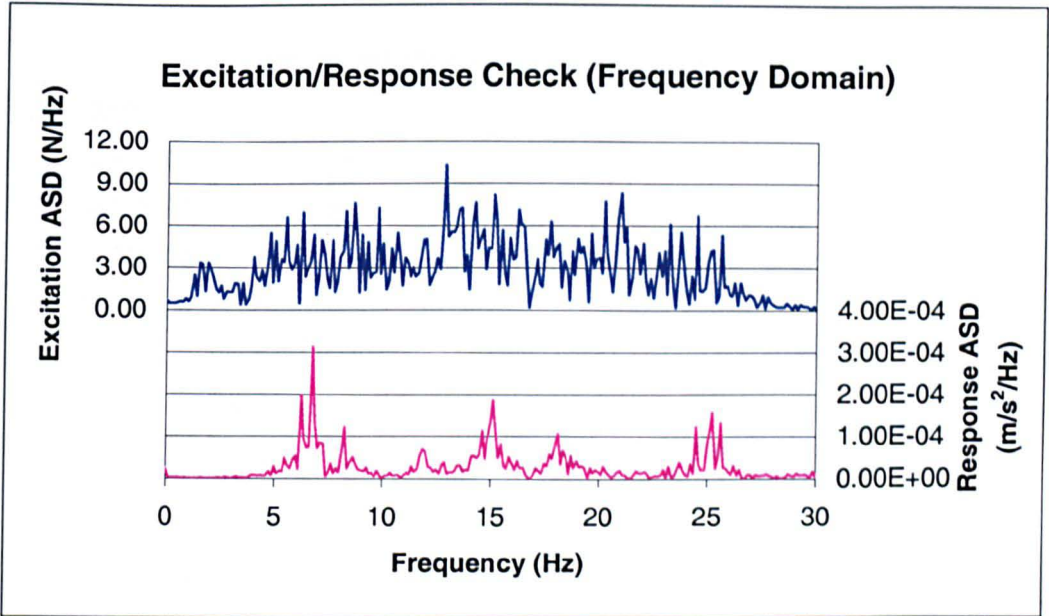


Figure 4.11: Structure A (Configuration 1) - Excitation/Response Check for BR Excitation (Frequency Domain).

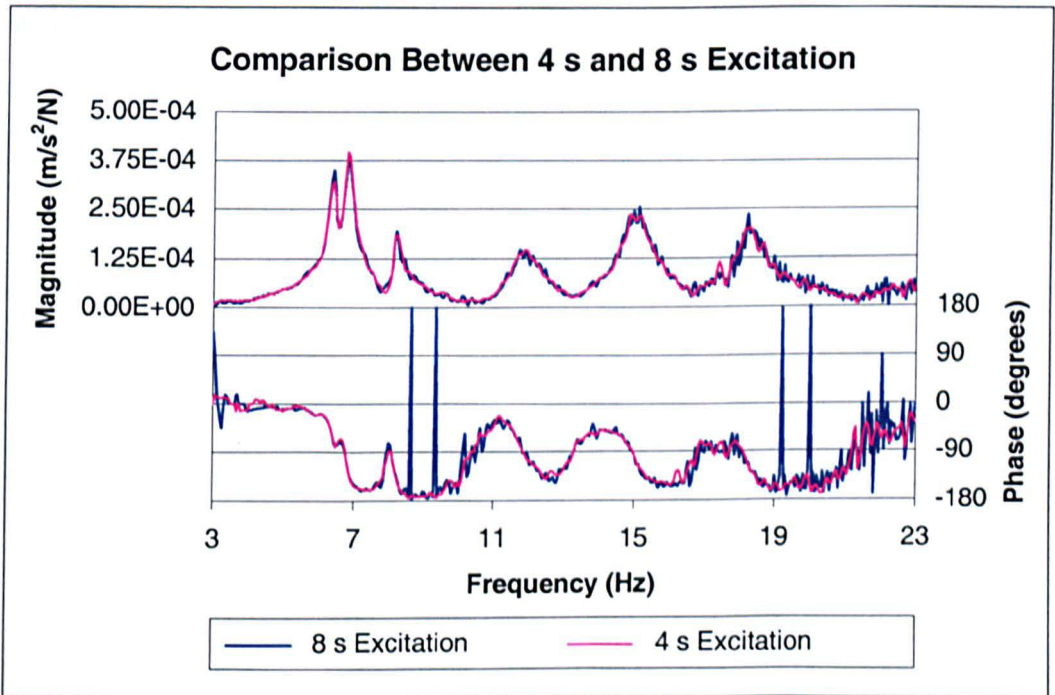


Figure 4.12: Structure A (Configuration 1) - Comparison Between 4 s and 8 s of BSS Excitation.

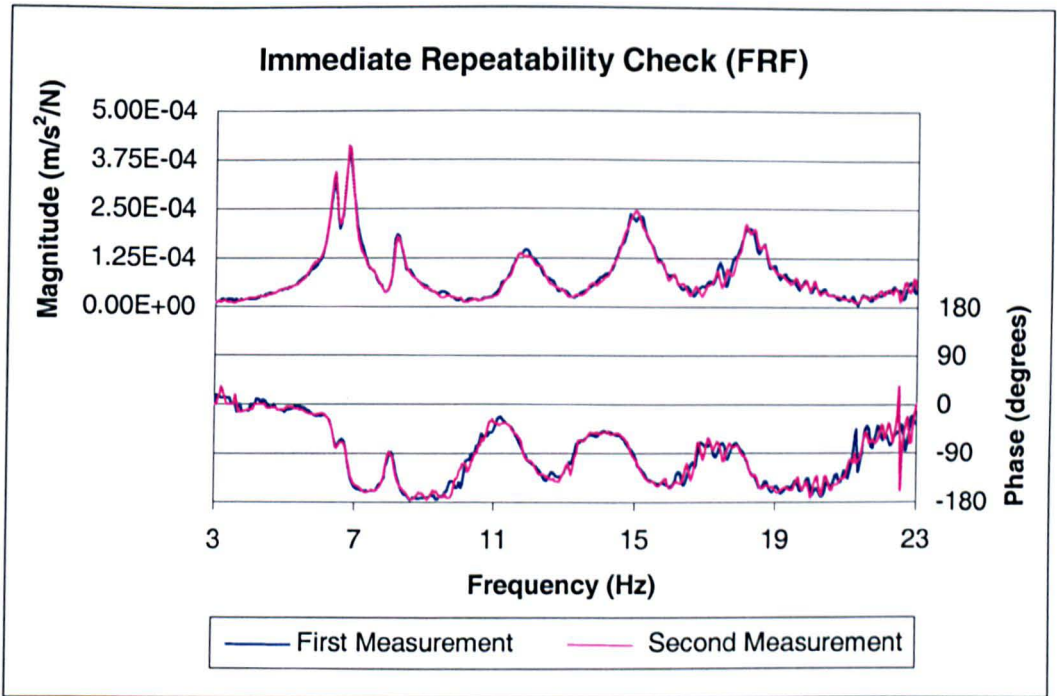


Figure 4.13: Structure A (Configuration 1) - Immediate Repeatability Check for BSS Excitation.

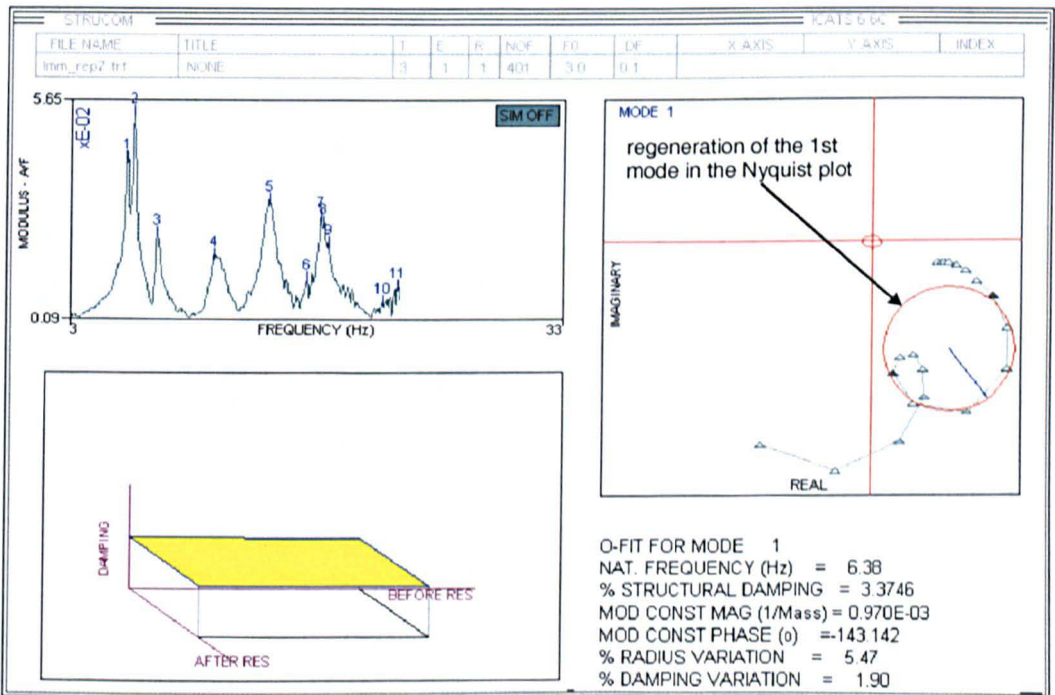


Figure 4.14: Structure A (Configuration 1) - SDOF Processing of Immediate Repeatability Check FRF.

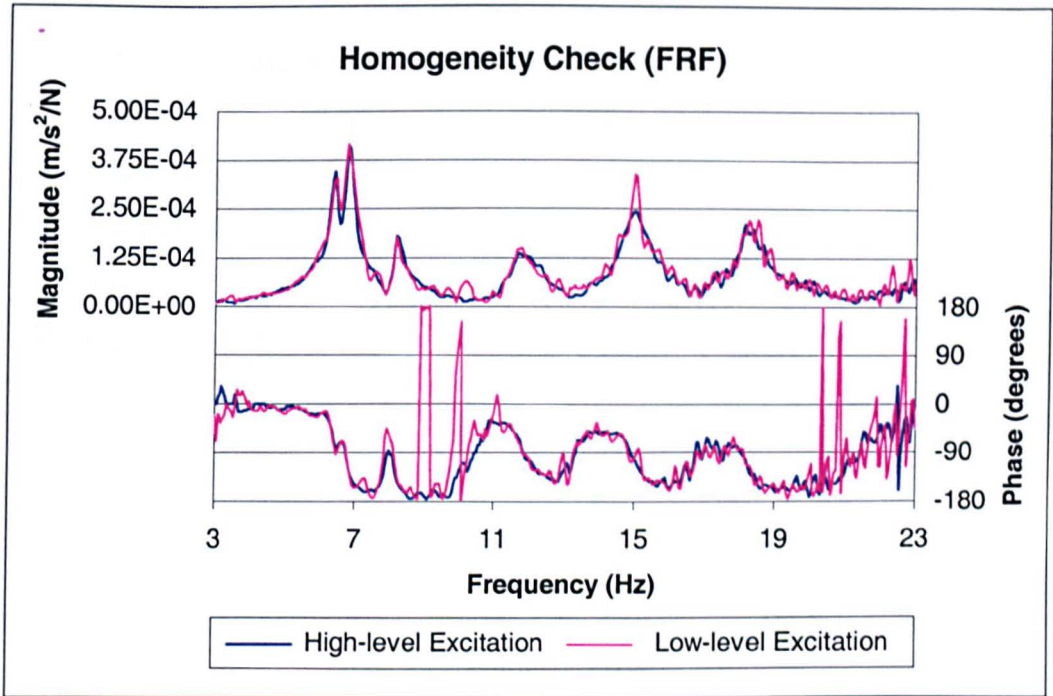


Figure 4.15: Structure A (Configuration 1) - Homogeneity Check for BSS Excitation.

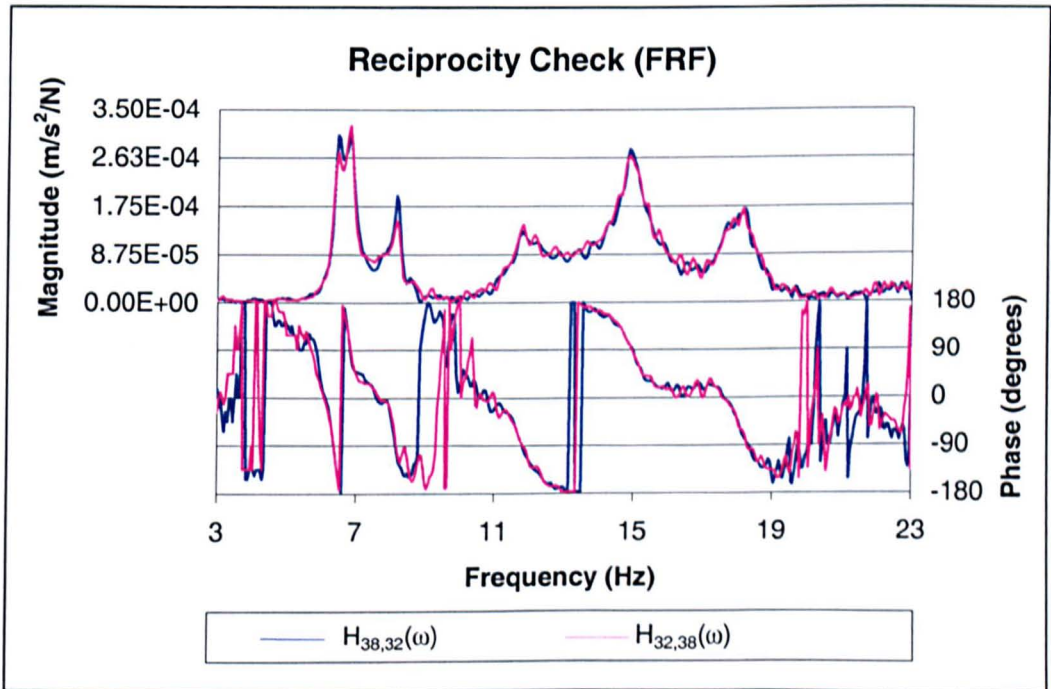


Figure 4.16: Structure A (Configuration 1) - Reciprocity Check for BSS Excitation.

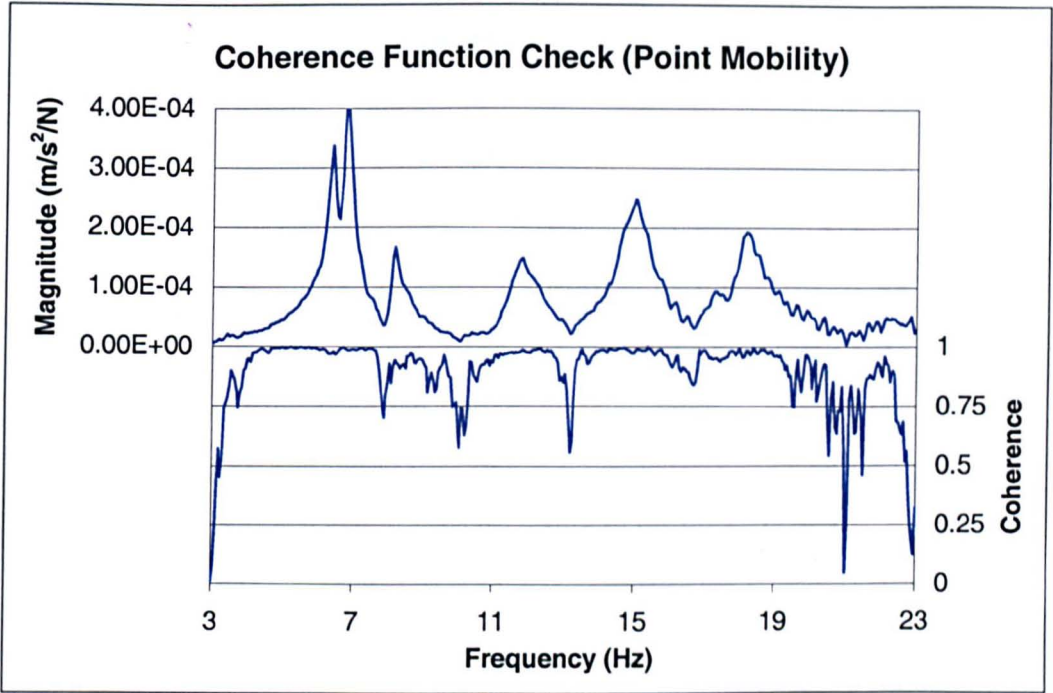


Figure 4.17: Structure A (Configuration 1) - Point Mobility Coherence Check for BSS Excitation.

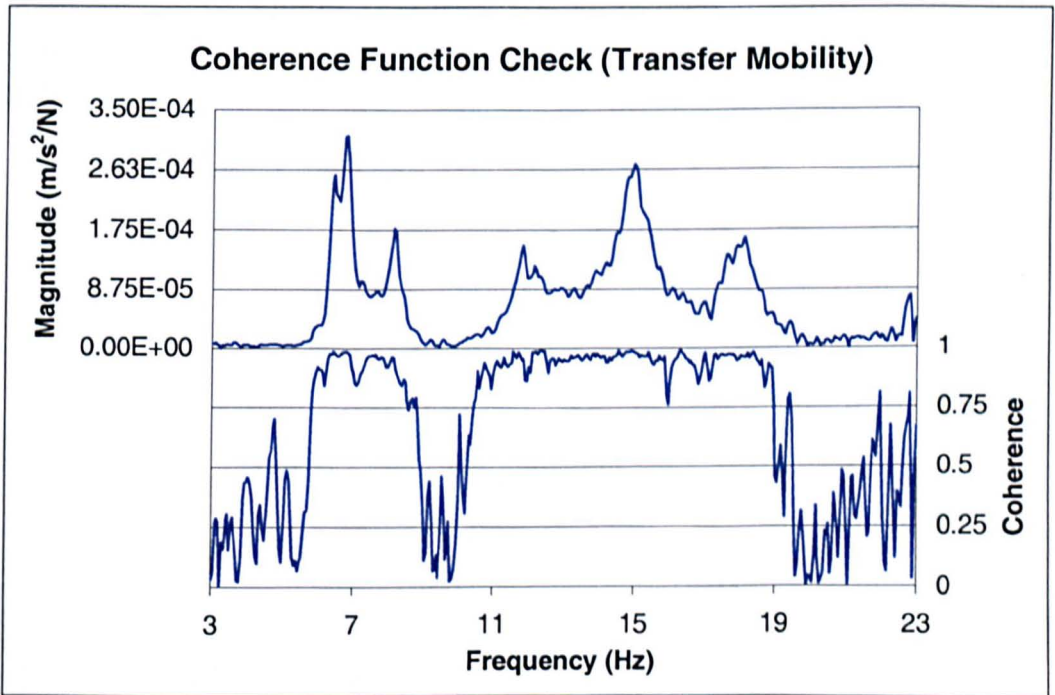


Figure 4.18: Structure A (Configuration 1) - Transfer Mobility Coherence Check for BSS Excitation.

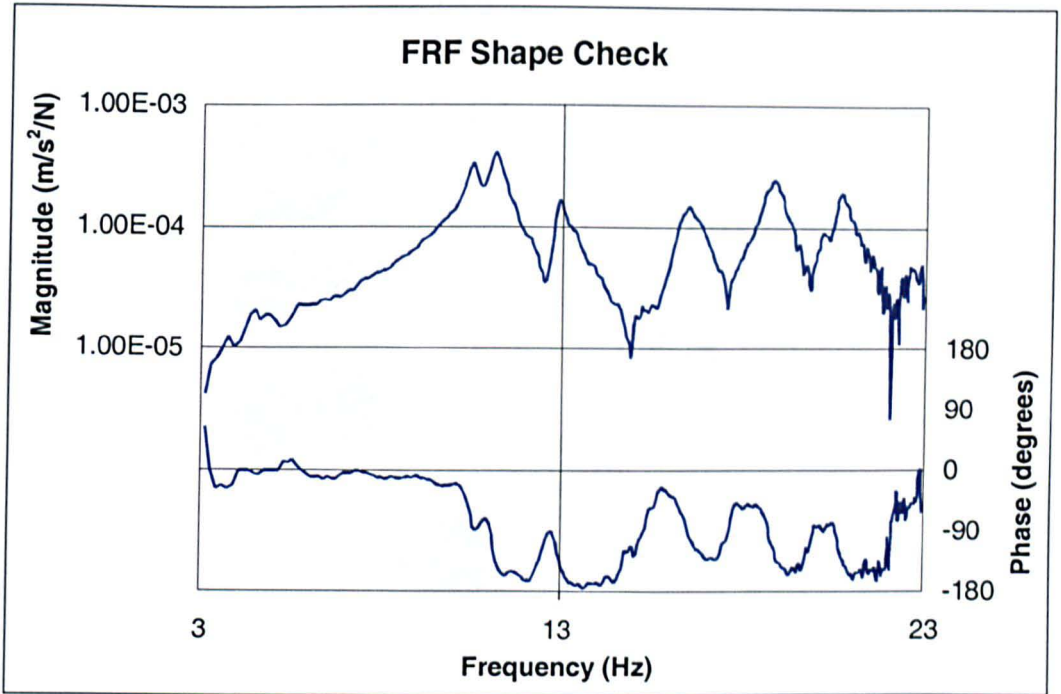


Figure 4.19: Structure A (Configuration 1) - FRF Shape Check for BSS Excitation.

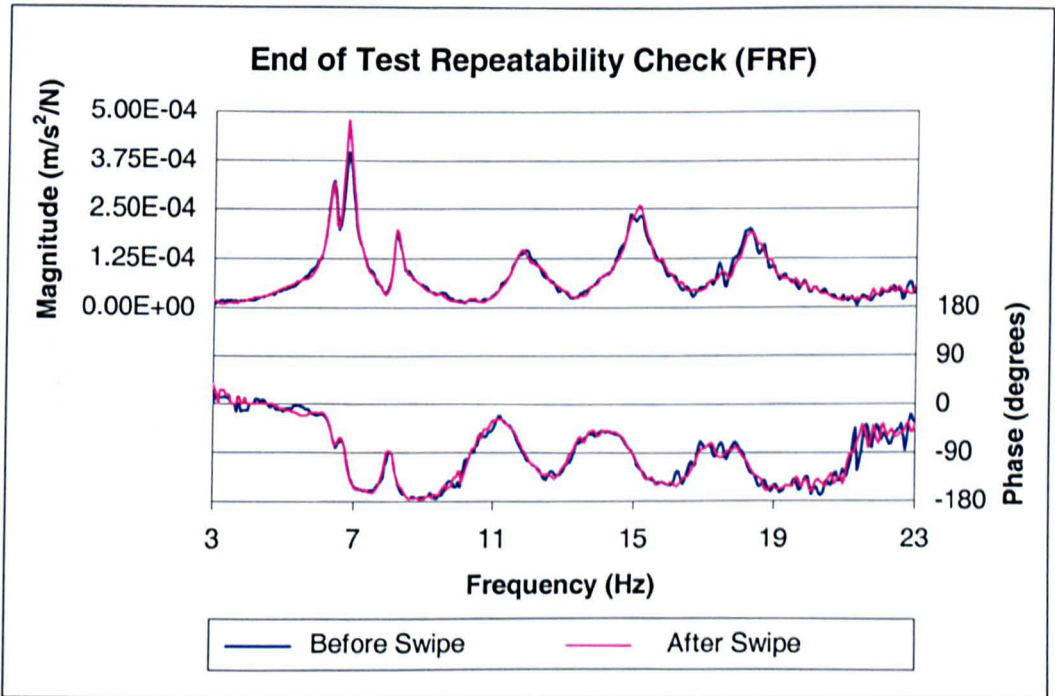


Figure 4.20: Structure A (Configuration 1) - End of Test Repeatability Check for BSS Excitation.

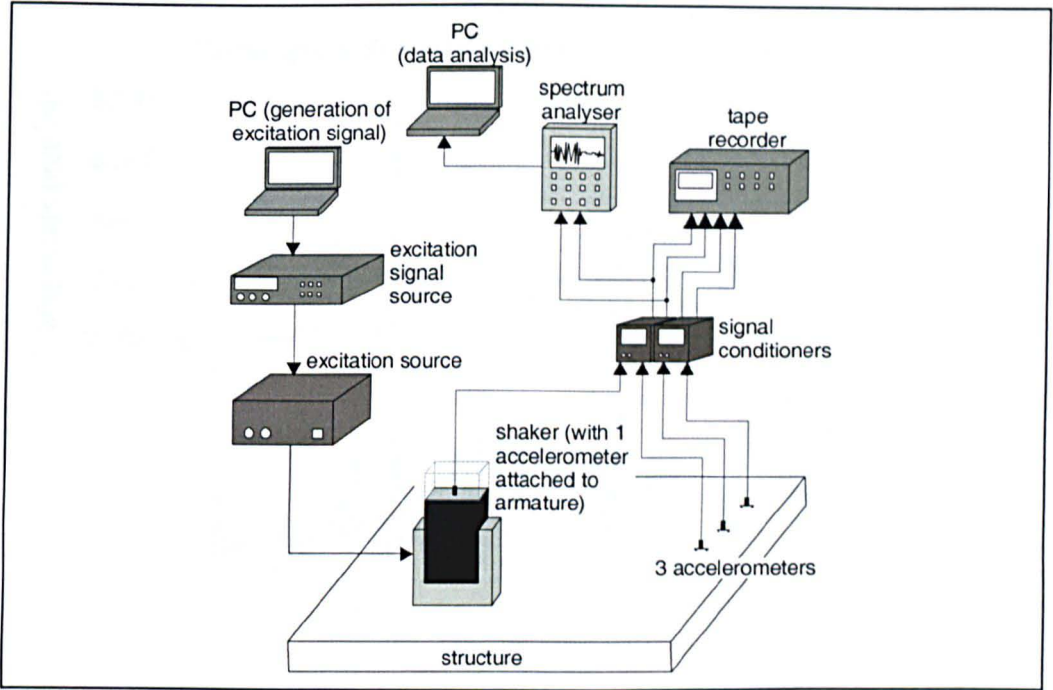


Figure 4.21: Schematic Illustration of the Instrumentation System.

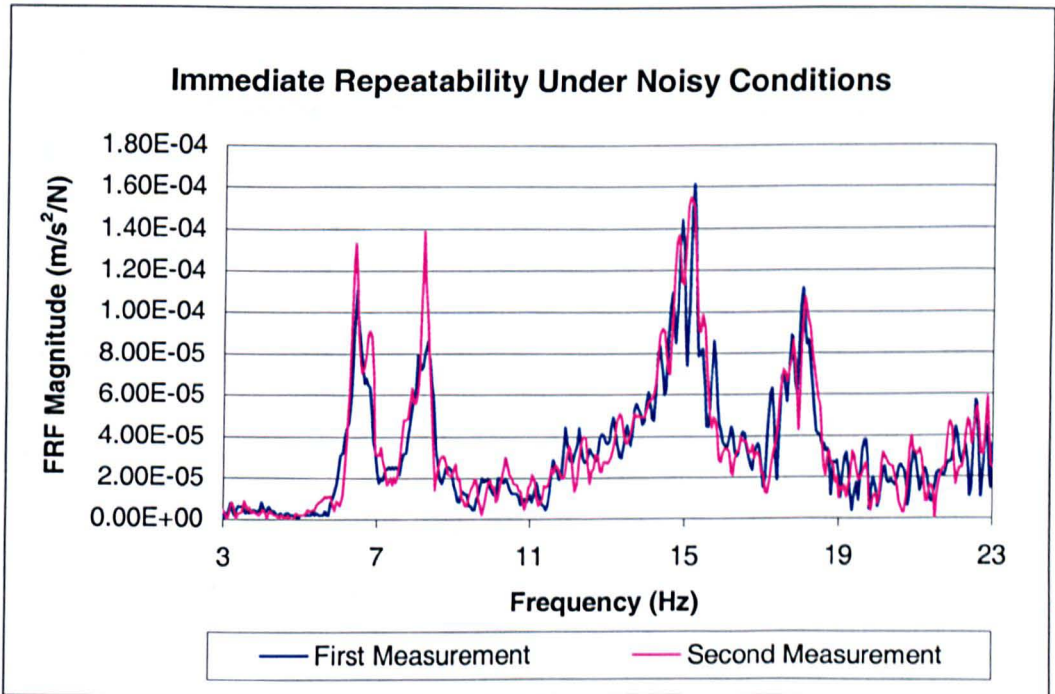


Figure 4.22: Structure A (Configuration 1) - Transfer Mobility Immediate Repeatability Check Under Noisy Conditions.

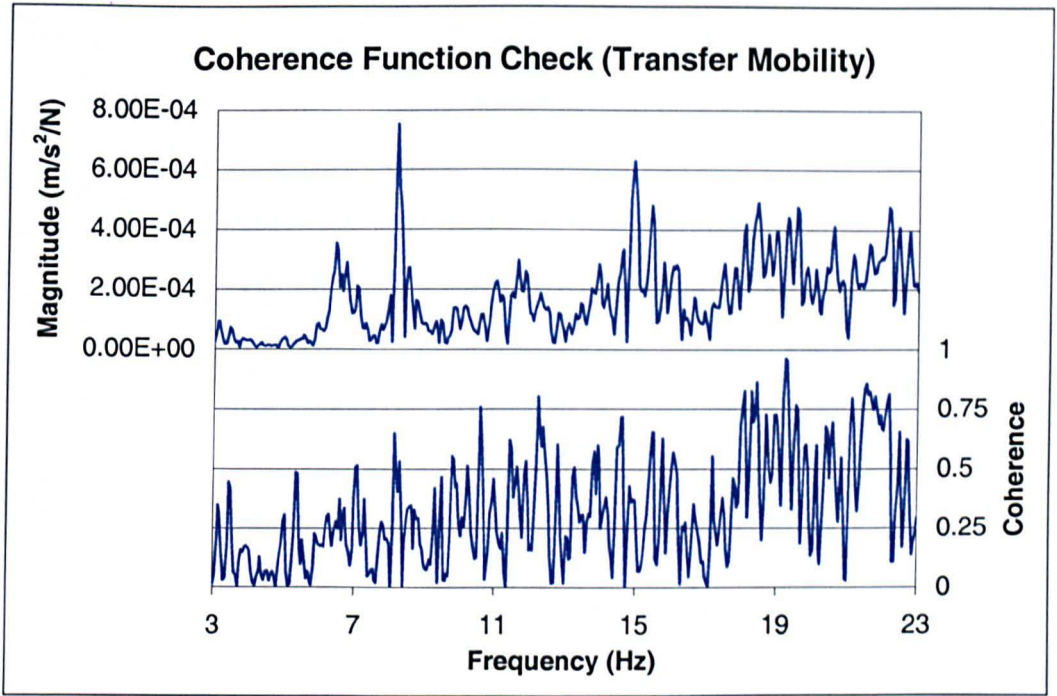


Figure 4.23: Structure A (Configuration 1) - Coherence Function for Transfer FRF Between Points 29 and 32.

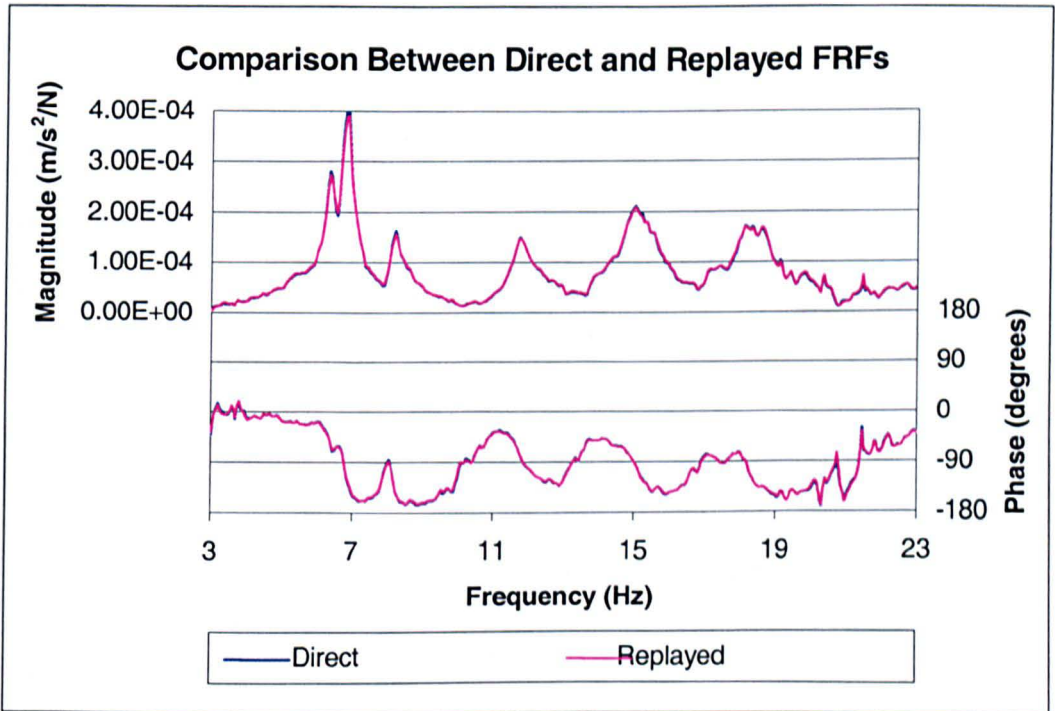


Figure 4.24: Structure A (Configuration 1) - Comparison of Direct and Replayed FRFs.

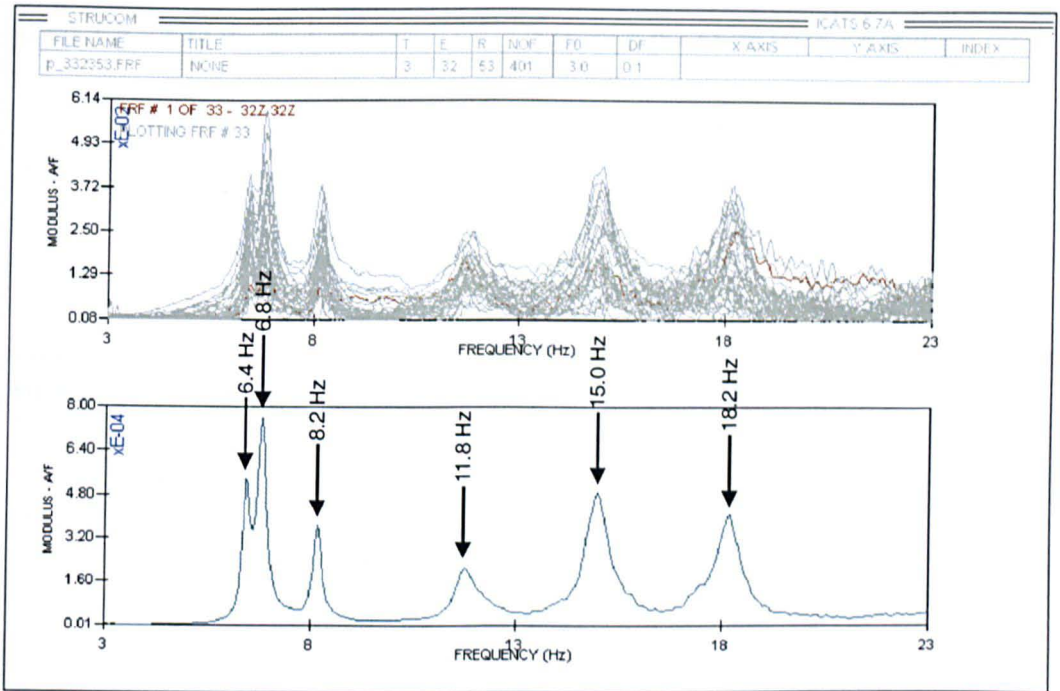


Figure 4.25: Structure A (Configuration 1) - Complex MIF for BSS Swipe Measured at Test Point 32.

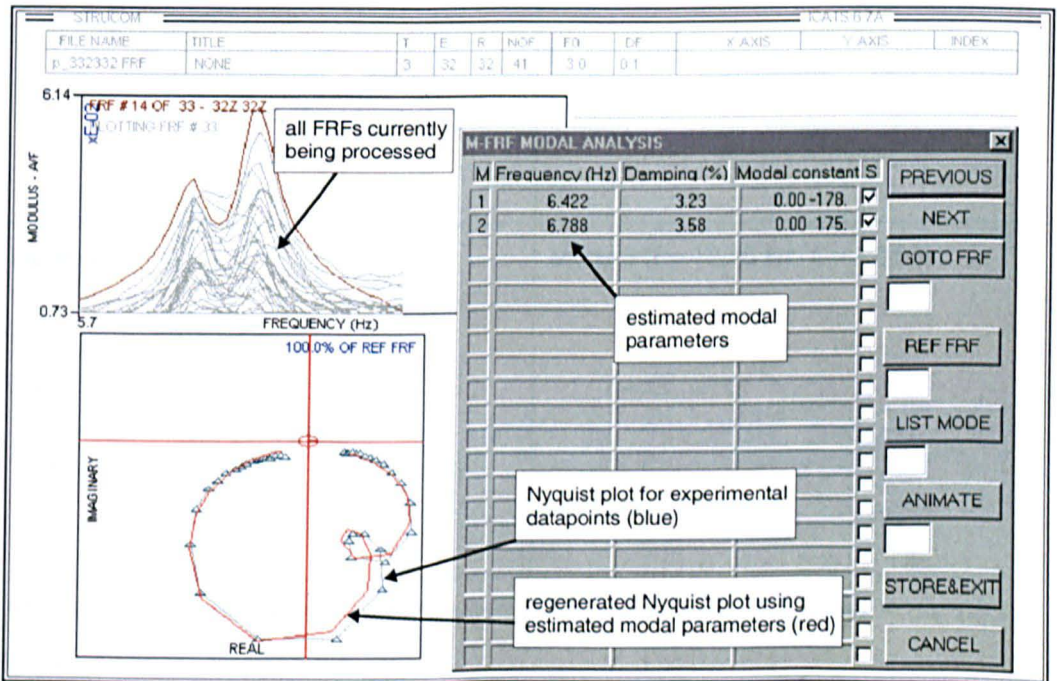


Figure 4.26: Structure A (Configuration 1) - MDOF Modal Parameter Estimation (Global-M) for BSS Swipe Measured at Test Point 32.

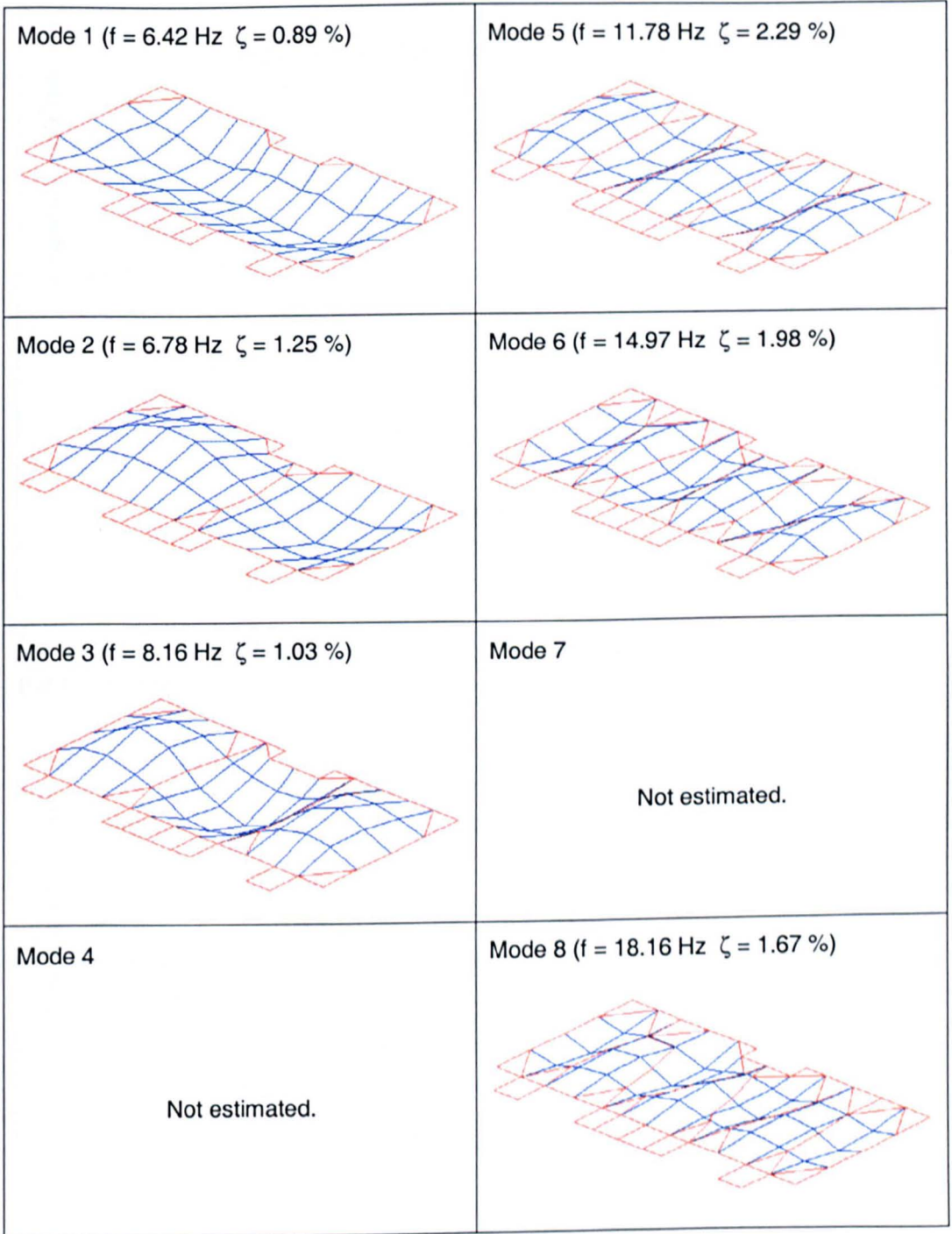


Figure 4.27: Structure A (Configuration 1) - Estimated Mode Shapes From BSS Swipe.

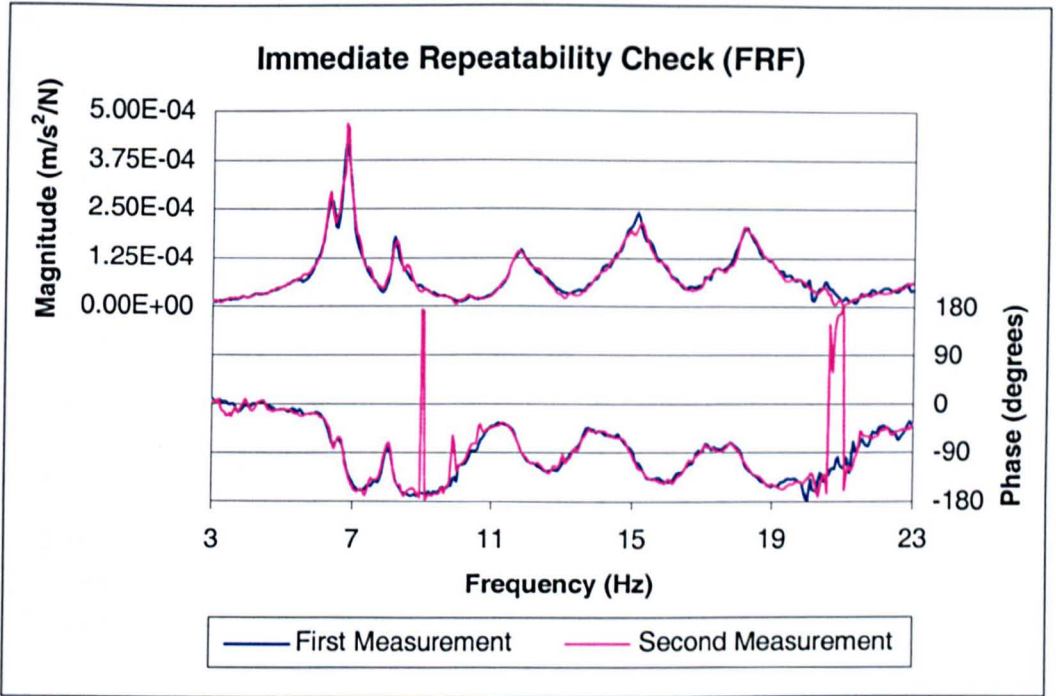


Figure 4.28: Structure A (Configuration 1) - Immediate Repeatability Check for BR Excitation.

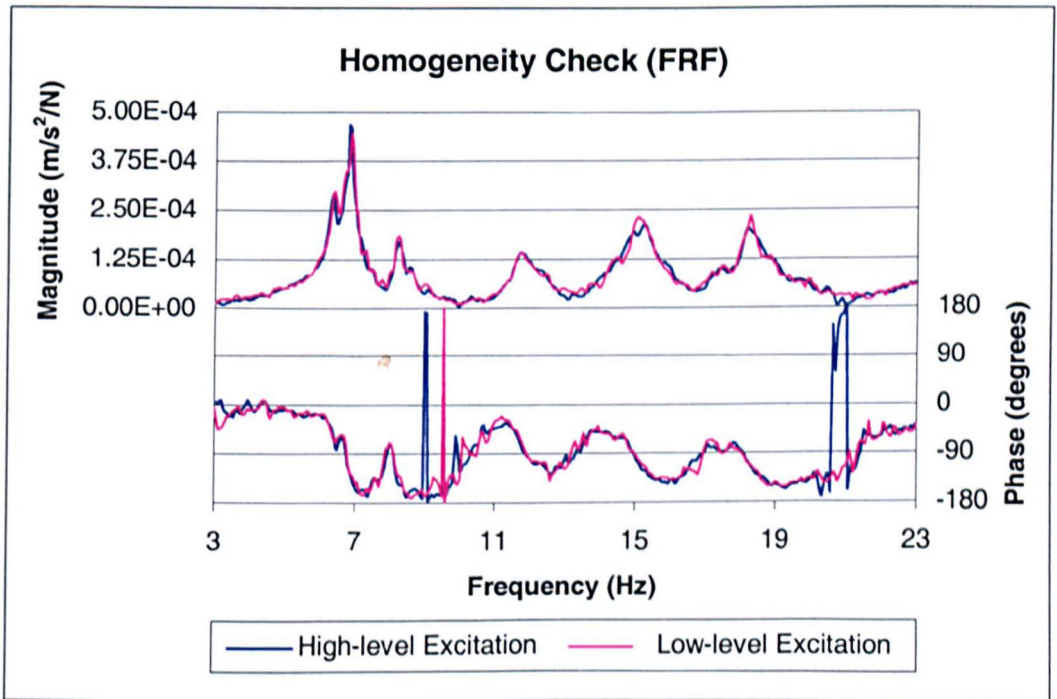


Figure 4.29: Structure A (Configuration 1) - Homogeneity Check for BR Excitation.

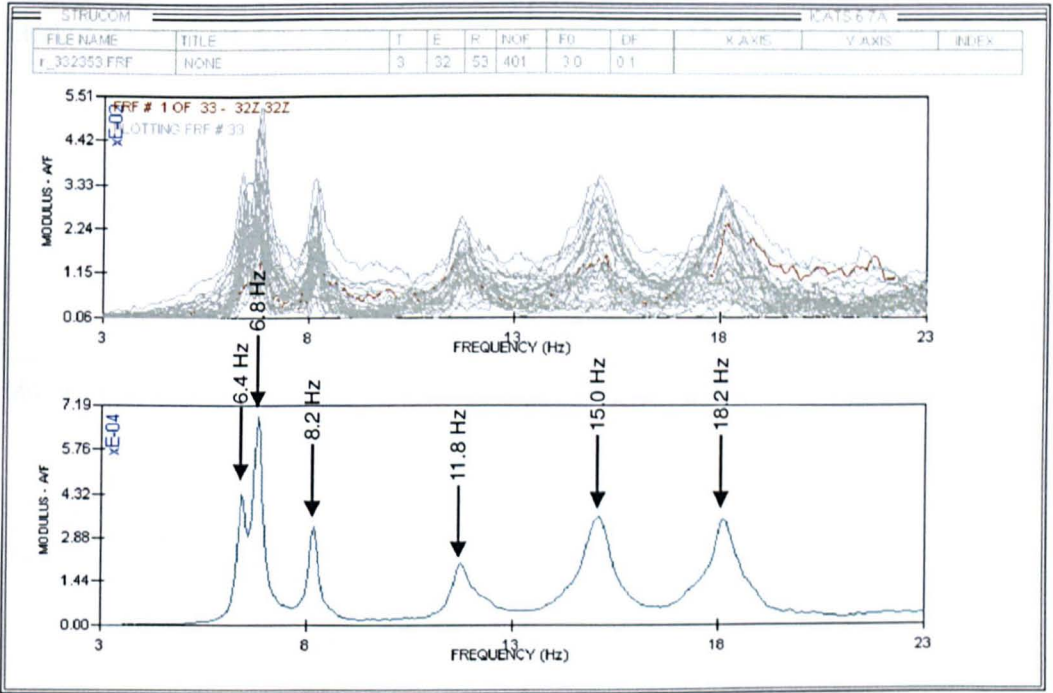


Figure 4.30: Structure A (Configuration 1) - Complex MIF for BR Swipe Measured at Test Point 32.

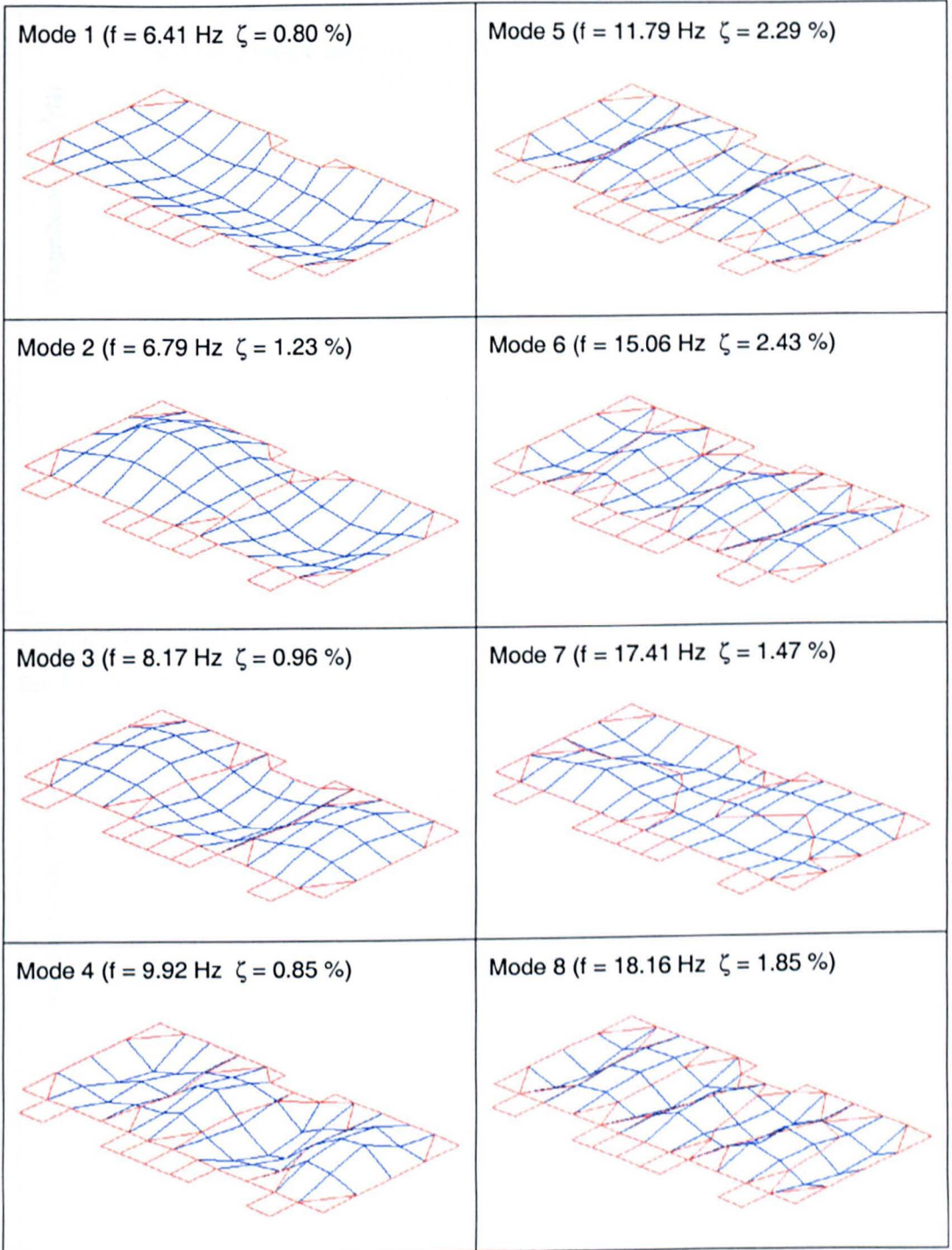


Figure 4.31: Structure A (Configuration 1) - Estimated Mode Shapes from BR Swipe.

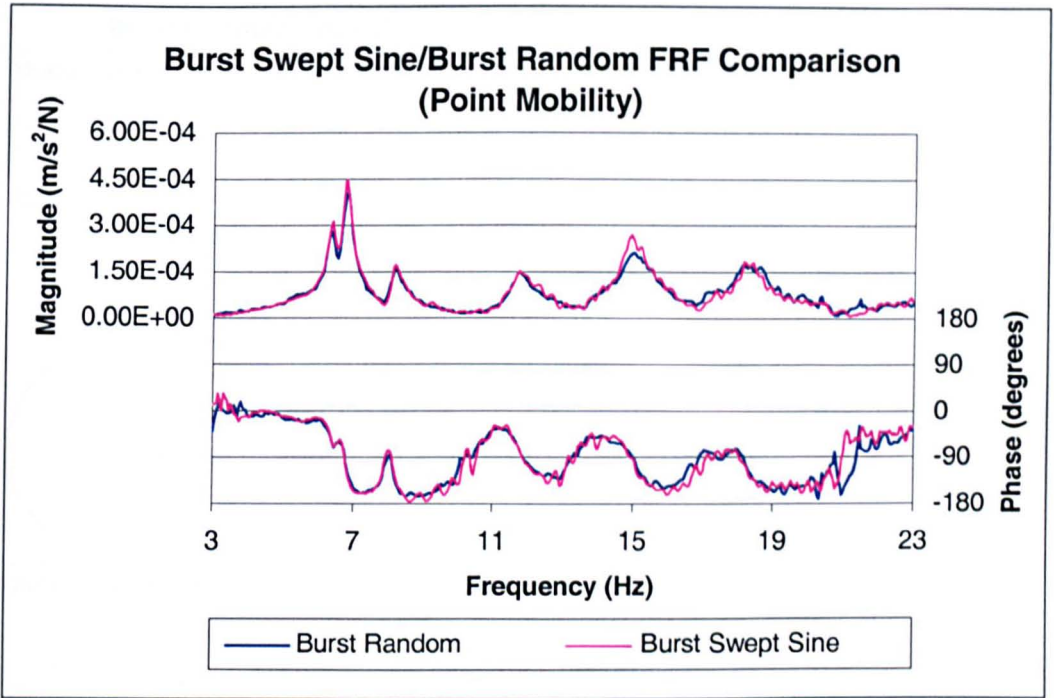


Figure 4.32: Structure A (Configuration 1) - Comparison of Point Mobility FRF for BR and BSS Excitation.

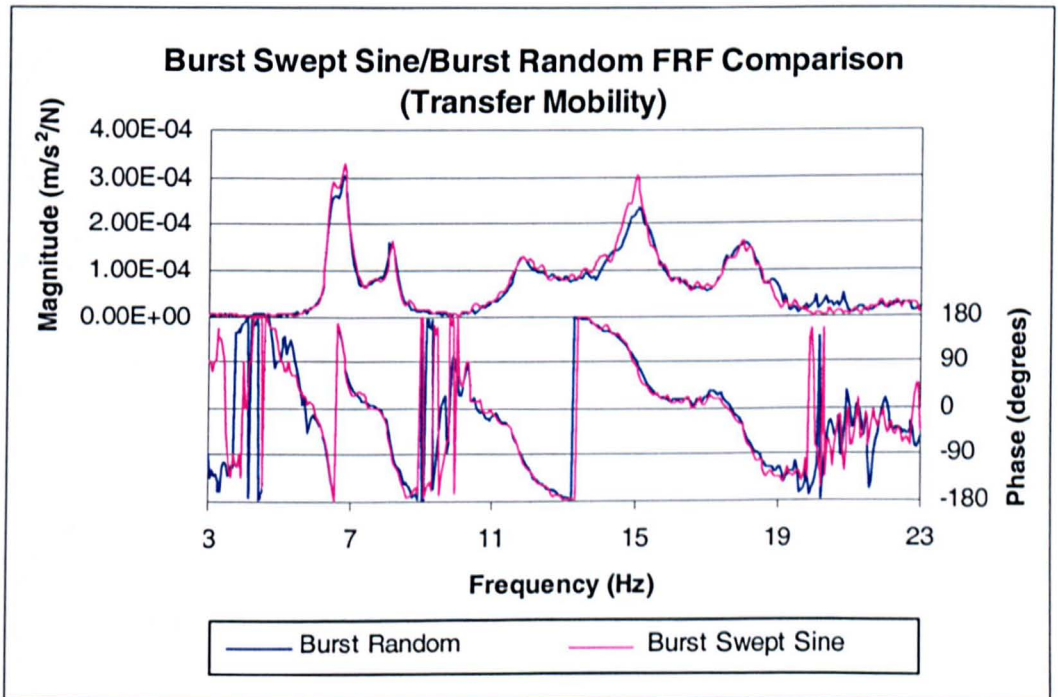


Figure 4.33: Structure A (Configuration 1) - Comparison of Transfer Mobility FRF for BR and BSS Excitation.

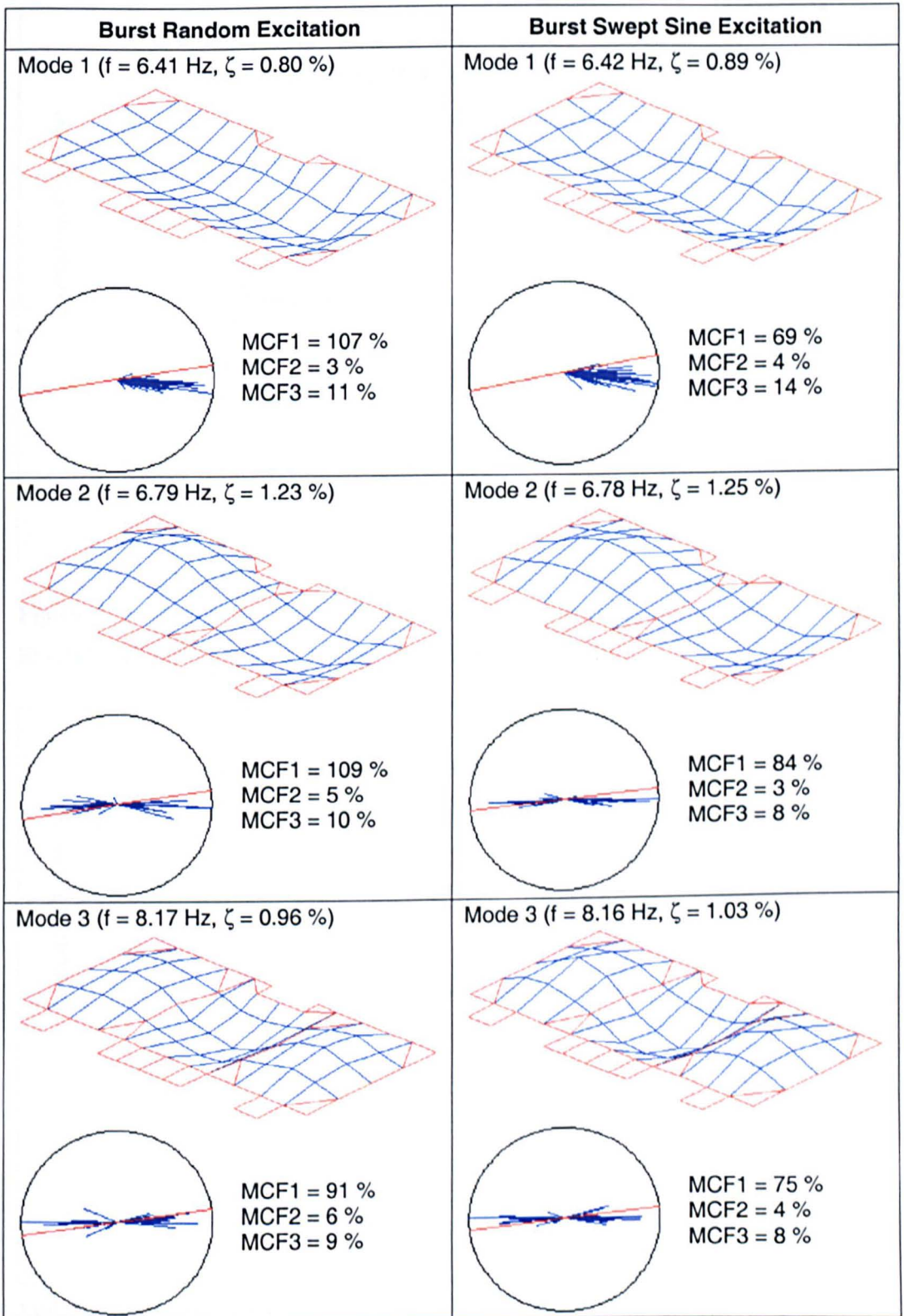


Figure 4.34: Structure A (Configuration 1) - Comparison of Mode Shapes and MCFs for BR and BSS Excitation.

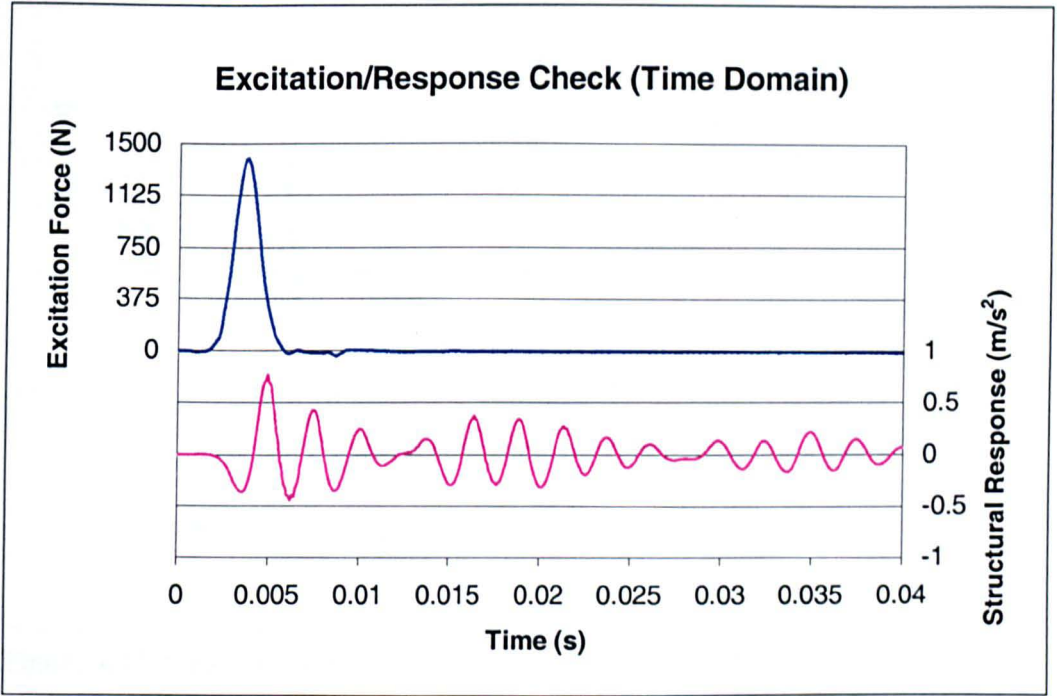


Figure 4.35: Structure A (Configuration 1) - Point Mobility Fast Sampling Excitation/Response Check for Hammer Excitation.

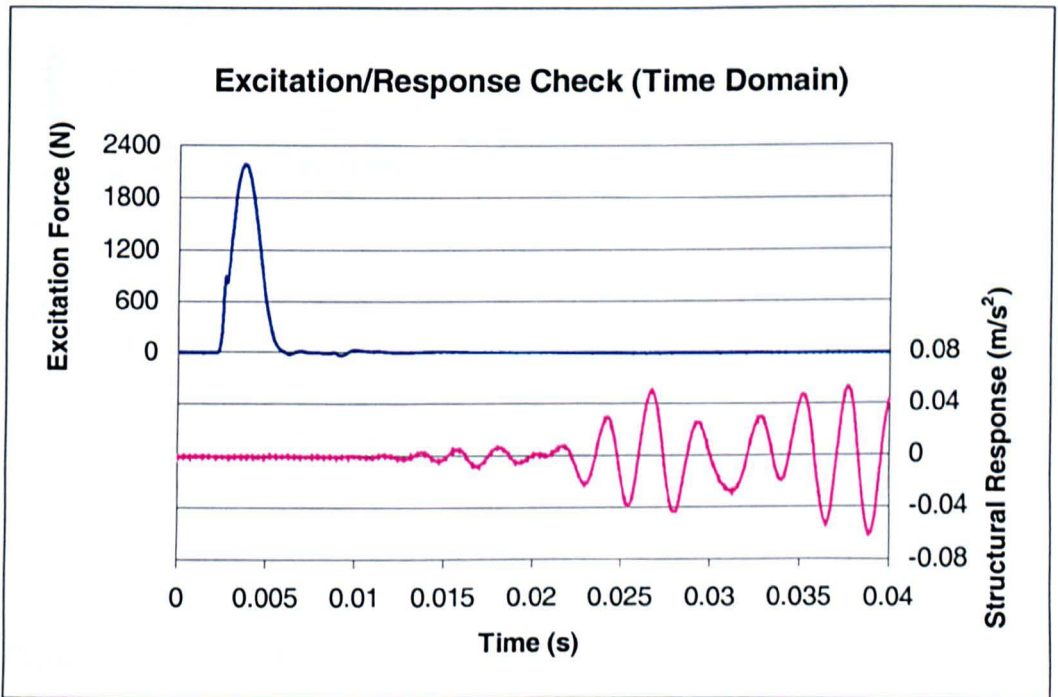


Figure 4.36: Structure A (Configuration 1) - Transfer Mobility Fast Sampling Excitation/Response Check for Hammer Excitation (Time Domain).

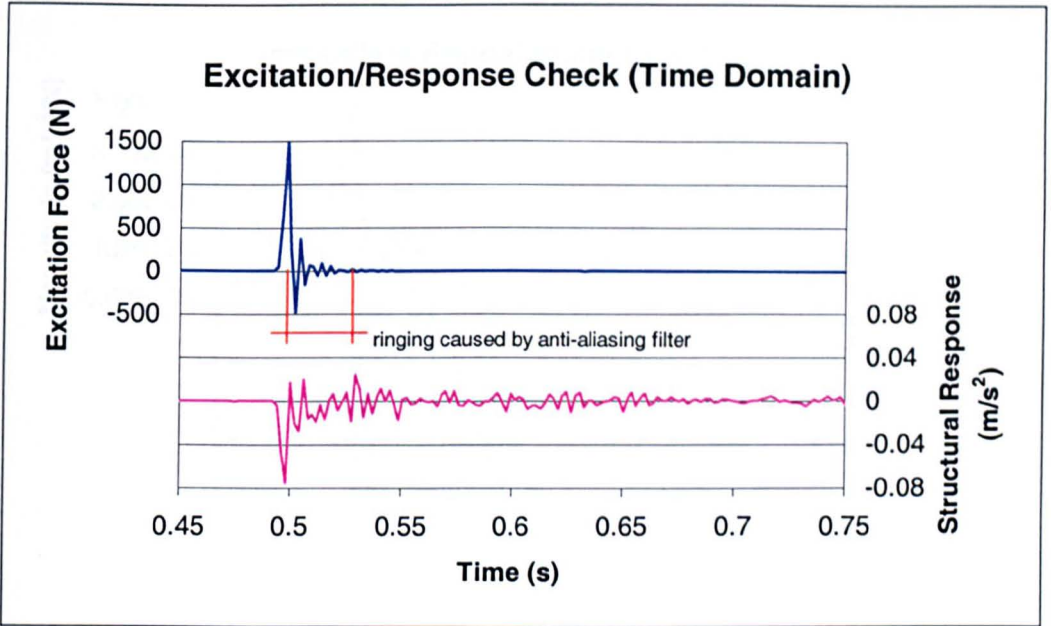


Figure 4.37: Structure A (Configuration 1) - Point Mobility Slow Sampling Excitation/Response Check for Hammer Excitation (Time Domain).

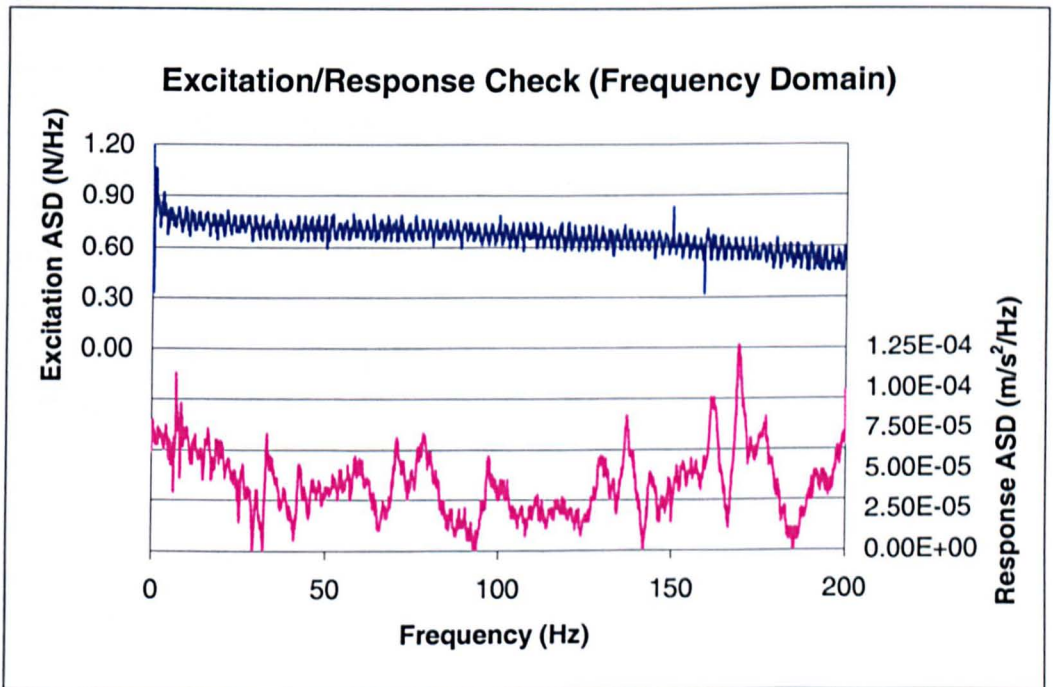


Figure 4.38: Structure A (Configuration 1) - Point Mobility Slow Sampling Excitation/Response Check for Hammer Excitation (Frequency Domain).

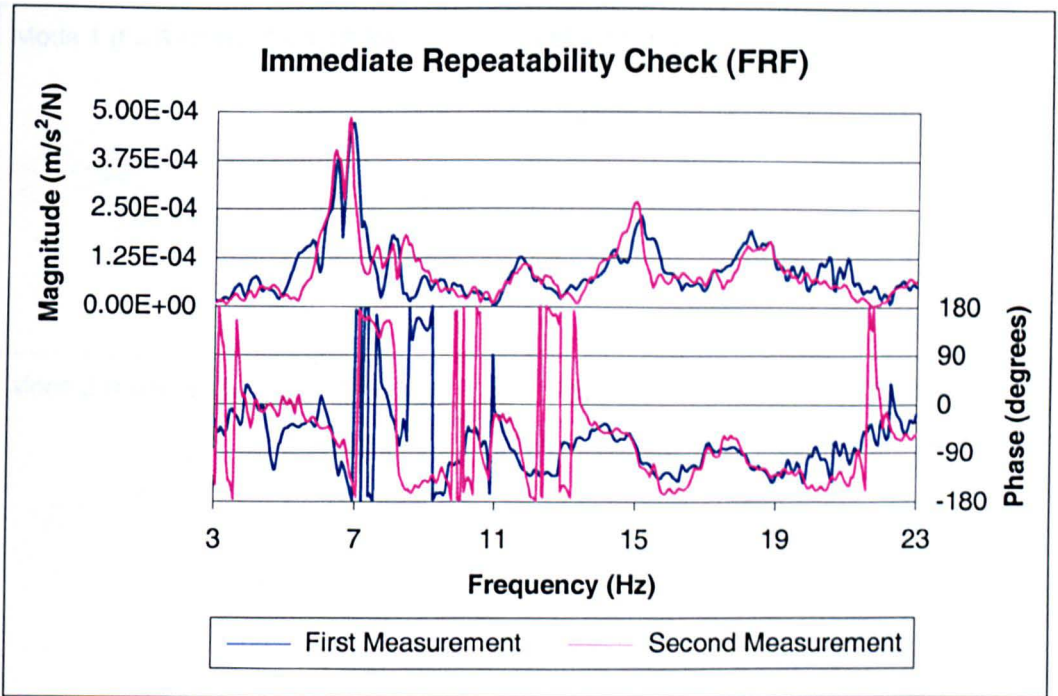


Figure 4.39: Structure A (Configuration 1) - Immediate Repeatability Check for Hammer Excitation.

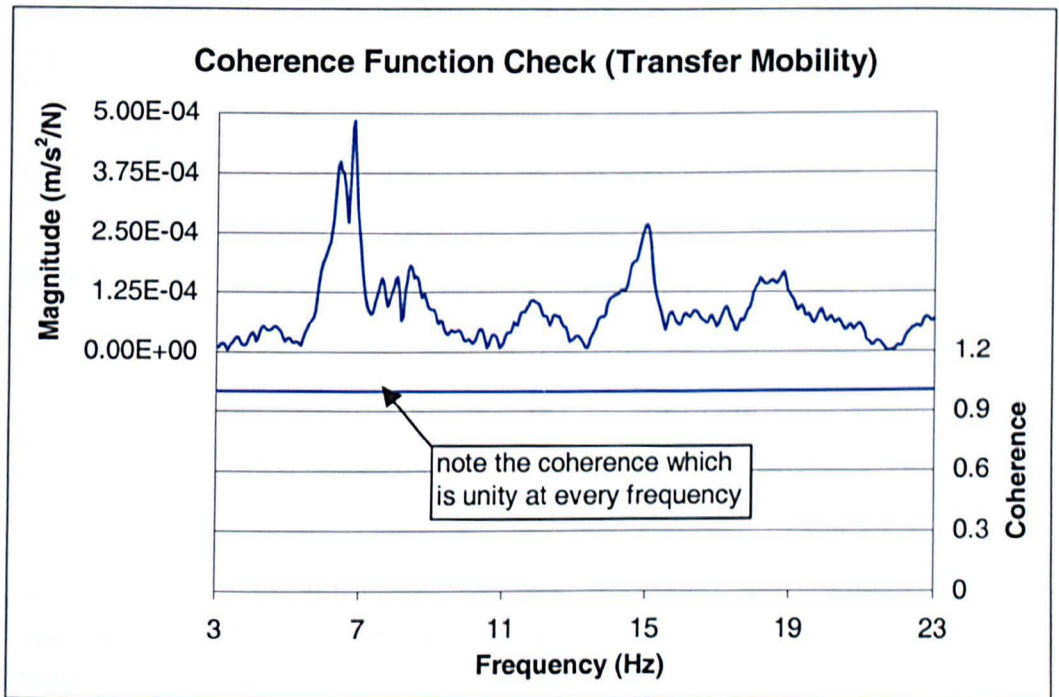


Figure 4.40: Structure A (Configuration 1) - Problematic Coherence Function Check for Hammer Excitation.

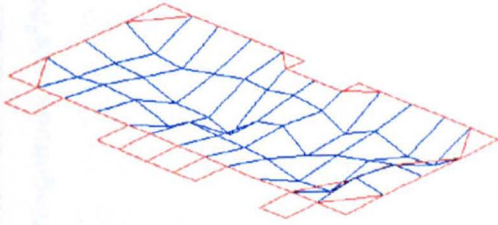
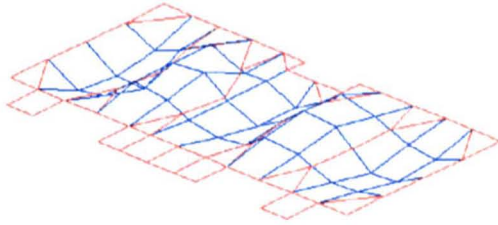
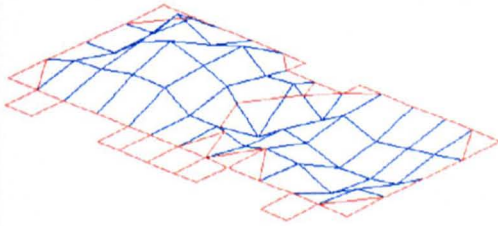
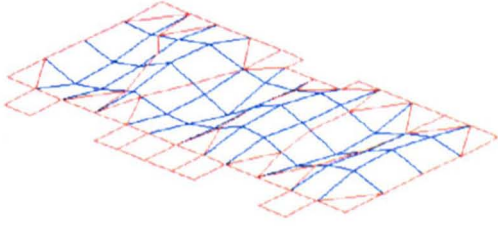
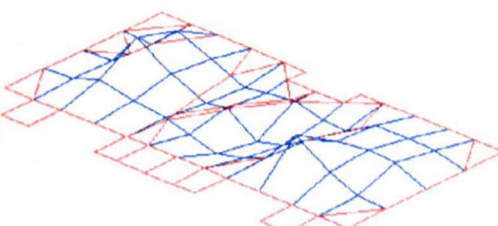
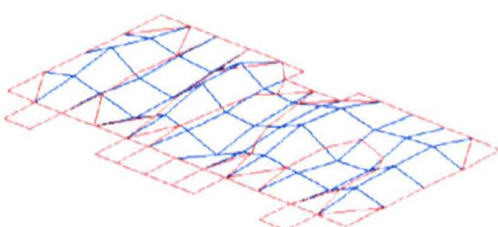
<p>Mode 1 (f = 6.43 Hz ζ = 1.13 %)</p> 	<p>Mode 5 (f = 11.77 Hz ζ = 1.99 %)</p> 
<p>Mode 2 (f = 6.79 Hz ζ = 0.64 %)</p> 	<p>Mode 6 (f = 15.03 Hz ζ = 1.98 %)</p> 
<p>Mode 3 (f = 8.18 Hz ζ = 0.74 %)</p> 	<p>Mode 7</p> <p>Not estimated.</p>
<p>Mode 4</p> <p>Not estimated.</p>	<p>Mode 8 (f = 18.10 Hz ζ = 1.65 %)</p> 

Figure 4.41: Structure A (Configuration 1) - Estimated Mode Shapes From Hammer Impact Swipe.

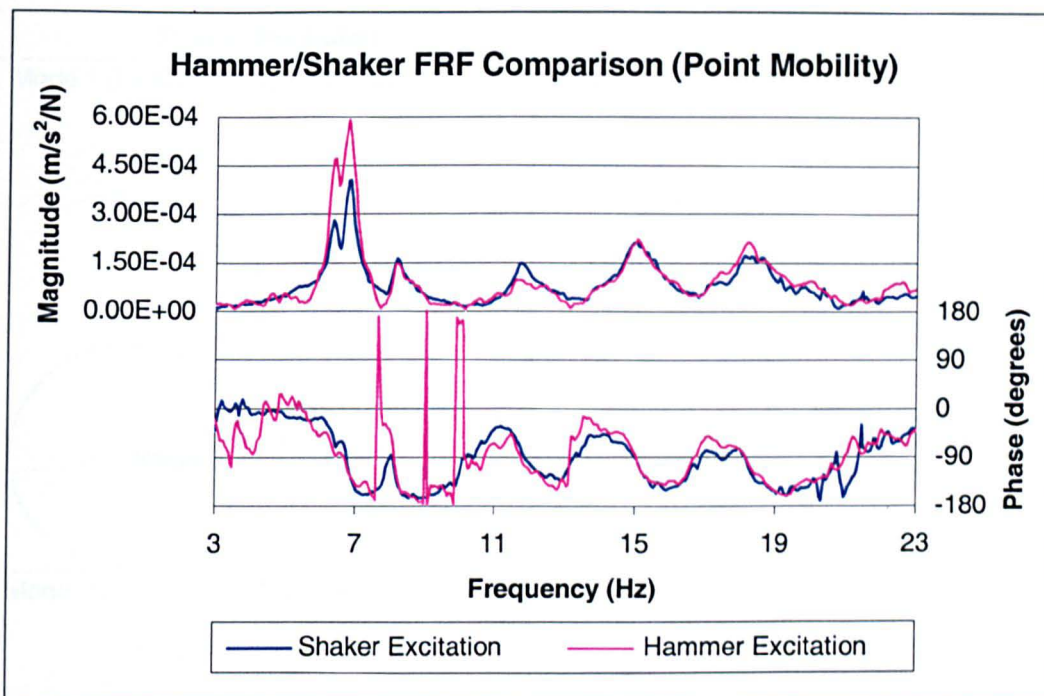


Figure 4.42: Structure A (Configuration 1) - Comparison of Point Mobility FRF for Hammer and Shaker Excitation.

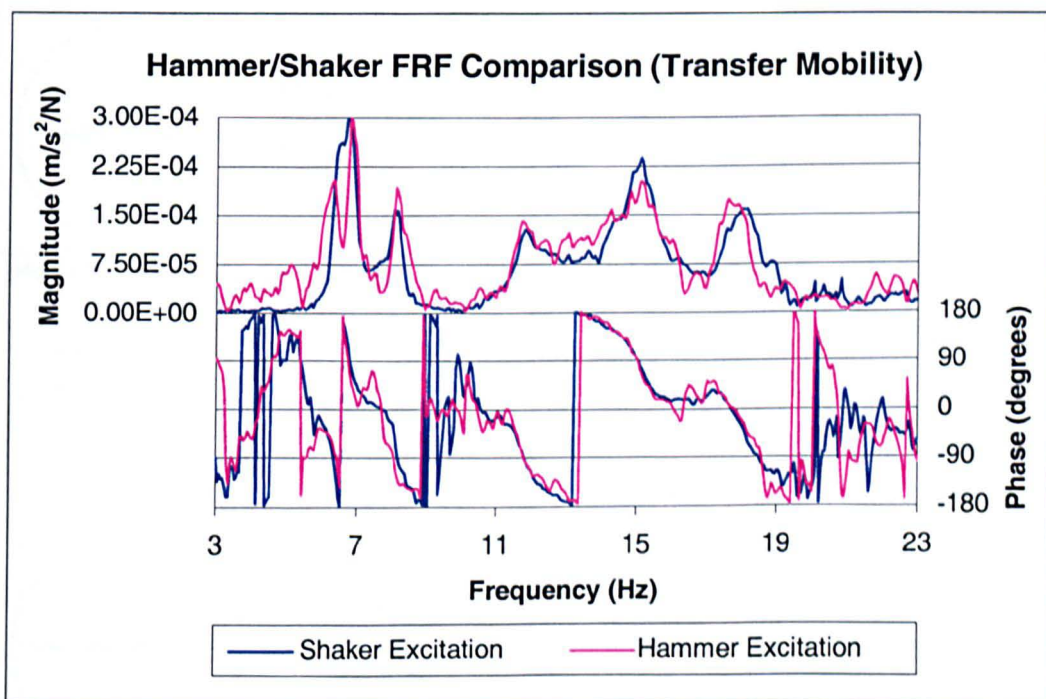


Figure 4.43: Structure A (Configuration 1) - Comparison of Transfer Mobility FRF for Hammer and Shaker Excitation.

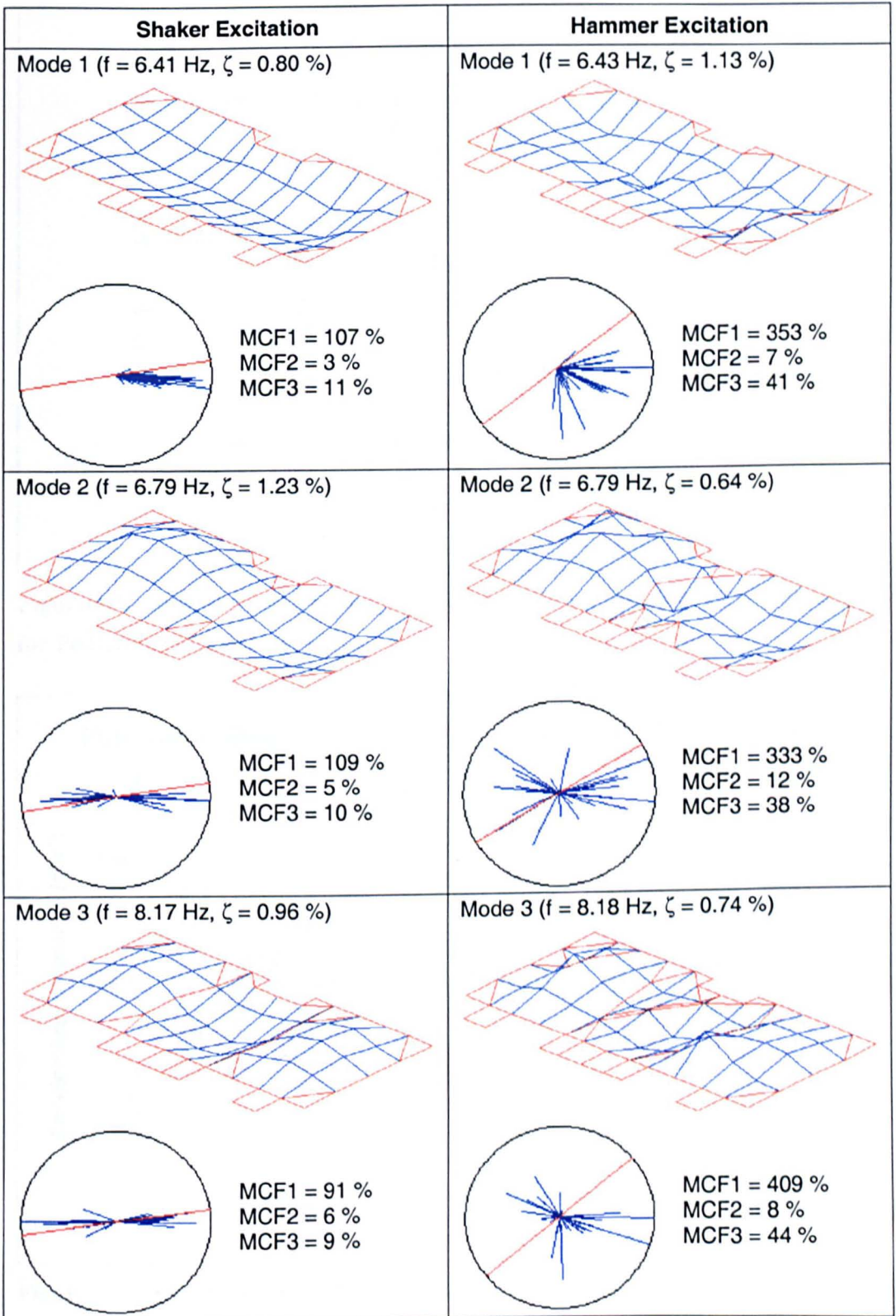


Figure 4.44: Structure A (Configuration 1) - Comparison of Mode Shapes and MCFs for Hammer and Shaker Excitation.

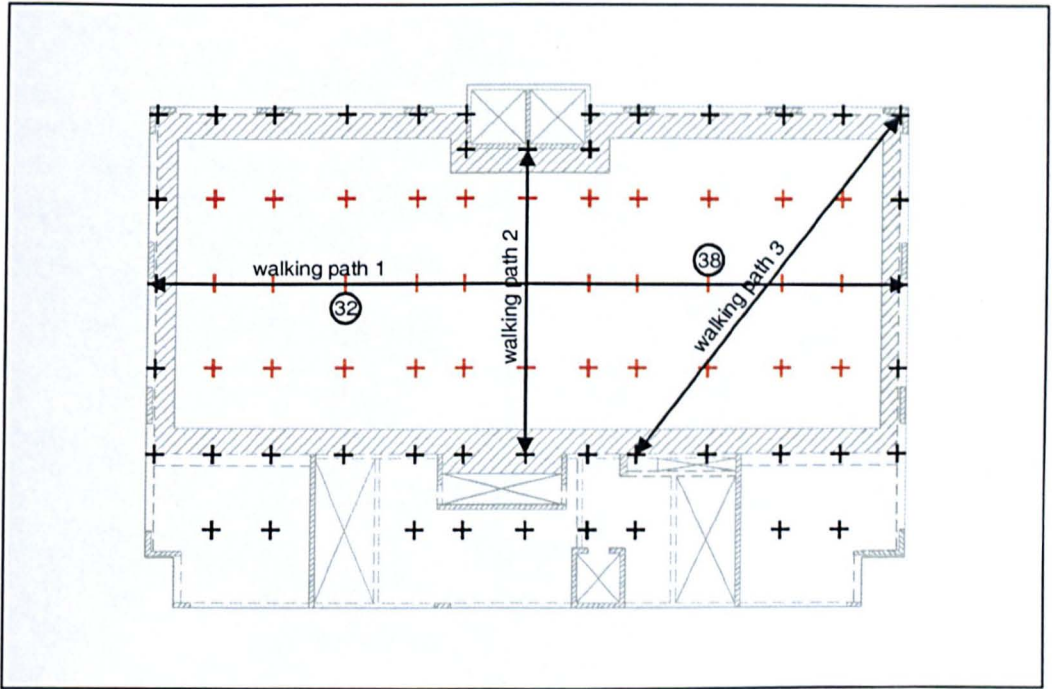


Figure 4.45: Structure A - Walking Paths and Response Measurement Locations for Pedestrian Response Tests.

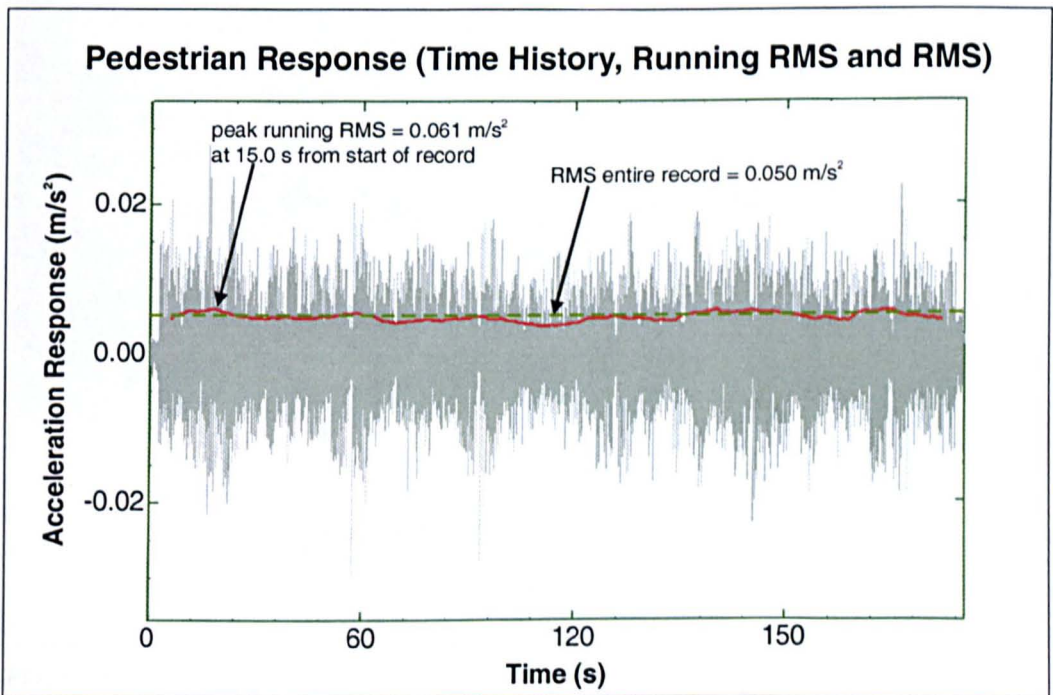


Figure 4.46: Structure A (Configuration 1) Pedestrian Response Measurement for Walking Path 1 (127 spm) with Response Measured at Test Point 32.



Figure 4.47: Structure A (Configuration 2) - General View.

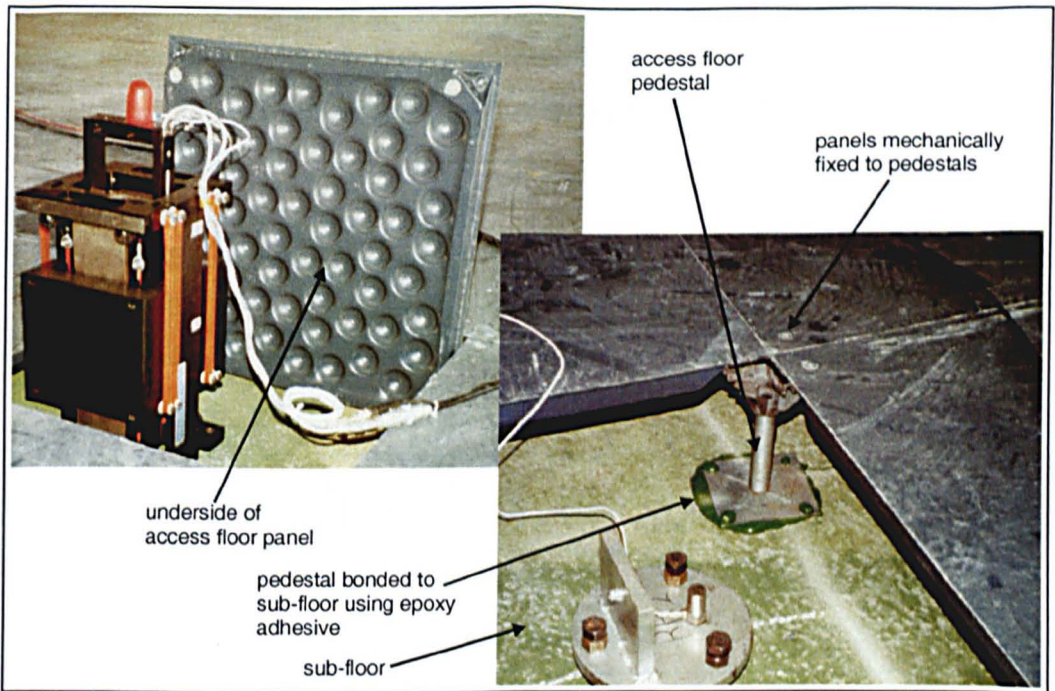


Figure 4.48: Structure A (Configuration 2) - General Construction of the Access Floor.

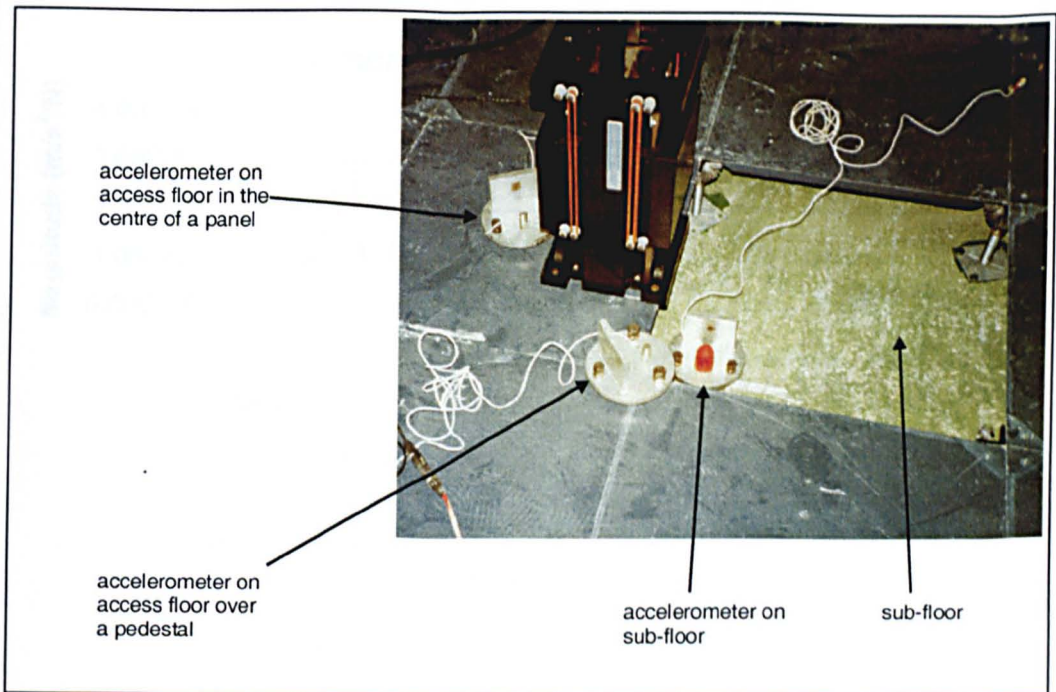


Figure 4.49: Structure A (Configuration 2) - Investigation of Accelerometer Position with Access Floors Installed.

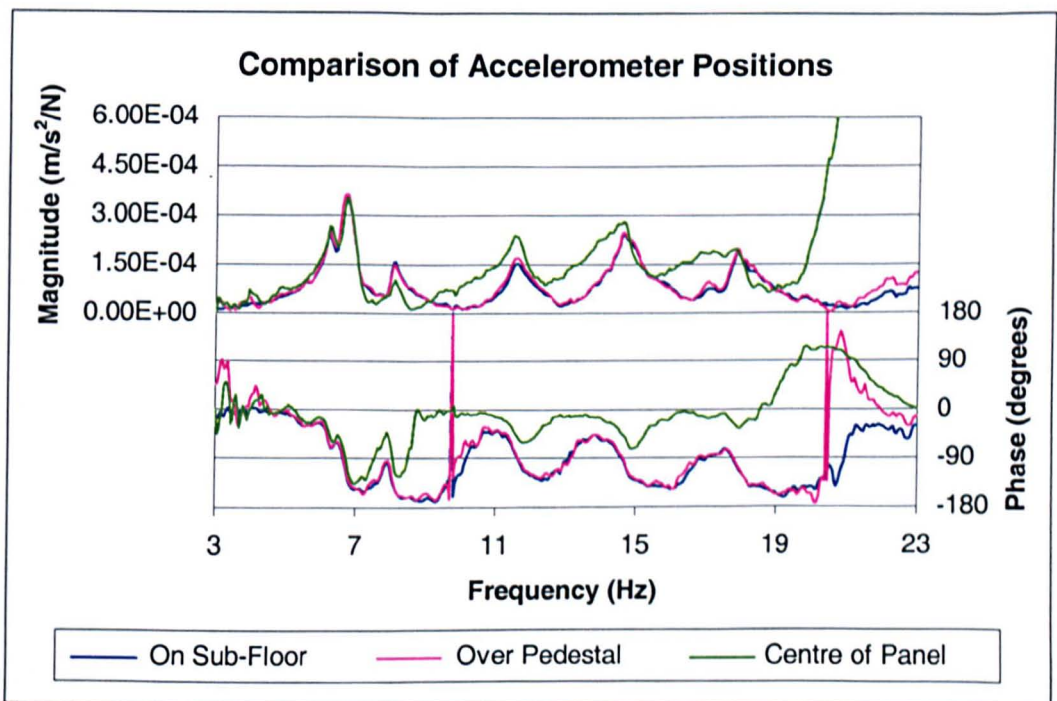


Figure 4.50: Structure A (Configuration 2) - Comparison of Accelerometer Positions (Point Mobility Nominally at Test Point 32).

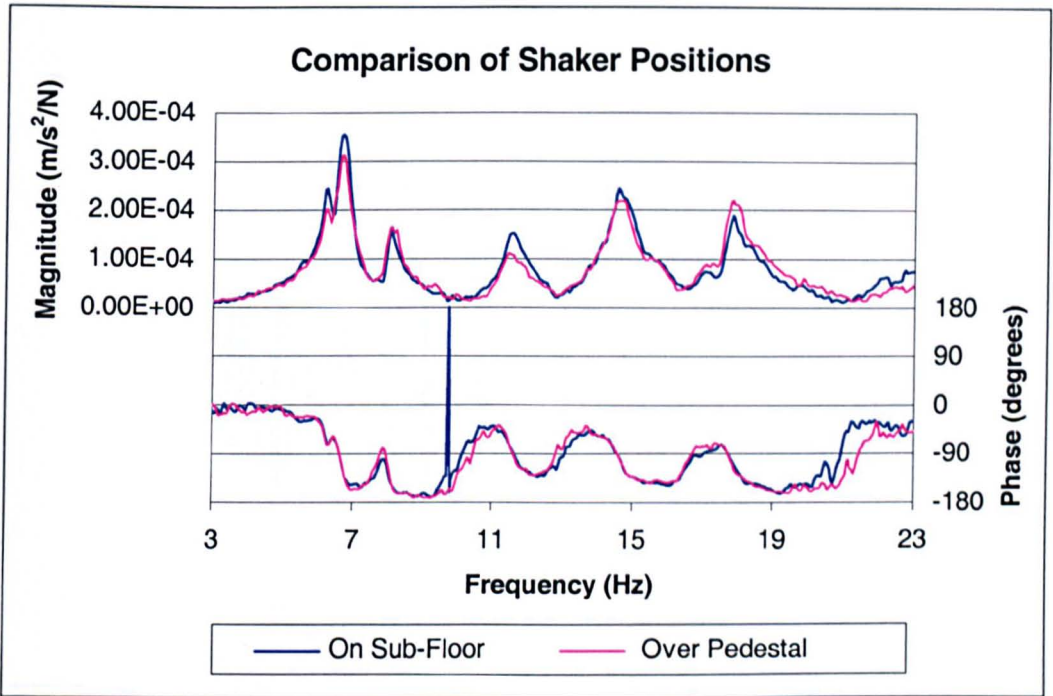


Figure 4.51: Structure A (Configuration 2) - Comparison of Shaker Positions (Point Mobility Nominally at Test Point 32).

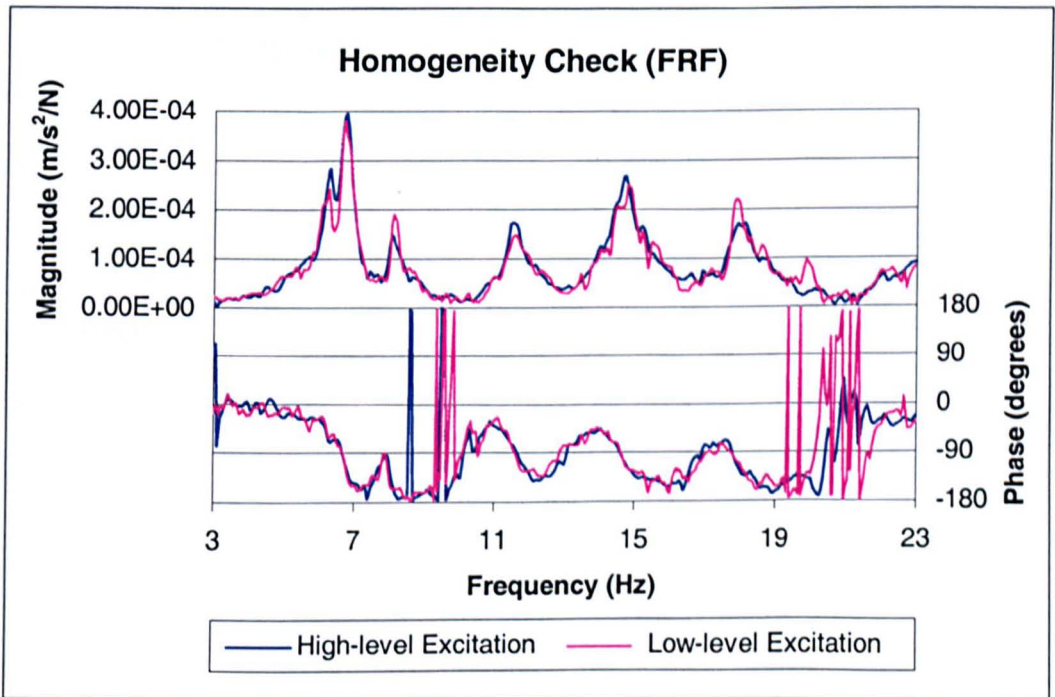


Figure 4.52: Structure A (Configuration 2) - Homogeneity Check Using BR Excitation.

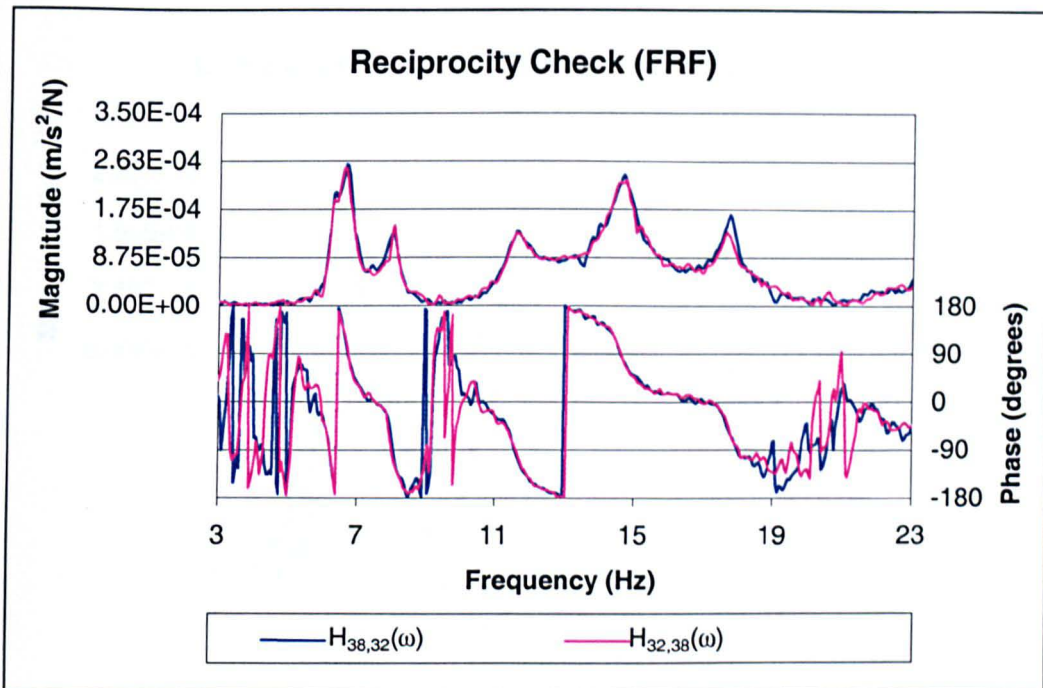


Figure 4.53: Structure A (Configuration 2) - Reciprocity Check Using BR Excitation.

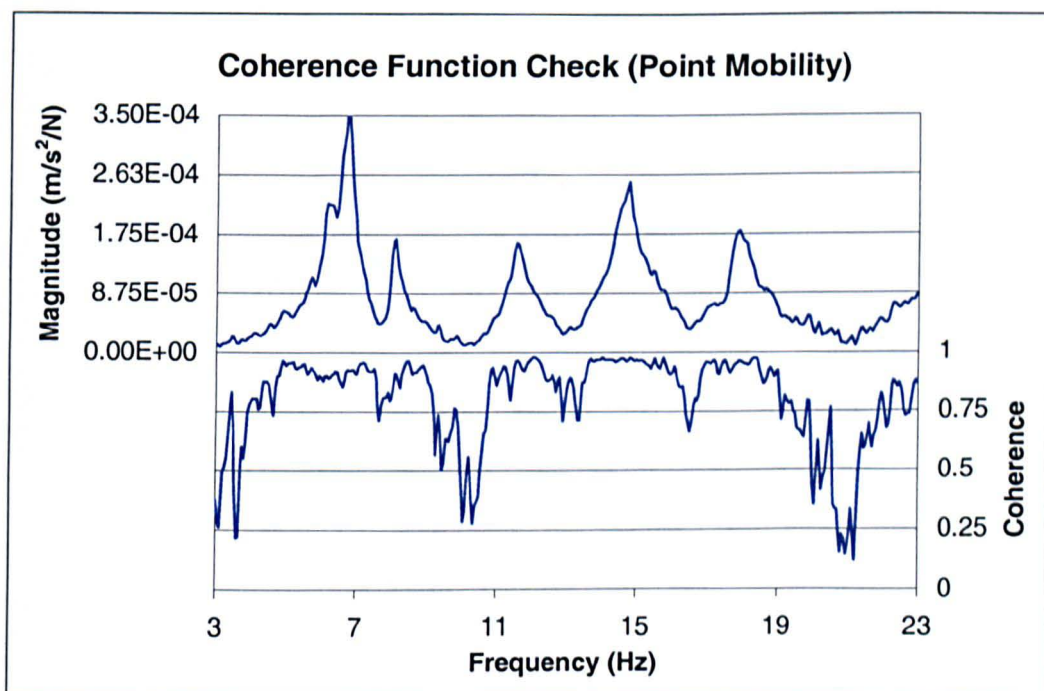


Figure 4.54: Structure A (Configuration 2) - Point Mobility Coherence Function Check Using BR Excitation.

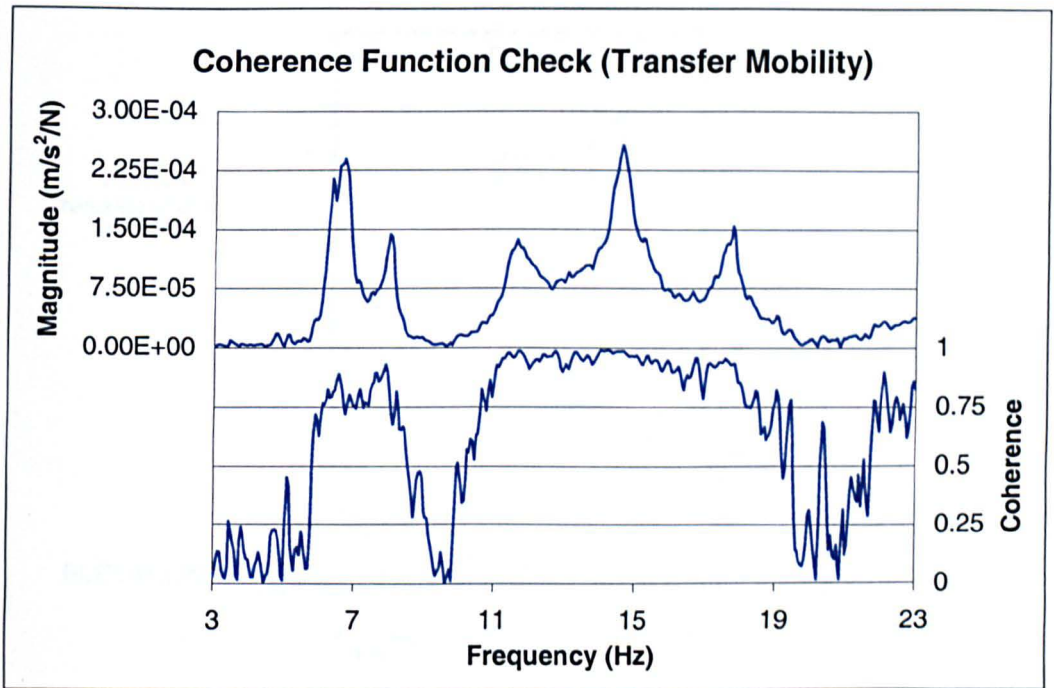


Figure 4.55: Structure A (Configuration 2) - Transfer Mobility Coherence Function Check Using BR Excitation.

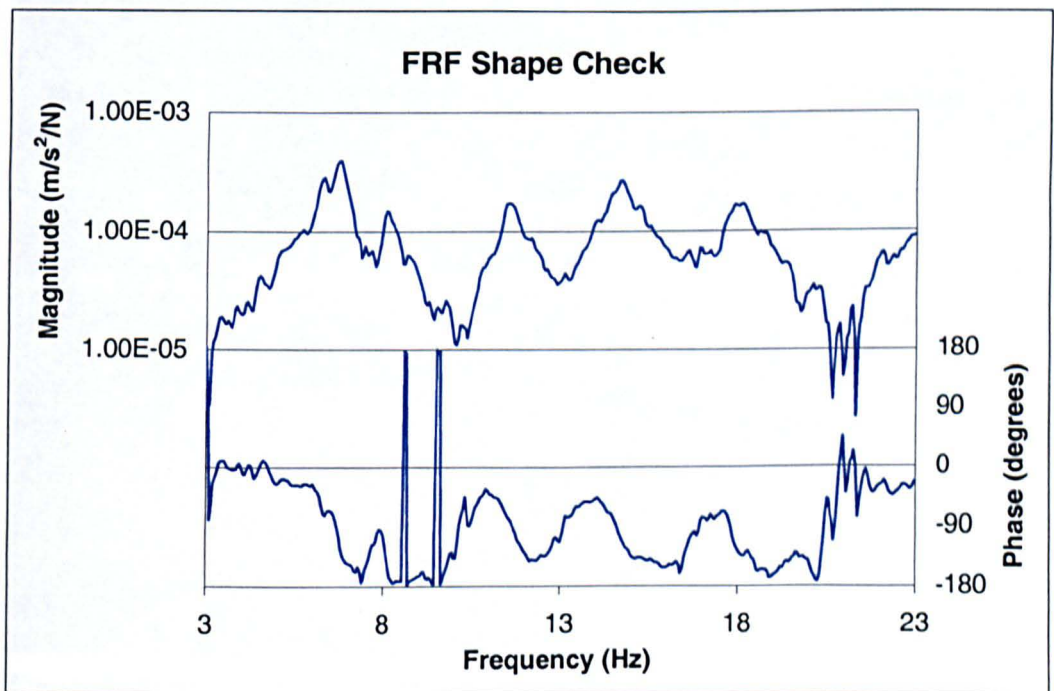


Figure 4.56: Structure A (Configuration 2) - FRF Shape Check Using BR Excitation.

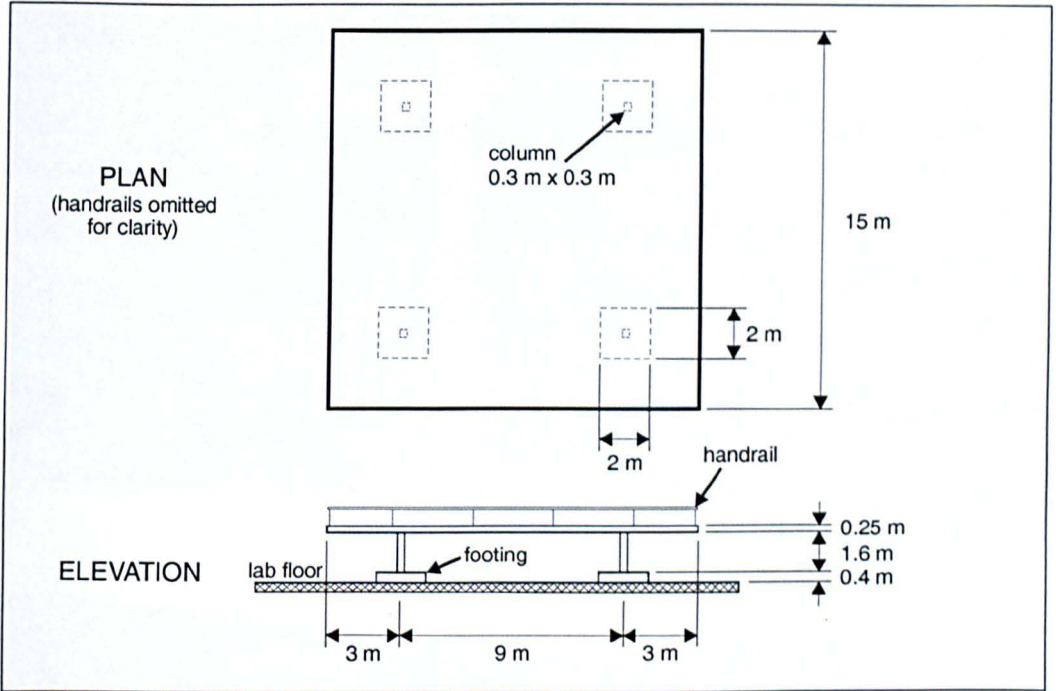


Figure 4.57: Structure B - Configuration.

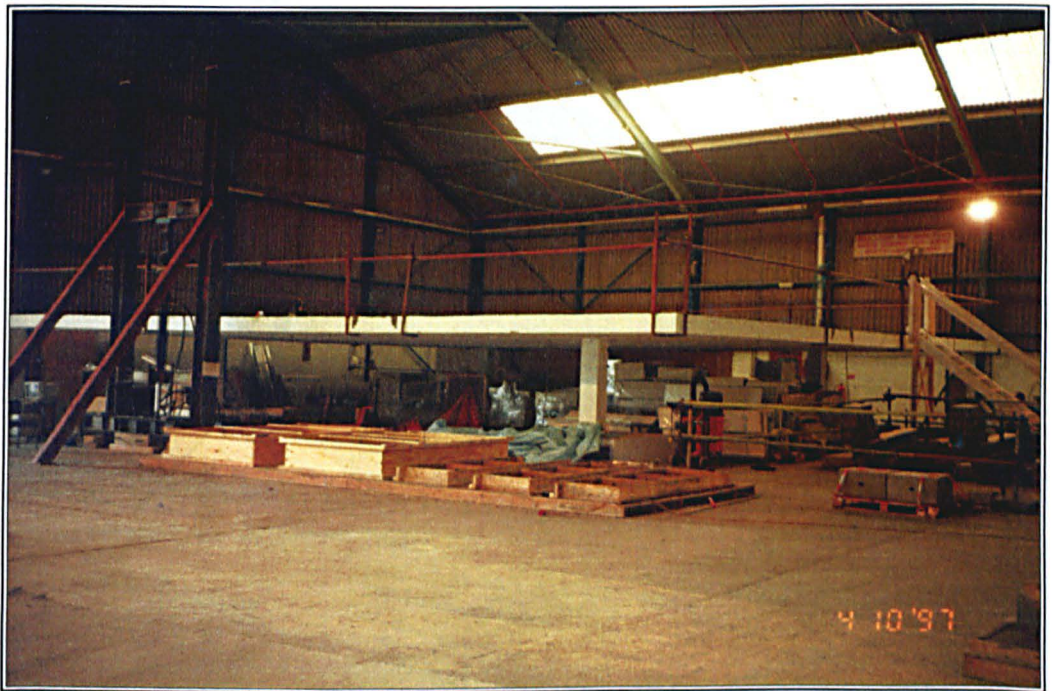


Figure 4.58: Structure B (Configuration 1) - General View of Structure B in its Bare Condition.

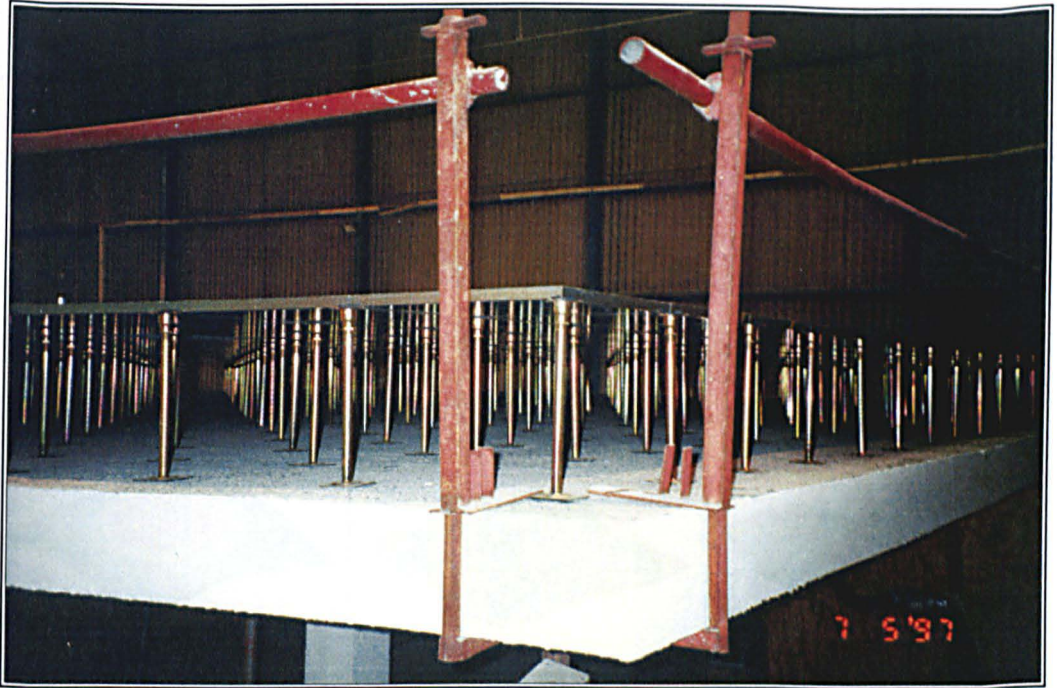


Figure 4.59: Structure B - General View with Access Floors Installed (Configurations 2 and 3).

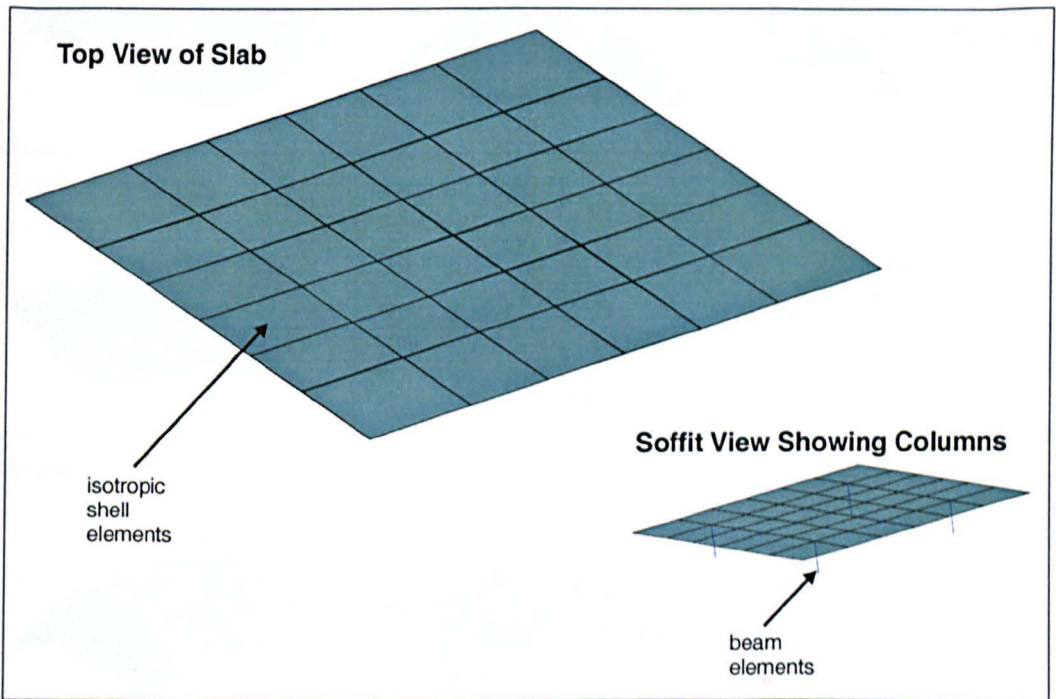


Figure 4.60: Structure B - Pre-Test FE Model.

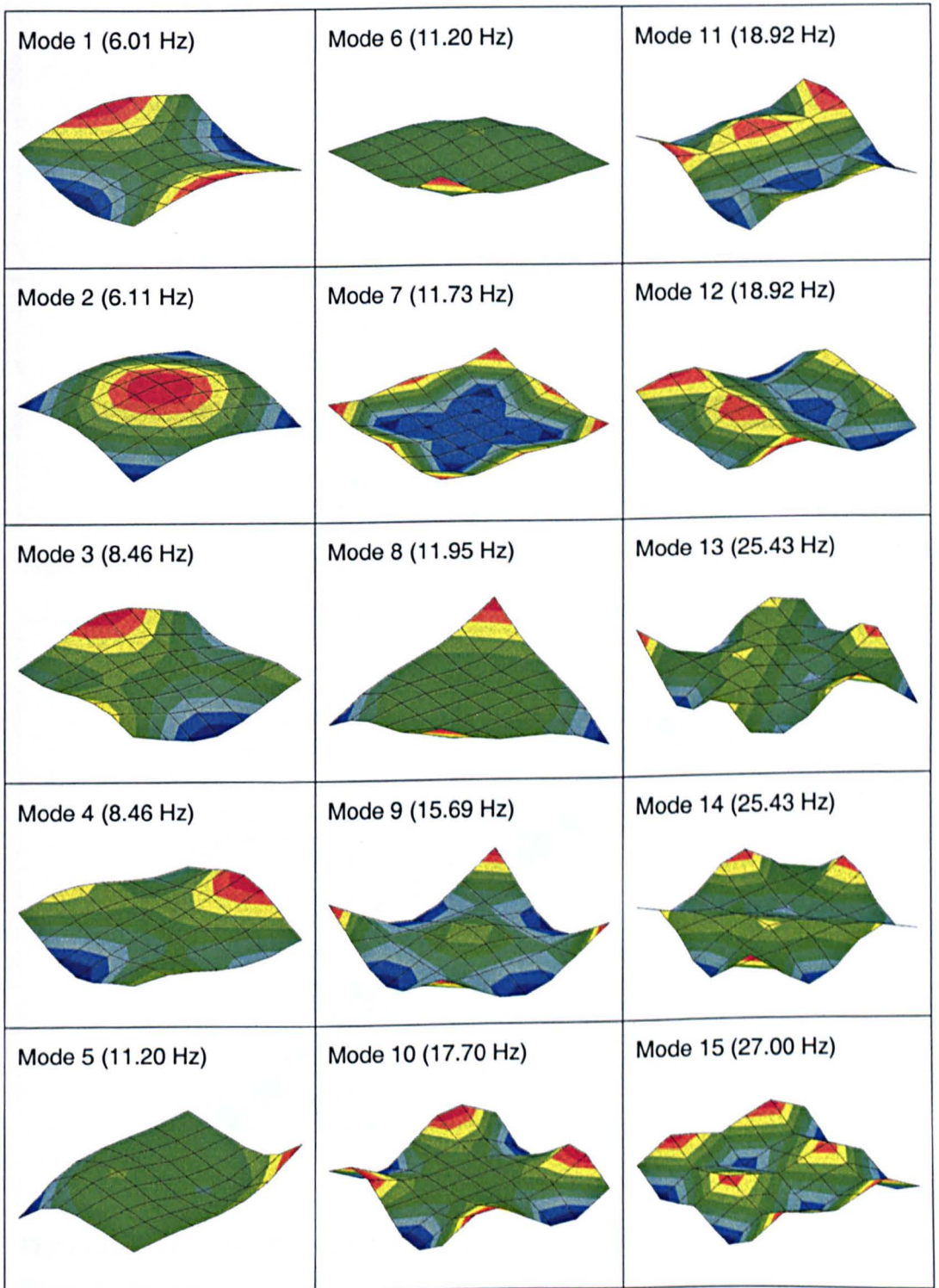


Figure 4.61: Structure B - First 15 Modes Calculated from Pre-Test FE Model.

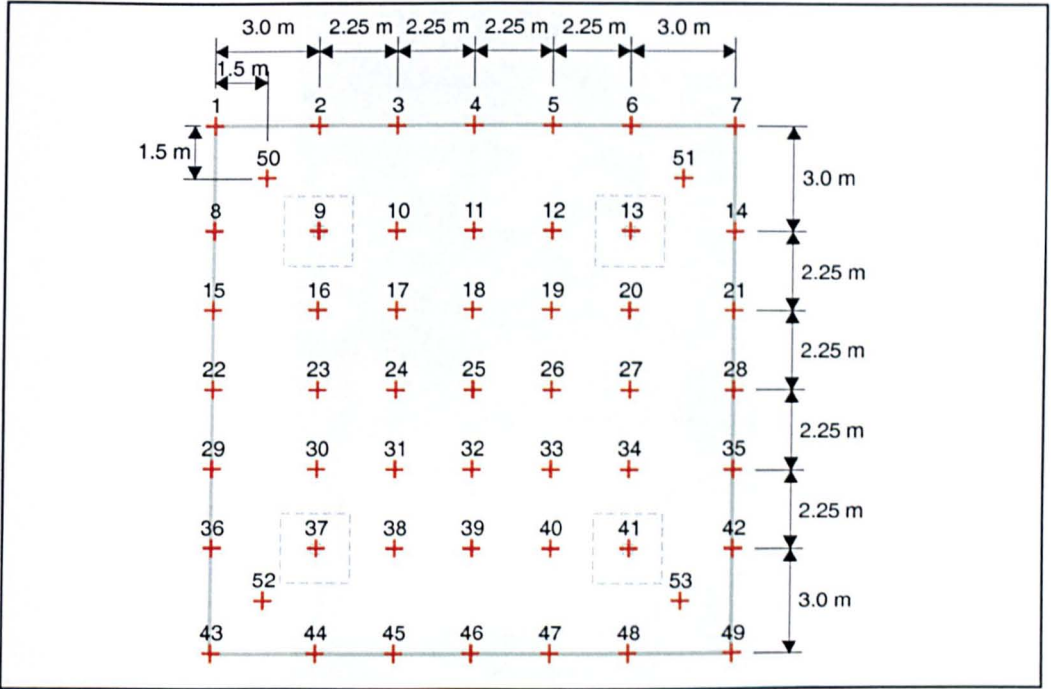


Figure 4.62: Structure B - Test Grid.

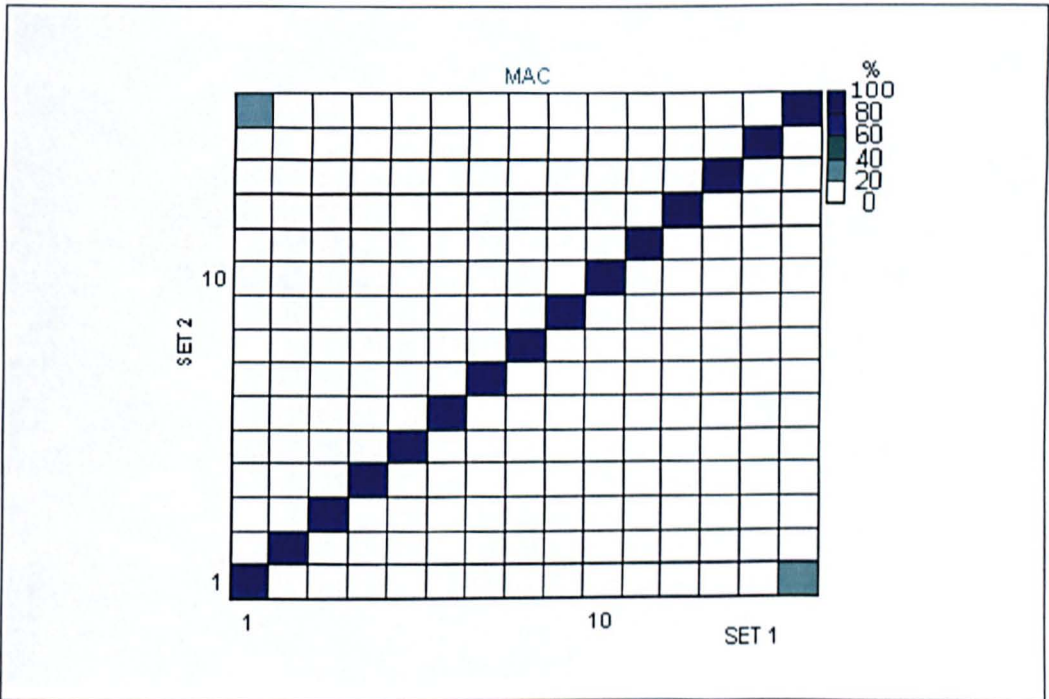


Figure 4.63: Structure B - Auto-MAC Calculated for Proposed Test Grid Using First 15 FE Calculated Modes of Vibration.

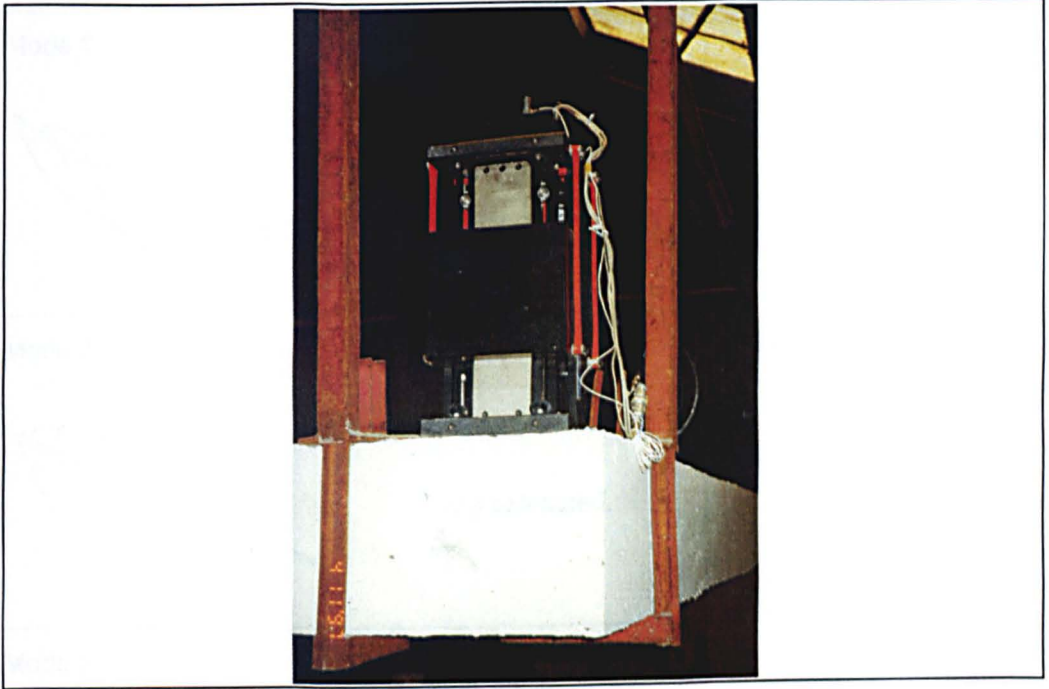


Figure 4.64: Structure B (Configuration 1) - Shaker on Bare Floor.

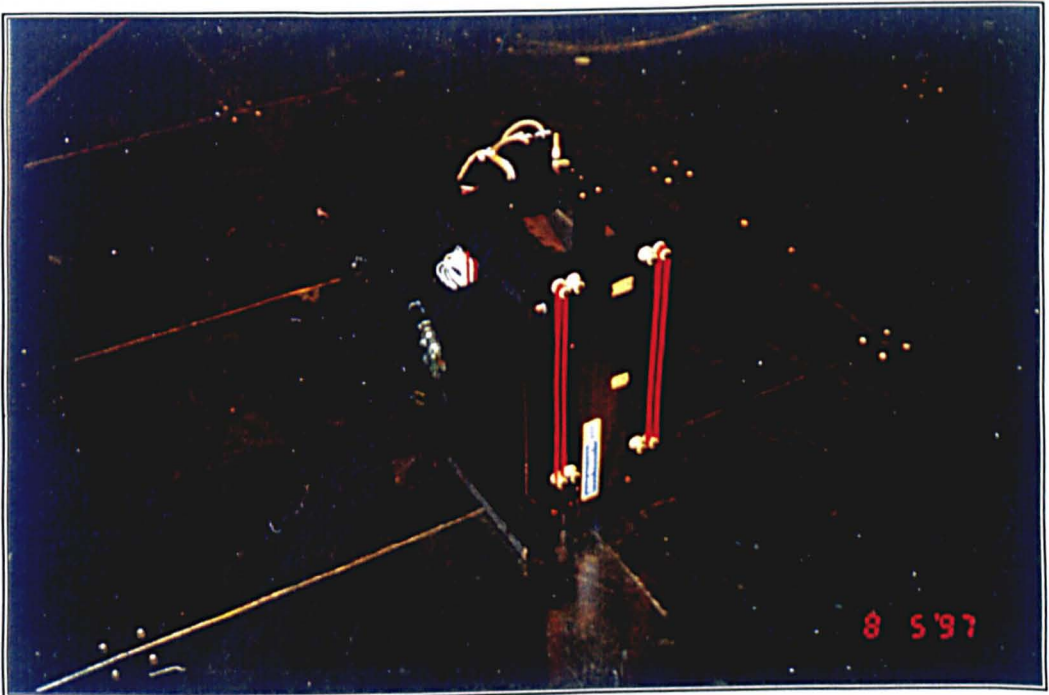


Figure 4.65: Structure B (Configurations 2 and 3) - Shaker on Access Floor Above a Pedestal.

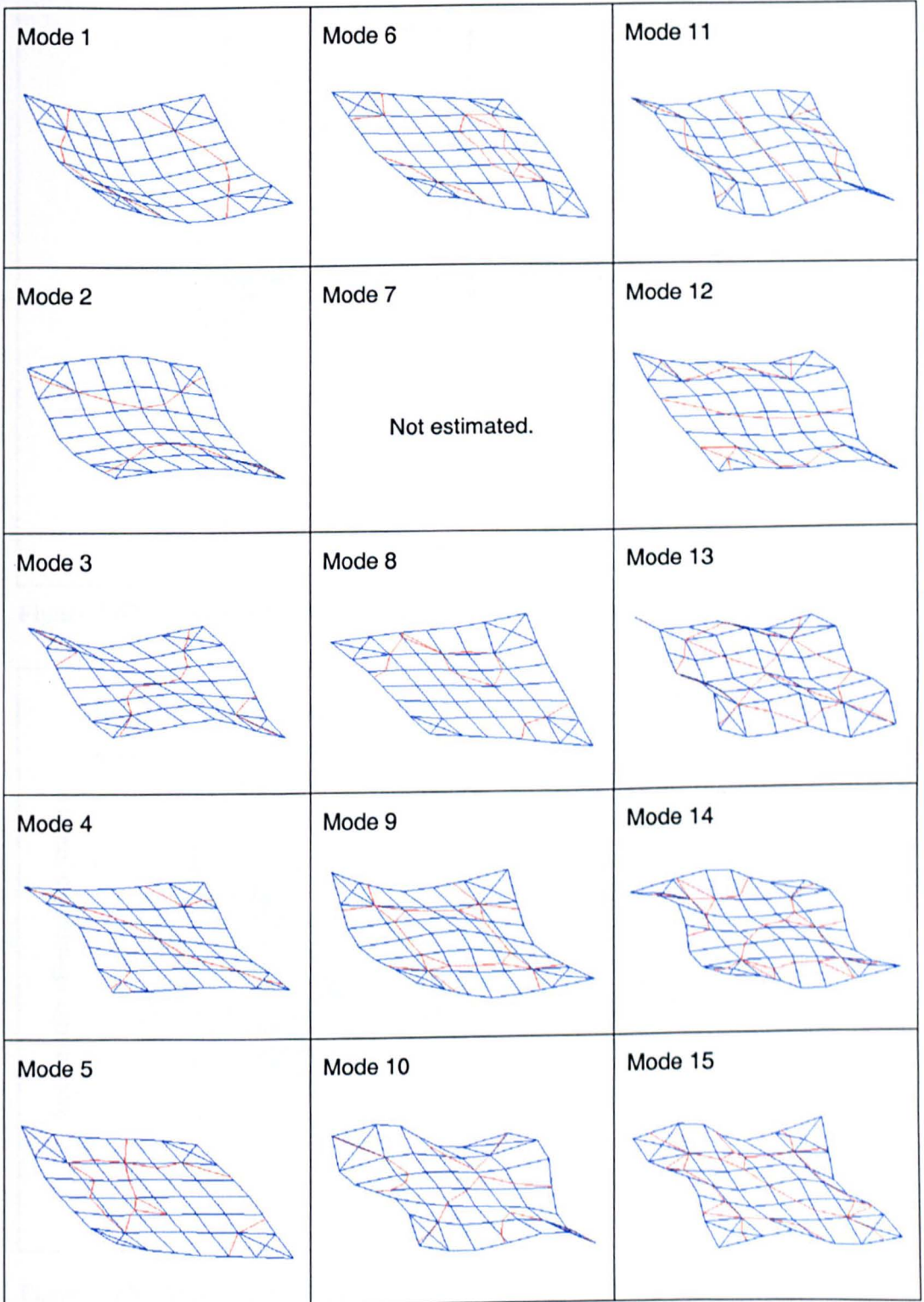


Figure 4.66: Structure B (All Configurations) - Estimated Mode Shapes.

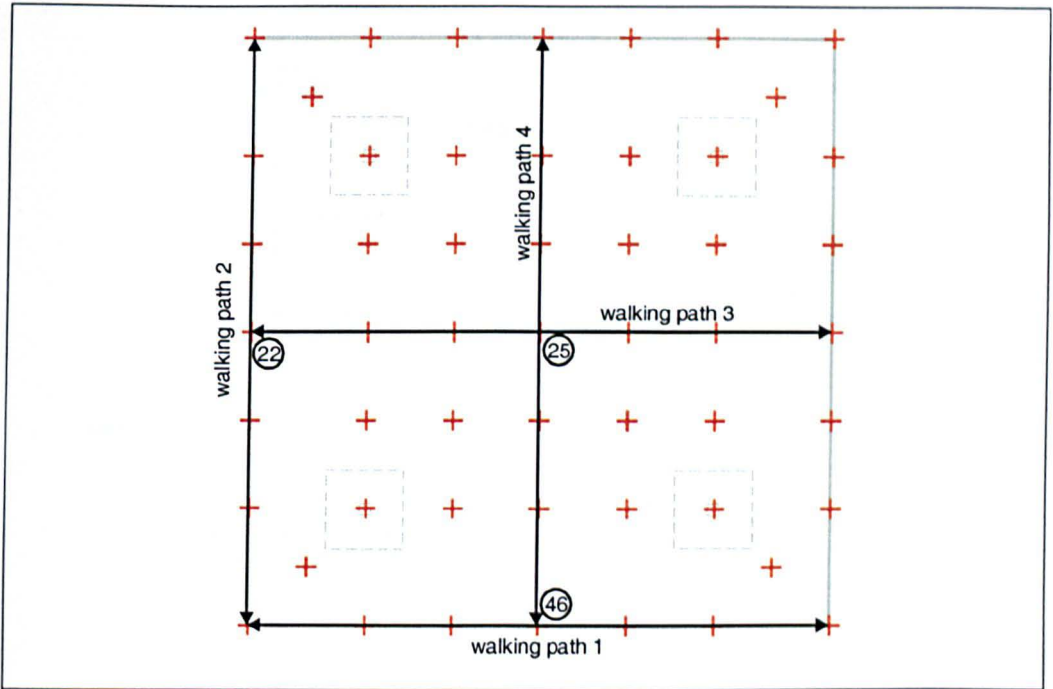


Figure 4.67: Structure B - Walking Paths for Pedestrian Response Measurements.

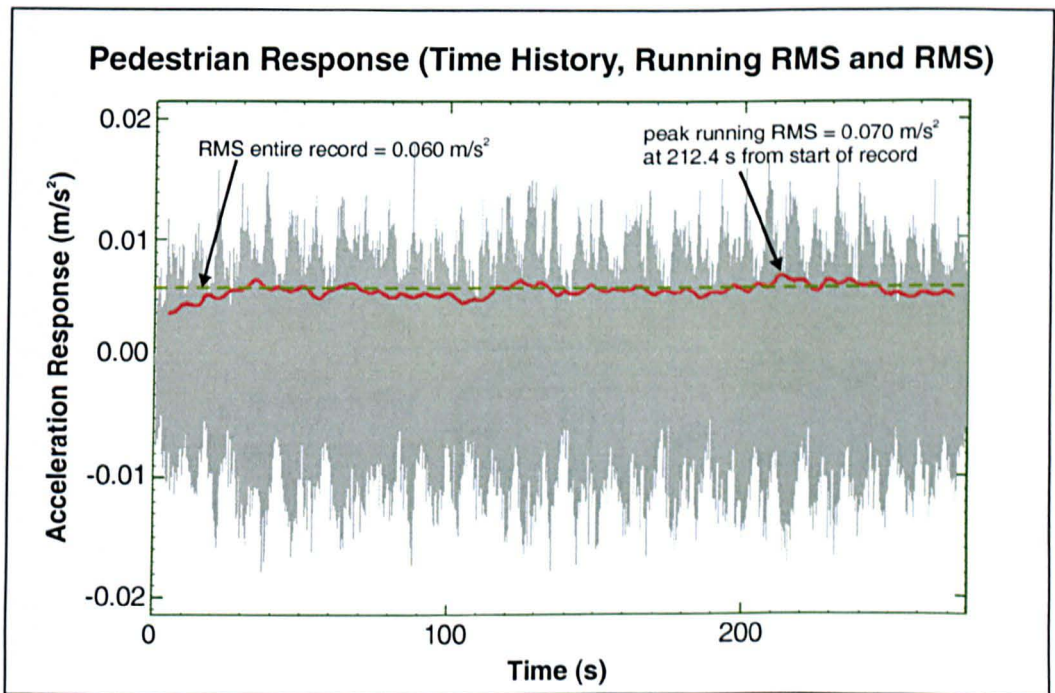


Figure 4.68: Structure B (Configuration 1) - Pedestrian Response Measurement for Walking Path 1 (138 spm) with Response Measured at Test Point 46.

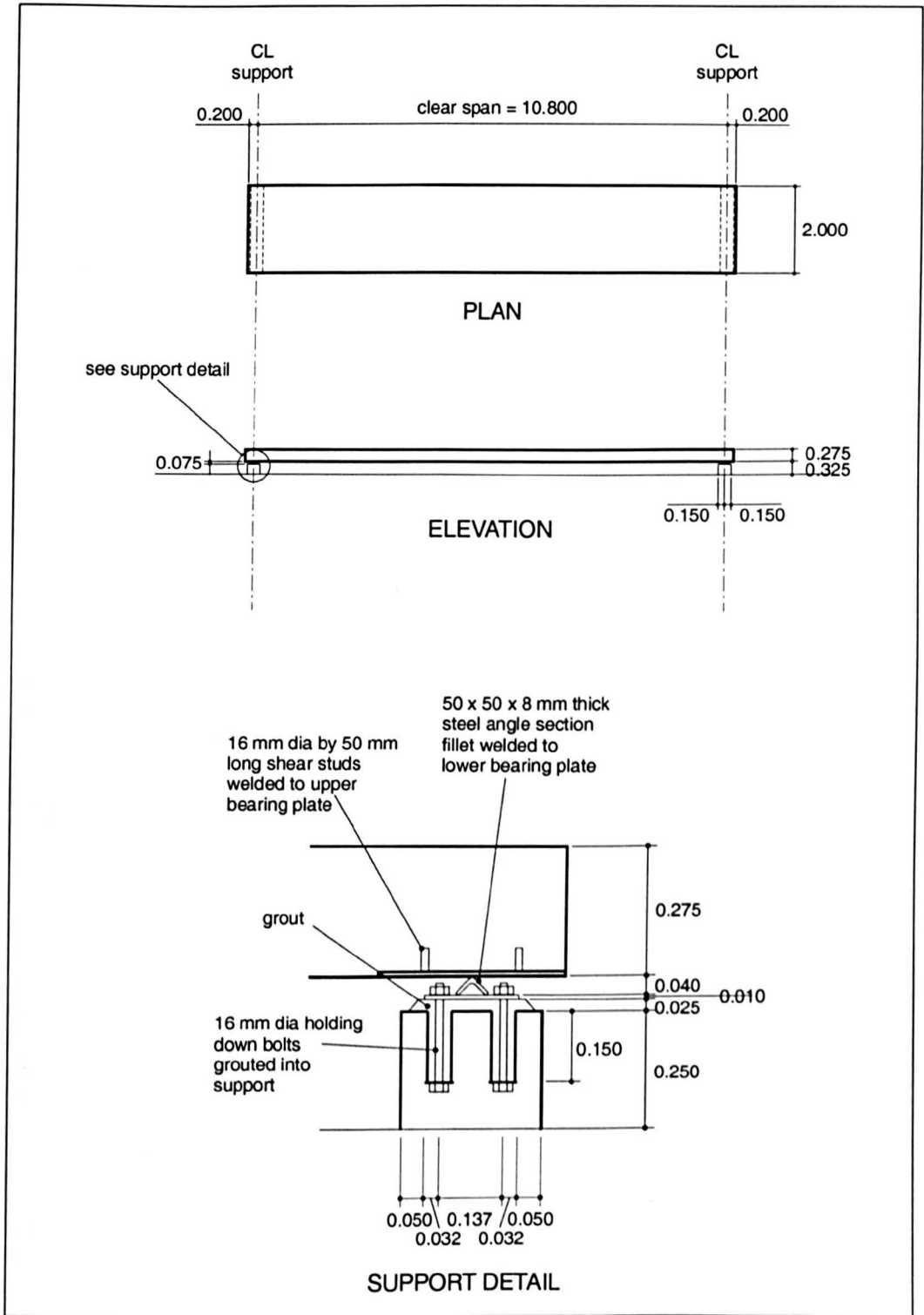


Figure 4.69: Structure C - General Arrangement Drawing.

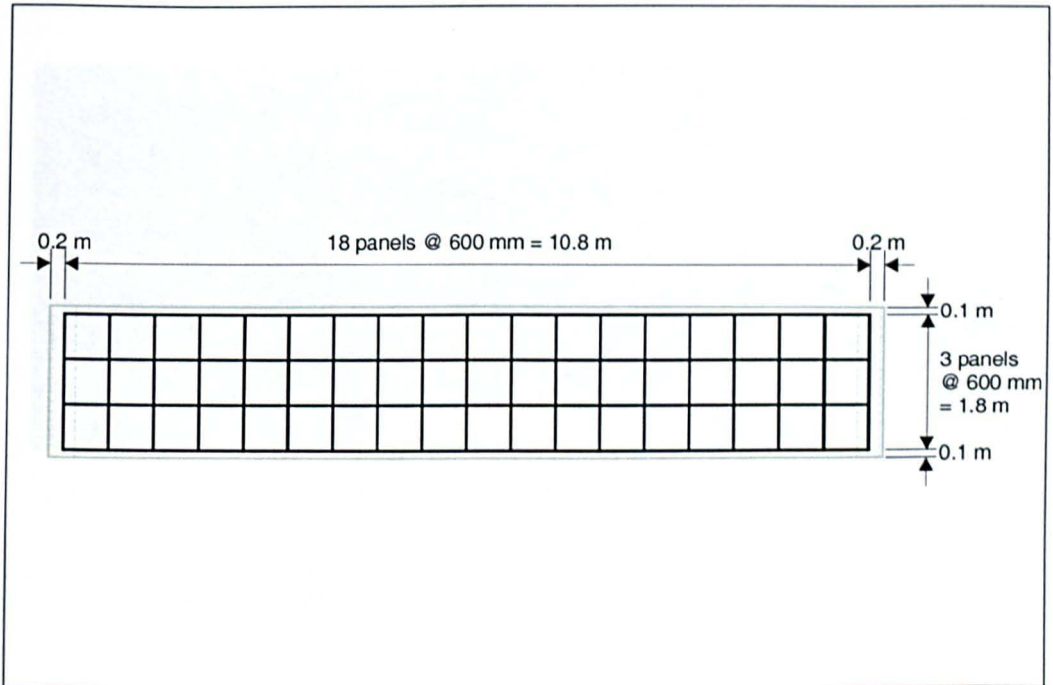


Figure 4.70: Structure C - Access Floor Grid Layout.



Figure 4.71: Structure C - Photograph of 'Knife-Edge' Support.

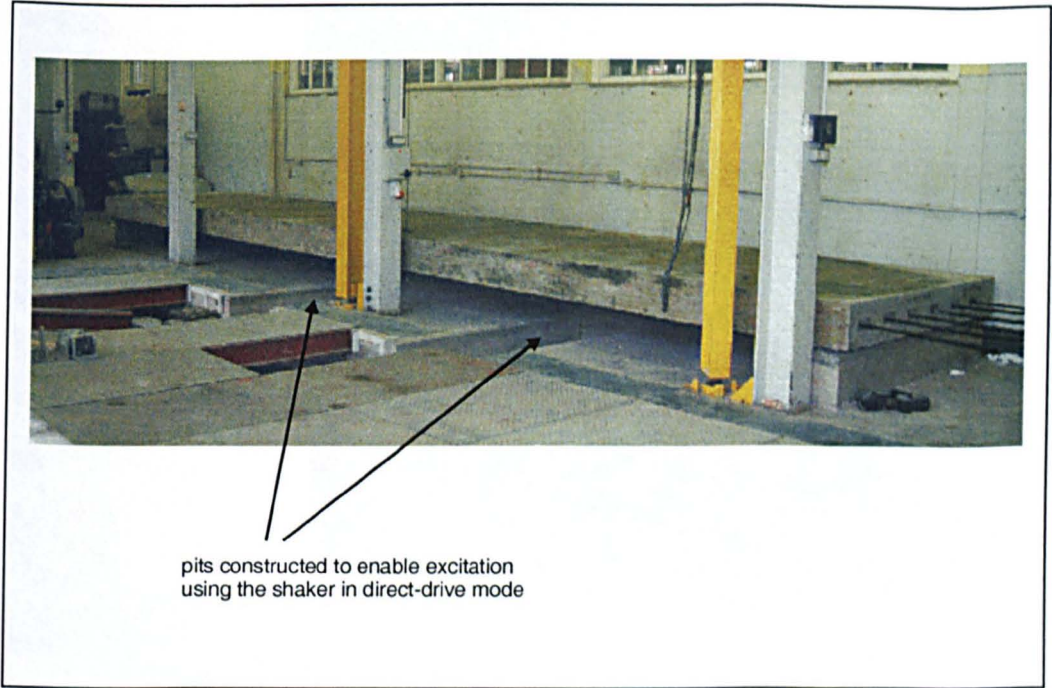


Figure 4.72: Structure C - Photograph of Showing Pits Constructed for Direct Drive Excitation.

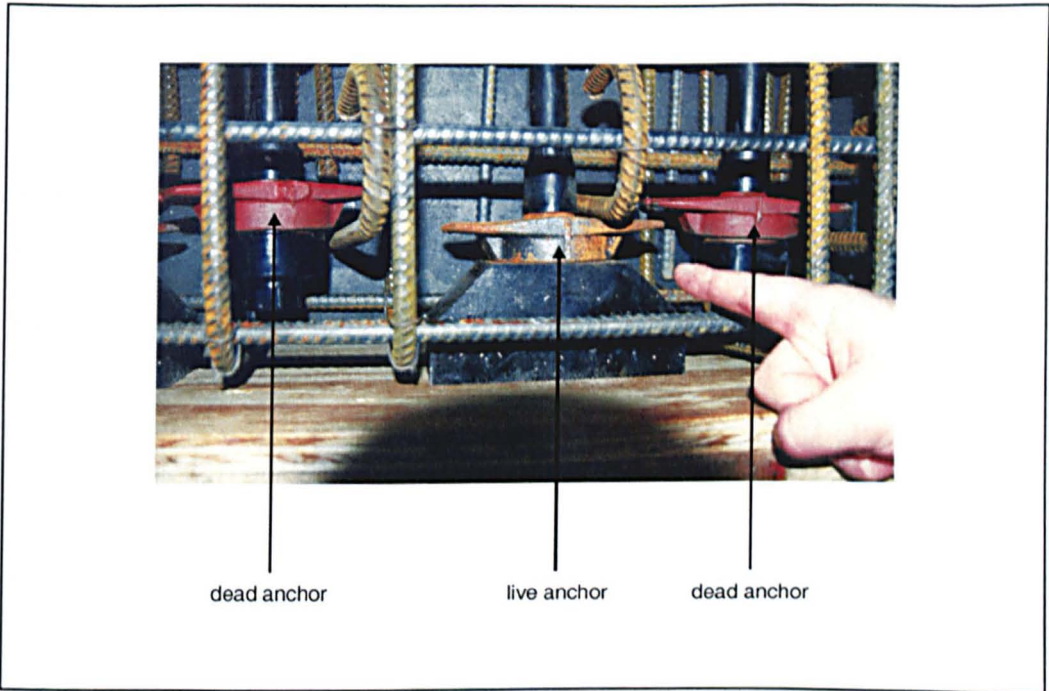


Figure 4.73: Structure C - Alternate Dead and Live Prestressing Anchors.



Figure 4.74: Structure C - Post-Tensioning in Progress.

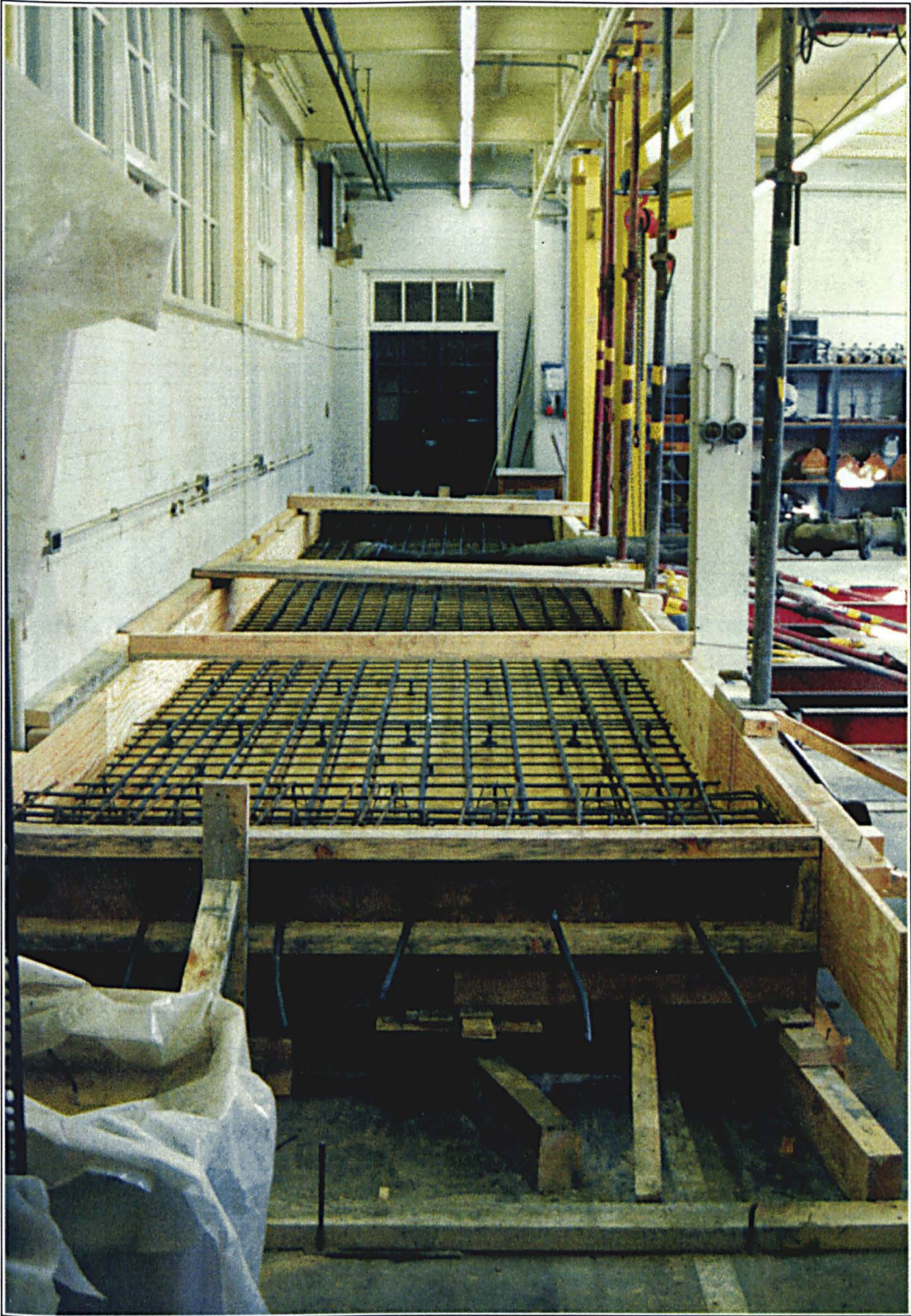


Figure 4.75: Structure C - Photograph Prior to Concreting Illustrating Formwork, Reinforcement and Prestressing.

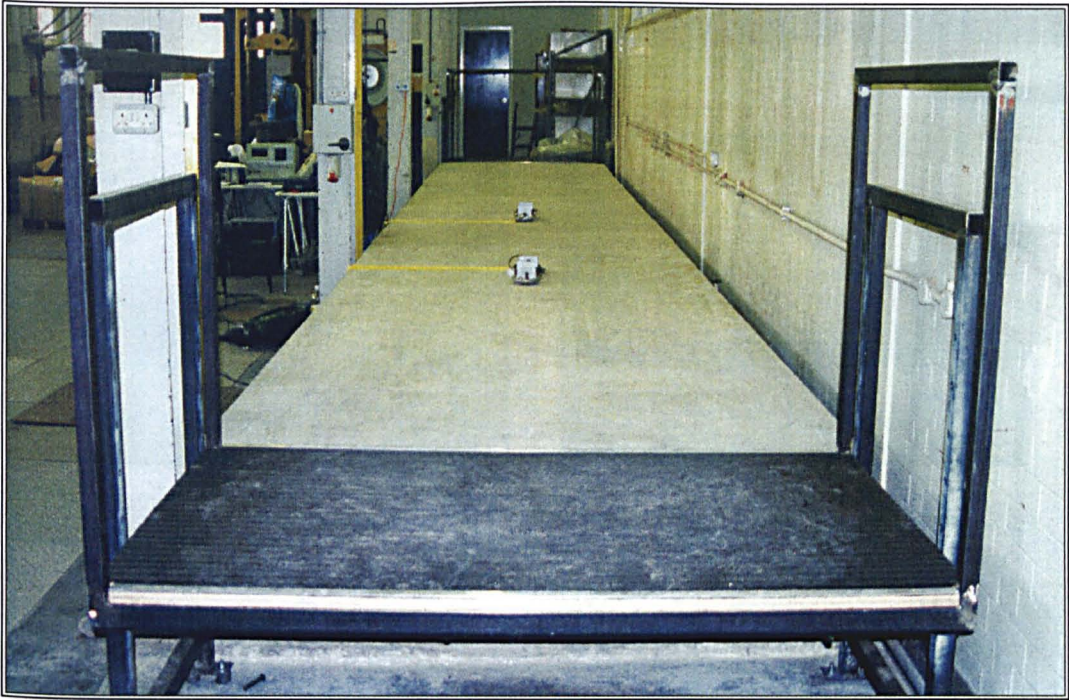
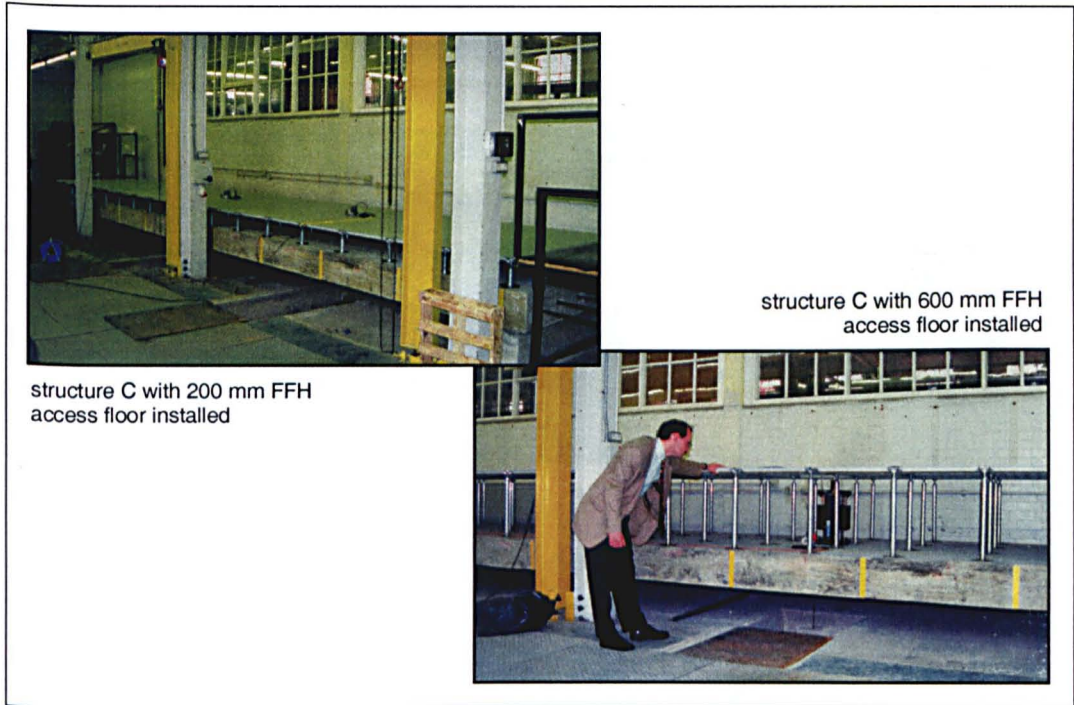


Figure 4.76: Structure C - Completed Structure with End Platforms Constructed.



structure C with 200 mm FFH access floor installed

structure C with 600 mm FFH access floor installed

Figure 4.77: Structure C - Comparison of 200 mm and 600 mm FFH Access Floors.



epoxy pedestal adhesive



polyurethane based pedestal adhesive

Figure 4.78: Structure C - Comparison of Epoxy and Polyurethane Based Pedestal Adhesives.



snap-on stringer system

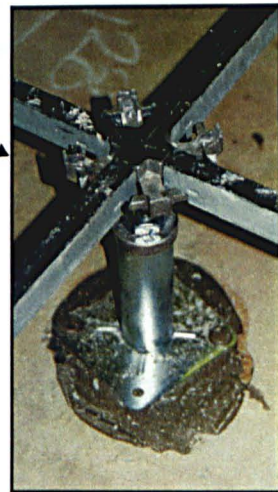


Figure 4.79: Structure C - Snap-On Stringer System.

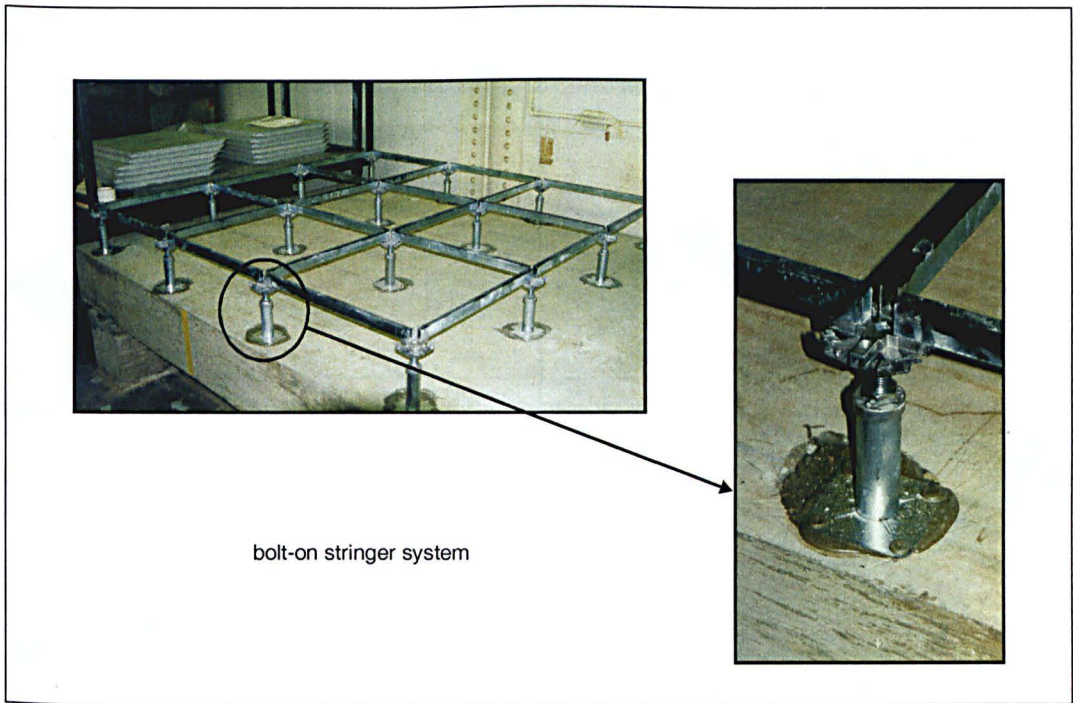


Figure 4.80: Structure C - Bolt-On Stringer System.

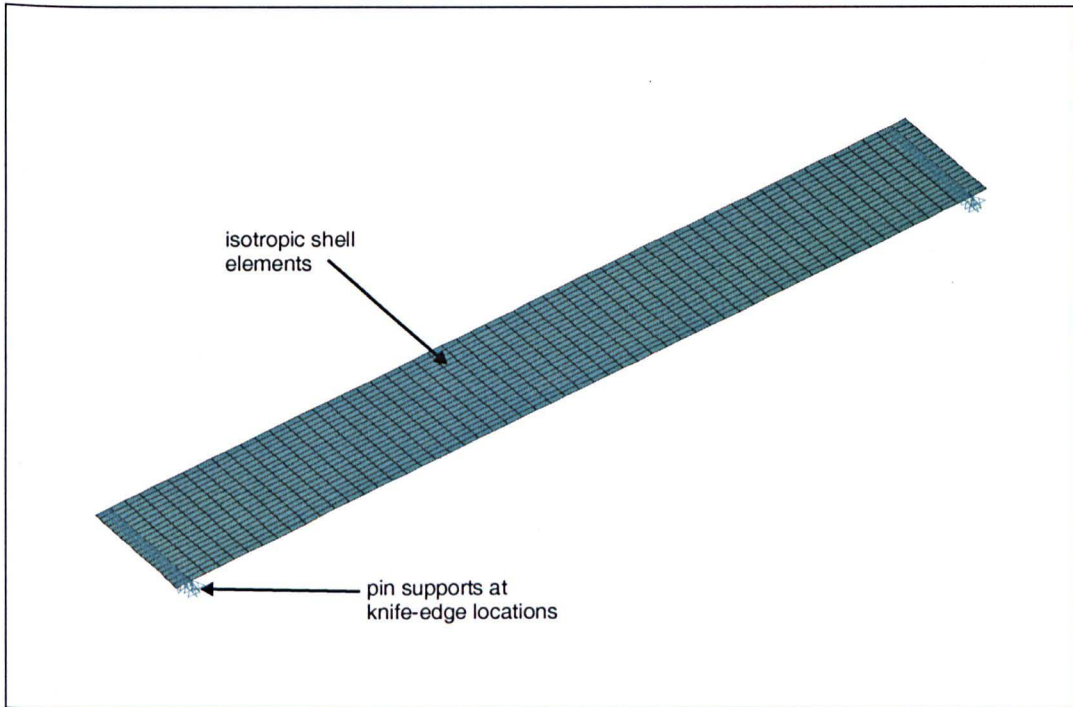


Figure 4.81: Structure C - Pre-Test FE Model.

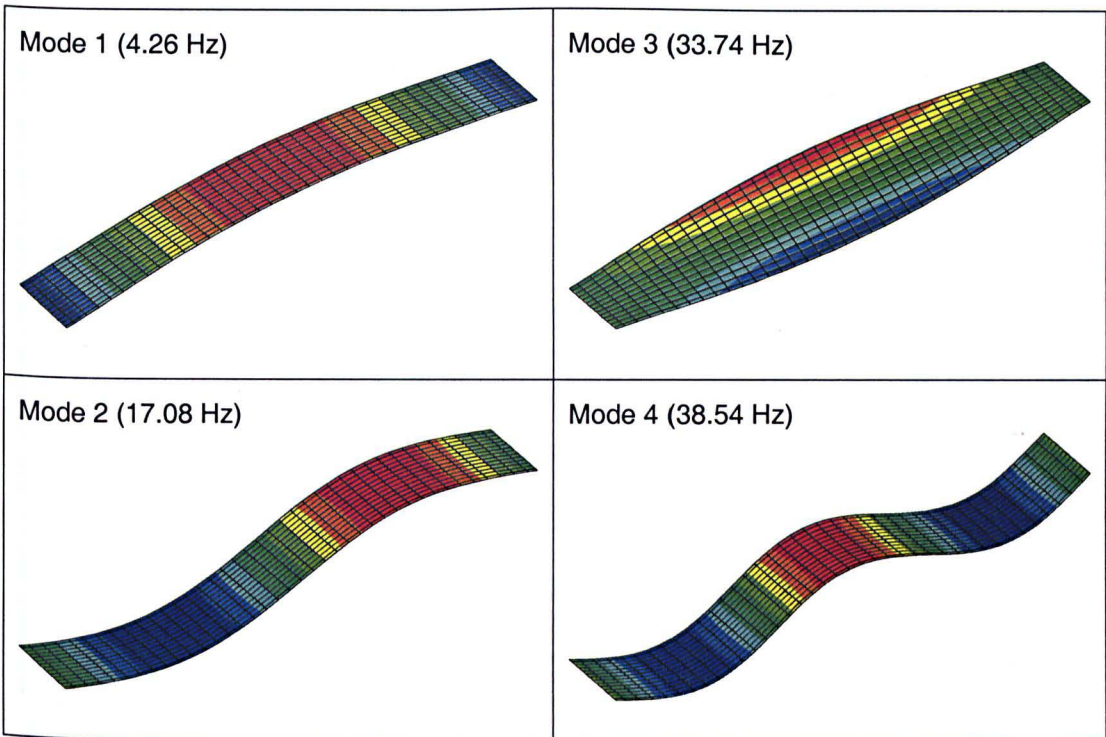


Figure 4.82: Structure C - First 4 Modes Calculated from Pre-Test FE Analysis.

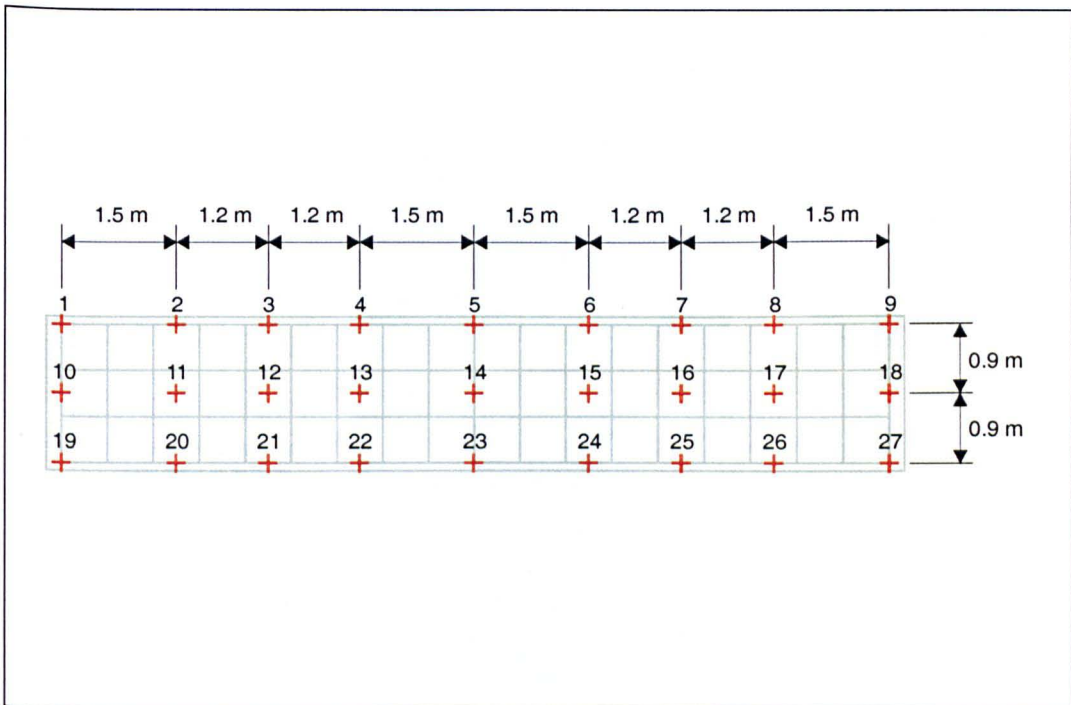


Figure 4.83: Structure C - Test Grid for EMA Swipes with Shaker in Free-Armature Mode.

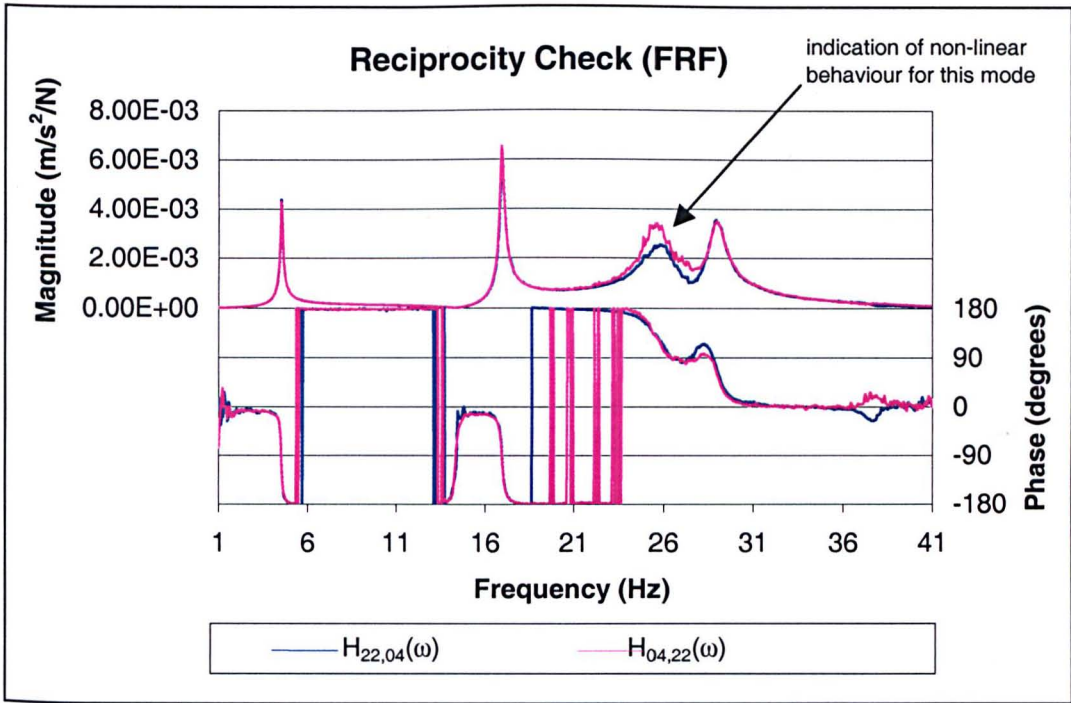


Figure 4.84: Structure C (Configuration 1) - Reciprocity Check Between Test Points 4 and 22.

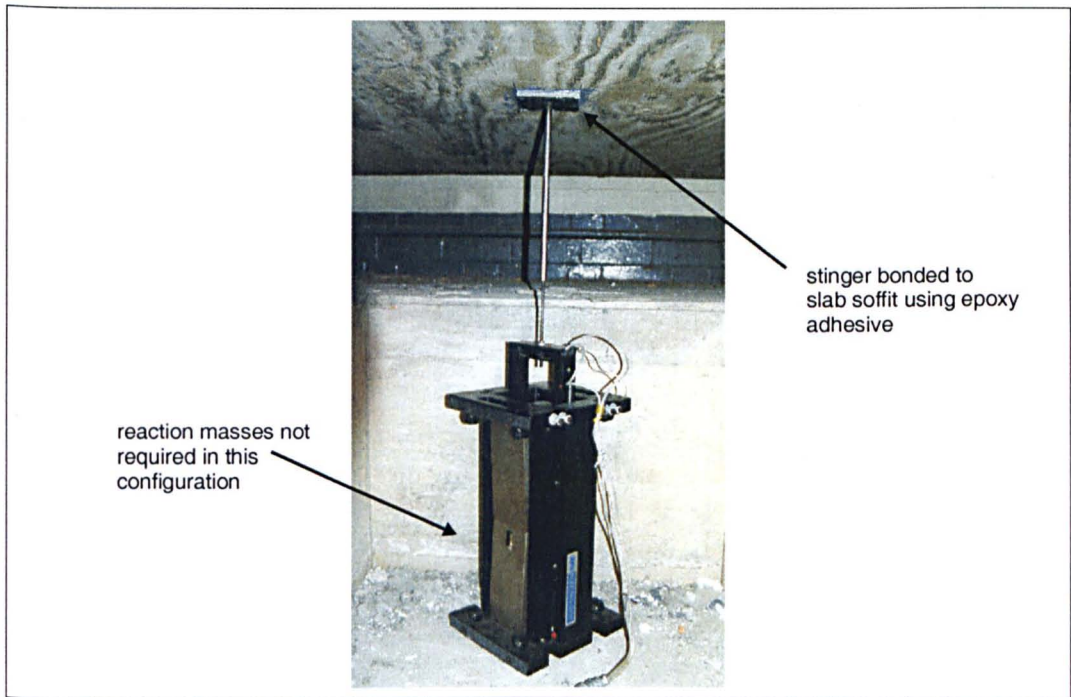


Figure 4.85: Structure C - Shaker Attached for Fixed-Armature Measurements.

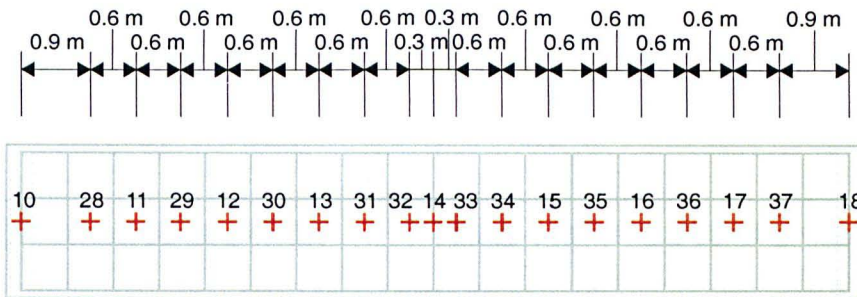


Figure 4.86: Structure C - Test Grid for EMA Swipes with Shaker in Fixed-Armature Mode.

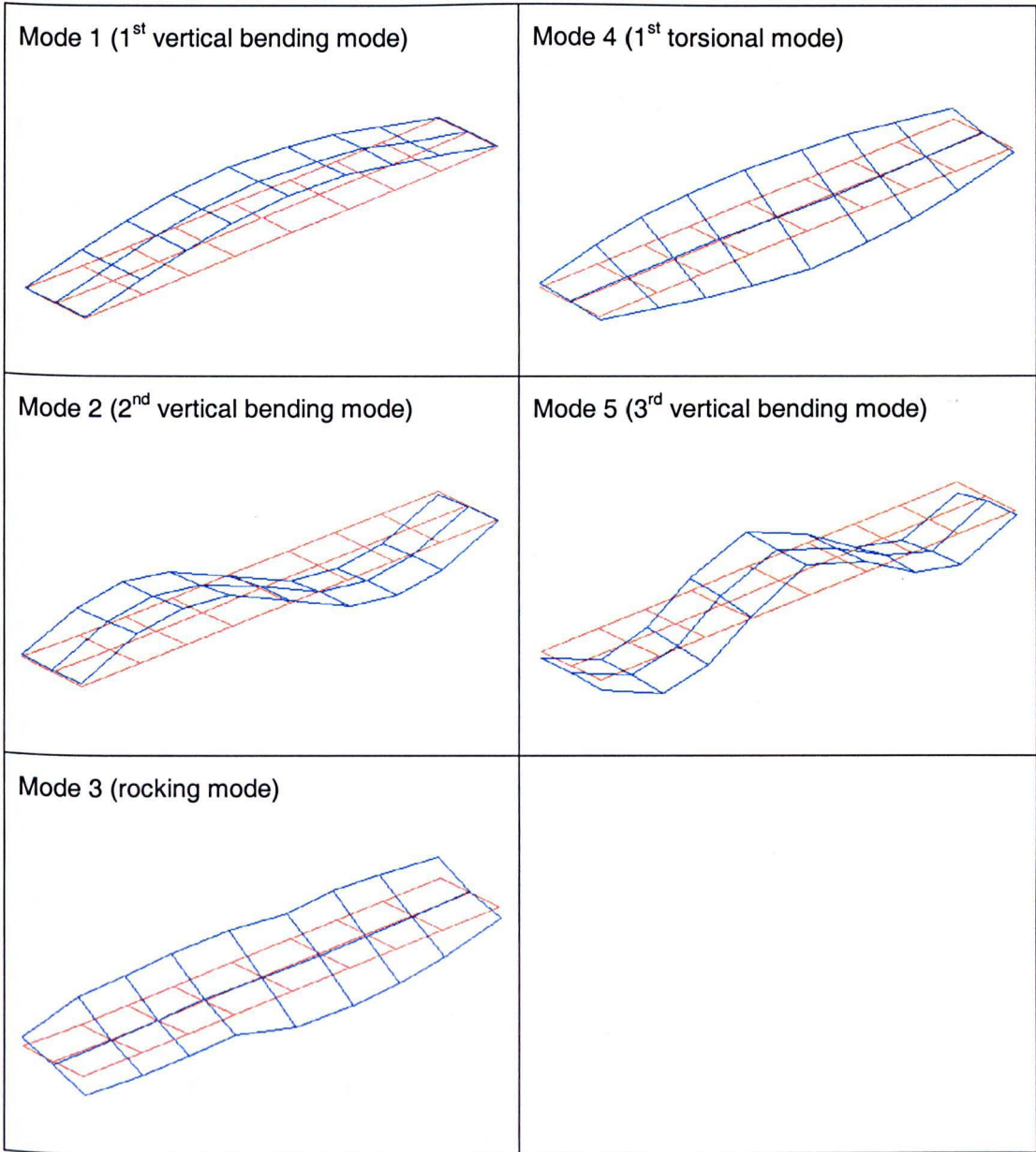


Figure 4.87: Structure C (All Configurations) - Estimated Mode Shapes.

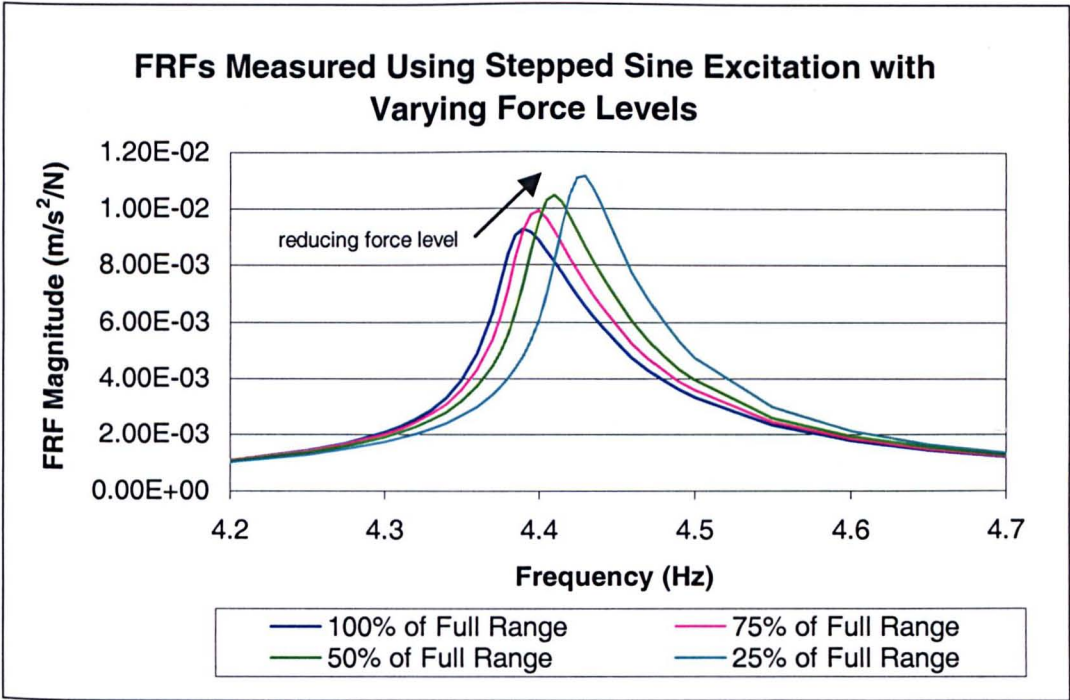


Figure 4.88: Structure C (Configuration 5) - FRFs Measured Using Stepped-Sine Excitation with Varying Force Levels.

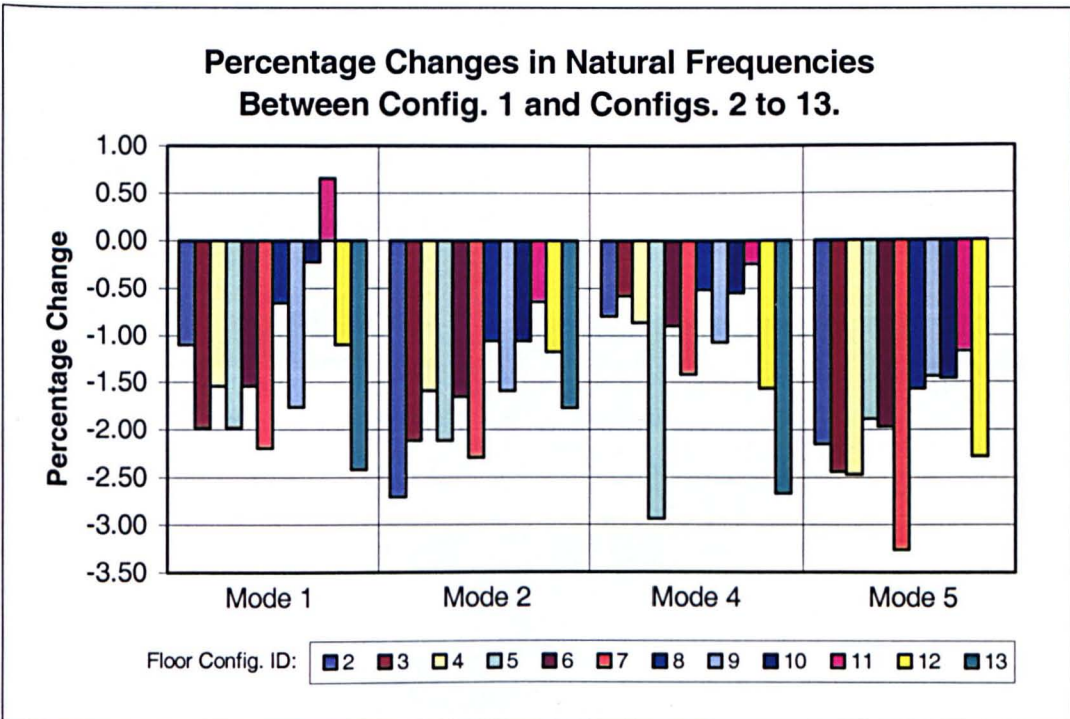


Figure 4.89: Structure C - Percentage Changes in Natural Frequencies Between Floor Configuration 1 and Configurations 2 to 13.

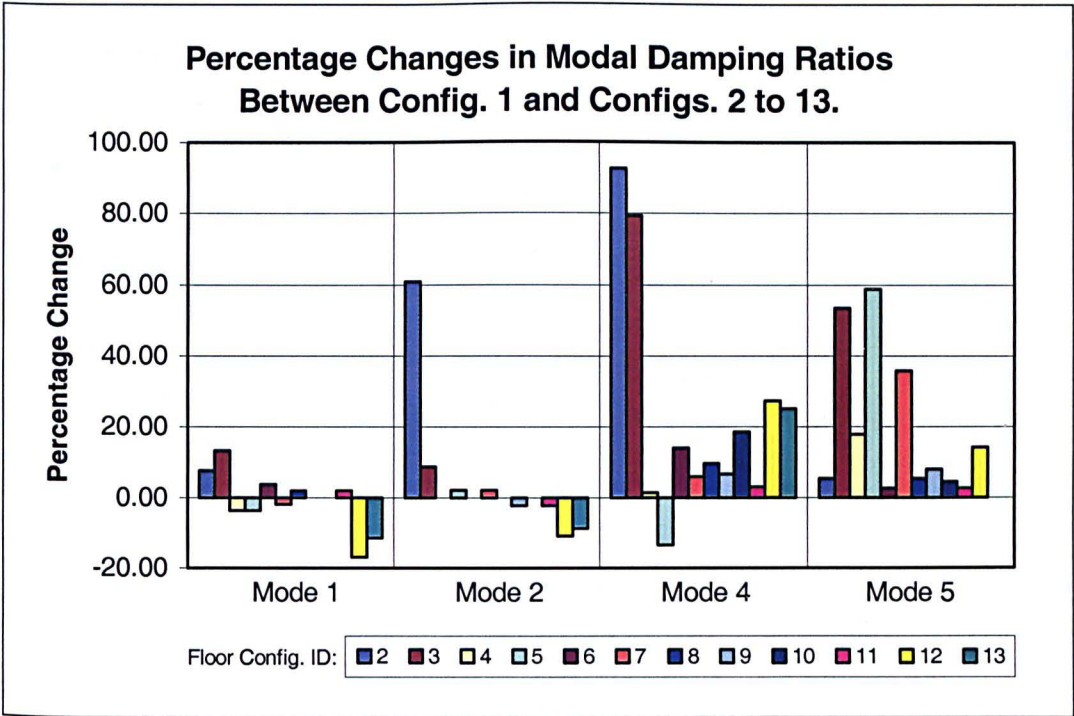


Figure 4.90: Structure C - Percentage Changes in Modal Damping Ratios Between Floor Configuration 1 and Configurations 2 to 13.

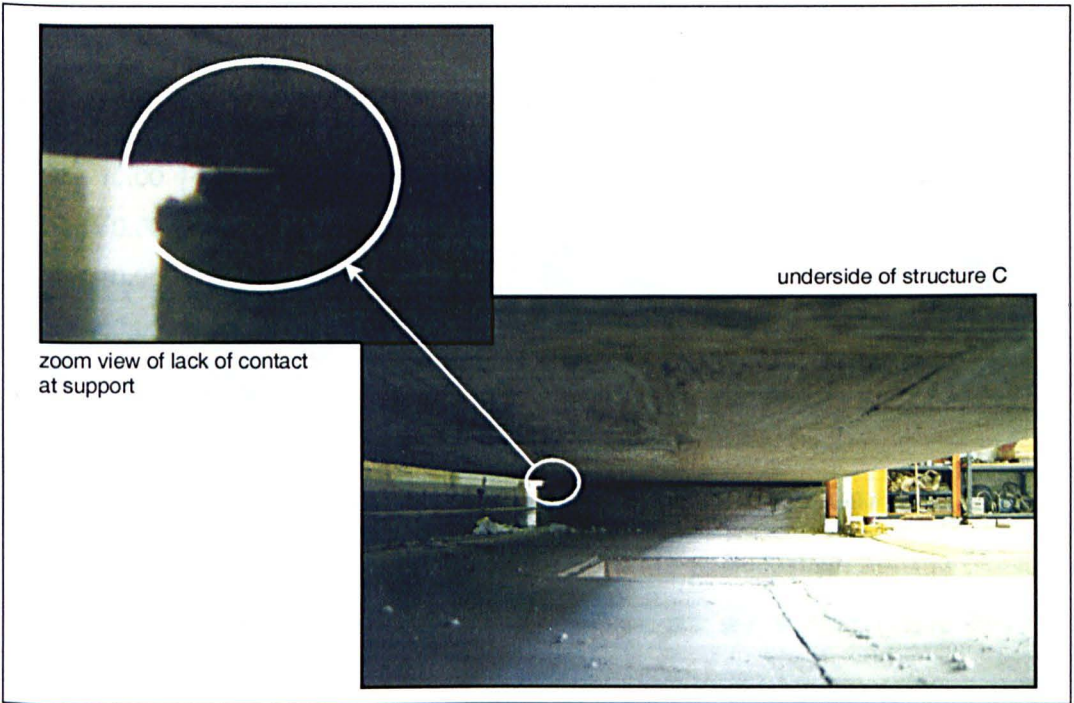


Figure 4.91: Structure C - Lack of Contact at Knife-Edge Support Beneath Test Point 9.

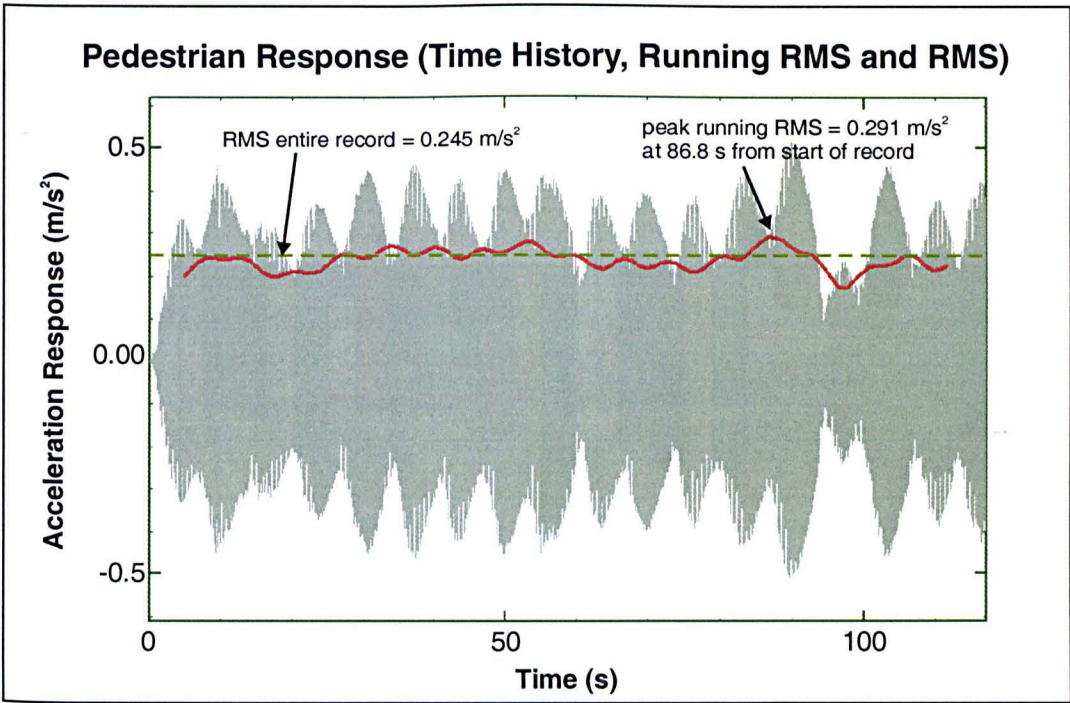


Figure 4.92: Structure C (Configuration 1) - Pedestrian Response Measurement for Pedestrian 1 at a Pacing Rate of 138 spm.

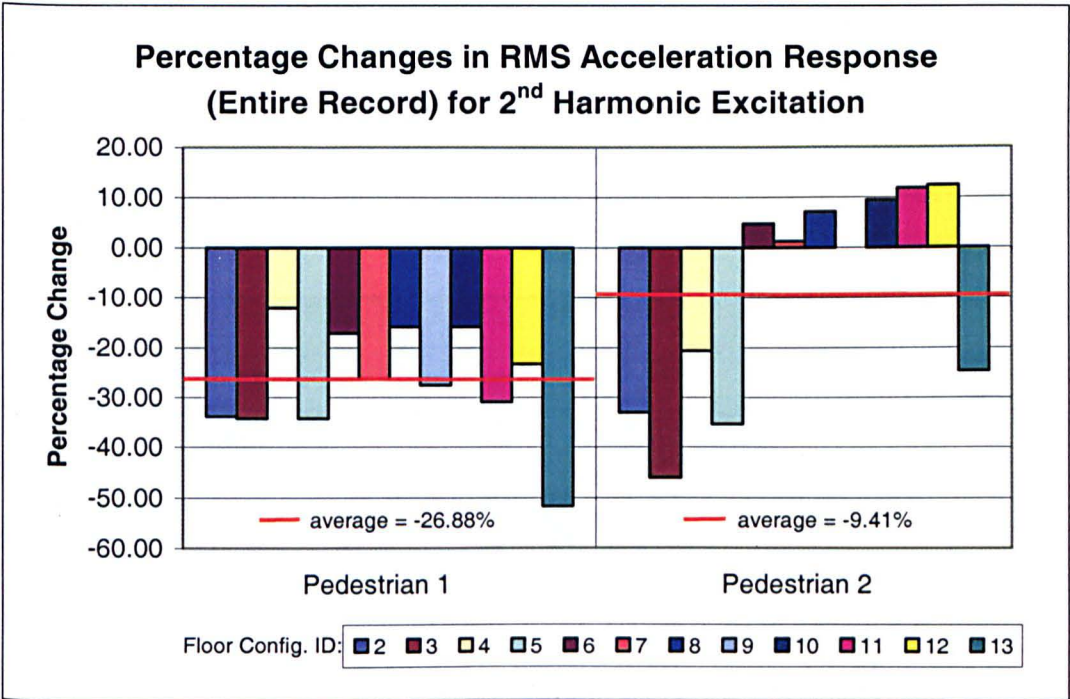


Figure 4.93: Structure C - Percentage Changes in RMS Acceleration Response (Entire Record) for 2nd Harmonic Excitation Between Floor Configuration 1 and Configurations 2 to 13.

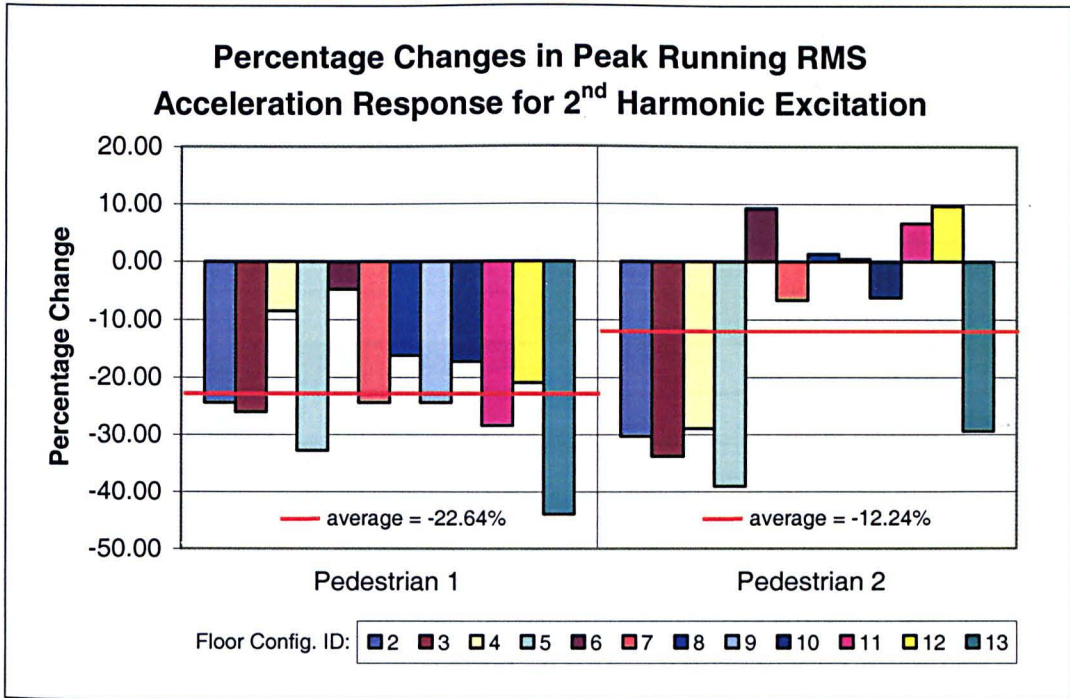


Figure 4.94: Structure C - Percentage Changes in Peak Running RMS Acceleration Response for 2nd Harmonic Excitation Between Floor Configuration 1 and Configurations 2 to 13.

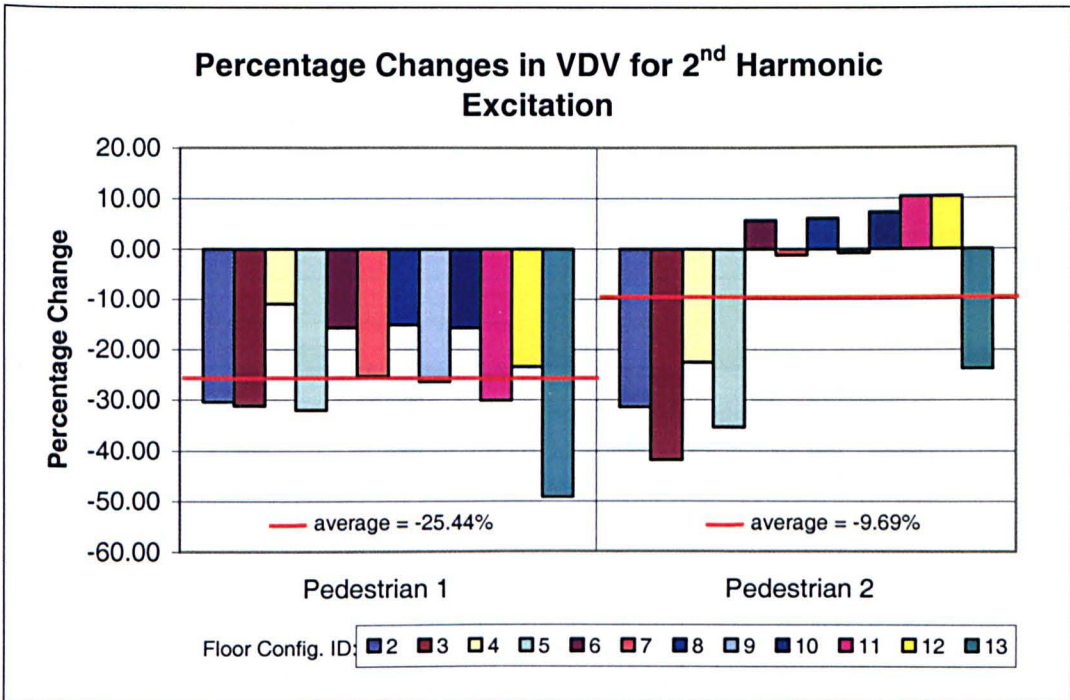


Figure 4.95: Structure C - Percentage Changes in VDV for 2nd Harmonic Excitation Between Floor Configuration 1 and Configurations 2 to 13.

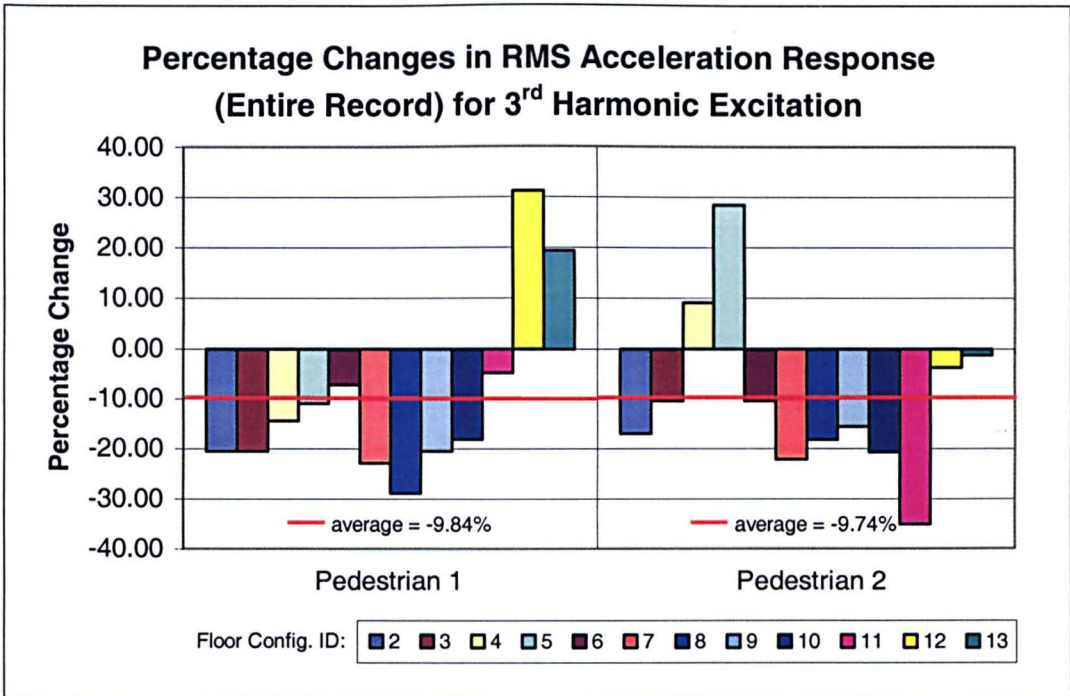


Figure 4.96: Structure C - Percentage Changes in RMS Acceleration Response (Entire Record) for 3rd Harmonic Excitation Between Floor Configuration 1 and Configurations 2 to 13.

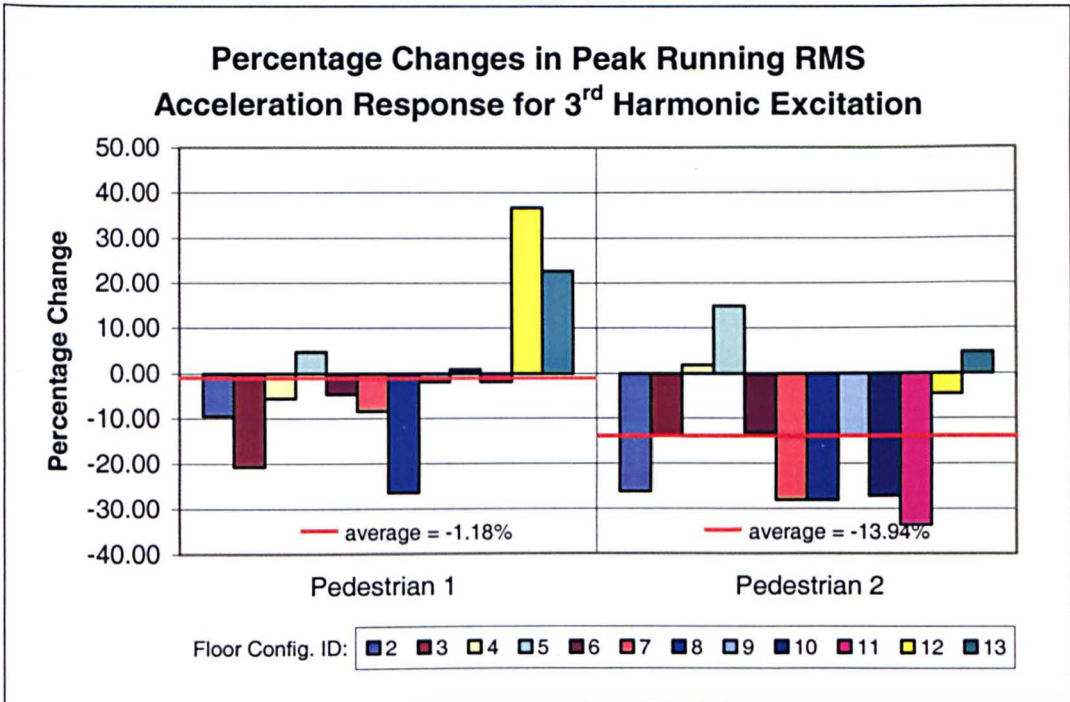


Figure 4.97: Structure C - Percentage Changes in Peak Running RMS Acceleration Response for 3rd Harmonic Excitation Between Floor Configuration 1 and Configurations 2 to 13.

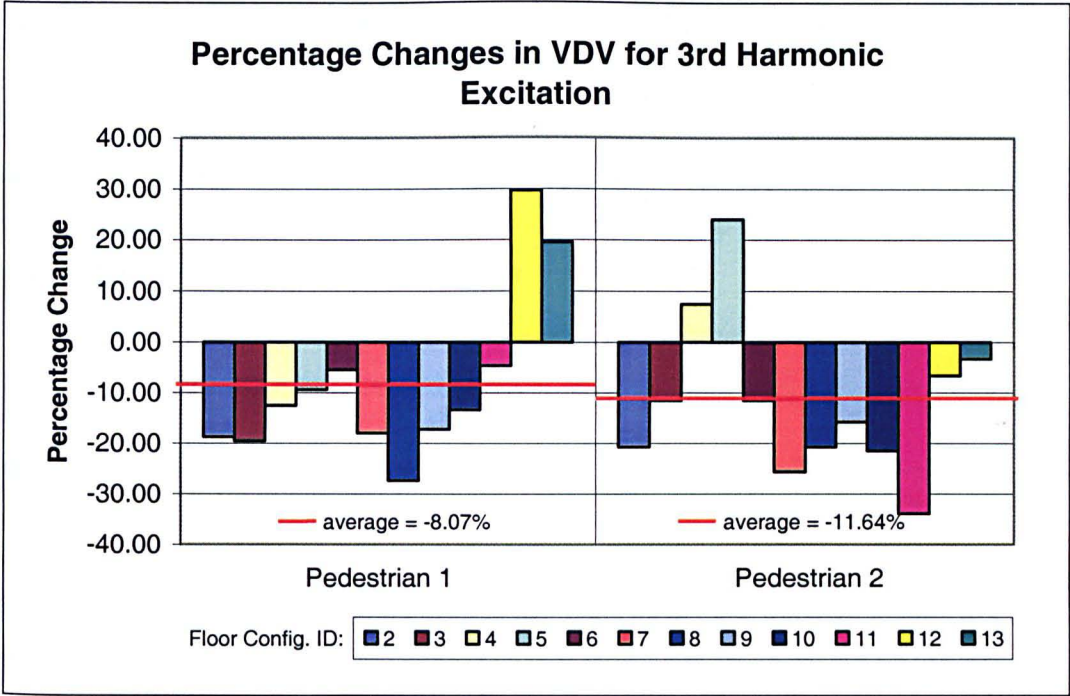


Figure 4.98: Structure C - Percentage Changes in VDV for 3rd Harmonic Excitation Between Floor Configuration 1 and Configurations 2 to 13.

5 Post-Test Analysis of Structures

This chapter presents the analytical work that was performed in order to simulate analytically the experimental results that were presented in Chapter 4. This combination of analysis and test data enables many useful observations to be made that would not be apparent through the use of either testing or analysis alone.

5.1 Structure A

The pre-test FE model constructed for Structure A was already quite realistic and a reasonable correlation between the results from this model and those estimated from the EMA was found.

5.1.1 Correlation Between Pre-Test Model and EMA Results

To determine the degree of correlation between the pre-test FE model and the results from the EMA, the following measures were utilised:

1. a plot of FE calculated natural frequencies versus EMA estimated natural frequencies,
2. a MAC matrix, and
3. a COMAC plot.

These measures were calculated using the MODESH program from the ICATS suite of software (ICATS, 1997) and are presented in Figure 5.1. In this figure, Set 1 corresponds to experimental data whereas Set 2 is the analytically calculated data. Examining firstly the natural frequencies plot, it can be seen that the points on this plot trace a reasonably straight line at an angle smaller than 45° from the abscissa. This suggests that the global spatial distribution of stiffness and mass in the FE model represents quite well that measured from the EMA, although the angle of less than 45° indicates a global lack of stiffness or an overestimation of mass in the pre-test FE model.

The MAC matrix showed that there was reasonable correlation between the FE model and the EMA results, with the first 6 modes of vibration having a MAC of above 60%,

three of which were above 80%. The correlated pairs of pre-test analytical and experimental modes are shown in Figure 5.2.

Finally, the COMAC plotted for all 33 correlated test points using the first 6 correlated mode pairs (CMPs) shows a reasonable correlation for all test points with only one of the test points having a value of COMAC below 60%.

5.1.2 FE Model Updating of Bare Structure A (Configuration 1)

Since the changes in modal properties caused by the installation of the access floors had been determined to be quite small, it was necessary to obtain as accurate an FE model of the structure as possible for further analytical investigation of the effects of the access floors. Failure to obtain a highly accurate FE model may have resulted in inappropriate conclusions being drawn from parametric studies performed on this model. For this reason, a manual FE model updating approach was utilised, as described in Section 3.8.2.

The updates made to the pre-test model to obtain better correlation with the EMA results can be divided into two groups:

1. FE model refinements, and
2. parameter adjustments.

FE model refinements were modifications made to the construction of the FE model, such as the explicit modelling of features omitted from the original model, changes in the way in which boundary conditions were modelled and the use of more appropriate element types.

Parameter adjustments were simply adjustments made to numerical values of uncertain modelling parameters, such as modulus of elasticity, spring constants for flexible supports and the ratio of orthotropic stiffnesses for the main area of the slab. At all stages, consideration was given to the physical meaning of these parameters and, consequently, unrealistic values were not utilised.

Taking all iterations of the model refinements and parameter adjustments into account, more than 50 FE analyses were performed to arrive at the final updated FE model.

5.1.2.1 Details of FE Model Refinements

Throughout the course of the FE model updating, the effects of various FE model refinements were investigated by constructing progressively more refined FE models, with only a single refinement being investigated at each stage. The following FE model refinements were implemented in sequence:

- The dowel connections between the lift shaft and the post-tensioned slab were modelled using linear elastic spring elements, as it was considered that this would represent more realistically the actual behaviour of these details.
- Shear walls were modelled using shell elements instead of pin supports. This was expected to simulate better the rotational restraint provided to the slab at these locations.
- As the columns in this structure were very wide and thin, they were modelled using shell elements, as opposed to beam elements as used in the pre-test FE model.

By examination of the MAC and COMAC calculated between the results of the intermediate FE models and the EMA results, it was found that each of the refinements improved the correlation to some extent. The final configuration of the FE model is illustrated in Figure 5.3.

5.1.2.2 Details of Parameter Adjustments

At each stage of the model refinements described above, it was necessary to 'tune' the FE model by adjusting various parameters to obtain the best possible correlation with the EMA results. This was done on a trial and error basis guided by engineering judgement. The following parameters were adjusted in this manner:

- The modulus of elasticity of the concrete.
- The ratio of stiffnesses between the two orthogonal directions of the ribbed slab.
- The spring stiffness of the elastic spring elements representing the dowel connection to the lift shaft (Figure 4.1).

It was found, as expected, that these parameters had different effects on the calculated dynamic behaviour of the system. The modulus of elasticity tended to change all natural frequencies, whereas the ratio of stiffness in orthogonal directions tended to alter the spacing between modes and the elastic spring stiffnesses tended to change only those modes in which they were engaged significantly.

Following the updating, each of the adjusted parameters had realistic and logical values. These are presented in Table 5.1.

Table 5.1: Structure A (Configuration 1) - Summary of Parameter Adjustments.

Parameter	Value Assumed for Pre-Test Analysis	Value Following FE Model Updating
E_{conc}	35 kN/mm ²	47.5 kN/mm ²
Ratio of Slab Orthogonal Stiffnesses	0.098	0.115
Spring Stiffnesses at Lift Shaft	infinite (pin supports)	500 kN/mm

It may seem at first glance that the modulus of elasticity in the updated FE model is rather high at a value of 47.5 kN/mm². However, at the time of testing there were suspended ceilings and electrical and mechanical services installed on the underside of the post-tensioned concrete slab, as shown in Figure 5.4. As some of these non-structural elements were quite robust, it is likely that they were contributing to the stiffness of the floor. By using an inflated value of modulus of elasticity, the stiffening effects of these non-structural elements were taken into account in a 'smeared' manner. In addition, the cube strength of the concrete was measured by the contractor to be 70 N/mm², which was higher than the designed strength of 50 N/mm² (Pavic, 1999). This would also probably have resulted in a slightly increased modulus of elasticity.

5.1.2.3 Correlation Between Updated FE Model and Results from EMA

The first 10 mode shapes calculated from the updated FE model are presented in Figure 5.5 together with the 8 modes from EMA with which they correlate. The calculated natural frequencies and modal masses are presented in Table 5.2 together with the natural frequencies and modal masses estimated from the EMA.

Table 5.2: Structure A (Configuration 1) - Natural Frequencies Calculated from the Updated FE Model.

FE Mode Number	Natural Frequency from Updated FE Model (Hz)	Natural Frequency from EMA (Hz)	Modal Mass from Updated FE Model (kg)	Modal Mass from EMA (kg)
1	6.42	6.41	58080	70000
2	6.72	6.79	47170	63000
3	8.13	8.16	38760	58000
4	10.06	9.92	55730	---
5	11.97	11.78	55840	68000
6	14.88	15.02	52870	48000
7	17.34	---	37440	---
8	17.53	17.40	34640	103000
9	18.22	18.18	59430	60000
10	20.26	---	38080	---

It can be seen from Table 5.2 that the modal masses calculated from the FE modelling were generally lower than those measured from EMA. This is expected since only a single floor in the multi-storey building was modelled in the updated FE model. In the real structure, it is likely that vibration energy would have been passed down through the columns to other parts of the structure, hence engaging a larger mass in the vibration. However, it was not practical to model the whole structure and the modal masses, calculated from the model of a single floor and its supporting columns, were assumed to be acceptably accurate for the purpose of this investigation.

Figure 5.6 shows the correlation measures calculated for these sets of modes. It can be seen that, with the exception of FE modes 7 and 10, which were not estimated from the EMA (Figure 4.31), the correlation between the two sets of data was good with no values of MAC or COMAC being below 60% and the majority being greater than 80%.

A final step in examining the correlation between the updated FE model and the test data recommended by Heylen et al. (1997) was to regenerate a measured FRF using the updated analytical model. A point mobility corresponding to point 32 of the test grid was calculated using a harmonic mode superposition analysis, taking the damping values estimated from the EMA which included the effects of the exponential window. Figure 5.7 shows this FRF superposed with an experimentally measured point mobility FRF at

the same point. As can be seen, the two FRFs having the same frequency resolution were comparable, giving more confidence in the ability of the updated FE model to represent accurately the measured dynamic behaviour of the structure.

5.1.2.4 Comparison with Previous FE Model Updating Exercises on Structure A

It should be noted here that similar FE model updating exercises were performed by Pavic (1999) on this structure. However, the EMA data used as a basis for updating were acquired using hammer impact excitation and were therefore of a lower quality than those obtained in this work using the more highly controlled electrodynamic shaker excitation. Probably as a result of the more uncertain estimated modal parameters, the values of MAC and COMAC calculated by Pavic between his updated FE model and the EMA results were typically lower than those presented in Figure 5.6. Pavic also failed to reproduce measured FRFs, such as that presented in Figure 5.7, by calculation using the updated FE model.

The increased reliability of the modal parameters estimated in this work, from tests performed using electrodynamic shaker excitation, facilitated a more detailed approach to the FE modelling of the structure. In particular, two model refinements which were not utilised by Pavic (1999) were the modelling of the columns using shell elements (as opposed to beam elements) and the inclusion of the shear walls in the analysis.

However, on the whole, the FE model updating exercises presented here resulted in similar conclusions to those drawn by Pavic regarding the modelling of this structure.

The most significant of these were:

1. the dynamic modulus of elasticity had to be higher than is commonly assumed,
2. the lateral floor stiffness is increased by the presence of the wide and shallow ribs relative to the stiffness of the slab alone, and
3. the columns must be modelled explicitly as they provide a significant contribution to the overall stiffness of the floor system.

The improved accuracy of the updated FE model described in this work was required for examination of the changes in modal properties exhibited by the floor following the installation of the access floors. This was because the aforementioned changes were quite small and it was important for them not to be obscured by inaccuracies in the FE modelling.

5.1.3 Simulation of the Effects of Access Floors

The updated FE model described in Section 5.1.2 was modified to include the access floors as an added mass of 33 kg/m² applied to floor areas only. This was implemented by changing the density of the floor elements, as appropriate. No other changes were made to the model. The mode shapes calculated did not change appreciably and were therefore the same as those presented in Figure 5.5. However, as expected, the calculated natural frequencies decreased and the modal masses increased. These results are presented in Table 5.3.

Table 5.3: Structure A (Configuration 2) - Natural Frequencies Calculated from the Updated FE Model with Access Floors Modelled as Added Mass Only.

FE Mode Number	Natural Frequency Including Added Mass (Hz)	Change in Natural Frequency from Updated FE Model (%)	Modal Mass Including Added Mass (kg)	Change in Modal Mass from Updated FE Model (%)
1	6.27	-2.34	60960	+4.96
2	6.56	-2.38	49500	+4.94
3	7.93	-2.46	40680	+4.95
4	9.82	-2.39	58480	+4.93
5	11.69	-2.34	58580	+4.91
6	14.52	-2.42	55470	+4.92
7	16.93	-2.36	39240	+4.81
8	17.12	-2.34	36310	+4.82
9	17.79	-2.36	62310	+4.85
10	19.78	-2.37	39910	+4.81

It is clear that, if the access floor acted as added mass only on the structure, all natural frequencies would be reduced by more or less the same percentage (-2.4%), and all modal masses would have increased by more or less the same percentage (+4.9%).

However, the changes in natural frequencies detected on the real structure following the installation of the access floor varied from -1.01% to -2.46%, depending on the mode under consideration (Table 4.12). This indicates that, in some modes, the access floor was likely to be providing a small amount of additional stiffness to the floor system.

This was simulated by increasing the modulus of elasticity of the floor shell elements in the updated FE model including the access floor mass. It was found that an increase in the bending stiffness of the floor elements of +3.6% was required to reduce the reduction in natural frequencies to a value of -1.01%, the lowest value observed on the actual structure. However, it should be noted that it was not possible to simulate the changes in stiffnesses for all modes simultaneously using this procedure. It would therefore appear that the measured phenomenon of increased stiffness caused by the access floors was more complicated than could be modelled using this FE modelling methodology.

5.2 Structure B

Due to extensive cracking of Structure B at the time of the testing, it was anticipated that a lot of FE model updating would be required to arrive at an FE model which would represent accurately the tested structure.

5.2.1 Correlation Between Pre-Test Model and EMA Results

Similarly as for Structure A, the plot of natural frequencies calculated from the FE model (Set 2) versus those estimated from EMA (Set 1) and the MAC matrix was produced using the ICATS software. These are presented in Figure 5.8. On examination of these, it is clear that the correlation between the two sets of data is less than perfect. The natural frequencies plot shows some scatter of the individual data points away from the line of best fit, indicating that it is not a global parameter such as stiffness of material density which is causing inaccuracies, but rather it is likely that there are local effects, such as the cracking, which must be included in the FE model. In addition, the line of best fit lies at an angle slightly greater than 45° which indicates that there is a probable global overestimation of stiffness considering the heavily cracked state of the slab (Figure 5.9).

The MAC matrix in Figure 5.8 shows that EMA mode 1 correlates with analytical mode 2 and vice versa. This also occurs for EMA and analytical modes 3 and 4 but since these calculated modes have repeated natural frequencies, analytical modes 3 and 4 may actually be interchanged. Since a global change in material properties would only serve

to shift the natural frequencies higher or lower, it is apparent that a different type of alteration to the FE model is warranted. The MAC matrix also shows a lack of correlation between analytical modes 5, 6 and 7 (Set 2) and EMA modes 5 and 6 (Set 1). This was caused by the fact that these modes of vibration were local corner modes of the slab structure (modes 5, 6 and 7 in Figure 4.61), which were consequently quite difficult to estimate.

The COMAC calculated for the first four CMPs (indicated in the MAC matrix) is also presented in Figure 5.8. However, this provides no clues as to how the FE model should be updated.

5.2.2 FE Model Updating

From examination of the correlation between the pre-test FE model and the results from EMA, it was confirmed that there were significant discrepancies between the FE model and the experimentally measured modal properties. Therefore, similar to the procedure used for Structure A, the manual FE model updating was performed through the use of FE model refinements and parameter adjustments.

5.2.2.1 Details of FE Model Refinements

Due to the simplicity of the overall geometry of this structure, there was no requirement for improvements in the geometry of the FE model. However, as has already been mentioned, the structure was very heavily cracked due to the prior performing of high level static load tests. The crack pattern recorded from the structure is illustrated in Figure 5.9.

It had already been established (Pavic, 1999) that the presence of these cracks was having a significant effect on the dynamic behaviour of the structure. For this reason, the first FE model refinement was to divide the slab into a number of areas as illustrated in Figure 5.9. Each of these areas of the slab could then take separate values of modulus of elasticity in both orthogonal directions. It was anticipated that the effects of the cracking could be simulated through the use of reduced values of modulus of elasticity wherever it was present. In addition to this, Poisson's ratio for cracked areas of the slab was reduced from 0.2 to 0.1.

Experimentation with the FE model refined as described above revealed that it was not possible to exchange the positions of the first 2 analytical modes of vibration, in terms of values of natural frequency, which was required to correlate the FE model with the EMA results. Therefore, a further refinement made to the FE model was to rotate the element coordinate axis for the column elements through 45° about the global z-axis. Through the use of this technique, it was possible to reduce the stiffness of the columns in the direction in the plane of the diagonal of the square slab, as illustrated in Figure 5.10. This was intended to represent a reduction in stiffness caused by the crack pattern observed on the columns (Figure 5.11).

5.2.2.2 Details of Parameter Adjustments

The first parameter adjustment made from the pre-test FE model was the value of density assumed for the concrete. As the concrete was very high strength, an initial estimate of 2600 kg/m^3 had been assumed for its density. However, the staff at the Taywood Engineering laboratory in which the slab was built performed measurements of the density of test cubes of the concrete, and obtained values between 2440 and 2490 kg/m^3 , for which they took an average value of 2465 kg/m^3 . Therefore, a value of 2500 kg/m^3 was assumed for the density of the concrete in the updated FE model. This included an allowance for the steel reinforcement.

The remainder of the parameter adjustments made in the course of the FE model updating were applied to the moduli of elasticity assumed for the various areas of the slab and the columns in two orthogonal directions. This was done largely on a systematic trial and error basis guided by engineering judgement, and resulted in the numerous analyses of the same FE model with slightly varying material properties. A summary of the modelling values which provided the best correlation between the updated FE model and the results from EMA is presented in Figure 5.12.

It can be seen from Figure 5.12 that significantly reduced moduli of elasticity were required to simulate the loss of stiffness in the cracked areas of the slab, compared with that assumed for the uncracked areas.

5.2.2.3 Correlation Between Updated FE Model and Results from EMA

The first 15 mode shapes calculated from the updated FE model area presented in Figure 5.13 together with the modes of vibration estimated from EMA with which they

correlate. The calculated natural frequencies and modal masses are presented in Table 5.4 together with the natural frequencies and modal masses estimated from the EMA.

Table 5.4: Structure B (Configuration 1) - Natural Frequencies Calculated from the Updated FE Model.

FE Mode Number	Natural Frequency from Updated FE Model (Hz)	Natural Frequency from EMA (Hz)	Modal Mass from Updated FE Model (kg)	Modal Mass from EMA (kg)
1	4.31	4.31	29750	25000
2	4.67	4.65	24910	20000
3	6.61	6.63	14250	16000
4	6.76	6.76	15030	15000
5	8.46	8.29	7900	5000
6	8.69	8.70	7950	6000
7	9.13	---	6920	---
8	9.22	9.04	22230	5000
9	12.45	12.42	12170	15000
10	14.65	15.02	19290	16000
11	15.08	15.09	28000	27000
12	15.70	15.32	29270	25000
13	20.98	20.03	18420	16000
14	21.01	20.75	17980	17000
15	21.95	21.09	23260	14000

The correlation measures calculated for these sets of modes are presented in Figure 5.14. Note that the COMAC was calculated using analytical modes 1 to 4 and 8 to 11. It is clear that there is a fairly good correlation between the FE model and the EMA results, although it is apparent that some lack of correlation starts to occur for higher modes of vibration. However, this updated FE model was considered to be acceptable for further simulation of the effects of the access floors.

Finally, similarly as for Structure A, to determine how representative the updated FE model was of the measured structure, an experimentally measured FRF was regenerated using the FE model. The point mobility FRF at test point 35 was calculated using a

harmonic mode superposition analysis (ANSYS, 1995), taking the damping value estimated from the EMA. This is presented in Figure 5.15 overlaid on the experimentally measured FRF. It can be seen that there is a very good correlation between these FRFs in the lower frequency region. These results satisfied the writer that the updated FE model was reasonably representative of the structure as tested.

5.2.2.4 Comparison with Previous FE Model Updating Exercises on Structure B

Similar as for Structure A, completely independent FE model updating exercises were also performed for this structure by Pavic (1999). However, his updating exercises were again performed using EMA data which was acquired using hammer impact excitation and, again, the resulting updated FE model was of a poorer quality. In fact, a good correlation between the analysis and test data was obtained only for the first three modes of vibration.

By far the most significant FE model refinement performed in this work, which was not performed by Pavic, was the rotation of the element coordinate system of the column elements. As described in Section 5.2.2.1, this measure was fundamental to the success of the FE model updating exercise as it provided the only realistic mechanism for the first two modes of vibration to exchange places without adversely affecting the correlation of higher modes of vibration.

5.2.3 Simulation of the Effects of Access Floors

The updated FE model described in Section 5.2.2 was modified to include the access floors as an added mass of 38 kg/m^2 applied to the whole of the slab area. No other changes were made to the model. The mode shapes did not change significantly and were therefore the same as those presented in Figure 5.13. The results from this analysis are presented in Table 5.5.

Table 5.5: Structure B (Configurations 2 and 3) - Natural Frequencies Calculated from the Updated FE Model with Access Floors Modelled as Added Mass Only.

FE Mode Number	Natural Frequency Including Added Mass (Hz)	Change in Natural Frequency from Updated FE Model (%)	Modal Mass Including Added Mass (kg)	Change in Modal Mass from Updated FE Model (%)
1	4.18	-3.02	31560	+6.08
2	4.54	-2.78	26430	+6.10
3	6.41	-3.03	15120	+6.11
4	6.56	-2.96	15950	+6.12
5	8.21	-2.96	8380	+6.08
6	8.44	-2.88	8430	+6.04
7	8.86	-2.96	23580	+6.07
8	8.95	-2.93	7340	+6.07
9	12.09	-2.89	12910	+6.08
10	14.23	-2.87	20460	+6.07
11	14.64	-2.92	29700	+6.07
12	15.24	-2.93	31050	+6.08
13	20.37	-2.91	19540	+6.08
14	20.40	-2.90	19070	+6.06
15	21.31	-2.92	24670	+6.06

Similar to Structure A, the updated FE model predicted a more or less uniform reduction in natural frequencies (-2.9%) and increase in modal mass (+6.1%) following the addition of the access floors as increased mass.

However, the results from the EMA (presented in Table 4.18) indicated that the natural frequencies reduced only between -0.15% and -2.43% for Configuration 2, depending on the which mode was being considered. Interestingly, the reduction in natural frequency corresponding to the 2nd measured mode of vibration, which was the most easily excited by normal walking, was only -0.22%. This effect was even more pronounced for Configuration 3 of the structure (Table 4.18), when the access floor panels were mechanically fixed to the pedestals. In this case, the maximum observed reduction in natural frequency was only -1.88%. Moreover, for the 2nd and the 4th measured modes, instead of decreasing, the natural frequencies actually increased following the

installation of the access floor, the increase corresponding to the 2nd mode being the largest at +1.94%.

Clearly, on this structure, the access floor was providing some additional stiffness to the slab system. This effect was more pronounced for the case when the access floor panels were mechanically fixed to the pedestals compared with when they were loose-laid on the pedestals. Another FE simulation was performed to investigate the actual increase in stiffness required to obtain the measured changes in natural frequencies. For Configuration 2, it was found that an increase in bending stiffness of 6% for the slab elements simulated the measured reduction of -0.22% in natural frequency. For Configuration 3, an increase in stiffness of 12% was required to simulate the +1.94% increase in natural frequency.

5.3 Structure C

Structure C, constructed under laboratory conditions at the University of Sheffield, had been designed to be as simple as possible to reduce the number of uncertainties in FE models constructed. However, even for such a simple structure, it was still necessary to pass through the FE model updating process to arrive at an accurate FE model which would represent the as-built structure.

5.3.1 Correlation Between Pre-Test Model and EMA Results

The natural frequencies comparison and MAC matrix were again calculated using the ICATS software and are presented in Figure 5.16. In addition, the visual correlation between the calculated and experimentally measured modes of vibration is presented in Figure 5.17.

It can be seen that, even though the structure was designed and constructed to be as simple and ideal as possible, there were significant differences between the calculated modal parameters and the results from EMA. In particular,

1. the error in the prediction of the natural frequency of the first bending mode was much more significant than the error in prediction of the natural frequencies of the second and third bending modes, and

2. the pre-test FE model failed to predict the occurrence of two closely spaced torsional modes of vibration.

The discrepancy between the analytical and measured natural frequencies for the 1st mode of vibration was considered not to be caused by an underestimation of stiffness or an overestimation of mass. If this was the case, it would be expected that the natural frequencies of higher vertical bending modes would also be underestimated, which was not apparent here. Therefore, it was hypothesised that the boundary conditions, whilst being as ideal as possible, were still influencing the structural dynamic behaviour in some way. This was scheduled for investigation in the FE model updating for this structure.

With regards to the two measured torsional modes of vibration, for which only one mode was predicted by the analysis, it was thought that the lack of contact at one of the supports (illustrated in Figure 4.91) was responsible for this. It was therefore decided to attempt to simulate this effect in the FE model updating.

It can also be seen from Figure 5.16 that the COMAC for the support points is zero. However, since full vertical displacement constraints were applied to these points in the FE model, any measured vertical motion at these points would be expected to produce a zero value of COMAC. This is the explanation for these 'anomalous' zero COMAC values.

5.3.2 FE Model Updating

Similar to Structures A and B, the FE model updating of Structure C consisted of making a number of modifications in terms of model refinements and parameter adjustments.

5.3.2.1 Updating of Pre-Test Model Using Parameter Adjustments Only

Concentrating mainly on the 1st mode of vibration, the pre-test FE model was updated using parameter adjustments only in an attempt to match the natural frequencies measured on the structure.

During the construction of the slab strip, test cubes were cast from the same batch of concrete that was used in the slab strip itself. These cubes, of known dimensions, were

weighed to determine a density of concrete which could be used to improve the modelling of the mass of the structure. The average density obtained from these cubes was 2300 kg/m³. This density was therefore used in all subsequent FE models of this structure. Due to the very light reinforcement in this structure, which can be seen in Figure 4.75, it was decided not to make an allowance for the weight of the steel.

Following the modification of the density of the concrete, another meaningful parameter which was adjusted on this model was the modulus of elasticity. To match the measured first natural frequency of 4.55 Hz, it was found that the modulus of elasticity had to be increased from the assumed 38 kN/mm² in the pre-test model to a value of 41.6 kN/mm². The natural frequencies of the first 4 modes of vibration calculated from this model are presented in Table 5.6, together with those estimated from EMA.

Table 5.6: Structure C (Configuration 1) - Natural Frequencies from Updated FE Model and from EMA.

Mode	Natural Frequency from Updated FE Model (Hz)	Natural Frequency from Testing (Hz)
1 (1 st vertical bending)	4.55	4.55
2 (2 nd vertical bending)	18.25	17.02
3 (1 st torsional)	36.09	26.02 or 28.92
4 (3 rd vertical bending)	41.18	37.71

Whilst the value of modulus of elasticity obtained (41.6 kN/mm²) was considered to be realistic, i.e. within 10% of the value of 38 kN/mm² recommended by Wyatt (1989), the model overestimated the natural frequencies of modes higher than the fundamental. For this reason, it was decided that it was unlikely that the value of modulus of elasticity should actually be that high, and that the higher fundamental natural frequency was probably caused by some effect other than a change in global stiffness alone.

5.3.2.2 Examination of Boundary Conditions

As already mentioned, the most likely source of the discrepancy between the calculated and measured natural frequencies corresponding to the first mode of vibration was considered to be the boundary conditions of the slab, i.e. the knife-edge supports (Figure 4.71).

Whilst the knife-edge supports could be considered to provide very little rotational restraint at the point of contact with the slab strip, they would be expected to provide some horizontal restraint in the direction along its length. This is due to friction between the top of the angle section and the bearing plate built into the slab (Figure 4.71). If this horizontal restraint was at the centroid of the slab strip section, no change in natural frequencies would be expected in theory. However, since this horizontal restraint was offset from the centroid of the slab strip at its soffit, it effectively provided some rotational restraint.

It was decided that this effect should be modelled by constructing an FE model of the slab strip using ANSYS SOLID73 elements (ANSYS, 1995). The exact position of the supports, offset from the centroid of the slab strip, could easily be modelled in this way.

5.3.2.3 Modelling of Structure C Using Solid Elements

Figure 5.18 shows the model which was constructed for bare Structure C (Configuration 1) using solid elements in place of the previously used shell elements. The first analysis performed using this model assumed a concrete density of 2300 kg/m^3 , Poisson's ratio of 0.2 and modulus of elasticity of 41.6 kN/mm^2 , which were the same parameters used in the previous model. At the nodes corresponding to the locations of the knife-edge supports, rigid constraints were applied in the x, y and z translation directions at one end and in the y and z directions at the other end. In other words, the beam was simply supported. The first four natural frequencies obtained from this model are presented in Table 5.7, together with those calculated from the previous model using shell elements.

Table 5.7: Structure C (Configuration 1) - Comparison of Natural Frequencies from FE Model Using Shell and Solid Elements.

Mode	Natural Frequency from FE Model Using Shell Elements (Hz)	Natural Frequency from FE Model Using Solid Elements (Hz)
1 (1 st vertical bending)	4.55	4.54
2 (2 nd vertical bending)	18.25	18.05
3 (1 st torsional)	36.09	33.67
4 (3 rd vertical bending)	41.18	40.08

It can be seen that there is not much difference between the natural frequencies obtained from these two FE models, with those calculated using solid elements being just slightly lower than those calculated using shell elements. This gave the writer confidence in the development of the new updated FE model using solid elements.

Having verified the FE model with solid elements, x-direction DOF constraints were applied to both ends of the slab. This model would simulate the extreme condition where friction between the support and the slab would not be overcome and no other deformation of the slab support existed. The natural frequencies obtained from this analysis are presented in Table 5.8, together with those from the simply supported condition.

Table 5.8: Structure C (Configuration 1) - Comparison of Natural Frequencies from FE Model Using Full Translational Constraints and Simple Supports.

Mode	Natural Frequency from FE Model Using Simple Supports (Hz)	Natural Frequency from FE Model Using Full Translational Constraints (Hz)
1 (1 st vertical bending)	4.54	7.20
2 (2 nd vertical bending)	18.05	18.06
3 (1 st torsional)	33.67	33.69
4 (3 rd vertical bending)	40.08	44.63

The natural frequencies for modes 1 and 4 were clearly significantly increased, whereas those for modes 2 and 3 remained almost unchanged. The increase of the two frequencies is the result of the additional strain energy required to produce the axial deformations necessary for the structure to deform with symmetric mode shapes, as illustrated in Figure 5.19. However, it is also clear that the increases in natural frequencies calculated in this model were too high. This was probably due to the assumption of perfect horizontal restraint at the locations of the knife-edge supports. In reality, it is likely that a less than perfect restraint would exist, due to the combined effect of overcoming of friction and horizontal deformation within the supports. For these reasons, the horizontal constraints at one end of the slab were replaced with linear elastic spring elements. The model was then tuned with the results from EMA by adjusting the spring stiffnesses at the supports and the modulus of elasticity of the concrete.

An additional modification was made to the support conditions to improve further the correlation with the test data. Examination of the experimental mode shapes (Figure 5.17) shows that there was some vertical movement at the test points corresponding to the supports. It was concluded that the knife-edge supports were not perfectly stiff, as assumed when vertical pin supports are used. Therefore, linear elastic spring elements were used to represent these supports.

After a number of 'manual' iterations of parameter adjustments, the parameters which gave the best correlation with the measured natural frequencies are given in Table 5.9. The natural frequencies calculated using this model are presented in Table 5.10.

Table 5.9: Structure C (Configuration 1) - Parameters for Best Correlation Between Updated FE Model and results from EMA Using Spring Supports.

Parameter	Updated Value
Modulus of Elasticity	37.55 kN/mm ²
Horizontal Support Spring Stiffness	50 kN/mm per m width
Vertical Support Spring Stiffness	525 kN/mm per m width

Table 5.10: Structure C (Configuration 1) - Comparison of Natural Frequencies from Updated FE Model Using Spring Supports and from EMA.

Mode	Natural Frequency from Updated FE Model (Hz)	Natural Frequency from EMA (Hz)
1 (1 st vertical bending)	4.55	4.55
2 (2 nd vertical bending)	17.02	17.02
3 (1 st torsional)	29.19	26.02 or 28.92
4 (3 rd vertical bending)	37.81	37.71

5.3.2.4 Simulation of the Lack of Contact Above Test Point 9

The final step in the updating process was to attempt to simulate the lack of contact above test point 9, which was described in Section 4.5.3.7 and is shown in Figure 4.91. Of particular interest was the simulation of the splitting of the 1st torsional mode into two separate torsional modes, one with a 'rocking' motion and the other with a classical torsional motion. This was attempted using several techniques, such as removal of DOF

constraints where the lack of contact was thought to occur, and reduction of vertical support stiffness at this location.

However, it was found not to be possible to split the single torsional mode into the two separate modes that were measured using standard linear elastic FE modelling of this structure. Reduction or elimination of the vertical stiffness of the supports only resulted in the torsional mode becoming more like the rocking mode, but two torsional modes never occurred. It was therefore thought that the rocking mode was probably the result of some kind of structural non-linearity, possibly a contact effect. This conclusion was backed up by the reciprocity check performed for this mode during testing, which had indicated the likelihood of non-linear behaviour.

For this reason, it was decided only to attempt to correlate the torsional mode with the updated FE model, and to ignore the rocking mode. The lack of contact of the knife-edge support beneath test point 9 was modelled by removing the DOF constraints at the ends of the vertical and horizontal spring elements, as illustrated in Figure 5.20. The updating parameters were therefore the modulus of elasticity of the concrete, and the spring stiffnesses of both the horizontal and vertical spring supports. The final updated parameters and the natural frequencies and modal masses calculated from the updated FE model are presented in Tables 5.11 and 5.12 respectively.

Table 5.11: Structure C (Configuration 1) - Parameters for Best Correlation Between Updated FE Model Considering Lack of Contact Above Test Point 9 and results from EMA.

Parameter	Updated Value
Modulus of Elasticity	37.6 kN/mm²
Horizontal Support Spring Stiffness	70 kN/mm per m width
Vertical Support Spring Stiffness	900 kN/mm per m width

Table 5.12: Structure C (Configuration 1) - Comparison of Natural Frequencies and Modal Masses from Updated FE Model and from EMA.

Mode	Natural Frequency from EMA (Hz)	Natural Frequency from Updated FE Model (Hz)	Modal Mass from EMA (kg)	Modal Mass from Updated FE Model (kg)
1 (1 st vertical bending)	4.55	4.55	6990	6700
2 (2 nd vertical bending)	17.02	17.03	6990	6180
3 (1 st torsional)	28.92	28.62	6990	2390
4 (3 rd vertical bending)	37.71	37.67	7700	4210

The mode shapes calculated from this FE model are presented in Figure 5.21 together with the experimentally measured mode shapes for the structure. Also, the correlation measures calculated between these two sets of data are presented in Figure 5.22. It can be seen that there is an excellent correlation between the two sets of modal data. In particular, the COMAC values were very high, even for many of the support points.

A calculated point mobility FRF produced for test point 22 is presented in Figure 5.23 overlaid on the same FRF measured during the EMA. Once again, there was good correlation between the analysis and test, except for the torsional modes, which have already been discussed. Based on these results, the updated FE model was considered to be adequate for the further examination of the effects of the access floors.

5.3.2.5 Comparison with Previous FE Model Updating Exercises on Structure C

As for Structures A and B, a limited amount of FE model updating had been performed for this structure by Pavic (1999). However, as he was only concerned with the response of the structure to excitation of the first mode of vibration, he did not consider it worthwhile to examine, in detail, the effects of the support conditions and to include these in the updated FE model. Instead, he merely increased the modulus of elasticity of the concrete so that the natural frequency of the first mode of vibration would be increased to match that measured from EMA. This resulted in the natural frequencies of the higher modes of vibration being overestimated. Such an approach was deemed too inaccurate for a detailed examination of the effects of the installation of access floors on the structure, and the more detailed approach described previously was adopted.

5.3.3 Simulation of the Effects of Access Floors

The updated FE model described in Section 5.3.2 was modified to include the access floors as an added mass of 35 kg/m² applied to the whole area of the slab strip. This additional mass was based on the assumption of a 200 mm FFH and no stringers on the access floor. No other changes were made to the model. The mode shapes were the same as those presented in Figure 5.21. The natural frequencies and modal masses calculated from this analysis are presented in Table 5.13.

Table 5.13: Structure C (Configurations 2 to 13) - Natural Frequencies Calculated from the Updated FE Model with Access Floors Modelled as Added Mass Only.

FE Mode Number	Natural Frequency Including Added Mass (Hz)	Change in Natural Frequency from Updated FE Model (%)	Modal Mass Including Added Mass (kg)	Change in Modal Mass from Updated FE Model (%)
1	4.43	-2.64	7070	+5.52
2	16.58	-2.64	6520	+5.50
3	27.86	-2.66	2520	+5.44
4	36.67	-2.65	4440	+5.46

Yet again, and as expected, the analysis performed using the updated FE model, including the added mass of the access floors, predicted a more or less uniform reduction in natural frequencies (-2.6%) and an increase in modal mass (+5.5%).

The configurations of Structure C which corresponded to the assumptions of 200 mm FFH with no stringers installed were Configurations 4, 5, 8, 9, 12 and 13 (Table 4.23). Considering only the fundamental mode of vibration, the changes in natural frequencies and modal mass from Configuration 1 (i.e. the bare slab) are presented in Table 5.14.

Table 5.14: Structure C - Percentage Changes in Natural Frequencies and Modal Masses from EMA Between Configuration 1 and Configurations 4, 5, 8, 9, 12 and 13.

Floor Configuration ID	Change in 1st Natural Frequency from Configuration 1 (%)	Change in 1st Modal Mass from Configuration 1 (%)
4	-1.54	+5.72
5	-1.98	+5.44
8	-0.66	+4.86
9	-1.76	+4.58
12	-1.10	+6.58
13	-2.42	+2.86

It can be seen that, whilst the increase in modal mass was roughly in line with that predicted by the analysis, the natural frequencies did not reduce by the predicted amount (-2.6%). This supports the conclusions of the FE modelling of Structures A and B in that it appears that the access floor contributes to the stiffness of the composite concrete/access floor system. The maximum increase in stiffness, with the smallest reduction in natural frequency (-0.66%) required an increase in the bending stiffness of +4.4%. Whilst it is difficult to make direct comparisons due to the different structural configurations, this increase in stiffness is similar to that calculated on Structure A for a similar configuration of access floors (+3.6%).

Interestingly, the tests on Structure C Configurations 2 and 3, which had a 600 mm FFH access floor installed, did not support the results obtained on Structure B with a 500 mm FFH. The stiffness increase here was only +3.4% when the panels were mechanically fixed, which compares with an increase of +12% on Structure B.

Finally, the EMA had shown that Configuration 11, with bolt-on stringers installed, had actually produced an increase in the fundamental natural frequency from 4.55 Hz to 4.58 Hz. Another FE analysis was run with these access floors modelled as an added mass of 38 kg applied to the whole of the slab strip. To obtain the measured fundamental natural frequency of 4.58 Hz, it was found to be necessary to increase the bending stiffness of the slab by 8.1%.

5.4 Summary of Conclusions from FE Analysis

The FE modelling presented in this Chapter has demonstrated that the installation of access floors on the structures tested did not only increase the mass of the composite concrete/access floor systems, but also the stiffness of the floors.

The EMA results and FE modelling also showed that different configurations of access floors appeared to alter the stiffness of the composite systems by different amounts. In particular:

1. the installation of stringers on the access floors on Structure C served to increase the stiffness of the system more significantly than when stringers were not used,
2. the 500 mm FFH access floor installed on Structure B, with its panels mechanically fixed to the pedestals, provided the greatest increase in stiffness of all the floors tested, and
3. only a small minority of the access floors tested appeared to have no effect on the floor stiffness.

It was also noted that for the majority of the access floor installations, the increase in stiffness was insufficient to counteract completely the effects of the additional mass due to the mass of the access floor.

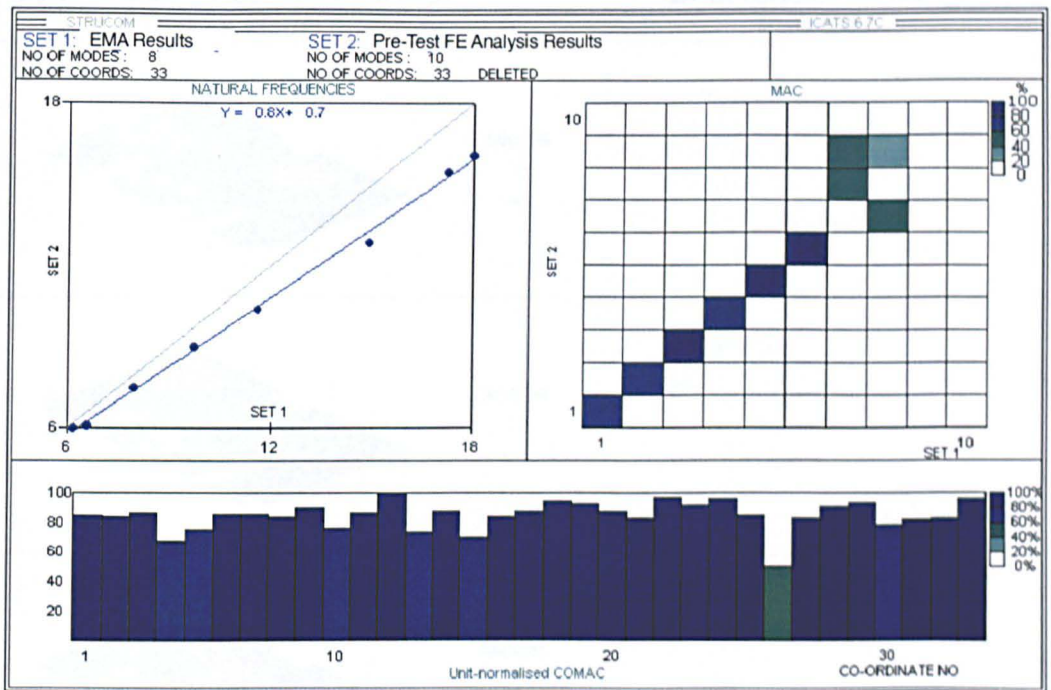


Figure 5.1: Structure A (Configuration 1) - Correlation Between Pre-Test FE Model and EMA Results.

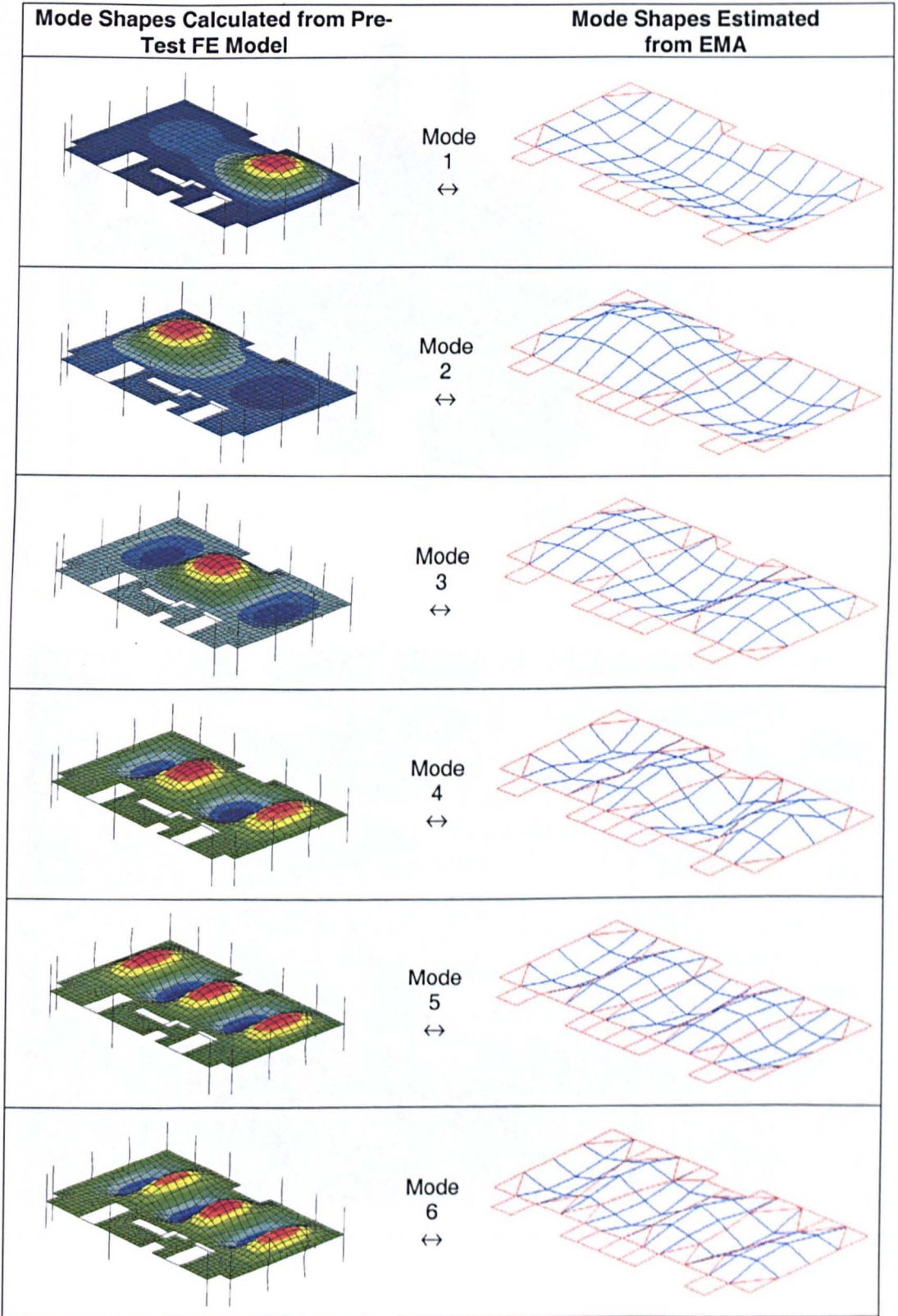


Figure 5.2: Structure A (Configuration 1) - Comparison of the First 6 Modes of the Pre-Test Model and the Results from EMA.

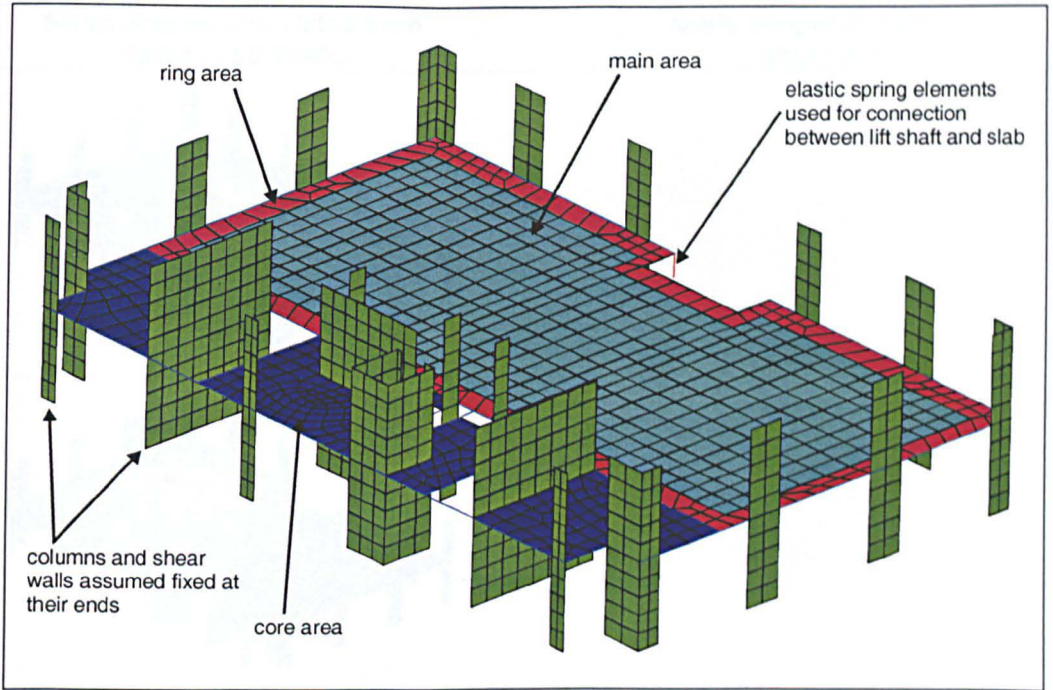


Figure 5.3: Structure A (Configuration 1) - Configuration of Updated FE Model.



Figure 5.4: Structure A (Configuration 1) - Attached Non-structural Elements.

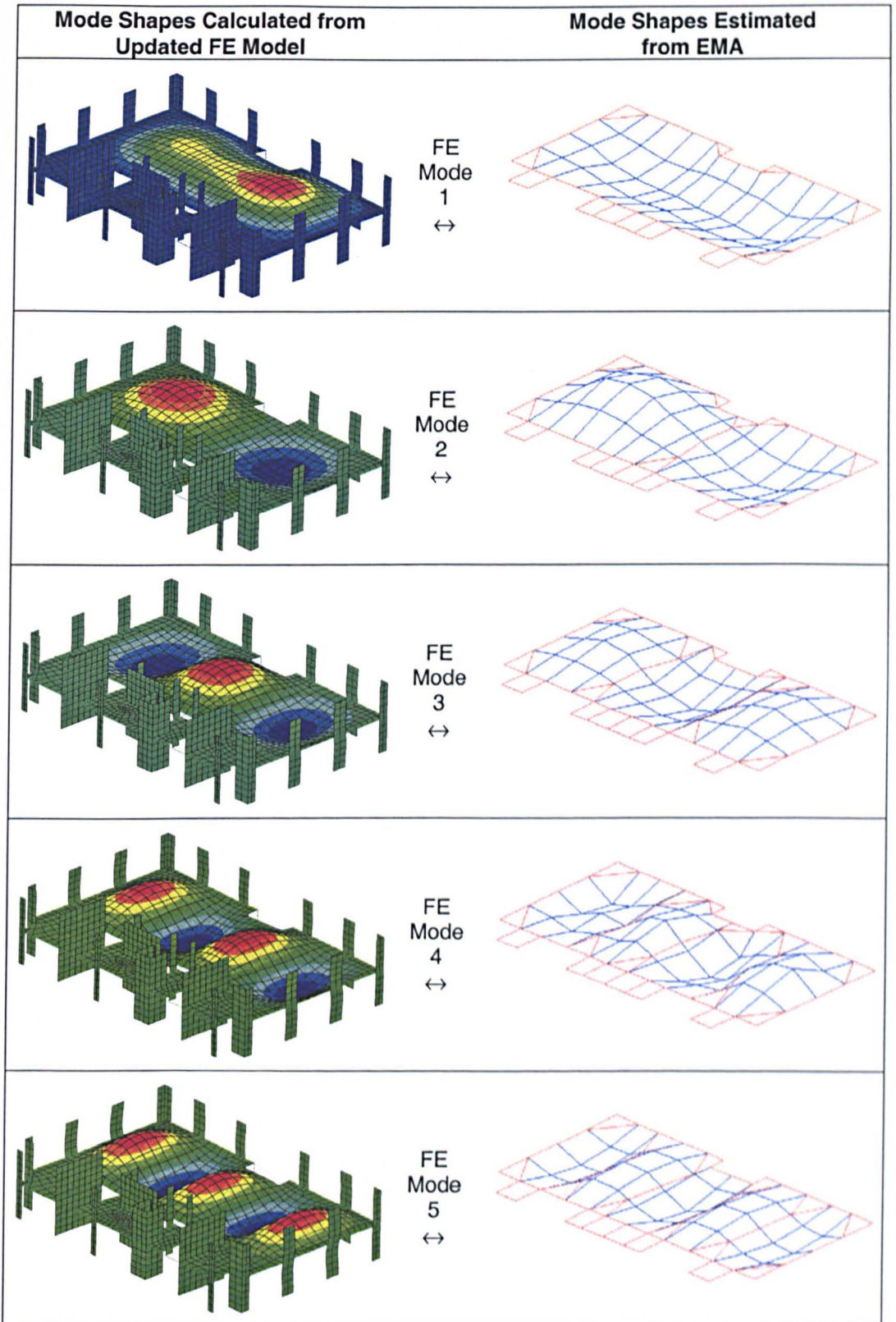


Figure 5.5: Structure A (Configuration 1) - Comparison of the First 10 Modes of the Updated FE Model and the Results from EMA. Continued Overleaf...

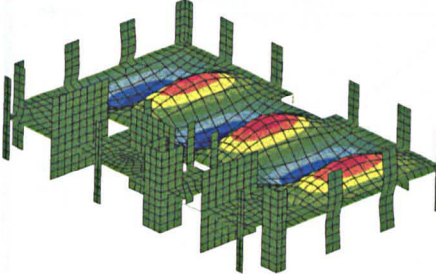
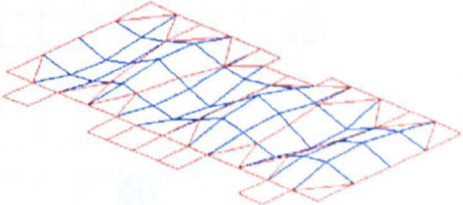
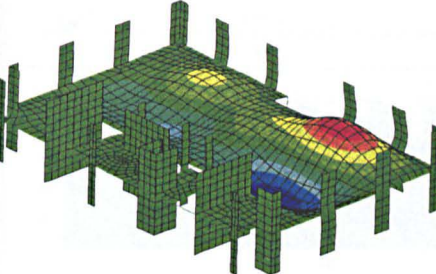
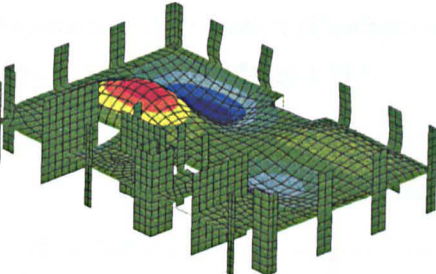
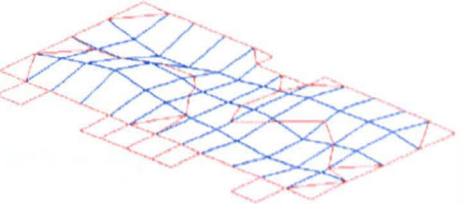
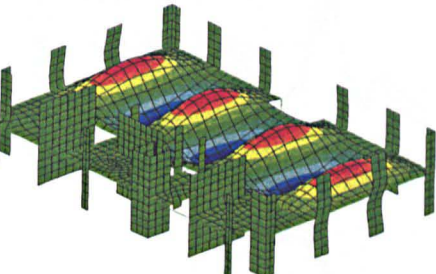
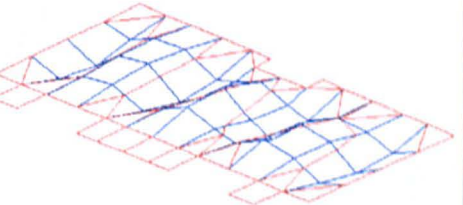
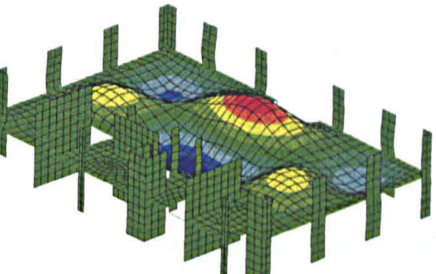
Mode Shapes Calculated from Updated FE Model	Mode Shapes Estimated from EMA
	<p data-bbox="672 267 742 390">FE Mode 6 ↔</p> 
	<p data-bbox="672 574 742 697">FE Mode 7 ↔</p> <p data-bbox="915 621 1093 652">Not Estimated.</p>
	<p data-bbox="672 880 742 1003">FE Mode 8 ↔</p> 
	<p data-bbox="672 1187 742 1310">FE Mode 9 ↔</p> 
	<p data-bbox="672 1494 742 1616">FE Mode 10 ↔</p> <p data-bbox="915 1541 1093 1571">Not Estimated.</p>

Figure 5.5 (Continued...): Structure A (Configuration 1) - Comparison of the First 10 Modes of the Updated FE Model and the Results from EMA.

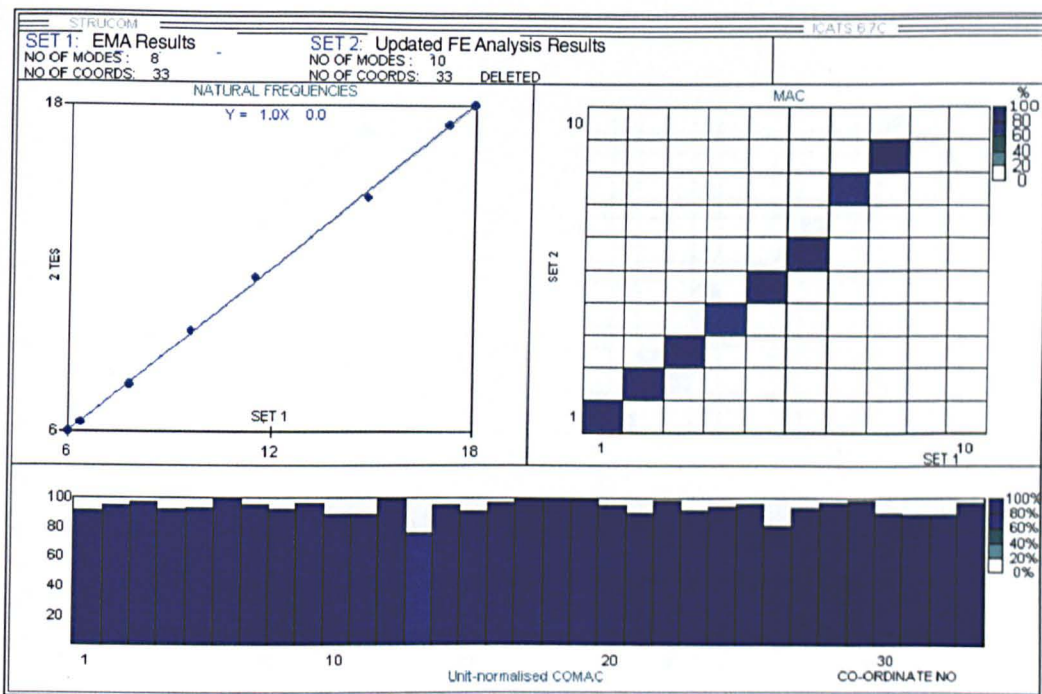


Figure 5.6: Structure A (Configuration 1) - Correlation Between the Updated FE Model and Results from EMA.

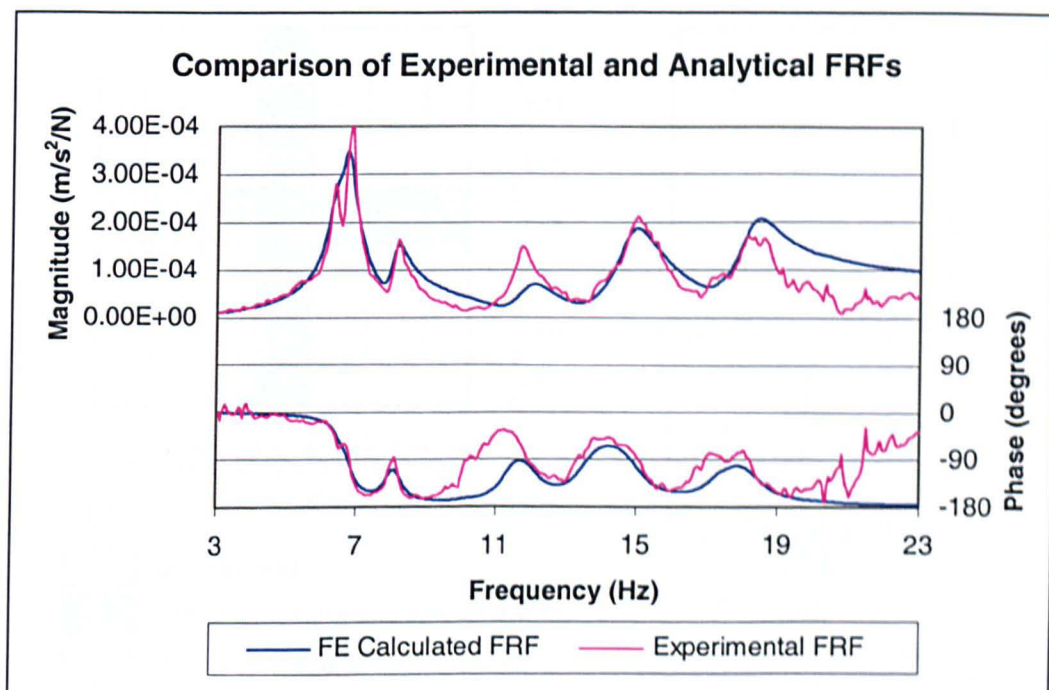


Figure 5.7: Structure A (Configuration 1) - Comparison of Experimental and Analytical FRFs.

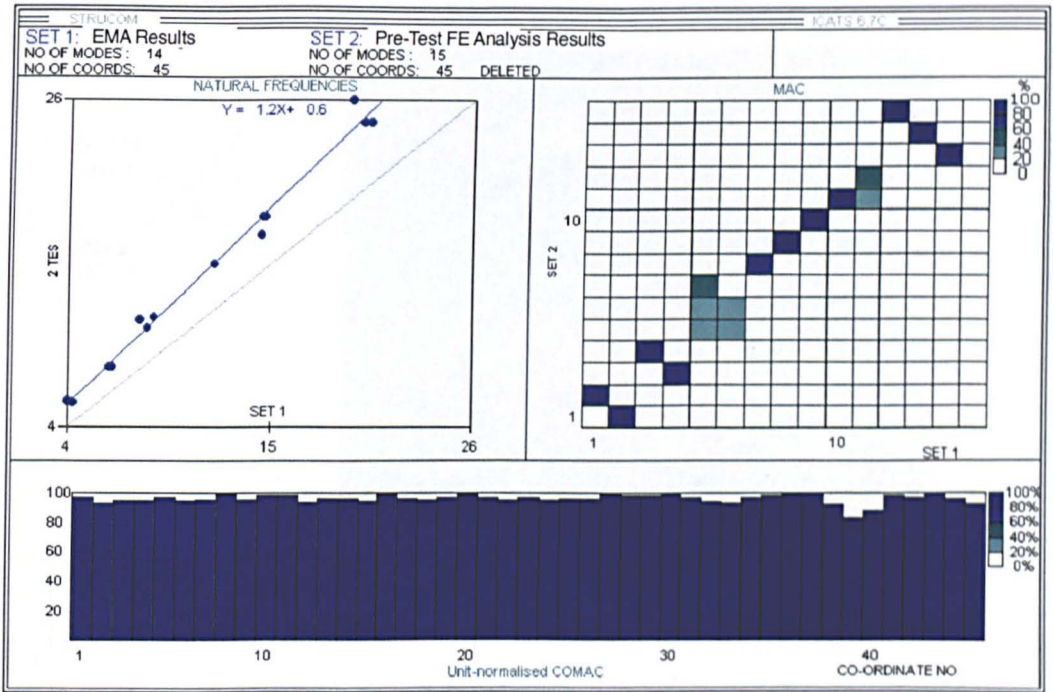


Figure 5.8: Structure B (Configuration 1) - Correlation Between Pre-Test FE Model and EMA Results.

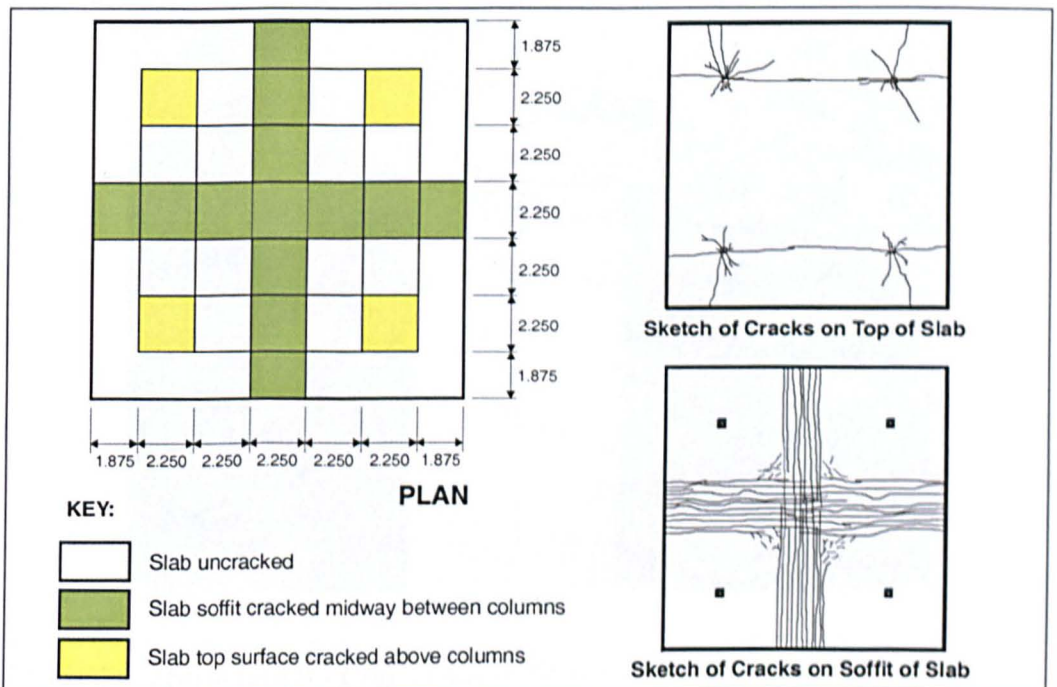


Figure 5.9: Structure B - Crack Pattern Observed During Tests and Corresponding Division of Slab into Areas for Simulation of the Effects of the Cracking.

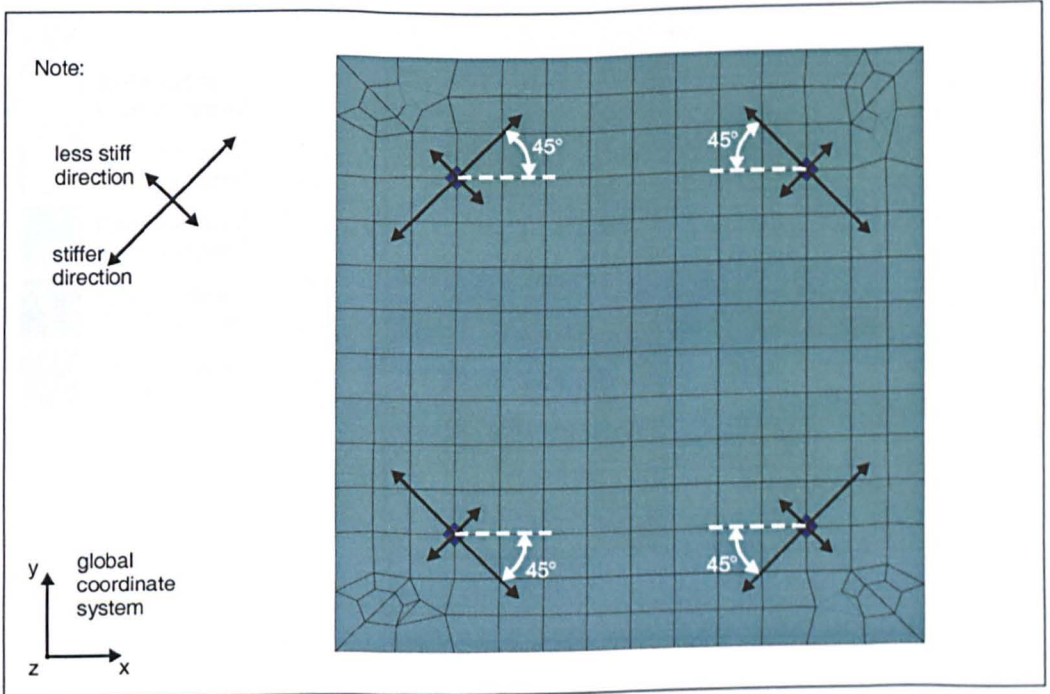


Figure 5.10: Structure B - Rotation of Columns Through 45° in FE Model.

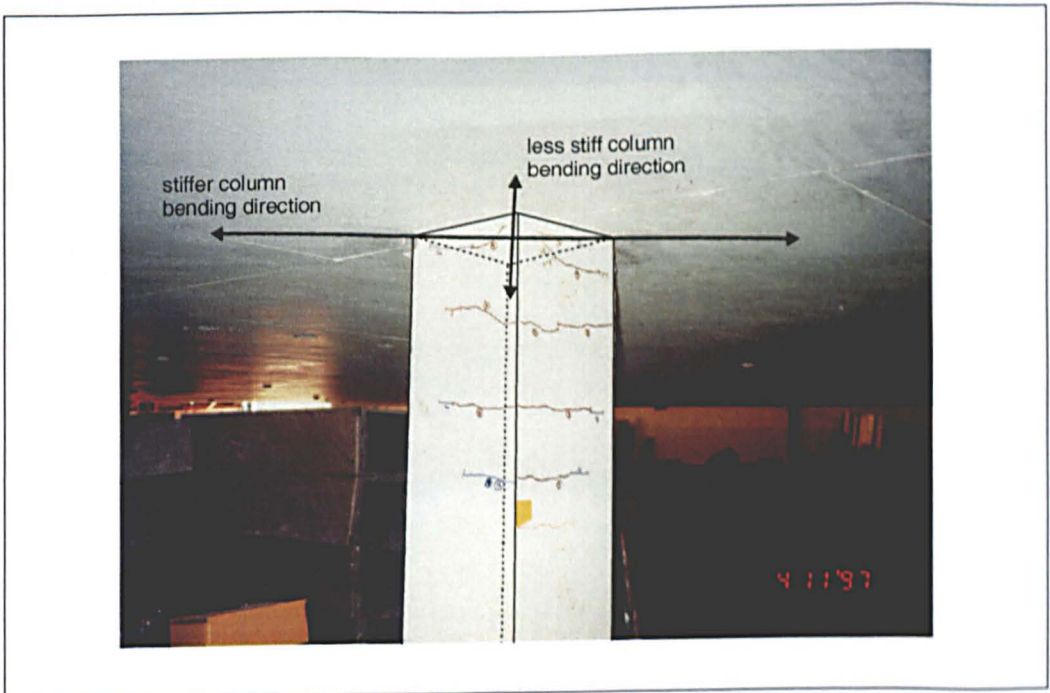


Figure 5.11: Structure B - Crack Pattern Observed on Columns.

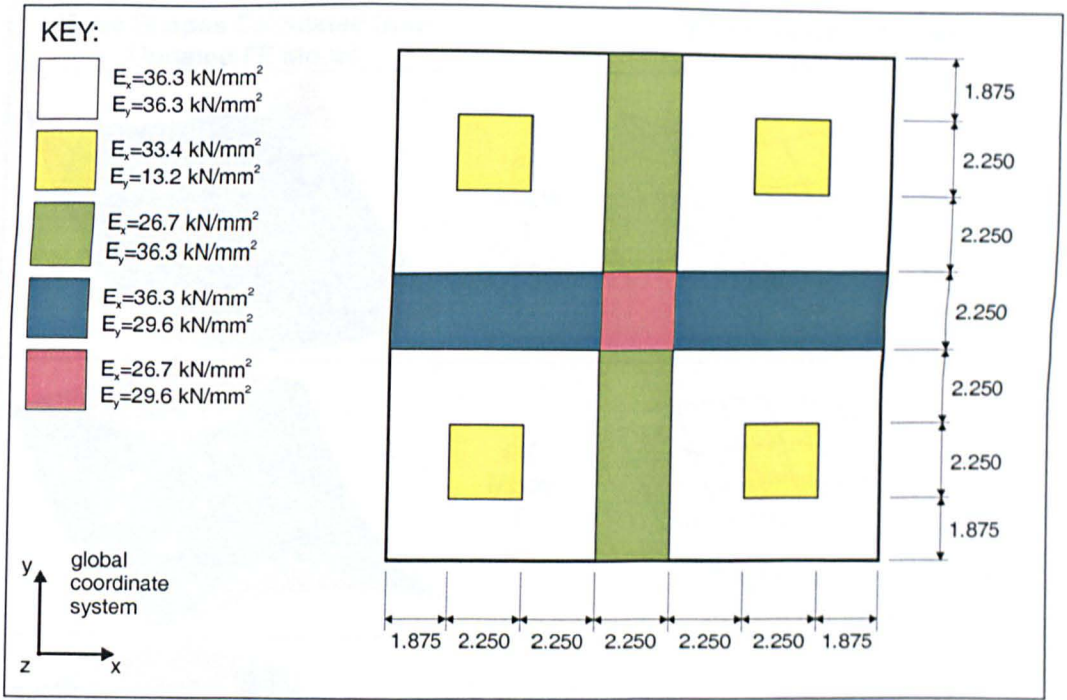


Figure 5.12: Structure B - Values of Modulus of Elasticity for Various Parts of the Structure Following FE Model Updating.

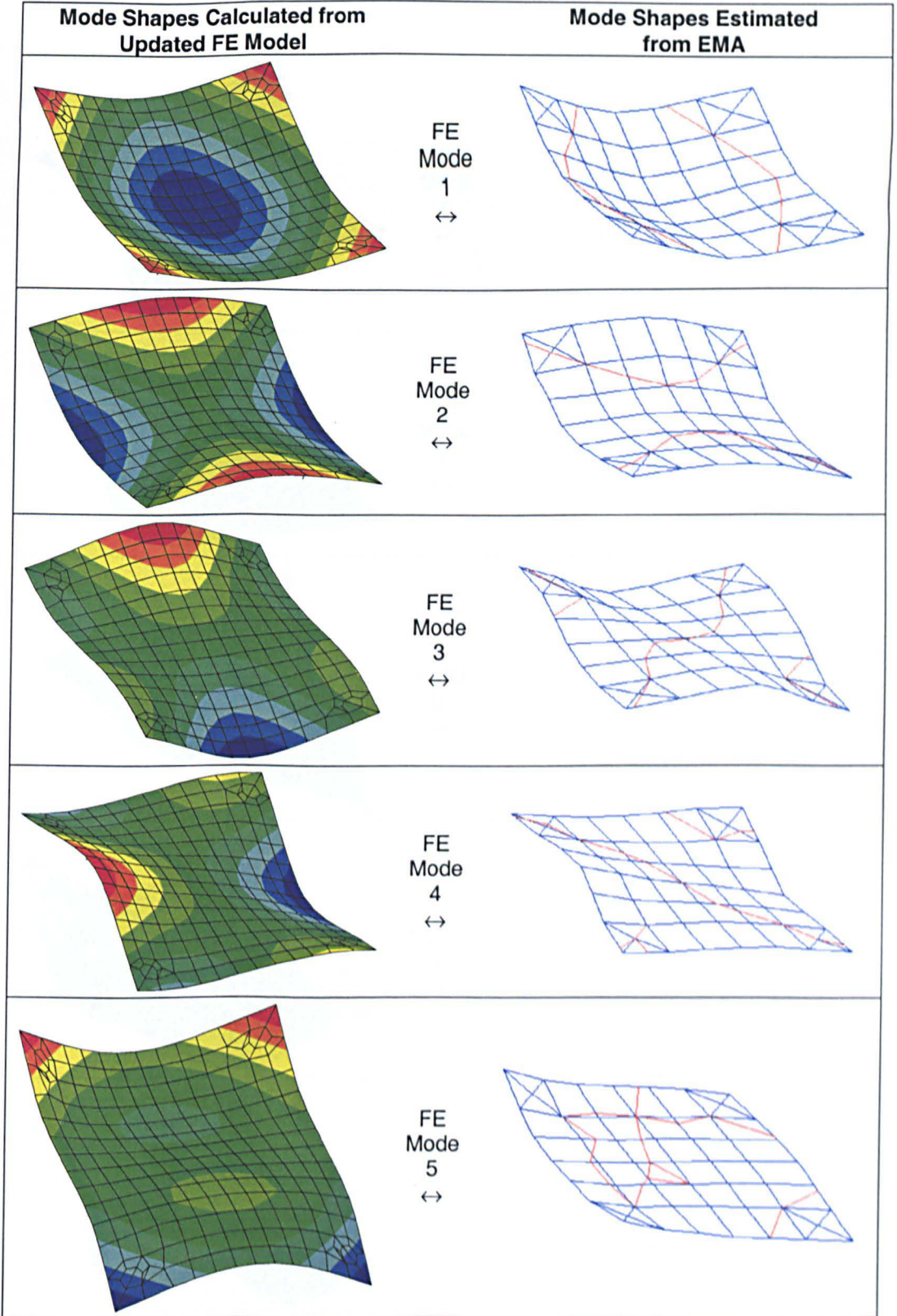


Figure 5.13: Structure B (Configuration 1) - Comparison of the First 15 Modes of the Updated FE Model and the Results from EMA. Continued Overleaf...

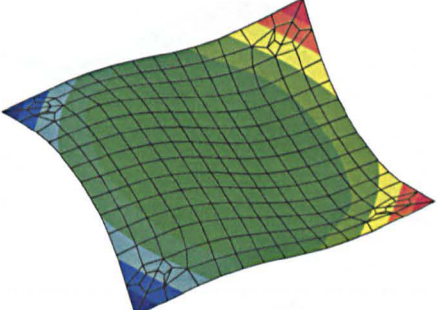
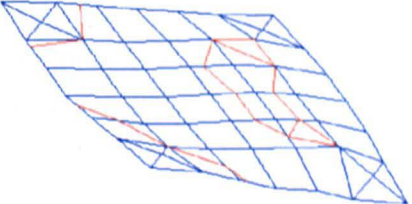
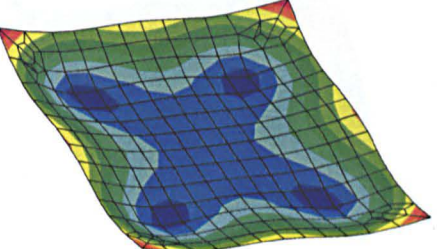
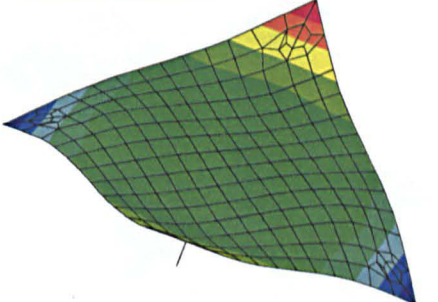
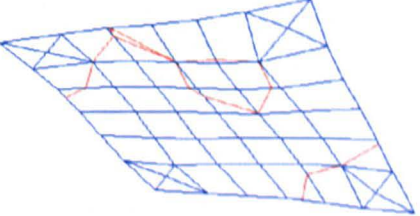
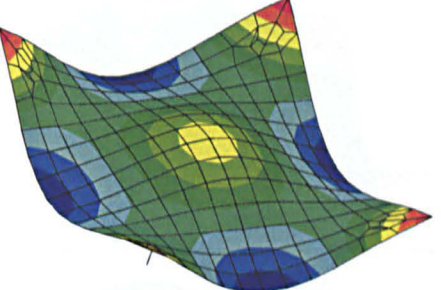
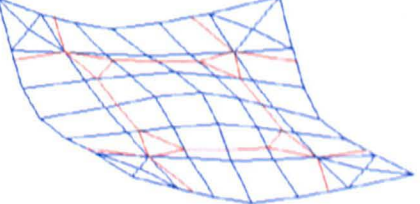
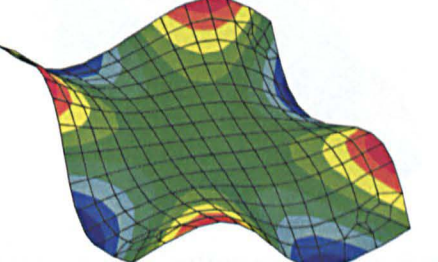
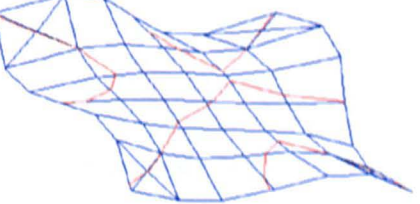
Mode Shapes Calculated from Updated FE Model	Mode Shapes Estimated from EMA
	<p data-bbox="668 290 739 404">FE Mode 6 ↔</p> 
	<p data-bbox="668 596 739 711">FE Mode 7 ↔</p> <p data-bbox="913 637 1089 670">Not Estimated.</p>
	<p data-bbox="668 891 739 1005">FE Mode 8 ↔</p> 
	<p data-bbox="668 1210 739 1324">FE Mode 9 ↔</p> 
	<p data-bbox="668 1516 739 1631">FE Mode 10 ↔</p> 

Figure 5.13 (Continued...): Structure B (Configuration 1) - Comparison of the First 15 Modes of the Updated FE Model and the Results from EMA. Continued Overleaf...

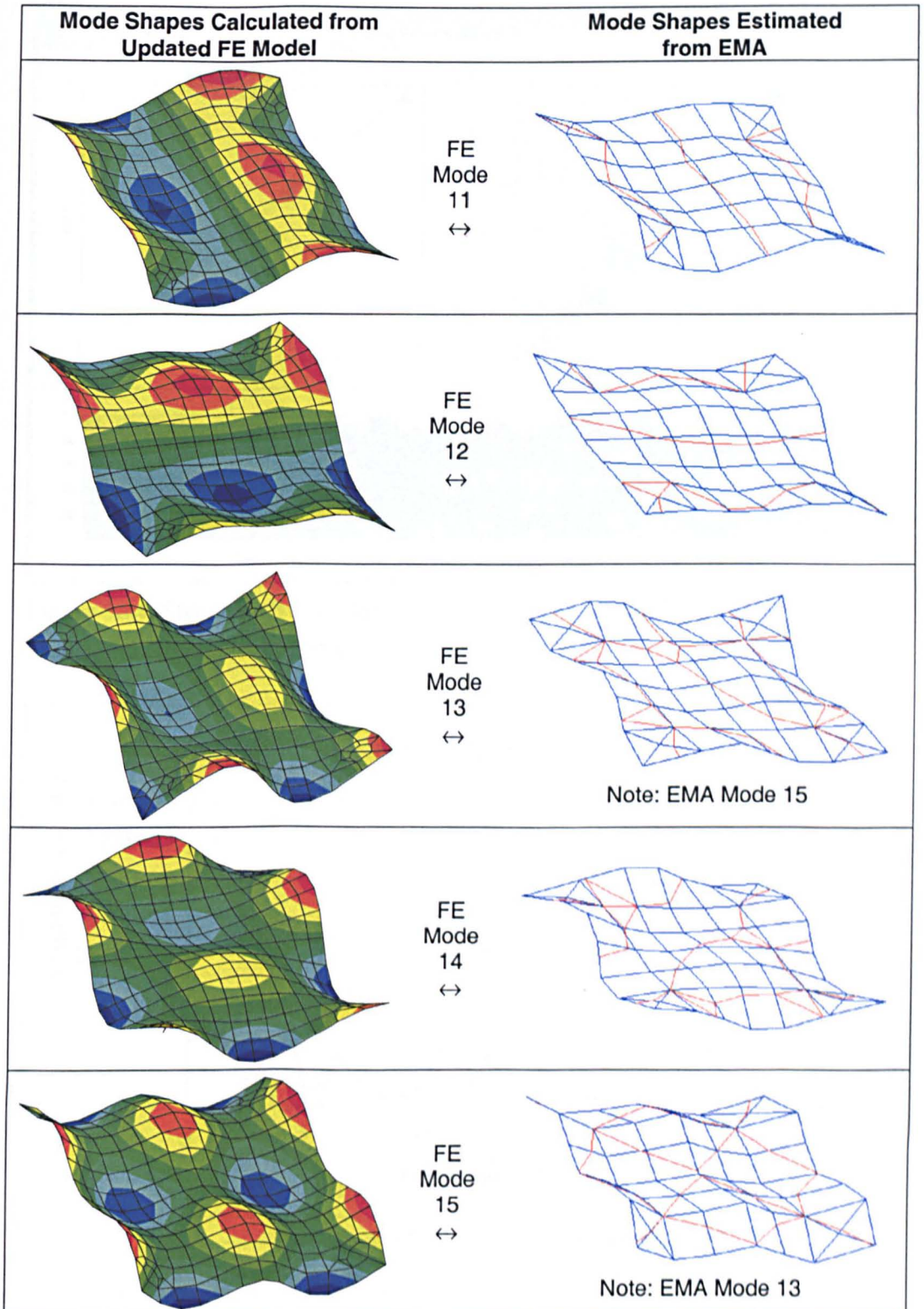


Figure 5.13 (Continued...): Structure B (Configuration 1) - Comparison of the First 15 Modes of the Updated FE Model and the Results from EMA.

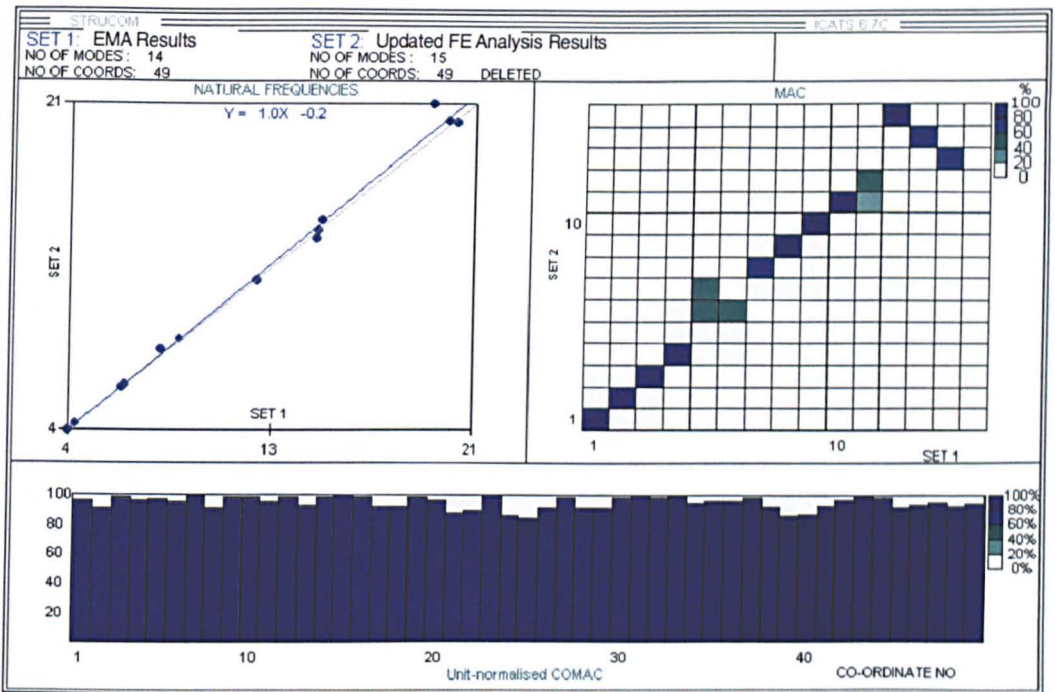


Figure 5.14: Structure B (Configuration 1) - Correlation Between the Updated FE Model and Results from EMA.

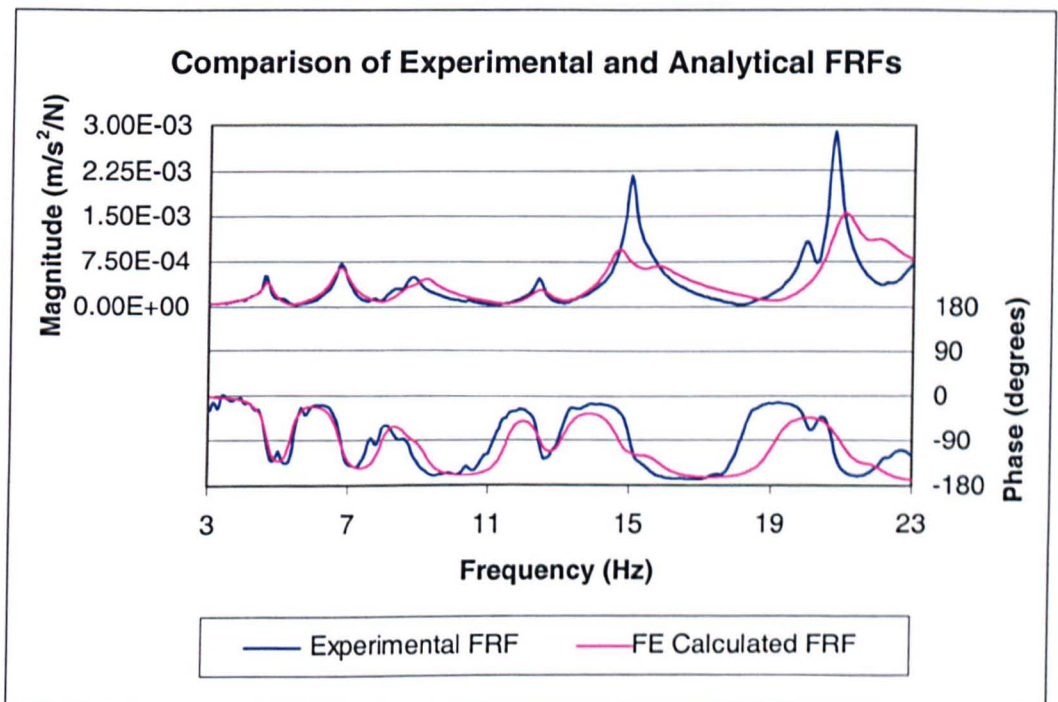


Figure 5.15: Structure B (Configuration 1) - Comparison of Experimental and Analytical FRFs.

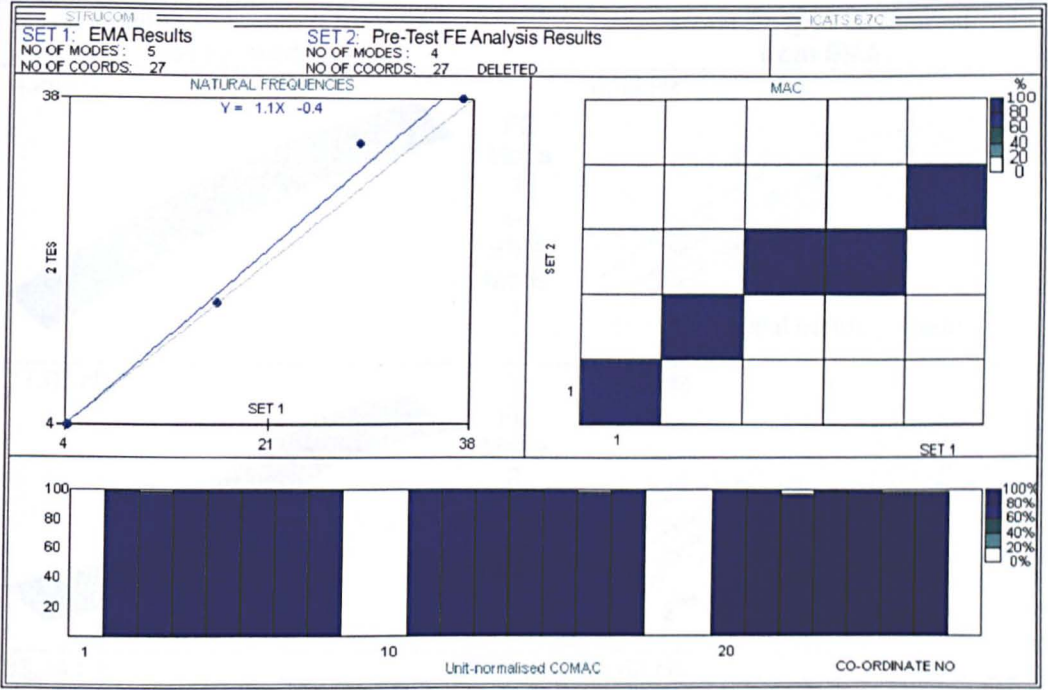


Figure 5.16: Structure C (Configuration 1) - Correlation Between Pre-Test FE Model and EMA Results.

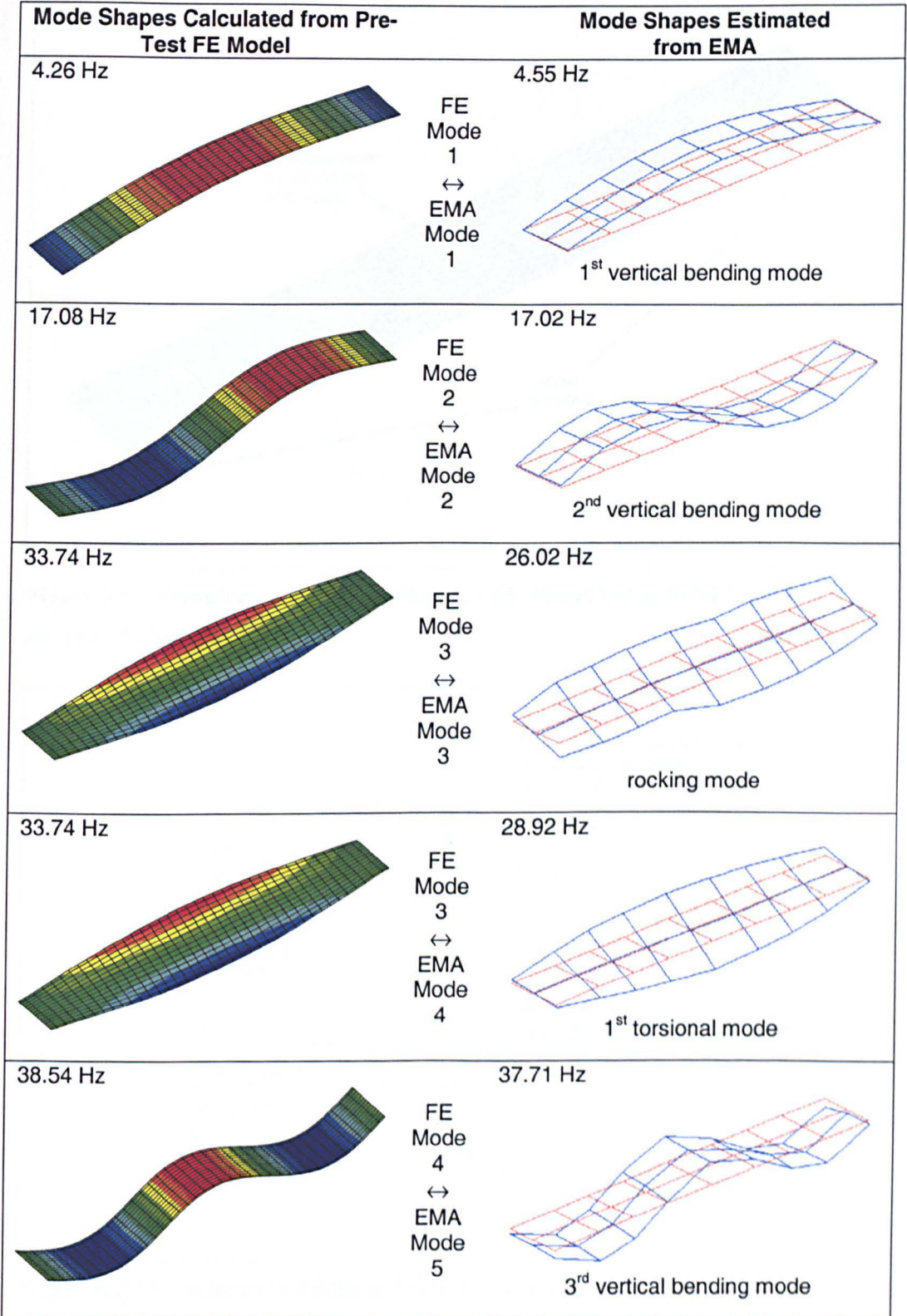


Figure 5.17: Structure C (Configuration 1) - Comparison of the First 4 Modes of the Pre-Test Model and the First 5 Modes from EMA.

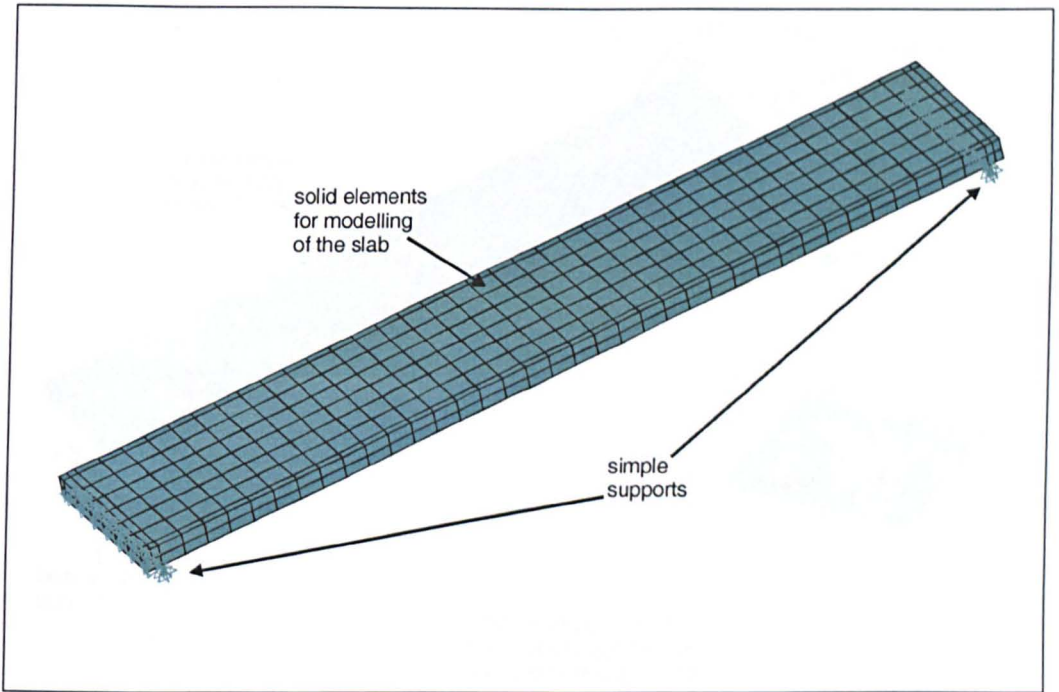


Figure 5.18: Structure C (Configuration 1) - FE Model Using Solid Elements Instead of Shell Elements.

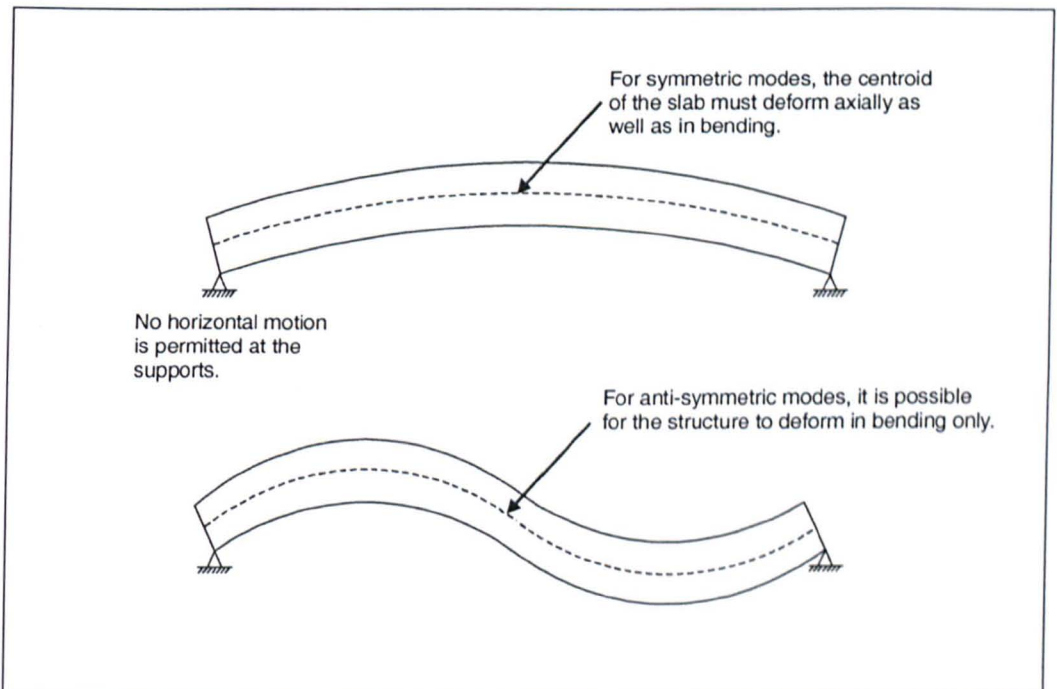


Figure 5.19: Structure C - Additional Axial Strain Caused by Friction at the Supports.

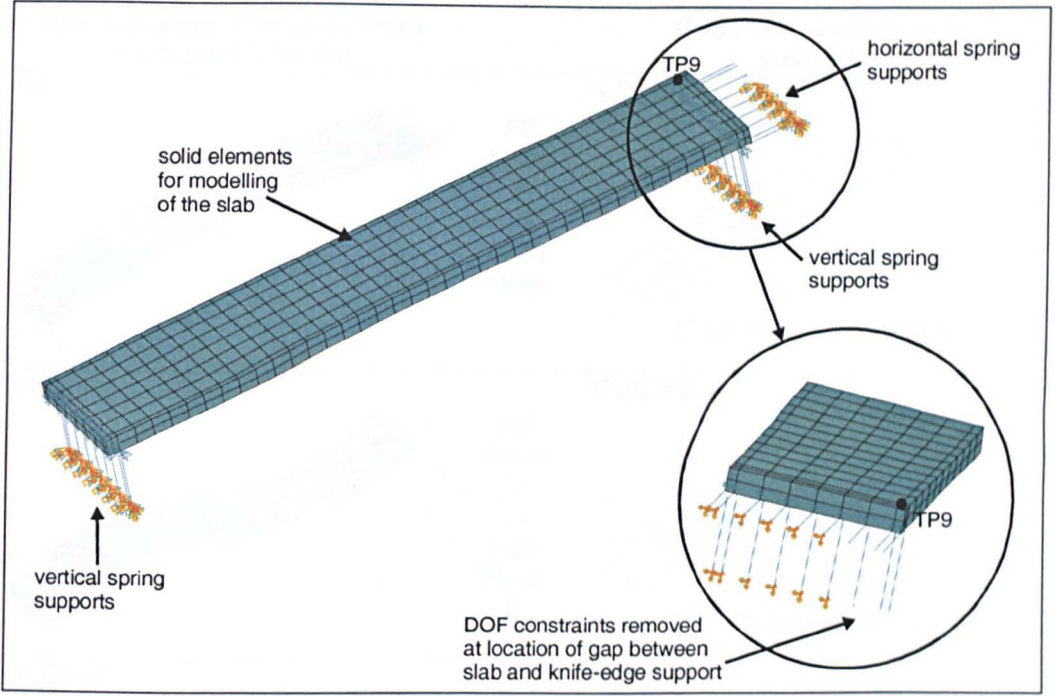


Figure 5.20: Structure C (Configuration 1) - Configuration of Updated FE Model with Vertical and Horizontal Spring Supports Removed at Point of Lack of Contact.

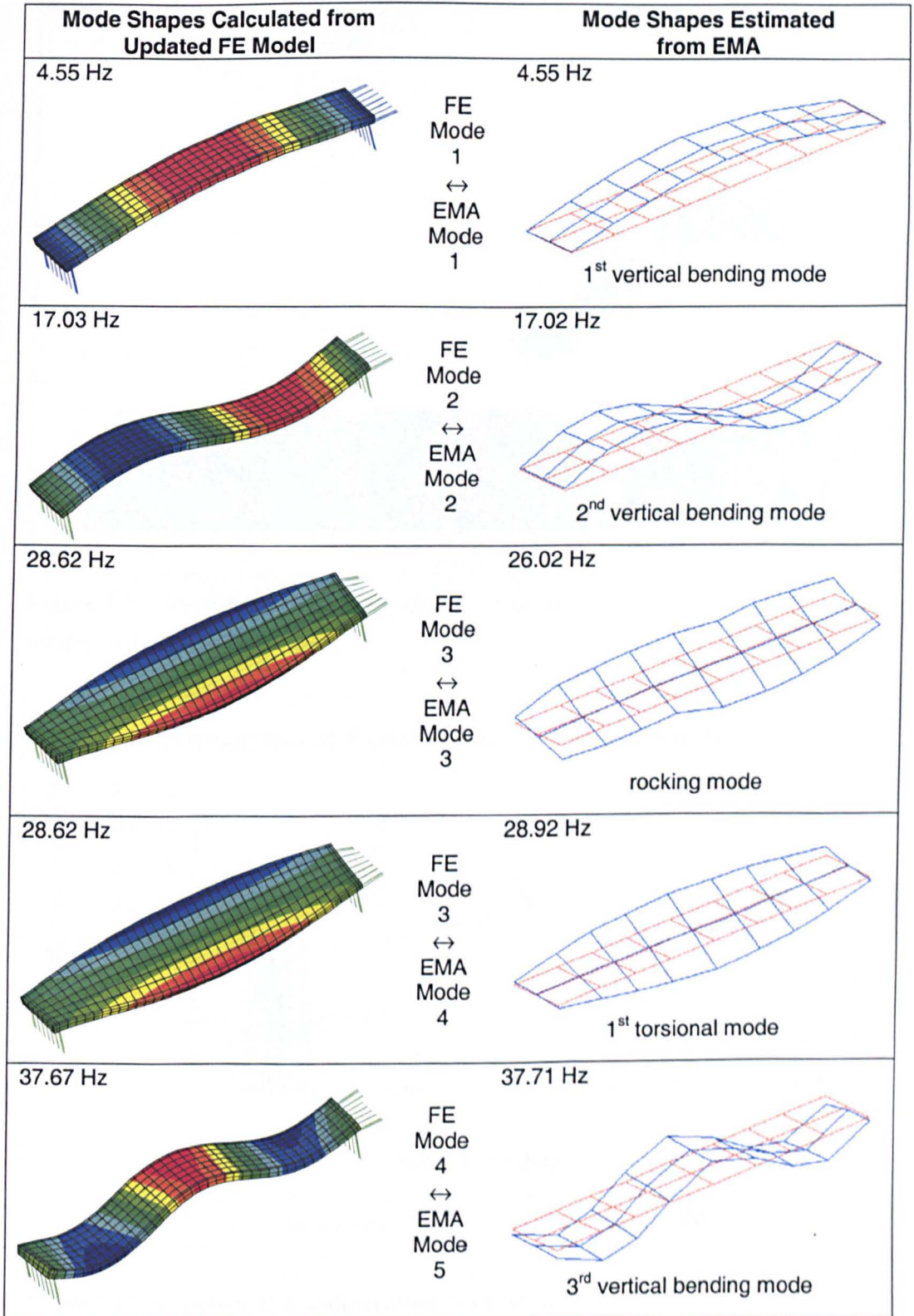


Figure 5.21: Structure C (Configuration 1) - Comparison of the First 4 Modes of the Updated Model and the First 5 Modes from EMA.

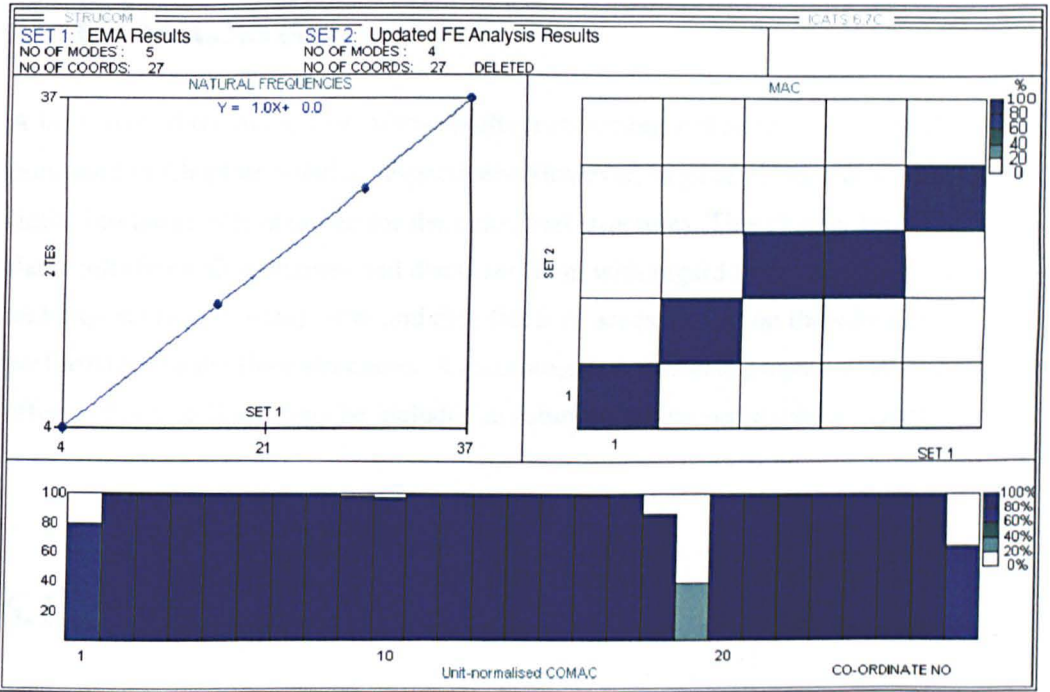


Figure 5.22: Structure C (Configuration 1) - Correlation Between the Updated FE Model and Results from EMA.

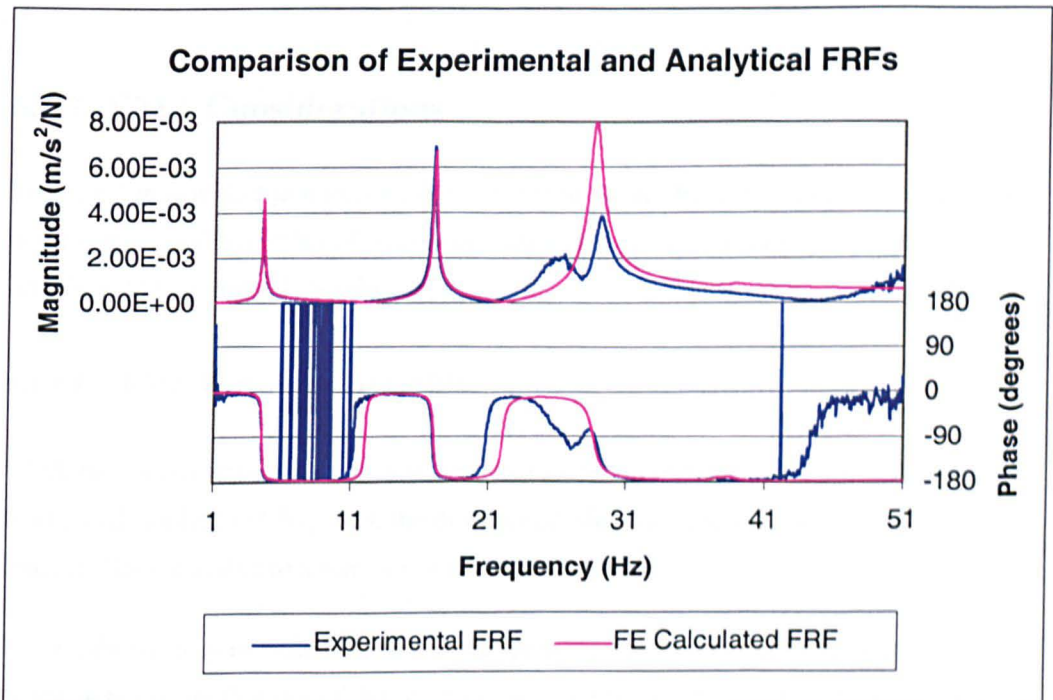


Figure 5.23: Structure C (Configuration 1) - Comparison of Experimental and Analytical FRFs.

6 Discussion

A large part of the discussion of the results from testing and analysis has already been presented in Chapters 4 and 5, respectively. However, in general, such discussion was limited to the results obtained for the individual structures. This chapter brings together the results from all structures and discusses them with regard to the experimental techniques utilised in this work and the effects of access floors on the vibration performance of the floor structures. A recommendation is also proposed for how the effects of access floors may be included in future vibration serviceability analyses.

6.1 Experimental Work Considerations

Through the course of the work presented in this thesis, a number of experimental facilities and procedures were developed. A summarised discussion of the most useful and successfully applied features of this new system will be given here.

6.1.1 EMA Considerations

The development and practical experience of the shaker EMA techniques used in this work highlighted a number of issues regarding how such techniques may best be implemented on large floor structures.

6.1.1.1 EMA Techniques Available

Of all the modal test excitation functions that were implemented and utilised in this work, as described in Chapter 3, the most successful was found to be band-limited burst random. This was due to a number of reasons.

Firstly, due to way in which the signal was generated, it was found to be more convenient on site that use of the burst swept sine excitation. More importantly, it was found that FRFs measured using burst random excitation were not adversely affected by the application of an exponential window. This is in contrast with the FRFs measured using burst swept sine excitation, which were adversely affected by the exponential windowing, as described in Section 4.2.6.2.

The application of burst random excitation, being a broadband excitation technique, was found to be much faster than using the stepped sine excitation, as expected. Moreover, the two main advantages of using stepped sine excitation are for the examination of non-linear behaviour and to enable the maximum excitation energy for the shaker to be applied to the structure. However, for the structures tested in this work, it was found that the shaker provided adequate excitation without having to resort to stepped sine excitation. Also, examination of the degree of non-linearity of Structure C, presented in Figure 4.88, revealed only very small changes with four excitation levels, where the highest level was four times greater than the lowest level. It is likely that similar insignificant non-linear effects would be measured on other floor structures undergoing EMA, because of the very low levels of excitation.

6.1.1.2 Practicalities of Performing EMA on Floors with Access Floors

As described in Chapter 4, problems were encountered when testing floors with access floors installed, due to local vibrations within the access floor system. Examination of the FRF data measured with the shaker and accelerometers positioned on the access floor and the sub-floor (Figure 4.49) revealed that the best data were acquired when they were positioned on the sub-floor. However, to save time on site, it was also found that positioning the shaker on the top surface of an access floor above a pedestal also gave good results. Positioning the shaker on top of an access floor away from a pedestal location was found to give quite poor EMA data, probably as a result of local deformations of the access floor system.

Therefore, it is recommended when testing future structures with access floors installed that, whenever possible, access floor panels should be removed and the excitation devices and response transducers should be located on the sub-floor. However, when time on site is limited, reasonable EMA data may be acquired by positioning the shaker (in the case of roving excitation) or the response transducer (in the case of roving response) on the surface of the access floor above a pedestal location. Positioning both the exciter and the response transducers on the access floor is not recommended.

6.1.2 Pedestrian Response Testing Considerations

6.1.2.1 Practicalities of Performing Tests on Floors with Access Floors

When performing pedestrian response tests on the floors with access floors, it was found that the response transducers located on the top of the access floors were frequently over-ranged by local high frequency accelerations within the access floor system. To eliminate this problem, similar to the FRF measurements, it is recommended that accelerometers should always be located on the sub-floor. The pedestrians in these tests may then walk on the access floors.

This advice seemingly contradicts that given in BS 6472 (1992) which suggests that measurements should be made at the “point of entry of vibration to the body”. In the case of a floor with an access floor installed, this would appear to suggest that measurements should be made on top of the access floor. However, in addition to the problems of the over-ranging of the response transducers due to high frequency vibrations, it is possible that measuring accelerations on top of access floors when a human being is not present may actually give a false assessment of the vibration to which a human body at the same location may experience. This is because the additional mass and damping of the human body would undoubtedly change the vibration characteristics of the access floor system in the vicinity.

This phenomenon was not examined in this work as the testing was aimed towards examining the global behaviour of the floors, rather than local effects. However, it is recommended that this effect is examined in more detail, since it may provide some more insight into why floors with access floors installed are commonly subjectively perceived to have improved vibration characteristics.

6.1.2.2 Selection of Vibration Response Assessment Parameter

The results of the vibration response tests, presented in Chapter 4, were given in terms of three different vibration response assessment parameters. These were:

1. RMS of the entire record,
2. peak running RMS with 10 s integration time, and
3. VDV assuming 8 h continuous exposure.

These assessment response parameters were described in more detail in Section 3.7.2.

Considering firstly the RMS for the entire record and the VDV assuming 8 h exposure time (which was also evaluated over the entire record), for all three structures, these two vibration assessment parameters gave proportionally very similar results (Tables 4.14 and 4.22, and Figures 4.93, 4.95, 4.96 and 4.98). In particular, the percentage changes in the response parameters, following the installation of the various systems of access floors, were very close.

This behaviour is expected for 'well-behaved' response signals in which the crest factor is below a value of about 6 (Griffin, 1996). This was determined to be the case for the majority of the vibration response signals analysed in this work. In fact, the VDV may be estimated from the measured RMS acceleration using the equation (BSI, 1992):

$$eVDV = 1.4a_{rms} t^{1/4} \quad \text{Equation 6.1}$$

where eVDV is known as the "estimated vibration dose value". The importance of this observation is in the way in which these parameters may be utilised in a vibration serviceability assessment of a structure.

The RMS accelerations in this work were calculated for a measured time history in which a pedestrian was exciting the structure with a pacing rate designed to produce the maximum possible response. To then use this RMS acceleration for a vibration serviceability assessment, it is necessary to assume that this vibration occurs continuously for comparison with vibration limits which are presented simply as threshold values for RMS acceleration. Obviously, typical office floors are unlikely to be subjected to this continuous excitation and, in reality, the most onerous realistic case is of a pedestrian traversing a floor with a repeat period dependent upon how busy the office floor is likely to be in normal use. Assessment of vibration using RMS accelerations cannot take account of this phenomenon.

However, VDV (and eVDV), by definition, represent a cumulative effect of vibration and are time dependant. The VDV results presented in this work were calculated on the assumption of continuous vibration for an 8 hour period. However, it is possible to take account of the intermittent nature of normal pedestrian excitation by adjusting the exposure time to a value which is more realistic. For example, if it takes a pedestrian 10 seconds to traverse a floor, and it is assumed that a likely repeat period in normal use is 1 minute, then the exposure time may be reduced by a factor of 10/60 (i.e. for an occupant who is on the floor for an assumed 8 hours, the actual equivalent non-stop exposure time would be $8/6 = 1.333$ hours). Since VDV is proportional to the fourth root

of the exposure time, it would be reduced by a factor of 0.639 using these assumptions, giving probably a more realistic assessment of the actual vibration conditions. Unfortunately, reliable data regarding vibration limits in terms of VDV are currently quite scarce and it appears that more research into such vibration limits is required.

An unfortunate consequence of assessing RMS acceleration from a complete time history is that it may be sensitive to the data acquisition duration and/or start-up or finishing transients. Because of this, Eriksson (1994) suggested that RMS accelerations should be assessed using a finite duration integration time of 10 s, and this should be adopted by the civil vibration engineering community as a standard. This technique also has the advantage that it represents the best possible attempt for a pedestrian to excite the floor. By using a standard integration time, Eriksson suggested that all future pedestrian response test results would be comparable and that this data would enable more satisfactory vibration limits to be specified. This call for standardisation was later reiterated by Pavic (1999) who used 10 s integration time in all RMS acceleration calculations presented in his doctoral thesis.

The results of the response tests performed in this work were also presented in terms of this standard assessment parameter in Chapter 4. These results showed that the running RMS values with 10 s integration time were found to be slightly higher than those values calculated for the entire record, as expected. However, the relative differences between the different tests appeared to be consistent with those calculated using the RMS accelerations of the entire records. It would therefore seem that the use of the 10 s integration time is likely to be consistent with other assessment parameters for similar floor structures, and the writer also recommends it in the interests of standardisation.

A typical vibration response assessment procedure of an existing floor structure would then be:

1. perform modal testing to establish natural frequencies and mode shapes and hence determine the most onerous pacing rates and walking paths,
2. measure the vibration response of the structure caused by pedestrian excitation for a duration considered appropriate by the test personnel (a minimum of 2 minutes is recommended by the writer),
3. perform frequency weighting on the measured time histories and calculate the peak running RMS value using a 10 s integration time,
4. calculate the eVDV using Equation 6.1 using an appropriate vibration exposure duration, and

5. compare the calculated eVDV value with pre-specified limits.

6.2 The Effects of Access Floors on the Vibration Performance of Long Span Concrete Floors

Chapters 4 and 5 presented respectively the experimental and analytical work applied to Structures A, B and C. This section seeks to bring together the results from the individual structures, and discuss them on the basis of all available data.

6.2.1 Changes in Estimated Modal Parameters

Drawing conclusions regarding the effects of access floors on the modal properties of the long span concrete floors on which they were installed was one of the aims of this work. If there were consistent changes to the modal properties, it would be possible to include such effects in future analytical models of the structures, and hence improve analytical vibration serviceability predictions.

6.2.1.1 Changes in Natural Frequencies

The EMA results for all of the structures presented in Chapter 4 (Table 4.12, Table 4.18 and Figure 4.89) indicated that for almost all configurations of access floors and individual modes of vibration, the natural frequencies reduced following the installation of the access floor. This indicated that the increased mass of the floor system due to the addition of the access floor had a more significant effect than any increase in stiffness. However, by modelling the access floors as increased mass on updated FE models of the bare floor structures, it was shown that the reductions in natural frequencies were normally not as much as would be expected if the access floors really were acting as added mass only. This indicated that the access floors were increasing the stiffness of the floor systems to some extent (up to +3.6% for Structure A, up to +12% for Structure B and up to +8.1% for Structure C).

Unfortunately, it was found that the increases in stiffness were not uniform for all modes of vibration of each particular structure. For example, for Structure A the +3.6% increase in stiffness was only applicable to the 4th mode of vibration. Other modes of

vibration exhibited smaller increases in stiffness and the 6th mode of vibration did not exhibit any increase in stiffness at all (i.e. the access floor was acting purely as added mass in this mode). Similar results were obtained for Structures B and C for most configurations of access floors. To complicate matters further, this phenomenon appeared to occur without any discernible pattern. This makes the prediction of the increase in stiffness following the installation of access floors practically impossible, bearing in mind the data obtained in this work.

6.2.1.2 Changes in Modal Damping Ratios

Similar observations were made regarding the changes in the estimated modal damping ratios as for the estimated natural frequencies. For all structures, it was noted that some modes exhibited an increase in modal damping, whereas other modes exhibited no increase or even a reduction in modal damping (Table 4.12, Table 4.18 and Figure 4.90). Again, this appeared to happen in a rather random fashion, precluding the possibility for predictive methods to be developed for future access floor installations.

An exception to this was observed for access floors with a relatively high FFH. Floors which came into this category were Structure B (Configurations 2 and 3) with an FFH of 500 mm and Structure C (Configurations 2 and 3) with an FFH of 600 mm. These access floors appeared to increase the modal damping ratios of the floors on which they were installed more consistently than the floors with lower FFHs (150 mm and 200 mm FFH).

6.2.2 Changes in Measured Vibration Response to Pedestrian Excitation

At first glance, the conclusions drawn in Section 6.2.1, regarding changes in modal properties caused by the installation of access floors, would seem to eliminate the possibility for analytical modelling of the beneficial effects of access floors with regards to vibration serviceability. Indeed, if the natural frequencies changed by only a small amount and the modal damping ratios were assumed to be unchanged, then reductions in response to pedestrian excitation would be predicted not to occur.

However, exactly the opposite was observed from the results of the pedestrian response measurements. Overall, all structures exhibited a reduction in response to controlled pedestrian excitation following the installation of the various configurations of access

floors. Taking the rather crude instrument of simple arithmetic averages of the reductions measured for all configurations of access floors and all tests for each structure, it was found that the vibration response to pedestrian excitation reduced by 16% for Structure A, by 33% for Structure B and by 13% for Structure C.

It is clear that some mechanism for dissipating excitation energy was being engaged in the tests performed using pedestrian excitation, which was not being engaged in the modal testing. This mechanism has not been positively identified in this research, but the writer speculates that this was caused by footfalls, which when applied directly to the panels of the access floor systems, were causing the panels to deflect locally (i.e. between pedestal supports). This effect may have engaged one or more local damping mechanisms, such as material damping within the panels and friction at the connections between the panels and the pedestals. However, on the basis of the work presented in this thesis, there is insufficient evidence to confirm this speculation. It is therefore recommended that further research is performed to confirm or disprove this hypothesis.

6.2.3 Influence of Access Floor Configuration

One of the objectives of the research was to determine which characteristics of access floors had most influence on the vibration serviceability of the floor on which they were installed. This was the reason for the testing of multiple configurations of access floors on both Structures B and C. It was not possible to perform such testing on Structure A due to the commercial nature of that building. Structure C, with 13 different configurations of access floors, was anticipated to provide the most detailed information in this regard.

Unfortunately, both the EMA results and the pedestrian response data for Structure C, presented in Figures 4.89 to 4.98, failed to provide conclusive evidence regarding precise effects of each individual configuration of access floors. However, three access floor configuration aspects were identified which appeared to have the most significant effect on the vibration behaviour of the structures. These were:

1. the finished floor height,
2. the mechanical fixing of panels to the pedestals, and
3. the presence of stringers.

6.2.3.1 Influence of the Finished Floor Height

It was already noted in Section 6.2.1.2 that relatively high FFH access floors appeared to increase the damping of the floor system more than relatively low access floors. It was also noted, through examination of the pedestrian response data for all structures, that the relatively high FFH access floors had the ability to reduce the response to pedestrian excitation to a greater extent than the relatively low FFH access floors.

Consider first the pedestrian response test results from Structures A and B. For structure A, with a 150 mm FFH access floor, the reduction in response averaged over all tests was 16%. Structure B, with a higher access floor FFH of 500 mm, exhibited on average a 33% reduction in response following the installation of the access floor.

Comparing the results of the pedestrian response measurements on Structures A and B may be misleading since the installed access floors were provided by different manufacturers. However, the results from Structure C, measured using high and low FFH access floors from the same manufacturer, appeared to support the observation of greater reductions in response for larger FFH access floors. Taking an average of all pedestrian response measurements made on Configurations 2 and 3 of Structure C, with 600 mm FFH access floors installed, it was found that the reduction in response following the installation of the access floors was 25%. This compares with 11% average reduction in response measured for Configurations 4 to 13 of Structure C, with 200 mm FFH access floors installed.

6.2.3.2 Influence of the Mechanical Fixing of Panels to Pedestals

On Structures B and C, tests were performed to compare identical access floor installations where the only difference was whether or not the access floor panels were mechanically fixed to the pedestals. Examination of the EMA results in Table 4.18 and Figure 4.89 indicated that for almost every access floor configuration, the mechanical fixing of the panels to the pedestals increased the natural frequency (and therefore stiffness) of the floor system. However, although an interesting and consistent observation, the changes in natural frequency were typically very small (less than 0.5%) and hence this characteristic is unlikely to be of any practical value.

The effects of the mechanical fixing of panels to pedestals could also be seen quite consistently in the results of the pedestrian response tests on Structures B and C. For Structure C, the results of the pedestrian response tests, which excited the fundamental

mode using the 2nd harmonic of walking (Figures 4.93 to 4.95), showed a greater reduction in response for every test in which the access floor panels were loose-laid compared with those when the panels were mechanically fixed. On the other hand, the pedestrian response test results from Structure B showed a greater reduction in response when the panels of that floor were mechanically fixed.

It is postulated by the writer that this seemingly contradictory behaviour was a result of the different access floor systems that were used in the testing. It is possible that for Structure B, with what was considered by the writer to be a relatively weak panel/pedestal connection, the larger reduction in response was caused by the increased friction present when the panels were mechanically fixed to the pedestals. For Structure C, with what the writer considered to be a relatively strong panel/pedestal connection, it is possible that the vibrating system was unable to overcome friction at the connection when the panels were mechanically fixed, whereas it was able to do this when the panels were loose laid. This would probably result in a reduction in friction damping at this connection and hence an increase in response. However, whilst the writer considers this to be a likely explanation for the observed phenomena, it is impossible from these measurements to be absolutely certain as to its validity.

Whilst the damping values measured from the EMA on Structure B appeared to confirm that mechanically fixing the pedestals increased the system damping (Table 4.18), the results from Structure C were less conclusive and any changes in system damping estimated from the EMA were quite insignificant. There are two possible reasons for this. Firstly, it is possible that friction at the panel/pedestal connections was engaged during pedestrian excitation, but not during the EMA. This is possible since the response levels due to pedestrian excitation were significantly higher than those due to the shaker excitation for EMA. Secondly, it is possible that the reduction in response is not being caused by increased system damping, but locally within the access floor by some mechanism which is enhanced when the panels are loose-laid and not mechanically fixed.

The tests reported in this thesis did not provide sufficient data to draw definite conclusions regarding this phenomenon and it was therefore considered inappropriate to make any recommendations regarding how it can be modelled for future structures.

6.2.3.3 Influence of the Presence of Stringers

Access floors with stringers installed were only tested on Structure C, where the effects of both snap-on and bolt-on stringers were examined. The results from the EMA (Figures 4.89 and 4.90) showed that both types of stringers had the ability to increase the natural frequency (and hence stiffness) of the floor system on which they were installed. This was particularly noticeable for the bolted stringers, which increased the natural frequency of the system above that measured on the bare structure. This corresponded to an increase in stiffness of +8.1%, as determined from the FE modelling presented in section 5.3.

However, there was very little difference between the modal damping ratios and responses due to pedestrian excitation measured when stringers were installed and when they were not.

6.2.4 Influence of the Sub-Floor Configuration

When examining the effects of the access floors on the modal properties of the three structures, it is interesting to note that the increase in damping was more pronounced for Structures A and B than it was for Structure C following the installation of the various configurations of access floors. This was particularly so for the first two modes of vibration.

In addition to this, the pedestrian response tests on Structure C demonstrated smaller reductions in response to those measured on Structures A and B, when similar access floor systems were installed. For relatively small FFH access floors, Structure A exhibited an average 16% reduction in response whereas Structure C exhibited an average 11% reduction. For the larger FFH access floors, Structure B exhibited an average 33% reduction in response whereas Structure C exhibited a 25% reduction.

It is possible that Structure C, being effectively a simple beam bending in only one direction, failed to engage the access floors in vibration as much as Structures A and B, which were effectively two-way acting plates. However, due to the limited number of structures tested, this conclusion is only tentative.

6.3 Inclusion of the Effects of Access Floors in Future Vibration Assessment Analyses

One of the main objectives of the work presented in this thesis was to determine how the beneficial (or otherwise) effects of access floors may be included in structural analyses for vibration serviceability. Section 6.2 discussed the various observations that were made from the test data and subsequent analysis. The purpose of this section is to indicate how it may be possible to include those effects into future vibration serviceability analyses.

6.3.1 Modification of Structural Dynamic Properties

Section 6.2.1 discussed the changes in modal parameters that were measured from each of the structures following the addition of access floors. In addition to the increase in mass of the vibrating system, it was found that there was a rather inconsistent increase in stiffness and damping.

However, due to the inconsistency and therefore unpredictability of these increases, it is the recommendation of the writer that attempting to model the effects of access floors in terms in changes in structural dynamic properties would be unwise. It is now well known (Eriksson, 1994; Pavic, 1999) that it is not necessarily the fundamental mode which is most critical from a vibration serviceability point of view, but that any of the modes in the frequency range excitable by pedestrian excitation is a candidate for being the most critical. Since it is not known which modes are likely to exhibit an increase in stiffness or damping, it seems unwarranted to assume an increase for any particular mode.

6.3.2 Application of a Vibration Response Reduction Factor

Sections 6.2.2 and 6.2.3 demonstrated that the reductions in response to pedestrian excitation were far more consistent than the changes in modal parameters. However, it was also demonstrated that it was very difficult to determine the effects of each of the individual configurations of access floors. The one exception to this was that there appeared to be quite a significant difference between the reduction in response detected

for small FFH access floors (150 – 200 mm) and that detected for relatively large FFH access floors (500 – 600 mm).

For these reasons, it is proposed that the most reliable and simple means of incorporating the effects of access floors into future vibration serviceability analyses is through the use of a reduction factor which will be called here a “Vibration Response Reduction Factor” (VRRF). The VRRF would be applied by calculating the vibration response of the bare structure on which access floors are to be installed, and then by multiplying the vibration response assessment parameter (say, VDV) by the relevant reduction factor. In the case of the retrofitting of existing buildings, it is recommended that the vibration response to pedestrian excitation is measured experimentally on the bare structure using the technique established by Pavic and Reynolds (1999) and presented in this thesis. The vibration response with access floors may then be estimated by multiplying the measured response on a bare floor by the VRRF.

Based on the results of the experimental and analytical work presented in this thesis, it is tentatively proposed that two reduction factors should be used. These are:

1. a reduction factor of 0.9 when the access floor FFH is less than 500 mm, and
2. a reduction factor of 0.8 when the access floor FFH is 500 mm or above.

As discussed in Section 6.1.2.2, all of the vibration response parameters evaluated in this work (RMS of the entire record, running RMS with 10 s integration time and VDV evaluated over the entire record) were found to give similar percentage changes in response following the installation of access floors. For this reason, it is proposed that the VRRF may equally be applied to any of these vibration response assessment parameters.

It is clear that the accuracy of the vibration response predicted for a structure with access floors installed is related directly to the accuracy of vibration response predictions for the bare structure. However, accurate analytical modelling of structures subjected to pedestrian excitation is very difficult, even using FE techniques. This is mainly due to the lack of accurate information about walking forcing functions. Pavic (1999) evaluated a number of existing walking forcing functions and determined that Eriksson’s (1994) walking forcing function most accurately predicted the vibration response measured on real structures. However, even this forcing function was quite conservative and it is therefore recommended by the writer that more work is carried out in the future to develop better models of pedestrian excitation.

6.4 Practical Use of Access Floors for Improvement of Vibration Serviceability

The results of the work presented in this thesis have indicated that access floors with relatively high FFHs tend to improve the vibration serviceability performance of floors more than access floors with relatively low FFHs. The proposed vibration response reduction factors reflect this phenomenon. However, simply utilising access floors with increased FFHs is unlikely to be an attractive proposition because it would result in increased building heights and, obviously, increased cost.

It is possible, however, to utilise increased FFH access floors without increasing overall building height by positioning electrical and mechanical services underneath the access floors instead of above suspended ceilings, as is the more common practice. This is, in fact, recommended in some of the sales literature for access floors (Tate Access Floors, 1997) and was illustrated in Figure 2.9. However, caution must be exercised regarding this recommendation, because it may be that the installation of services beneath the access floors actually provides less of a mechanism for damping and stiffness than when attached to the underside of the sub-floor. This effect was not investigated in this work and additional testing would be required to examine this possibility.

7 Conclusions and Recommendations for Further Work

7.1 Conclusions

1. A system for performing experimental modal analysis (EMA) on full scale floor structures was implemented using an electrodynamic shaker as an excitation source. It was utilised successfully for the estimation of natural frequencies, modal damping ratios and mode shapes of full scale classically reinforced and post-tensioned floor structures. Of the excitation signals which had been developed in this work, burst random excitation was the most appropriate for such floor structures. Of all model parameters estimated, modal masses proved to be least reliable.
2. Pedestrian response tests were performed successfully in this work. However, when performing such tests on floors with access floors installed, it was found to be necessary to locate the response transducers on the sub-floor. Mounting of the transducers on the access floor resulted in them being overloaded by local high frequency accelerations caused by footfall impacts.
3. A number of vibration response assessment parameters were calculated for the pedestrian response tests presented in this work. However, in the interests of standardisation of test procedures, it is recommended that the running RMS with 10 s integration time is adopted. This may subsequently be utilised for calculation of the eVDV with the appropriate exposure time, which was shown for these structures to be a reasonable approximation to the VDV.
4. The installation of access floors was found to cause only minor changes in the modal parameters estimated from EMA for all structures tested in this work. In most cases, the reductions in natural frequencies caused by the additional mass of the system were offset to some extent by a small increase in stiffness. Increases in modal damping ratios were found to be quite sporadic with some modes showing no increase and others showing quite large increases. Since any of the modes excitable by pedestrian excitation may be critical, it would not be conservative to assume an increase in damping for modelling purposes.

5. The results from pedestrian response measurements made before and after the installation of various types and configurations of access floors indicated that, in general, a reduction in response is likely. Such a reduction in response was measured on all of the structures tested in this work.
6. Examination of the pedestrian response data revealed that there was not much difference between the reductions in response measured for the different configurations of access floors tested in this work. The only exception to this was the influence of the finished floor height of the access floors. The relatively high FFH access floors tested in this work (500 - 600 mm) appeared to provide a greater reduction in response to pedestrian excitation than the relatively low FFH access floors (150 - 200 mm), when compared with the responses measured on the bare floor.
7. Based on the results of the pedestrian response tests, it is recommended that the effects of access floors may be included in future vibration serviceability analyses by applying a reduction factor to predicted responses to pedestrian excitation assuming a bare floor. The proposed reduction factors are:
 - 0.9 for access floors where the FFH is less than 500 mm, and
 - 0.8 for access floors where the FFH is 500 mm or greater.
8. It is suggested that the beneficial effects of increased FFH access floors on vibration serviceability may be incorporated into new buildings by installing electrical and mechanical services beneath the access floors instead of above the suspended ceilings. This would not require an increase in overall building height. This installation approach is also recommended by access flooring manufacturers but for ease of access to services.

7.2 Recommendations for Further Work

1. A methodology has been presented in this thesis for the verification of analytical models through experimental testing of real structures. However, due to the limited time and resources available to this project, only a small number of structures was actually tested. For this reason, it is recommended that a programme of research is initiated in which a large number of structures of various configurations is tested,

utilising this feasible and powerful technology, so that their vibration behaviour may be understood better leading to improved design guidelines.

2. In this work, the effects of the installation of access floors were investigated using only a limited number of tests on long-span concrete floors before and after the installation of access floors. It is recommended that, to increase confidence in the conclusions drawn in this thesis, a larger number of tests is required.
3. The influence of other types of non-structural elements on the vibration serviceability performance of floors is poorly understood. It is recommended that the procedures applied in this thesis, which investigated the effects of access floors, should be applied to determine the effects of other types of non-structural elements (such as suspended ceilings, electrical and mechanical services, partition walls, furniture and human beings).
4. To achieve recommendations 1 to 3, it is recommended that, whenever possible, new built and retrofit floor structures should be tested in their bare condition and at various stages of completion when non-structural elements have been installed. Such testing should also include an 'occupied' condition (i.e. with human beings present on the structure) so that the possibly beneficial effects of human occupants may be included.
5. It is possible that the reductions in response under pedestrian excitation were caused by local deformations in the access floor panels, which engaged damping mechanisms that reduced the amount of excitation energy transmitted to the floor structures. However, further research is required to confirm or disprove this hypothesis.
6. It is likely that occupants of floors with an access floor installed modify the vibration characteristics of the access floor in their vicinity. It is also possible that such an effect may be beneficial with respect to vibration serviceability. This phenomenon was not investigated in this work and it is recommended that further testing and analysis is performed to verify whether or not this effect actually occurs.
7. Current limits for vibration serviceability, such as the acceptable VDV in office buildings, are scarce and not widely verified. It is recommended that a large number of structures, both with and without vibration serviceability problems, is tested to provide data which may be used to determine improved limits for floor vibrations.

References

- Allen, D. L. (1974). Vibrational Behaviour of Long-Span Floor Slabs. Canadian Structural Engineering Conference. Ontario, Canada. pp1-19.
- Allen, D. E. (1990). Building Vibrations from Human Activities. Concrete International: Design and Construction, 12(6). pp66-73.
- Allen, D. E. and Murray, T. M. (1993). Design Criterion for Vibrations Due to Walking. AISC Engineering Journal, 30(4). pp117-129.
- Allen, D. E. and Rainer, J. H. (1975). Floor Vibration. Canadian Building Digest, 173. Ottawa, Canada: Division of Building Research, NRCC. pp173.1-173.4.
- Allen, D. E. and Rainer, J. H. (1976). Vibration Criteria for Long-Span Floors. Canadian Journal of Civil Engineering, 3(2). pp165-173.
- Allen, D. E. and Swallow, J. C. (1975). Annoying Floor Vibrations - Diagnosis and Therapy. Sound and Vibration, 3. pp12-17.
- ANSYS (1995). ANSYS User's Manual - Revision 5.2: Theory (Volume IV). Houston, USA: Author.
- APS Dynamics Inc. (undated). Instruction Manual: ELECTRO-SEIS Model 113 Shaker. Carlsbad, CA, USA: Author.
- Bachmann, H. and Ammann, W. (1987). Vibrations in Structures - Induced by Man and Machines. Zürich, Switzerland: IABSE.
- Bachmann, H., Ammann, W. J., Deischl, F., Eisenmann, J., Floegl, I., Hirsch, G. H., Klein, G. K., Lande, G. J., Mahrenholtz, O., Natke, H. G., Nussbaumer, H., Pretlove, A. J., Rainer, J. H., Saemann, E-U., Steinbeisser, L. (1995). Vibration Problems in Structures - Practical Guidelines. Basel, Boston, Berlin: Birkhäuser.
- Blanchard, J., Davies, B. L. and Smith, J. W. (1977). Design Criteria and Analysis for Dynamic Loading of Footbridges. DoE and DoT TRRL Symposium on Dynamic Behaviour of Bridges. Crowthorne, UK. 19 May. pp90-106.

- Blevins, R. D. (1979). Formulas for Natural Frequency and Mode Shape. Malabar, Florida: Krieger Publishing Company.
- Brown, D., Carbon, G. and Ramsey, K. (1977). Survey of Excitation Techniques Applicable to the Testing of Automotive Structures. Society of Automotive Engineers: International Automotive Engineering Congress and Exposition. Detroit, USA. 28 February - 4 March. pp1-15.
- BSI. (1978). BS 5400 Part 2: Steel, concrete and composite bridges. Specification for loads. (Appendix C: Simplified Method for Deriving Maximum Vertical Acceleration). London, UK: Author.
- BSI. (1990). BS 6897 Part 2: Method for Experimental Determination of Mechanical Mobility - Measurements Using Single-Point Translation Excitation with an Attached Vibration Exciter. London, UK: Author.
- Caetano, E. and Cunha, A. (1993). Experimental Identification of Modal Parameters on a Full-scale Structure. 6th International Conference on Computational Methods and Experimental Measurements (Vol. 2 - Stress Analysis). Italy. pp321-335.
- Caverson, R. G. (1992). Vibration Characteristics of Suspended Concrete Slabs. MSc Thesis. Bristol, UK: University of Bristol.
- Clough, R. W. and Penzien, J. (1993). Dynamics of Structures. Singapore: McGraw-Hill Book Co.
- Craig, R. R. (1981). Structural Dynamics: An Introduction to Computer Methods. USA: John Wiley and Sons.
- Concrete Society. (1994). Post-Tensioned Concrete Floors Design Handbook (Technical Report 43). Slough, UK: Author.
- CSA. (1974). Steel Structures for Buildings - Limit States Design. (Appendix G - Guide for Floor Vibrations.) Toronto, Canada: Author.
- CSA. (1989). Limit States Design of Steel Structures - A National Standard of Canada (S16.1-1989). (Appendix G - Guide for Floor Vibrations.) Toronto, Canada: Author. pp127-134.

- CSA. (1994). Limit States Design of Steel Structures - A National Standard of Canada (S16.1-94). (Appendix G - Guide for Floor Vibrations.) Toronto, Canada: Author. pp116-123.
- CVCP. (1995). Code of Practice for Safety in Fieldwork. London, UK: Author.
- DI. (undated). Real Time FFT Analyser/DSO: Applications Manual. West Lothian, UK: Diagnostic Instruments Ltd.
- DI. (1995). Real Time FFT Analyser/DSO: Operating Manual. West Lothian, UK: Diagnostic Instruments Ltd.
- DTA. (1993a). DTA Handbook - Volume 3 - Modal Testing. London, UK: Author.
- DTA. (1993b). DTA Handbook - Volume 4 - Non-linearity in Dynamic Testing. London, UK: Author.
- Dytran. (undated). Operating Guide - Model 5803A Instrumented Impulse Hammer Twelve Pound Sledge. Chatsworth, California, USA: Dytran Instruments Inc.
- Ellingwood, B. R. (1989). Serviceability Guidelines for Steel Structures. AISC Engineering Journal, 26(1). pp1-8.
- Eriksson, P-E. (1994). Vibration of Low-Frequency Floors - Dynamic Forces and Response Prediction. PhD Thesis (in English). Göteborg, Sweden: Chalmers University of Technology.
- Eriksson, P-E. (1996). Dynamic Service Actions for Floor Systems - Human Activity. Proceedings of Structures Congress XIV (Vol. 1). Chicago, Illinois, USA: ASCE. 15-18 April. pp413-419.
- Eriksson, P-E. and Ohlsson, S. V. (1988). Dynamic Footfall Loading from Groups of Walking People. Symposium/Workshop on Serviceability of Buildings (Movements, Deformations, Vibrations). Ottawa, Canada: University of Ottawa. 16-18 May. pp497-511.
- Ewins, D. J. (1995). Modal Testing: Theory and Practice. Taunton, UK: Research Studies Press and John Wiley & Sons Inc.

- Fahy, F. J. and Westcott, M. E. (1978). Measurement of Floor Mobility at Low Frequencies in Some Buildings with Long Floor Spans. Journal of Sound and Vibration, 57(1), pp101-129.
- Filloid R., Lallement, G. Piranda, J. and Raynaud, J. L. (1985). Global Method of Modal Identification. Proceedings of the 3rd International Modal Analysis Conference. Orlando, Florida, USA: SEM. pp1145-1151.
- Fladung, W. and Rost, R. (1997). Application and Correction of the Exponential Window for Frequency Response Functions. Mechanical Systems and Signal Processing, 11(1), pp23-36.
- Flanigan, C. C. and Hunt, D. L. (1993). Integration of Pretest Analysis and Model Correlation Methods for Modal Surveys. Proceedings of the 11th International Modal Analysis Conference. Kissimmee, Florida, USA: SEM. pp444-448.
- Friswell, M. I. and Mottershead, J. E. (1995). Finite Element Model Updating in Structural Dynamics. Dordrecht, The Netherlands: Kluwer Academic Publishers.
- Galbraith, F. W. and Barton, M. V. (1970). Ground Loading from Footsteps. Journal of the Acoustical Society of America, 48(5), pp1288-1292.
- Goldman, D. E. A. (1948). A Review of Subjective Responses to Vibratory Motion of the Human Body in the Frequency Range 1 to 70 cps. Report NM-004-001. Washington, USA: Naval Medical Research Institute.
- Griffin, M. J. (1996). Handbook of Human Vibration. London, UK: Academic Press.
- Guignard, J. C. (1971). Human Sensitivity to Vibration. Journal of Sound and Vibration, 15(1), pp11-16.
- Harper, Warlow and Clarke. (1961). The Forces Applied to the Floor by the Foot in Walking. National Building Studies, Research Paper 32. Department of Scientific and Industrial Research (DSIR). UK: HMSO.
- Heylen, W., Lammens, S. and Sas, P. (1997). Modal Analysis Theory and Testing. Leuven, Belgium: Katholieke Universiteit Leuven.
- ICATS. (1997). Modent, Modesh, Modacq, Meshgen Reference Manual (Version 6). London, UK: Author.

Imregun, M. and Ewins, D. J. (1995). Complex Modes - Origins and Limits. Proceedings of the 13th International Modal Analysis Conference. Nashville, Tennessee, USA: SEM. pp496-506.

ISO. (1992). ISO 10137: Bases for Design of Structures - Serviceability of Buildings Against Vibration. Geneva, Switzerland: Author.

ISO. (1994). ISO 7626: Vibration and Shock - Experimental Determination of Mechanical Mobility: Part 5 - Measurements Using Impact Excitation with an Exciter which is not Attached to the Structure. Geneva, Switzerland: Author.

ISO. (1997). ISO 2631: Mechanical vibration and shock - Evaluation of human exposure to whole-body vibration - Part 1: General requirements. Geneva, Switzerland: Author.

Khan, A. Z. (1996). Frequency Estimation of Prestressed and Composite Floors. PhD Thesis. London, UK: City University.

Khan, S. and Williams, M. (1995). Post-Tensioned Concrete Floors. Oxford, UK: Butterworth-Heinemann Ltd.

Lenzen, K. H. (1962). Final Report - Vibration of Steel Joist-Concrete Slab Floor Systems. Studies in Engineering Mechanics (Report Number 16). Lawrence, Kansas: Center for Research in Engineering Science, University of Kansas, USA.

Lenzen, K. H. (1966). Vibration of Steel Joist-Concrete Slab Floors. Journal of the American Institute of Steel Construction Engineering, 3, pp133-136.

Lenzen, K. H. and Murray, T. M. (1969). Vibration of Steel Beam-Concrete Slab Floor Systems. Studies in Engineering Mechanics (Report Number 29). Lawrence, Kansas: Center for Research in Engineering Science, University of Kansas, USA.

Lieven, N. A. J. and Ewins, D. J. (1988). Spatial Correlation of Mode Shapes: The Coordinate Modal Assurance Criterion (COMAC). Proceedings of the 6th International Modal Analysis Conference. Kissimmee, Florida, USA: SEM. 1-4 February. pp690-695.

Maia, N. M. M., Silva, J. M. M., He, J., Lieven, N. A. J., Lin, R. M., Skingle, G. W., To, W.-M., Urgueira, A. P. V. (1997). Theoretical and Experimental Modal Analysis, ed. Maia and Silva. Taunton, UK: Research Studies Press Ltd.

- Matsumoto, Y., Nisioka, T., Shiojiri, H. and Matsuzaki, K. (1978). Dynamic Design of Footbridges. IABSE Proceedings P-17/78. Zürich, Switzerland: IABSE. pp1-15.
- McConnell, K. G. (1995). Vibration Testing: Theory and Practice. New York, USA: John Wiley and Sons.
- Mercer, C. A. (1997). Communication between A. Pavic and C. A. Mercer, Prosig UK Ltd. Fareham, UK.
- Mouring, S. E. and Ellingwood, B. R. (1993). Minimising Floor Vibration Caused by Building Occupants. IABSE International Colloquium. Göteborg, Sweden: IABSE. 9-11 June. pp125-132.
- Murray, T. M. (1981). Acceptability Criterion for Occupant-Induced Floor Vibrations. AISC Engineering Journal, 18(2). pp62-70.
- Murray, T. M. (1985). Building Floor Vibrations. 3rd Conference on Steel Developments. Australian Institute of Steel Construction, Melbourne, Australia, 20-22 May. pp145-149.
- Murray, T. M. (1988). Practical Aspects of Floor Serviceability Design. Symposium/Workshop on Serviceability of Buildings (Movements, Deformations, Vibrations). Ottawa, Canada, 16-18 May. pp495-496.
- Murray, T. M. and Allen, D. E. (1993). Floor Vibrations: A New Design Approach. IABSE International Colloquium: Structural Serviceability of Buildings. Göteborg, Sweden: IABSE. pp119-124.
- NAFEMS (1992a). A Finite Element Primer. Glasgow, UK: Author.
- NAFEMS (1992b). A Finite Element Dynamics Primer. Glasgow, UK: Author.
- Ohlsson, S. V. (1982). Floor Vibrations and Human Discomfort. PhD Thesis (in English). Göteborg, Sweden: Chalmers University of Technology.
- Ohlsson, S. V. (1988). Ten Years of Floor Vibration Research - A Review of Aspects and Some Results. Symposium/Workshop on Serviceability of Buildings (Movements, Deformations, Vibrations). Ottawa, Canada: University of Ottawa. 16-18 May. pp435-451.

- Olsen, N. (1984). Excitation Functions for Structural Frequency Response Measurements. Proceedings of the 2nd International Modal Analysis Conference. Orlando, Florida, USA: SEM. pp894-902.
- Osborne, K. P. and Ellis, B. R. (1990). Vibration Design and Testing of a Long-Span Lightweight Floor. The Structural Engineer, 68(10), pp181-186.
- Parsons, K. C. and Griffin, M. J. (1988). Whole-Body Vibration Perception Thresholds. Journal of Sound and Vibration, 121(2), pp237-258.
- Pavic, A. (1999). Vibration Serviceability of Long-Span Cast In-Situ Concrete Floors. PhD Thesis. Sheffield, UK: University of Sheffield.
- Pavic, A., Pimentel, R. L. and Waldron, P. (1998a). Instrumented Sledge Hammer Impact Excitation: Worked Examples. Proceedings of the 16th International Modal Analysis Conference. Santa Barbara, USA:SEM. 2-5 February. pp929-935.
- Pavic, A. and Reynolds, P. (1999). Experimental Assessment of Vibration Serviceability of Existing Office Floors under Human-Induced Excitation. Experimental Techniques, 23(5), pp41-45.
- Pavic, A., Waldron, P. and Reynolds, P. (1998b). Vibration of Post-tensioned Concrete Floor Slabs. DETR PiT Contract Ref. CI 39/3/393(cc0952) Final Report. University of Sheffield, UK.
- Pernica, G. (1987). Effect of Architectural Components on the Dynamic Properties of a Long-Span Floor System. Canadian Journal of Civil Engineering, 14(4), pp461-467.
- Petyt, M. (1990). Introduction to Finite Element Vibration Analysis. Cambridge, UK: Cambridge University Press.
- Pimentel, R. L. (1997). Vibrational Performance of Pedestrian Bridges Due to Human-Induced Loads. PhD Thesis. Sheffield, UK: University of Sheffield.
- Press, W. H., Teukolsky, S. A., Vetterling, W. T. and Flannery, B. P. (1992) Numerical Recipes in Fortran - The Art of Scientific Computing, 2nd Edition. Cambridge, UK: Cambridge University Press.
- Price, W. (1996). Stronger, Bigger, Better. Concrete, 30(1), pp28-29.

- PSA. (1992). Platform Floors (Raised Access Floors) – Performance Specification. Croydon, UK: The Property Services Agency Specialist Services.
- Racal. (1994). Racal StorePlus VL Operation. Southampton, UK: Racal Recorders Ltd.
- Rades, M. (1994). A Comparison of Some Mode Indicator Functions. Mechanical Systems and Signal Processing, 8(4), pp367-377.
- Rainer, J. H. and Pernica, G. (1981). Damping of a Floor Sample. 2nd Speciality Conference on Dynamic Response of Structures. Atlanta, Georgia, USA. pp859-873.
- Rainer, J. H. and Pernica, G. (1986). Vertical Dynamic Forces from Footsteps. Canadian Acoustics, 14(2), pp12-21.
- Rainer, J. H., Pernica, G. and Allen, D. E. (1988). Dynamic Loading and Response of Footbridges. Canadian Journal of Civil Engineering, 15, pp66-71.
- Rainer, J. H. and Swallow, J. C. (1986). Dynamic Behaviour of a Gymnasium Floor. Canadian Journal of Civil Engineering, 13(3), pp270-277.
- Randall, R. B. (1987). Frequency Analysis. Nærum, Denmark: Brüel & Kjær.
- Reynolds, P. (1996a). Documentation for In-House Software "RANGEN". CCC Reference: CCC/96/0055A. UK: University of Sheffield.
- Reynolds, P. (1996b). Documentation for In-House Software "SG_CTRL". CCC Reference: CCC/96/0054A. UK: University of Sheffield.
- Reynolds, P. and Pavic, A. (1996). Excitation Signals for Shaker Testing. CCC Reference: CCC/96/0052A. UK: University of Sheffield.
- Reynolds, P. and Pavic, A. (2000). Impulse Hammer versus Shaker Excitation for the Modal Testing of Building Floors. Experimental Techniques. Paper submitted for review.
- Reynolds, P., Pavic, A. and Waldron, P. (1998). Model Testing, FE Analysis and FE Model Correlation of a 600 tonne Post-Tensioned Concrete Floor. 23rd International Seminar on Modal Analysis. Leuven, Belgium. pp1129-1136.
- Richardson, M. H. and Formenti, D. L. (1985). Global Curve Fitting of Frequency Response Measurements using the Rational Fraction Polynomial Method. Proceedings

of the 3rd International Modal Analysis Conference. Orlando, Florida, USA:SEM. pp390-397.

Spectral Dynamics (1994) STAR System - Reference Manual. San Jose, California, USA: Spectral Dynamics.

Steffens, R. J. (1974). Structural Vibration and Damage. London, UK: HMSO.

Taber, R. C., Brown, D. L., Vold, H. and Rocklin, G. T. (1985). Exponential Window for Burst Random Excitation. Proceedings of the 3rd International Modal Analysis Conference. Orlando, Florida, USA: SEM. 28-31 January. pp840-844.

Tate Access Floor Systems Ltd. (1996). Concore II – The Next Step. (Sales Literature) Walsall, UK.

Tate Access Floor Systems Ltd. (1997). An Introduction to Tate Access Floor Systems Ltd. (Sales Literature) Walsall, UK.

Tilly, G. P., Cullington, D. W. and Eyre, R. (1984). Dynamic Behaviour of Footbridges. IABSE Periodica 2/1984. Zürich, Switzerland: IABSE. pp13-24.

Ungar, E. E. and White, R. W. (1979). Footfall-Induced Vibrations of Floors Supporting Sensitive Equipment. Sound and Vibration, October 1979, pp10-13.

University of Manchester (1991). Introduction to the Analysis of Dynamic Test Data (Part 1). Course notes from seminar held on 21-24 September 1991 at the University of Manchester, UK.

Waller, R. A. (1969). Building on Springs. Oxford, UK: Pergamon Press.

Williams, M. S. and Falati, S. (1999). Modal Testing of a Post-tensioned Concrete Model Floor Slab. Proceedings of the 17th International Modal Analysis Conference. Kissimmee, Florida, USA: SEM. 8-11 February. pp14-20.

Williams, M. S. and Waldron, P. (1994). Evaluation of methods for predicting occupant-induced vibrations in concrete floors. The Structural Engineer, 72(20), pp334-340.

Wright, D. T. and Green, R. (1959). Human Sensitivity to Vibration. Report No. 7. Kingston, Ontario, Canada: Queen's University.

Wyatt, T. A. (1989). Design Guide on the Vibration of Floors (SCI Publication 076). Ascot, UK: SCI.

Wyatt, T. A. and Dier, A. F. (1989) Floor Serviceability Under Dynamic Loading. Proceedings of the International Symposium "Building in Steel - The Way Ahead". ECCS Publication No. 57, Stratford on Avon, UK. 19-20 September. pp20.1-20.22.

Appendix I

This appendix contains the modal parameters estimated from individual modal tests on the structures considered in this thesis. For each configuration of each floor, the estimated modal parameters presented in the thesis body were arithmetic averages of the values presented in this appendix. Estimated modal parameters presented in ~~striketrough~~ form were judged by the writer to be unreliable and were therefore not included in the arithmetic average calculation.

For ease of referencing, each dataset is assigned a unique identification code. This comprises the following elements:

1. Structure identification letter (A, B or C)
2. Structural configuration number (##)
3. Underscore character
4. Sequential swipe number (##)
5. Letter to indicate site measurement (S) or replayed measurement (R).
6. Underscore character
7. Swipe reference test point (##)
8. Letter to indicate response reference (R) or excitation reference (E)

Therefore, an example reference to a particular set of EMA data is:

B02_02S_35R

which represents data corresponding to the second swipe made on configuration 2 of structure B, measured directly on site with a reference accelerometer location at point 35.

Table A1.1: Structure A (Configuration 1) - Summary of Estimated Modal Parameters.

Dataset ID	Mode 1			Mode 2			Mode 3			Mode 4		
	Freq. (Hz)	Damp. (%)	M. Mass (kg)	Freq. (Hz)	Damp. (%)	M. Mass (kg)	Freq. (Hz)	Damp. (%)	M. Mass (kg)	Freq. (Hz)	Damp. (%)	M. Mass (kg)
A01_01S_32R	6.42	0.89	89900	6.78	1.25	61800	8.16	1.03	59800	---	---	---
A01_01R_32R	6.42	0.97	67900	6.78	1.22	64200	8.16	1.06	60700	---	---	---
A01_01R_35R	6.41	1.01	65000	---	---	---	8.16	1.04	58200	---	---	---
A01_01R_38R	6.41	1.11	68200	6.78	1.40	54000	8.16	1.04	52500	---	---	---
A01_02S_32R	6.43	1.13	---	6.79	0.64	---	8.18	0.74	---	---	---	---
A01_02R_51R	6.39	0.70	---	6.80	0.93	---	8.18	0.46	---	---	---	---
A01_03S_32R	6.41	0.80	76300	6.79	1.23	65900	8.17	0.96	56900	9.92	0.85	460800
A01_03R_32R	6.41	0.86	73900	6.79	1.22	63200	8.16	0.97	55800	---	---	---
A01_03R_35R	6.40	0.97	67200	---	---	---	8.16	0.94	58000	---	---	---
A01_03R_38R	6.41	1.01	70800	6.77	1.41	62500	8.16	0.97	59700	---	---	---

Table A1.1: Structure A (Configuration 1) - Summary of Estimated Modal Parameters (continued).

Dataset ID	Mode 5			Mode 6			Mode 7			Mode 8		
	Freq. (Hz)	Damp. (%)	M. Mass (kg)	Freq. (Hz)	Damp. (%)	M. Mass (kg)	Freq. (Hz)	Damp. (%)	M. Mass (kg)	Freq. (Hz)	Damp. (%)	M. Mass (kg)
A01_01S_32R	11.78	2.29	66200	14.97	1.98	58000	---	---	---	18.16	1.67	56900
A01_01R_32R	11.79	2.60	68300	14.98	1.91	53700	---	---	---	18.15	1.59	51100
A01_01R_35R	11.77	2.36	62400	---	---	---	---	---	---	18.18	1.73	58000
A01_01R_38R	11.78	2.26	72000	14.96	1.90	53800	---	---	---	18.20	1.63	57100
A01_02S_32R	11.77	1.99	---	15.03	1.98	---	---	---	---	18.10	1.65	---
A01_02R_51R	11.79	2.05	---	---	---	---	---	---	---	---	---	---
A01_03S_32R	11.79	2.29	69700	15.06	2.43	43500	17.41	1.47	118600	18.16	1.85	54100
A01_03R_32R	11.79	2.24	70700	15.07	2.44	40500	17.40	1.66	88100	18.18	1.80	76000
A01_03R_35R	11.79	2.15	67200	---	---	---	---	---	---	18.20	1.94	62200
A01_03R_38R	11.78	2.16	83300	15.07	2.31	40300	---	---	---	18.22	1.96	62800

Table A1.2: Structure A (Configuration 2) - Summary of Estimated Modal Parameters.

Dataset ID	Mode 1			Mode 2			Mode 3			Mode 4			Mode 5		
	Freq. (Hz)	Damp. (%)	M. Mass (kg)	Freq. (Hz)	Damp. (%)	M. Mass (kg)	Freq. (Hz)	Damp. (%)	M. Mass (kg)	Freq. (Hz)	Damp. (%)	M. Mass (kg)	Freq. (Hz)	Damp. (%)	M. Mass (kg)
A02_01S_32R ¹	6.27	1.01	48100	6.68	1.68	61200	8.03	0.95	58500	---	---	---	11.57	2.21	72400
A02_01R_32R ²	6.27	1.02	66400	6.67	1.46	57200	8.03	0.91	56100	---	---	---	11.58	2.23	73100
A02_01R_32R ³	6.27	0.97	58200	6.68	1.66	57300	8.03	0.98	59900	9.80	1.66	106200	11.58	2.19	63500
A02_02S_37R ¹	6.28	0.99	70900	6.71	1.59	59500	---	---	---	9.83	1.36	94500	11.62	2.02	70900
A02_02R_35R ¹	6.28	1.08	58900	---	---	---	8.06	0.83	61600	---	---	---	11.60	2.07	64200
A02_02R_51R ¹	6.28	1.13	60300	6.72	1.83	37800	8.05	0.74	69300	---	---	---	11.62	1.97	65600

Notes: ¹ Measurements made with accelerometer located on the sub-floor.

² Measurements made with accelerometer located over the false floor pedestal closest to the test point being measured.

³ Measurements made with accelerometer located over the centre of the false floor panel closest to the test point being measured.

Table A1.2: Structure A (Configuration 1) - Summary of Estimated Modal Parameters (continued).

Dataset ID	Mode 6			Mode 7			Mode 8			Mode 9			Mode 10		
	Freq. (Hz)	Damp. (%)	M. Mass (kg)	Freq. (Hz)	Damp. (%)	M. Mass (kg)	Freq. (Hz)	Damp. (%)	M. Mass (kg)	Freq. (Hz)	Damp. (%)	M. Mass (kg)	Freq. (Hz)	Damp. (%)	M. Mass (kg)
A02_01S_32R ¹	14.63	2.13	65200	17.16	1.91	81000	17.79	1.45	61500	---	---	---	---	---	---
A02_01R_32R ²	14.63	2.09	58500	17.13	1.57	210800	17.80	1.31	74000	---	---	---	---	---	---
A02_01R_32R ³	14.61	2.08	70100	---	---	---	17.74	1.23	115200	---	---	---	---	---	---
A02_02S_37R ¹	14.67	1.81	53200	---	---	---	17.77	1.68	79500	---	---	---	21.42	1.55	79000
A02_02R_35R ¹	---	---	---	---	---	---	17.78	1.74	70600	20.11	2.12	58000	---	---	---
A02_02R_51R ¹	14.69	1.75	18300	---	---	---	---	---	---	---	---	---	---	---	---

Notes: ¹ Measurements made with accelerometer located on the sub-floor.

² Measurements made with accelerometer located over the false floor pedestal closest to the test point being measured.

³ Measurements made with accelerometer located over the centre of the false floor panel closest to the test point being measured.

Table A1.3 Structure B (Configuration 1) - Summary of Estimated Modal Parameters.

Dataset ID	Mode 1			Mode 2			Mode 3			Mode 4			Mode 5		
	Freq. (Hz)	Damp. (%)	M. Mass (kg)	Freq. (Hz)	Damp. (%)	M. Mass (kg)	Freq. (Hz)	Damp. (%)	M. Mass (kg)	Freq. (Hz)	Damp. (%)	M. Mass (kg)	Freq. (Hz)	Damp. (%)	M. Mass (kg)
B01_01S_05R	---	---	---	4.66	0.55	19100	6.64	0.80	17600	---	---	---	8.28	1.87	7000
B01_01R_25R	4.31	0.74	26600	---	---	---	---	---	---	---	---	---	8.29	1.67	5900
B01_01R_43R	4.31	0.74	22900	---	---	---	---	---	---	---	---	---	8.30	1.67	3900
B01_02S_22R	---	---	---	4.64	0.52	23300	---	---	---	6.76	0.94	15300	8.26	1.73	6100
B01_02R_18R	4.31	0.70	25800	---	---	---	6.62	0.81	14900	---	---	---	8.31	1.51	3800
B01_02R_35R	---	---	---	4.64	0.54	16800	---	---	---	6.76	0.90	14800	8.29	1.62	5000

Table A1.3: Structure B (Configuration 1) - Summary of Estimated Modal Parameters (continued).

Dataset ID	Mode 6			Mode 7			Mode 8			Mode 9			Mode 10		
	Freq. (Hz)	Damp. (%)	M. Mass (kg)	Freq. (Hz)	Damp. (%)	M. Mass (kg)	Freq. (Hz)	Damp. (%)	M. Mass (kg)	Freq. (Hz)	Damp. (%)	M. Mass (kg)	Freq. (Hz)	Damp. (%)	M. Mass (kg)
B01_01S_05R	8.70	1.53	8900	9.08	1.49	6100	---	---	---	12.43	0.49	13800	15.03	0.52	17300
B01_01R_25R	---	---	---	---	---	---	---	---	---	12.43	0.45	16600	---	---	---
B01_01R_43R	8.66	1.70	4100	9.00	1.23	3200	---	---	---	12.43	0.44	13000	---	---	---
B01_02S_22R	---	---	---	---	---	---	---	---	---	12.41	0.46	15000	---	---	---
B01_02R_18R	---	---	---	---	---	---	---	---	---	12.41	0.46	17900	---	---	---
B01_02R_35R	8.73	1.48	5900	---	---	---	---	---	---	12.41	0.47	14800	15.00	0.43	14800

Table A1.3: Structure B (Configuration 1) - Summary of Estimated Modal Parameters (continued).

Dataset ID	Mode 11			Mode 12			Mode 13			Mode 14			Mode 15		
	Freq. (Hz)	Damp. (%)	M. Mass (kg)	Freq. (Hz)	Damp. (%)	M. Mass (kg)	Freq. (Hz)	Damp. (%)	M. Mass (kg)	Freq. (Hz)	Damp. (%)	M. Mass (kg)	Freq. (Hz)	Damp. (%)	M. Mass (kg)
B01_01S_05R	---	---	---	15.25	1.25	23700	20.04	0.53	15600	---	---	---	21.10	0.38	15600
B01_01R_25R	---	---	---	---	---	---	---	---	---	---	---	---	---	---	---
B01_01R_43R	---	---	---	---	---	---	---	---	---	20.77	0.38	22100	21.10	0.38	13200
B01_02S_22R	15.09	1.23	26700	---	---	---	20.04	0.55	44000	20.75	0.39	18700	21.06	0.39	16200
B01_02R_18R	---	---	---	15.38	1.54	29900	20.02	0.54	15900	20.75	0.40	14600	21.07	0.41	11300
B01_02R_35R	---	---	---	15.34	1.40	22500	20.03	0.53	16000	20.75	0.39	14000	---	---	---

Table A1.4: Structure B (Configuration 2) - Summary of Estimated Modal Parameters.

Dataset ID	Mode 1			Mode 2			Mode 3			Mode 4			Mode 5		
	Freq. (Hz)	Damp. (%)	M. Mass (kg)	Freq. (Hz)	Damp. (%)	M. Mass (kg)	Freq. (Hz)	Damp. (%)	M. Mass (kg)	Freq. (Hz)	Damp. (%)	M. Mass (kg)	Freq. (Hz)	Damp. (%)	M. Mass (kg)
B02_01S_05R¹	---	---	---	4.65	0.82	20900	6.46	0.88	17500	6.76	1.14	15500	8.12	1.67	6400
B02_01R_18R¹	4.22	0.68	29000	---	---	---	6.46	0.89	19900	---	---	---	8.19	1.50	4600
B02_01R_22R¹	---	---	---	4.64	0.57	20800	---	---	---	6.76	1.12	15300	8.17	1.89	11800
B02_02S_25R¹	4.23	0.46	33800	4.62	0.60	23300	---	---	---	---	---	---	8.14	1.51	6100
B02_02R_35R¹	4.22	0.59	20400	4.63	0.59	20400	---	---	---	6.74	1.13	14900	8.15	1.83	5500
B02_02R_43R¹	4.22	0.69	28900	---	---	---	---	---	---	---	---	---	8.17	1.87	3600
B02_03S_39R²	4.23	0.65	33800	4.64	0.49	25600	6.48	0.92	17200	---	---	---	---	---	---
B02_03R_39R¹	4.23	0.70	27500	4.64	0.42	26000	6.48	0.91	17500	---	---	---	8.14	1.58	2100

Notes: ¹ Measurements made with accelerometer located on the concrete floor.

² Measurements made with accelerometer located over the false floor pedestal closest to the test point being measured.

Table A1.4: Structure B (Configuration 2) - Summary of Estimated Modal Parameters (continued).

Dataset ID	Mode 6			Mode 7			Mode 8			Mode 9			Mode 10		
	Freq. (Hz)	Damp. (%)	M. Mass (kg)	Freq. (Hz)	Damp. (%)	M. Mass (kg)	Freq. (Hz)	Damp. (%)	M. Mass (kg)	Freq. (Hz)	Damp. (%)	M. Mass (kg)	Freq. (Hz)	Damp. (%)	M. Mass (kg)
B02_01S_05R ¹	8.53	1.85	6700	8.85	1.58	7800	---	---	---	12.18	0.59	16000	14.70	0.56	16000
B02_01R_18R ¹	---	---	---	---	---	---	---	---	---	12.19	0.57	14800	---	---	---
B02_01R_22R ¹	---	---	---	---	---	---	---	---	---	12.19	0.59	14700	14.74	1.22	26200
B02_02S_25R ¹	---	---	---	---	---	---	---	---	---	12.19	0.55	17500	---	---	---
B02_02R_35R ¹	8.54	1.50	6900	---	---	---	---	---	---	12.18	0.55	17200	---	---	---
B02_02R_43R ¹	8.52	1.45	5000	8.79	1.05	3600	---	---	---	12.19	0.53	13900	---	---	---
B02_03S_39R ²	---	---	---	8.81	1.31	7400	---	---	---	12.22	0.56	12700	---	---	---
B02_03R_39R ¹	---	---	---	---	---	---	---	---	---	12.22	0.57	15900	---	---	---

Notes: ¹ Measurements made with accelerometer located on the concrete floor.

² Measurements made with accelerometer located over the false floor pedestal closest to the test point being measured.

Table A1.4: Structure B (Configuration 2) - Summary of Estimated Modal Parameters (continued).

Dataset ID	Mode 11			Mode 12			Mode 13			Mode 14			Mode 15		
	Freq. (Hz)	Damp. (%)	M. Mass (kg)	Freq. (Hz)	Damp. (%)	M. Mass (kg)	Freq. (Hz)	Damp. (%)	M. Mass (kg)	Freq. (Hz)	Damp. (%)	M. Mass (kg)	Freq. (Hz)	Damp. (%)	M. Mass (kg)
B02_01S_05R ¹	---	---	---	---	---	---	19.63	0.48	18300	---	---	---	20.64	0.39	16700
B02_01R_18R ¹	---	---	---	15.03	1.75	35200	19.62	0.49	29100	20.32	0.41	19700	20.64	0.40	14200
B02_01R_22R ¹	---	---	---	---	---	---	19.62	0.49	26200	20.33	0.40	22100	20.64	0.40	14800
B02_02S_25R ¹	---	---	---	---	---	---	19.61	0.48	25000	---	---	---	---	---	---
B02_02R_35R ¹	---	---	---	15.03	1.50	419200	19.62	0.51	17400	20.34	0.39	16800	---	---	---
B02_02R_43R ¹	---	---	---	15.03	1.54	24900	---	---	---	20.34	0.41	16300	20.65	0.37	16400
B02_03S_39R ²	---	---	---	15.05	1.48	30600	19.65	0.51	21300	---	---	---	20.68	0.42	8100
B02_03R_39R ¹	---	---	---	15.07	1.66	30600	19.65	0.47	18600	20.37	0.38	13200	20.69	0.36	17000

Notes: ¹ Measurements made with accelerometer located on the concrete floor.

² Measurements made with accelerometer located over the false floor pedestal closest to the test point being measured.

Table A1.5: Structure B (Configuration 3) - Summary of Estimated Modal Parameters.

Dataset ID	Mode 1			Mode 2			Mode 3			Mode 4			Mode 5		
	Freq. (Hz)	Damp. (%)	M. Mass (kg)	Freq. (Hz)	Damp. (%)	M. Mass (kg)	Freq. (Hz)	Damp. (%)	M. Mass (kg)	Freq. (Hz)	Damp. (%)	M. Mass (kg)	Freq. (Hz)	Damp. (%)	M. Mass (kg)
B03_01S_05R¹	---	---	---	4.73	0.97	21400	6.58	1.10	16400	---	---	---	8.19	1.64	7600
B03_01R_18R¹	4.25	0.63	22500	---	---	---	6.57	1.04	21300	---	---	---	8.23	1.32	5500
B03_01R_22R¹	---	---	---	4.73	0.93	22400	---	---	---	6.80	1.19	16000	8.23	1.77	12000
B03_02S_25R¹	4.26	0.71	29400	4.75	1.06	20400	---	---	---	---	---	---	8.24	1.51	8200
B03_02R_35R¹	4.26	0.56	21700	4.74	1.27	17200	---	---	---	6.81	1.19	18500	8.20	1.51	9600
B03_02R_43R¹	4.26	0.67	24200	---	---	---	---	---	---	---	---	---	8.26	1.57	4700
B03_03S_39R²	4.24	0.66	30000	4.74	0.91	20500	6.56	1.04	17700	---	---	---	---	---	---
B03_03R_39R¹	4.24	0.71	29800	4.72	0.97	17900	6.56	1.06	20100	---	---	---	---	---	---

Notes: ¹ Measurements made with accelerometer located on the concrete floor.

² Measurements made with accelerometer located over the false floor pedestal closest to the test point being measured.

Table A1.5: Structure B (Configuration 3) - Summary of Estimated Modal Parameters (continued).

Dataset ID	Mode 6			Mode 7			Mode 8			Mode 9			Mode 10		
	Freq. (Hz)	Damp. (%)	M. Mass (kg)	Freq. (Hz)	Damp. (%)	M. Mass (kg)	Freq. (Hz)	Damp. (%)	M. Mass (kg)	Freq. (Hz)	Damp. (%)	M. Mass (kg)	Freq. (Hz)	Damp. (%)	M. Mass (kg)
B03_01S_05R ¹	8.55	2.05	6500	8.89	1.54	5800	---	---	---	12.26	0.60	16300	14.74	0.78	14300
B03_01R_18R ¹	---	---	---	---	---	---	---	---	---	12.27	0.56	8700	14.76	0.56	18700
B03_01R_22R ¹	---	---	---	8.85	1.41	13000	---	---	---	12.27	0.53	15700	14.79	0.36	24500
B03_02S_25R ¹	---	---	---	---	---	---	---	---	---	12.27	0.51	18500	14.76	0.44	32400
B03_02R_35R ¹	8.56	1.49	7200	---	---	---	---	---	---	12.27	0.54	16500	---	---	---
B03_02R_43R ¹	---	---	---	---	---	---	10.60	3.67	14600	12.27	0.55	12600	14.81	0.54	27500
B03_03S_39R ²	---	---	---	---	---	---	---	---	---	12.25	0.55	12600	14.74	0.53	23600
B03_03R_39R ¹	---	---	---	---	---	---	---	---	---	12.25	0.50	19200	14.74	0.66	16500

Notes: ¹ Measurements made with accelerometer located on the concrete floor.

² Measurements made with accelerometer located over the false floor pedestal closest to the test point being measured.

Table A1.5: Structure B (Configuration 3) - Summary of Estimated Modal Parameters (continued).

Dataset ID	Mode 11			Mode 12			Mode 13			Mode 14			Mode 15		
	Freq. (Hz)	Damp. (%)	M. Mass (kg)	Freq. (Hz)	Damp. (%)	M. Mass (kg)	Freq. (Hz)	Damp. (%)	M. Mass (kg)	Freq. (Hz)	Damp. (%)	M. Mass (kg)	Freq. (Hz)	Damp. (%)	M. Mass (kg)
B03_01S_05R¹	---	---	---	15.06	1.46	11800	19.73	0.49	15600	---	---	---	20.73	0.39	17100
B03_01R_18R¹	---	---	---	15.11	1.69	32400	19.73	0.49	21600	20.48	0.45	16900	20.72	0.41	19800
B03_01R_22R¹	14.89	1.21	20200	---	---	---	19.71	0.43	11600	20.47	0.33	20000	20.75	0.40	19100
B03_02S_25R¹	---	---	---	---	---	---	19.73	0.46	24300	---	---	---	20.72	0.37	8700
B03_02R_35R¹	---	---	---	---	---	---	19.74	0.49	17800	20.47	0.42	17500	---	---	---
B03_02R_43R¹	---	---	---	15.05	1.57	19500	19.73	0.49	21900	20.47	0.40	16700	20.73	0.40	16200
B03_03S_39R²	---	---	---	15.07	1.63	35200	19.69	0.49	21500	---	---	---	---	---	---
B03_03R_39R¹	---	---	---	15.06	1.61	29600	19.71	0.56	25600	20.44	0.45	12400	20.69	0.35	10000

Notes: ¹ Measurements made with accelerometer located on the concrete floor.

² Measurements made with accelerometer located over the false floor pedestal closest to the test point being measured.

Table A1.6: Structure C (All Configurations) - Summary of Estimated Modal Parameters.

Dataset ID	Mode 1			Mode 2			Mode 3			Mode 4			Mode 5		
	Freq. (Hz)	Damp. (%)	M. Mass (kg)	Freq. (Hz)	Damp. (%)	M. Mass (kg)	Freq. (Hz)	Damp. (%)	M. Mass (kg)	Freq. (Hz)	Damp. (%)	M. Mass (kg)	Freq. (Hz)	Damp. (%)	M. Mass (kg)
C01_01S_16R	4.54	0.53	7140	16.96	0.47	6450	---	---	---	---	---	---	37.61	1.12	4370
C01_01R_14R	4.54	0.54	6940	---	---	---	---	---	---	---	---	---	37.61	1.10	5560
C01_01R_22R	4.54	0.53	6620	16.96	0.46	6940	26.02	2.55	3550	28.92	1.35	6990	---	---	---
C01_02S_14E	4.55	0.52	7090	---	---	---	---	---	---	---	---	---	37.71	1.12	7810
C01_03S_16E	4.55	0.50	7140	17.02	0.46	7580	---	---	---	---	---	---	37.71	1.13	7580
C02_01S_16R	4.49	0.57	7140	16.46	0.75	7300	---	---	---	---	---	---	36.84	1.18	5920
C02_01R_14R	4.49	0.56	7140	---	---	---	---	---	---	---	---	---	36.84	1.14	5590
C02_01R_22R	4.49	0.58	7040	16.50	0.73	5490	27.00	1.64	4980	28.69	2.60	7350	---	---	---
C02_02S_14E	4.50	0.58	7580	---	---	---	---	---	---	---	---	---	36.90	1.17	8550
C02_03S_16E	4.50	0.57	7250	16.56	0.43	13190	---	---	---	---	---	---	36.89	1.22	7810

Notes: All measurements made with accelerometer located on the concrete floor.

Results from stepped sine tests not presented here.

Table A1.6: Structure C (All Configurations) - Summary of Estimated Modal Parameters (continued).

Dataset ID	Mode 1			Mode 2			Mode 3			Mode 4			Mode 5		
	Freq. (Hz)	Damp. (%)	M. Mass (kg)	Freq. (Hz)	Damp. (%)	M. Mass (kg)	Freq. (Hz)	Damp. (%)	M. Mass (kg)	Freq. (Hz)	Damp. (%)	M. Mass (kg)	Freq. (Hz)	Damp. (%)	M. Mass (kg)
C03_01S_16R	4.45	0.60	7250	16.62	0.49	6990	---	---	---	---	---	---	36.79	1.72	7040
C03_01R_14R	4.45	0.60	7250	---	---	---	---	---	---	---	---	---	---	---	---
C03_01R_22R	4.45	0.60	6760	16.62	0.50	7690	26.49	1.62	5350	28.75	2.42	9900	---	---	---
C03_02S_14E	4.46	0.60	7520	---	---	---	---	---	---	---	---	---	---	---	---
C03_03S_16E	4.47	0.58	7400	16.66	0.50	8000	---	---	---	---	---	---	---	---	---
C04_01S_16R	4.47	0.50	7460	16.71	0.45	6410	---	---	---	---	---	---	36.74	1.36	4900
C04_01R_14R	4.47	0.51	7140	---	---	---	---	---	---	---	---	---	36.76	1.37	5650
C04_01R_22R	4.47	0.51	7300	16.71	0.46	7300	24.78	1.95	9620	28.67	1.37	6410	---	---	---
C04_02S_14E	4.48	0.51	7350	---	---	---	---	---	---	---	---	---	36.78	1.28	8470
C04_03S_16E	4.49	0.51	7690	16.75	0.46	8000	---	---	---	---	---	---	36.84	1.28	8130

Notes: All measurements made with accelerometer located on the concrete floor.

Results from stepped sine tests not presented here.

Table A1.6: Structure C (All Configurations) - Summary of Estimated Modal Parameters (continued).

Dataset ID	Mode 1			Mode 2			Mode 3			Mode 4			Mode 5		
	Freq. (Hz)	Damp. (%)	M. Mass (kg)	Freq. (Hz)	Damp. (%)	M. Mass (kg)	Freq. (Hz)	Damp. (%)	M. Mass (kg)	Freq. (Hz)	Damp. (%)	M. Mass (kg)	Freq. (Hz)	Damp. (%)	M. Mass (kg)
C05_01S_16R	4.45	0.51	6990	16.66	0.47	6990	---	---	---	---	---	---	36.77	1.42	5750
C05_01R_14R	4.45	0.51	7410	---	---	---	---	---	---	---	---	---	36.76	1.47	6410
C05_01R_22R	4.45	0.51	7520	16.66	0.46	7520	23.30	2.08	19490	28.07	1.17	4650	---	---	---
C05_02S_14E	4.46	0.51	7350	---	---	---	---	---	---	---	---	---	37.09	2.34	5100
C05_03S_16E	4.46	0.50	7580	16.69	0.47	7940	---	---	---	---	---	---	36.94	1.89	7520
C06_01S_16R	4.48	0.52	7300	16.69	0.47	6710	---	---	---	---	---	---	36.96	1.15	5240
C06_01R_14R	---	---	---	---	---	---	---	---	---	---	---	---	36.96	1.13	5410
C06_01R_22R	---	---	---	16.70	0.46	7300	25.17	1.95	7460	28.66	1.54	7630	---	---	---
C06_02S_14E	4.48	0.60	7460	---	---	---	---	---	---	---	---	---	36.98	1.15	7810
C06_03S_16E	4.48	0.53	7460	16.74	0.46	8130	---	---	---	---	---	---	36.97	1.15	8060

Notes: All measurements made with accelerometer located on the concrete floor.

Results from stepped sine tests not presented here.

Table A1.6: Structure C (All Configurations) - Summary of Estimated Modal Parameters (continued).

Dataset ID	Mode 1			Mode 2			Mode 3			Mode 4			Mode 5		
	Freq. (Hz)	Damp. (%)	M. Mass (kg)	Freq. (Hz)	Damp. (%)	M. Mass (kg)	Freq. (Hz)	Damp. (%)	M. Mass (kg)	Freq. (Hz)	Damp. (%)	M. Mass (kg)	Freq. (Hz)	Damp. (%)	M. Mass (kg)
C07_01S_16R	4.44	0.52	7870	16.60	0.48	6580	---	---	---	---	---	---	36.44	1.52	4670
C07_01R_14R	4.43	0.51	7090	---	---	---	---	---	---	---	---	---	36.44	1.52	4900
C07_01R_22R	4.44	0.52	7300	16.60	0.47	7520	24.64	2.06	10260	28.51	1.43	7190	---	---	---
C07_02S_14E	4.45	0.53	7460	---	---	---	---	---	---	---	---	---	36.58	1.62	8330
C07_03S_16E	4.45	0.52	7350	16.63	0.47	8000	---	---	---	---	---	---	36.48	1.46	8000
C08_01S_16R	4.51	0.54	7300	16.80	0.46	6800	---	---	---	---	---	---	37.09	1.18	5400
C08_01R_14R	4.51	0.54	7090	---	---	---	---	---	---	---	---	---	37.11	1.18	5650
C08_01R_22R	4.51	0.54	7460	16.80	0.46	7250	25.31	1.86	7190	28.77	1.48	8260	---	---	---
C08_02S_14E	4.52	0.57	7350	---	---	---	---	---	---	---	---	---	37.17	1.13	8470
C08_03S_16E	4.52	0.54	7460	16.84	0.46	7940	---	---	---	---	---	---	37.09	1.21	8620

Notes: All measurements made with accelerometer located on the concrete floor.

Results from stepped sine tests not presented here.

Table A1.6: Structure C (All Configurations) - Summary of Estimated Modal Parameters (continued).

Dataset ID	Mode 1			Mode 2			Mode 3			Mode 4			Mode 5		
	Freq. (Hz)	Damp. (%)	M. Mass (kg)	Freq. (Hz)	Damp. (%)	M. Mass (kg)	Freq. (Hz)	Damp. (%)	M. Mass (kg)	Freq. (Hz)	Damp. (%)	M. Mass (kg)	Freq. (Hz)	Damp. (%)	M. Mass (kg)
C09_01S_16R	4.46	0.52	7300	16.72	0.46	6540	---	---	---	---	---	---	---	---	---
C09_01R_14R	4.46	0.52	7040	---	---	---	---	---	---	---	---	---	---	---	---
C09_01R_22R	4.46	0.52	7040	16.72	0.46	7190	24.96	1.90	7350	28.61	1.44	7580	---	---	---
C09_02S_14E	4.47	0.55	7580	---	---	---	---	---	---	---	---	---	37.17	1.21	12790
C09_03S_16E	4.47	0.53	7580	16.75	0.45	7940	---	---	---	---	---	---	---	---	---
C10_01S_16R	4.53	0.52	7090	16.80	0.46	6370	---	---	---	---	---	---	37.10	1.22	5430
C10_01R_14R	4.53	0.52	7090	---	---	---	---	---	---	---	---	---	37.10	1.23	5320
C10_01R_22R	4.53	0.53	7250	16.81	0.46	7090	25.29	1.81	7630	28.76	1.60	7520	---	---	---
C10_02S_14E	4.54	0.54	7410	---	---	---	---	---	---	---	---	---	37.16	1.13	8400
C10_03S_16E	4.54	0.53	7190	16.84	0.46	7940	---	---	---	---	---	---	37.17	1.11	8330

Notes: All measurements made with accelerometer located on the concrete floor.

Results from stepped sine tests not presented here.

Table A1.6: Structure C (All Configurations) - Summary of Estimated Modal Parameters (continued).

Dataset ID	Mode 1			Mode 2			Mode 3			Mode 4			Mode 5		
	Freq. (Hz)	Damp. (%)	M. Mass (kg)	Freq. (Hz)	Damp. (%)	M. Mass (kg)	Freq. (Hz)	Damp. (%)	M. Mass (kg)	Freq. (Hz)	Damp. (%)	M. Mass (kg)	Freq. (Hz)	Damp. (%)	M. Mass (kg)
C11_01S_16R	4.57	0.54	7300	16.88	0.45	6670	---	---	---	---	---	---	37.18	1.15	5710
C11_01R_14R	4.57	0.54	7090	---	---	---	---	---	---	---	---	---	37.18	1.17	3770
C11_01R_22R	4.57	0.54	7140	16.88	0.45	6940	25.20	1.78	6490	28.85	1.39	8700	---	---	---
C11_02S_14E	4.58	0.54	7300	---	---	---	---	---	---	---	---	---	37.24	1.14	8060
C11_03S_16E	4.59	0.52	7300	16.91	0.44	7870	---	---	---	---	---	---	37.27	1.13	7940
C12_01S_16R	4.50	0.43	7520	16.81	0.41	6800	---	---	---	---	---	---	36.78	1.29	4780
C12_01R_14R	4.50	0.44	7250	---	---	---	---	---	---	---	---	---	36.77	1.29	5240
C12_01R_22R	4.50	0.44	7250	16.80	0.41	7090	24.50	1.78	5490	28.47	1.72	8400	---	---	---
C12_02S_14E	4.50	0.46	7460	---	---	---	---	---	---	---	---	---	36.85	1.22	8000
C12_03S_16E	4.51	0.44	7750	16.82	0.41	7690	---	---	---	---	---	---	36.85	1.28	7300

Notes: All measurements made with accelerometer located on the concrete floor.

Results from stepped sine tests not presented here.

Table A1.6: Structure C (All Configurations) - Summary of Estimated Modal Parameters (continued).

Dataset ID	Mode 1			Mode 2			Mode 3			Mode 4			Mode 5		
	Freq. (Hz)	Damp. (%)	M. Mass (kg)	Freq. (Hz)	Damp. (%)	M. Mass (kg)	Freq. (Hz)	Damp. (%)	M. Mass (kg)	Freq. (Hz)	Damp. (%)	M. Mass (kg)	Freq. (Hz)	Damp. (%)	M. Mass (kg)
C13_01S_16R	4.41	0.46	7690	16.67	0.42	6540	---	---	---	---	---	---	---	---	---
C13_01R_14R	4.41	0.47	6670	---	---	---	---	---	---	---	---	---	---	---	---
C13_01R_22R	4.41	0.47	6760	16.67	0.42	6990	23.98	1.50	7040	28.15	1.69	9010	---	---	---
C13_02S_14E	4.43	0.50	7410	---	---	---	---	---	---	---	---	---	---	---	---
C13_03S_16E	4.45	0.46	7410	16.72	0.42	7810	---	---	---	---	---	---	---	---	---

Notes: All measurements made with accelerometer located on the concrete floor.

Results from stepped sine tests not presented here.